To my mother who encouraged
me to do this work and to the
memory of my father . . . .

DECAY SCHEMES FROM THE (n,γ) REACTION ON ^{151}Eu AND ^{181}Ta

JAMAL KADOM JABBER

B. Sc. (Baghdad)

A Thesis submitted for the Degree of
Doctor of Philosophy
in the
University of London

Department of Physics
Royal Holloway and Bedford New College
Egham Surrey England

May 1989

ProQuest Number: 10096229

All rights reserved

INFORMATION TO ALL USERS
The quality of this reproduction is dependent upon the quality of the copy submitted.

In the unlikely event that the author did not send a complete manuscript
and there are missing pages, these will be noted. Also, if material had to be removed,
a note will indicate the deletion.
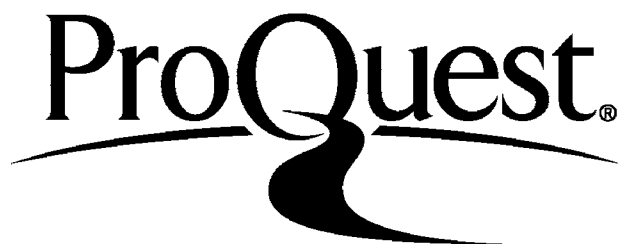
ProQuest 10096229

Published by ProQuest LLC(2016). Copyright of the Dissertation is held by the Author.

ABSTRACT

Gamma-rays were detected in both singles and coincidence in order to establish the decay schemes of the nuclei ^{152}Gd, ^{152}Sm and ^{182}W, which arise from the radioactive decay of ^{152}Eu and ^{182}Ta prepared from the (n,γ) reaction on ^{151}Eu and ^{181}Ta.

Two high resolution Ge(Li) detectors and one intrinsic germanium detector were employed for the measurements of the γ-ray energies and relative intensities, allowing the logft values, multipolarities, spins/parities and transition probabilities to be deduced for the ^{152}Gd, ^{152}Sm and ^{182}W. The fast-slow coincidence technique was used with two Ge(Li) detector and data recorded with a microcomputer for off-line analysis. Consequently, following these measurements, the level schemes of the above nuclei were built up incorporating several new energy levels and transitions.

Comparisons are made with the predictions of current nuclear models. In particular, the application of the group theoretical symmetries of the Interacting Boson Model (IBM) are discussed. The calculations were carried out using the program package PHINT for determing the energy levels, in conjunction with FBEM for evaluating the transition rates. The nuclei investigated test the SU(5) $\rightarrow$ SU(3) transitional region in the case of ^{152}Gd and ^{152}Sm, and the SU(3) rotational limit for the ^{182}W.

3

CONTENTS

4

CHAPTER V   **STUDIES OF THE LOW-LYING STATES IN ^{152}Sm ISOTOPE**

CHAPTER VI   STUDIES OF THE EXCITED STATES IN ^{182}W ISOTOPE

LIST OF FIGURES

11

LIST OF TABLES

14

CHAPTER I
GENERAL

1.1 Introduction

The main objective of nuclear spectroscopy is to further the understanding of the structure of a nucleus. One can describe the bound states of atomic nuclei in terms of interactions among all of the constituent neutrons or protons. For medium-to-heavy mass nuclei, however, this is not feasible. Even in a shell model calculation, where the energy spectrum is assumed to result only from a valence nucleon, the number of possible states with a given angular momentum is enormous. Yet the low-lying energy levels in most medium- to-heavy mass nuclei show very regular features. The energy levels of even-even nuclei for instance, which have only a few neutrons and protons outside a closed major shell, are reminiscent of a harmonic vibrator. When there are many valence neutrons and protons (i.e in mid-shell region), the energy levels of even-even nuclei have a distinct rotational character. Such energy levels are generally known as "collective", as they result from a combination of all the available shell model states. One naturally seeks a simple description of these energy states.

The geometrical model of Rainwater[1], and Bohr and Mottelson[2,3,4], provides an appealing physical description of the semi-classical picture of a vibrating or rotating "liquid drop". The problem with the geometrical model is that there is no simple procedure for describing the transition of a series of isotopes or isotones from rotational nuclei to vibrational nuclei. Attempts have also been

made to describe these collective properties in terms of boson degrees of freedom, instead of fermion degrees of freedom[5]. A common problem connected with this formulation is that the boson Hamiltonian cannot be restricted to a two-body interaction. That is, these methods involve infinite expansions[6].

Recently, two methods have been developed which contain boson operators of finite order. One is the method of Jenssen, Jolos and Dönav[7] which contains quadrupole operators that obey the commutation relation of a U(6) Lie algebra. Since their method utilizes only quadrupole operators, their expansion consists solely of quadrupole (J=2 or d) bosons. The second approach is that of Arima and Iachello[8-12], known as the "Interacting Boson Model" (IBM), which contains monopole (J=0 or S) bosons as well as quadrupole bosons.

The IBM differs fundamentally from the others in that the total number of bosons $(n_s + n_d)$ is conserved. This is because the number of active bosons in the IBM corresponds to the number of valence nucleons, thus providing a direct link to the underlying single particle or shell model structure of the nucleus[13-15]. The IBM thus provides us with a method of simultaneously interpreting nuclear collective properties in terms of a very simple model, and understanding this model and its parameters in term of the underlying fermionic structure.

Another advantage of the IBM is that it is a purely quantum mechanical description of the nucleus, rather than a semi-classical one, as in a geometrical model. The observed vibrational and rotational energy spectra which occur in many nuclei, arise due to dynamical symmetries (or approximate dynamical symmetries) of the effective IBM Hamiltonian. The relationship of the IBM to the geometrical model is currently an area of great interest and controversy[16-19].

In this chapter, theoretical considerations relevent to the present work are introduced. The theory of some important nuclear models will be discussed in Chapter Two where the IBM is emphasized. Experimental techniques for Gamma-ray spectroscopy are described in Chapter Three. Chapters Four, Five and Six are dedicated to the studies of the decay schemes of ^{152}Gd, ^{152}Sm and ^{182}W following the radioactive decays of ^{152}Eu and ^{182}Ta respectively.

1.2 Radioactive Decay

Radioactivity involves the changes of the nucleus of an atom not its extra nuclear electrons, and is an attempt by an unstable nucleus to become more stable. The emission of an Alpha or Beta particle from the nucleus of a radioactive atom produces the nucleus of a different atom called the "daughter" or "decay atom" which may itself be unstable. The disintegration process proceeds at a definite rate through a certain number of stages until a stable end-product is formed.

It was shown by Rutherford[20] that the decay of a radioactive atom is a random process, and the rate of decay can only be described statistically. Any sample of radioactive material likely to be of practical interest, however, contains so many atoms that a statistical prediction about its behaviour turns out to be very accurate.

The decay was observed to follow an exponential law with great accuracy. The solution for the number of radioactive atoms (N) left in a sample after time t is:

$$N = N_o e^{-\lambda t} \tag{1.2.1}$$

where N_o is the number of radioactive atoms at time t=0.

λ is the probability per unit time that a particular atom will decay.

A characteristic of each radionuclide is its half-life. The half-life is defined as the time for a number of radioactive atoms to be reduced to one half of the original value. Applying this definition to Eq. (1.2.1) we get

$$N = N_o e^{-0.693t/T_{\frac{1}{2}}} \tag{1.2.2}$$

The radioactive material can occur either naturally, like Uranium, or can be obtained either by bombardment of suitable target materials with neutrons or from fission products. In this study, radioisotopes are produced by neutron bombardment in a nuclear reactor, which is the most useful source of neutrons. This reaction involves the capturing of one neutron by the target nucleus. Such a reaction is normally written in simplified form by A(n,γ)B, where n represents the captured neutron and γ represents the photon. A and B are the "initial" and "final" nuclides, respectively.

Since the product of this type of reaction is an isotope of the target element, a chemical separation cannot generally be carried out. Thus the specific activity obtainable by the (n,γ) reaction is limited. For "short" irradiations and irradiation in low fluxes, the burn up of the target nuclei can be neglected, and the neutron absorption cross-section of the product isotope is frequently negligible. Then the specific activity S of the product is given by[21]

$$S = \frac{0.6\phi\sigma(1 - e^{-0.693t/T_{\frac{1}{2}}})}{3.7\times10^{10}W} \tag{1.2.3}$$

where

S is in Ci g^{-1} of the target element,

ϕ is the effective neutron flux in sample in n.cm^{-2}.sec^{-1},

σ is the neutron capture cross-section in barns,

W is the atomic weight of target material,

t is the radiation time, and

$T_{\frac{1}{2}}$ is the half-life of the product isotope.

1.3 Beta Decay

Beta decay can be described as the process in which the mass number remains unchanged for the nucleus under consideration but the atomic number changes by unity. The process is classified further into three types shown below.

$$n \rightarrow p + e^- + \bar{\nu} \qquad \beta^-\text{-decay} \qquad (1.3.1)$$

$$p \rightarrow n + e^+ + \nu \qquad \beta^+\text{-decay} \qquad (1.3.2)$$

$$p + e^- \rightarrow n + \nu \qquad \text{electron capture} \qquad (1.3.3)$$
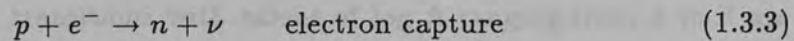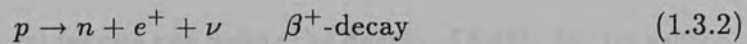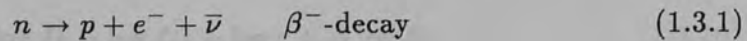
All the above processes are controlled by the weak interaction force of nature. For the present discussion, however we shall concentrate on the first two types of decay processes. The β^- and the β^+ decays which contain broad spectra from zero to finite maximum energy. This is also called the end-point energy of the process and is a characteristic of the nuclide under consideration. The spectra involved with the intermediate excited state proceed to the ground state in an appreciable fraction by a process of internal conversion which is observed as a line spectrum superimposed on the continuous β-ray spectrum.

Beta transitions can be classified as either allowed or forbidden. Allowed transitions are those in which the emitted particles (electron and neutrino) do not carry away any angular momentum. This means that the parity of the nuclear states do not change. If in the decay the parity of the nuclear states changes,

22

then the particles cannot be emitted. The angular momentum carried now is no longer zero. Such a transition is termed as forbidden transition.

It is customary to define the "comparative life time" of a beta transition, ft, where f is the function which includes the coulomb correction factor resulting from an interaction of the orbital electron with the daughter nucleus. t is half-life of beta decay.

The evaluation of log ft is obtained from the graph of Maszkouski[22] and Verrall et al[23] which is based on

$$\log ft = \log f_o t + \log c + \Delta \log ft \qquad (1.3.10)$$

On the basis of the log ft values one can define the degree of forbidden transition. It can be seen that transitions with values of log ft ranging from 3 to 6 are allowed, those between 6 and 9 constitute "first forbidden", higher than 9 constitute "second forbidden" and so on until the higher degrees of forbiddeness. The transition having values of log ft less than 4 are called "super allowed transitions"[24].

As far as the selection rules are concerned, the β-decay process is taken as a reaction where an electron and a neutrino are emitted. The conservation of angular momentum then gives

$$J_i = J_f + L_{e\nu} + S_{e\nu} \qquad (1.3.11)$$

Where J_i is the angular momentum of the nucleus before emission, J_f is the angular momentum after the emission, and $L_{e\nu}$ and $S_{e\nu}$ is the orbital angular momentum and spin of the emitted pair.

If the pair (e,ν) is emitted with antiparallel spins then the spin is zero and

$$J_i = J_f + L_{e\nu}$$

where again $L_{e\nu} = 0$ if the parity has to remain unchanged. This means the pair are emitted without angular momentum.

The selection rule is therefore $\Delta J = 0$ and the transitions are called the Fermi transitions (allowed β-decay). However, $S_{e\nu} \neq 0$ i.e the spin of the pair is parallel and this results in change of the angular momentum so that in this case

$$J_i = J_f + 1$$

for $L_{e\nu} = 0$ to retain parity. $\Delta J = 0$, or ± 1 (for all $0 \rightarrow 0$ not allowed).

These transitions are called the Gamow-Teller transitions. The selection rules for first forbidden transition can be obtained when the emission of the light particles cannot be as an S-wave consequently leads to their emission as a P-wave resulting in change of parity as $L_{e\nu} = 1$ for a P-wave. For tables see Ref. (25).

Another important note to be made is the de-excitation of the daughter nucleus by the emission of a γ-ray after the emission of a β-ray from the parent nucleus.

1.4 Electromagnetic Transitions

A great deal of information about the nuclei has come from the study of the electromagnetic transitions. The basic reason for this is the fact that the interaction is known, while the nucleus forces are still elusive in nature.

The basic information comes from the study of gamma emission of the nuclei. The semiclassical description of gamma radiation is well documented and a review of the general principles of the spectroscopy along with the basic aspects of multipole radiation is discussed by Blatt and Weisskopf[26]. The classical picture describes the nucleus as a charge-current distribution of confined periodic motion the frequency of which is ω with the relationship between it and the energy of transition as

$$\omega = \frac{E_i - E_f}{\hbar}$$

The power radiated from an oscillating charge assembly involves the solution of Maxwell's equation outside and inside the charge region (the nucleus) and by the integration of Poynting's vector over an area surrounding the nucleus. The simplest treatment of the problem is to assume the wavelength of the radiation as large when compared to the nuclear dimensions. This implies that the probability of emission of the radiation decreases rapidly with the increase of multipole order.

Since each nuclear state has a definite angular momentum I, component m and parity π then a transition results in an change of angular momentum L with eigenvalue λ and component μ and parity π such that the conservation laws are retained, therefore

$$L = I_i - I_f \qquad (1.4.1)$$

$$\pi_i \times \pi_f = \pi \qquad (1.4.2)$$

where i and f mean the initial and final state.

The angular momentum of the photon indicates the multipolarity of the radiation. Hence for multipolarity λ, for example the two kinds of radiations are electric with 2^λ pole (Eλ) and magnetic 2^λ pole (Mλ).

25

In addition the two multipoles have different symmetry properties and therefore the selection rule could be obtained using the parity properties of the wavefunction of the relevant nuclear state. As a consequence, the electric multiple radiation of order L has parity $\pi_i.\pi_f = (-1)^L$ and magnetic multipole has $\pi_i.\pi_f = (-1)^{L+1}$.

As the two momentum selection rules restrict the possible multipolarities, one therefore has the triangle relation:

$$|\,I_i - I_f| \leq L \leq |\,I_i + I_f| \tag{1.4.3}$$

The above conditions, though necessary, are not sufficient for radiative transitions e.g. transitions from 0_i to 0_f states are always forbidden and occur by a mechanism different from E.M γ-ray emission e.g by a conversion electron or by formation of electron positron pairs.

The types of radiations observed are E1 to E6 and M1 to M5 (inclusive). In all cases, with the exception of E2/M1 and E1/M2, only single type of radiation occurs for a given transition.

If for a certain order of multipole, the matrix elements which determine the transition probability vanish, then that transition is forbidden and that multipole component of the E.M field is absent.

The transition probability is the main feature of E.M transitions in general and for the analysis of empirical data in particular. The formula is described in Blatt and Weisskopf[26,27].

$$T(\sigma\lambda,\mu) = \frac{8\pi(\lambda+1)}{\lambda[(2\lambda+1)!]^2\hbar}\left(\frac{\omega}{c}\right)^{2\lambda+1)} |< f \mid M(\sigma\lambda,\mu) \mid i > I \mid^2 \tag{1.4.4}$$

$$T(\lambda : I_i \rightarrow I_f) = \sum_{\mu,m_f} T(\lambda,\mu : I_i m_i \rightarrow I_f m_f)$$

$$T(\lambda : I_i \rightarrow I_f) = \frac{8\pi(\lambda + 1)}{\lambda[(2\lambda + 1)!]^2 \hbar}(\frac{\omega}{c})^{2\lambda+1)}B(\lambda : I_i \rightarrow I_f) \qquad (1.4.5)$$

Where σ is meant for electric or magnetic radiation and

$$B(\lambda : I_i \rightarrow I_f) = \sum_{\mu,m_f} |< I_f m_f \mid M(\lambda,\mu) \mid I_i m_i >|^2 \qquad (1.4.6)$$

is the reduced transition probability.

It is seen that the transition probability depends on the transition energy whereas the reduced transition probability is independent of energy but it is the square of the transition matrix element. It is usually advantageous to convert $T(\lambda)$ into $B(\lambda)$ where

$B(E\lambda)$ is expressed in a units of $e^2 R^2 \lambda$

and $B(M\lambda)$ is expressed in a units of $\mu_N^2 R^{2\lambda-2}$

The formula such as $B(\sigma\lambda)$ require detailed knowledge of the nucleus but detailed calculations are available only for the low lying state. A simple case is that of a single nucleon radiating system. This single particle assumes the excitation of only one nucleon and provides avaliable reference to nuclear models. The rough and simple estimate for a single particle transition probability for each multipolarity is given by the Weisskopf estimate. In calculating the Weisskopf estimate, the statistical factor S is assumed to be unity and the nuclear radius is taken as 1.2 A$^{\frac{1}{3}}$ fm.

$$B_w(E\lambda) = \frac{1}{4\pi}(\frac{3}{\lambda + 3})^2(1.2)^{2\lambda}A^{\frac{2\lambda}{3}} \quad e^2 fm^{2\lambda} \qquad (1.4.7)$$

$$B_w(M\lambda) = \frac{10}{\pi}(\frac{3}{\lambda + 2})^2(1.2)^{2\lambda-2}A^{\frac{2\lambda-2}{3}} \quad \mu_N^2 fm^{2\lambda-2} \qquad (1.4.8)$$

In practice, when a small admixture of magnetic multipole with the electric multipole radiations are present like, E2 and M1, the relative magnitudes and phases of the E2 and M1 matrix element can yield information on the nature

and size of the non-vibrational component of the excited states and is given by the ratio

$$\delta = \frac{<I_f|E2|I_i>}{<I_f|M1|I_i>} \tag{1.4.9}$$

The total transition probabilities of the nuclear level say the P-level is the sum of the transition probabilities of all depopulating (electromagnetic and particles) transitions P_d, and can be measured by knowing the half-life τ or the level width T of that level

$$P(\text{level}) = \sum_d P_d = [\tau(\text{level})]^{-1} \quad \text{per sec} \tag{1.4.10}$$

$$\tau(\text{level})T(\text{level}) = \hbar = 6.58 \times 10^{-22} \; MeV \sec \tag{1.4.11}$$

The experimental gamma-ray transition probability is related to the theoretical partial gamma-ray transition probability

$$T(\sigma\lambda) = P_\gamma(E\lambda)$$

which is given by

$$P_\gamma(\sigma\lambda) = \frac{P(\text{level})I_\gamma(\sigma\lambda)}{\sum_d I_d} \tag{1.4.12}$$

where $\sum I_d$ is the sum of the intensities of all transitions depopulating the level of interest in the same units as that of the intensity $I_\gamma(\sigma\lambda)$ of the gamma-ray transition with multipolarity $\sigma\lambda$. Now $\sum I_d$ is obtained using the following relation

$$\sum_d I_d = \sum_d I_\gamma(1 + \alpha_T) \tag{1.4.13}$$

where interference between electric and magnetic multipoles are ruled out. The total electron conversion coefficient α_T is obtained from the theory of internal conversion discussed in section (1.5). Using Eq. (1.4.5) one gets

$$B(E1 : I_i \rightarrow I_f) = 6.288 \times 10^{-16} E_\gamma^{-3} P_\gamma(E1 : I_i \rightarrow I_f)$$

$$B(E2 : I_i \rightarrow I_f) = 8.161 \times 10^{-10} E_\gamma^{-5} P_\gamma(E2 : I_i \rightarrow I_f) \tag{1.4.14}$$

$$B(M1 : I_i \rightarrow I_f) = 5.687 \times 10^{-14} E_\gamma^{-3} P_\gamma(M1 : I_i \rightarrow I_f)$$

where E_γ is in MeV and is the transition energy.

For a single depopulating gamma-ray transition with E2/M1 mixing the partial gamma-ray transition probability and the total transition probability are related to each other as a function of the total internal conversion coefficient α_T and multipole ratio δ.

$$P_\gamma(M1) = \frac{P(\text{level})}{[1 + \delta^2 + \alpha_T(M1) + \delta^2 \alpha_T(E2)]} \tag{1.4.15}$$

$$P_\gamma(E2) = \frac{P(\text{level})}{[1 - \delta^{-2} + \alpha_T(E2) + \delta^{-2} \alpha_T(E2)]} \tag{1.4.16}$$

For transitions with a different multipole mixing order one may refer to Löbner[28]. The above relations are used for calculations in chapter IV, V and VI.

1.5 Internal Conversion

The observations of well defined peaks in the electron spectrum that are emitted in radioactive decay processes were interpreted by Hahn and Meit ner[29] as decay energy resulting from the internal conversion of nuclear gamma radiation in various shells of the atom. In this process a quantum is directly exchanged, without the intermediate emission of a photon, between the nucleus and the electron. The total system involved consists of the nucleus, the electrons in various shells and the quantized field. The conversion electron energy is equal to the nuclear transition energy less the binding energy of the orbital electron. In fact, the ease with which the exact energies of these conversion lines could be measured with magnetic spectrometers, made the observation of conversion

electrons the most accurate practical method of determining gamma energies until about 1950.

For an electromagnetic transition , gamma-ray emission and internal conversion compete. Excluding other possible modes of decay, for instance β-decay, the total transition probability can be written as

$$\lambda = I_\gamma + I_e \tag{1.5.1}$$

where I_γ is the probability for emission of a gamma-ray per second and I_e is the probability for emission of a conversion electron per second. The ratio between the two decay constants is

$$\alpha = \frac{I_e}{I_\gamma} \tag{1.5.2}$$

and α is called the conversion coefficient and is the intensity ratio of conversion electrons and γ-ray for a given transition. Thus α may be any positive number. The total probability for internal conversion I_e can also be broken up into partial probabilities for ejection of K, L and M electrons, etc which can be written as

$$I_e = I_K + I_L + I_M + ... \tag{1.5.3}$$

Thus, Eq. (1.5.2) can be written as

$$\alpha = \frac{I_K + I_L + I_M}{I_\gamma} = \frac{I_K}{I_\gamma} + \frac{I_L}{I_\gamma} + \frac{I_M}{I_\gamma} = \alpha_K + \alpha_L + \alpha_M \tag{1.5.4}$$

where α_K, α_L and α_M are called the K, L, and M conversion coefficients, respectively. From Eq. (1.5.4), one can relate the mean lifetime τ of the total transition and τ_γ for the gamma transition in the following way

$$\tau = \frac{1}{\lambda} = \frac{1}{(I_\gamma + I_e)} = \frac{\frac{1}{I_\gamma}}{1 + \frac{I_e}{I_\gamma}}$$

or

$$\tau = \frac{\tau_\gamma}{1 + \alpha}$$

30

i.e

$$\tau_\gamma = \tau(1 + \alpha) \tag{1.5.5}$$

In the point nucleus approximation, the interaction of the electron and nuclear currents and charge via the electromagnetic field is exactly proportional to the product of the atomic (electronic) and nuclear (gamma transition) matrix elements involved[30]. Because the atomic wave functions are well known, the form of electromagnetic field for a point nucleus depends only on the nuclear charge number Z, the energy of the nuclear transition, the type of transition, electric or magnetic, and its multipolarity. It is clear that the internal conversion can be calculated very precisely from the theory of electromagnetism and is reasonably independent of the detailed features of the nuclear transitions. The earliest tabulations were based on the Dirac wave function for the electron in the atomic field of a point nucleus[31]. The conversion coefficients for the K and L shells have been calculated by Rose [31,32] as a function of atomic number Z, transition energy and multipole order (both electric and magnetic) for multipole order from 1 to 5. The well understood theory of internal conversion therefore, can be used to determine multipolarities and admixture of multipolarities for nuclear transitions. The present theoretical α_k, which are needed in chapters IV, V and VI are obtained from Ref. (33).

CHAPTER II
NUCLEAR MODELS

2.1 Shell Model

With the accumulation of data on nuclei through the 1930's and 40's, it became apparent that the nucleus does exhibit a shell structure in much the same way as the atom. If one plots the binding energy of the valence electron as a function of atomic number, Z, for the elements, one sees discontinuities at values of Z corresponding to the noble gases, due to shell closing effects. Plots of neutron separation energy as a function of mass number A show discontinuities at values of the neutron number N = 28, 50, 82 and 126. Similar plots of the proton separation energy show gaps at Z = 28, 50 and 82[34]. Thus, closed shell effects similar to those present in the noble gases in atomic physics, are present in the nucleus and occur at nucleon numbers Z or N = 2, 8, 20, 28, 50, 82 and 126[35,36]. These are so called "magic numbers" of the nucleus and are associated with a large binding energy. Other experimental evidence related to the large binding energy of the magic number nuclei are the abundance of stable isotopes at magic Z and stable isotones for magic N.

As in the case of the atomic shell model, where each electron is considered to be moving in a fixed orbit in an average potential due to the nucleus and other electrons, the nuclear model considers each nucleon in the nucleus to be moving on a fixed path in an average potential created by all the other nucleons[37]. The early models used a spherically symmetric, Square-Well potential which reproduced the observed regularities in nuclear structure up to Z or N = 20[37-39].

However, such a potential alone will not reproduce the observed structure at the higher values of Z and N.

In 1949, in two independently published papers[37,38] a strong coupling between the spin and orbital angular momentum of each nucleon was postulated. The form of this interaction is given by

$$V_{\ell s}(r) = V_{\ell s}(\frac{\hbar}{m_\pi c})^2 \quad \mathbf{L.S} \quad (\frac{1}{r}\frac{df}{dr})$$

where L denotes the orbital angular momentum vector, S is the spin vector, f gives the profile of the central potential and $(\frac{\hbar}{m_\pi c})^2$ Compton wavelength of the pion is introduced for dimensional reasons.

There are two possible couplings of the orbital angular momentum and spin

$$J = \ell + \frac{1}{2} \quad or \quad J = \ell - \frac{1}{2}$$

where J is the total angular momentum of the particle. If one assumes the Woods-Saxon potential as the central potential, it can be shown that the levels are split with states having $J = \ell + \frac{1}{2}$ lowered and states with $J = \ell - \frac{1}{2}$ raised.

In the shell model terminology, each level is designated by a principle quantum number N, an orbital angular momentum value ℓ, and a total angular momentum value $J = \ell \pm \frac{1}{2}$, and is referred to as a single-particle or shell model state. The lowest states are filled first, up to the maximum number of (2J+1) like particle in a given shell.

For even-even nuclei, i.e even number of neutrons and even number of protons, the assignment of the ground state spin and parity is quite simple (0^+). This is a consequence of the pairing interaction which tends to couple pairs of particles to zero spin.

33

In the case of odd mass nuclei, where either N or Z is odd, the ground state angular momentum and parity are given by the half integral angular momentum J and the parity $(-1)^{\ell}$ of the unpaired particle.

2.2 The Collective Model

In this section, to understand the nuclear excitations in terms of the specific interactions of the single nucleons comprising a nucleus is the primary goal of nuclear physics. The shell model has been shown to provide this level of understanding in many nuclear systems. This success has been limited in even-even nuclei, however, to systems with relatively few particles outside of closed shells or the region $A \leq 50$. To date, no complete shell model description of a heavy even-even nucleus far from a closed shell exists.

Multiparticle nuclear systems, however, exhibit structures that can be easily understood when the gross properties of their nuclei are taken into account. For example, there is considerable evidence that the low-lying excitations of even-even nuclei with $A \geq 100$ are predominantly of a collective nature, the correlated oscillations of many particles with respect to a core of spectator nucleons. In addition, the onset of structures that can be attributed to the excitation of only a few (2 to 4) particles occurs at a much higher energy.

The most successful of the macroscopic descriptions of nuclear excitation is that of Bohr and Mottelson (BM)[3,4]. An excellent detailed description of the collective properties of nuclei is presented in their text Ref. (45). In addition, there are numerous excellent review articles[40-44], which present (BM) model in great detail; so, the discussion here will be restricted to a general presentation

of the model and the characteristic features of the different excitations expected from a phenomenological approach.

2.2.1 Vibrational Shape

In the BM description, the competition of short-range and long-range interactions between nucleons gives rise to surface vibrations about an equilibrium shape that can be spherical or deformed, whether or not axially symmetric.

The surface of a nucleus can be expressed in term of [43]

$$R = R_\circ \left[1 + \sum_{\lambda,\mu} \alpha_{\lambda\mu} Y_\lambda^\mu(\theta,\phi) \right] \tag{2.2.1.1}$$

where $R_\circ$ is the constant and Y_λ^μ are the usual Legendre polynomials. The collective motions can then obtained by the time variation of the $\alpha_{\lambda\mu}$'s. In the usual quadratic approximation, the kinetic energy can be written as[43]

$$T = \frac{1}{2} \sum_{\lambda,\mu} B_\lambda \mid \dot{\alpha}_{\lambda\mu} \mid^2 \tag{2.2.1.2}$$

Similarly, the expression for the potential energy becomes[43]

$$V = \frac{1}{2} \sum_{\lambda,\mu} C_\lambda \mid \alpha_{\lambda\mu} \mid^2 \tag{2.2.1.3}$$

Equation (2.2.1.2) and (2.2.1.3) correspond to the familar simple harmonic oscillator for each variable $\alpha_{\lambda\mu}$, where the associated frequency for each $\alpha_{\lambda\mu}$ is given[43]

$$\omega_\lambda = \left(\frac{C_\lambda}{B_\lambda} \right)^{\frac{1}{2}} \tag{2.2.1.4}$$

The oscillations associated with $\lambda = 0$ and $\lambda = 1$ are not of concern here, since they correspond to density oscillations (which will occur at high excitation

energies) and vibrations of the centre of mass, respectively. The frequency, ω_λ, rapidly increases[42] as a function of λ. The lowest order vibrations will, therefore, be of order $\lambda = 2$, or quadrupole oscillations. Since we are only interested in low-lying excitations, the only other order which will be discussed is $\lambda = 3$.

Consider first the situation for $\lambda = 2$. A phonon, a quantum of vibration, of type λ carries angular momentum equal to λ and parity $(-)^\lambda$. For a nucleus which can oscillate about a spherical shape, therefore, the first excited state will have spin-parity of 2^+. The next quadrupole excitation will correspond to the coupling of two $\lambda = 2$ phonons, i.e., $n_{(\lambda=2)} = 2$, and will be a degenerate triplet of states with J^π values of $0^+, 2^+, 4^+$ at twice the excitation energy of the first 2^+ state. (Remember the energy for a simple harmonic oscillator is of the form $E_n = \hbar\omega(n+\frac{3}{2})$). An example of a typical spectrum of levels for a spherical nucleus exhibiting quadrupole oscillations is shown in Fig. (2.1a). In the actual situation, one expects that the degeneracies will be broken, but the predicted occurrence of levels at approximately the appropriate energies should correspond to those actually observed.

An energy spectrum is not sufficient to identify the structure of a nucleus; knowledge of the wave functions of the states is also critical. The usual method of probing the wave functions is by investigating the reduced transition probability, B(E2), for the γ-ray decay of one level to another, since this involves the overlap of two wave functions connected by the transition operator, which is a familiar multipole operator M(Eλ). The B(Eλ) values are simply related to the multipole operator, M(Eλ), through [40]

$$B(E\lambda, L_i \rightarrow L_f) = \frac{1}{2L_f + 1} < L_i \| M(E\lambda) \| L_f >^2 \qquad (2.2.1.5)$$

36
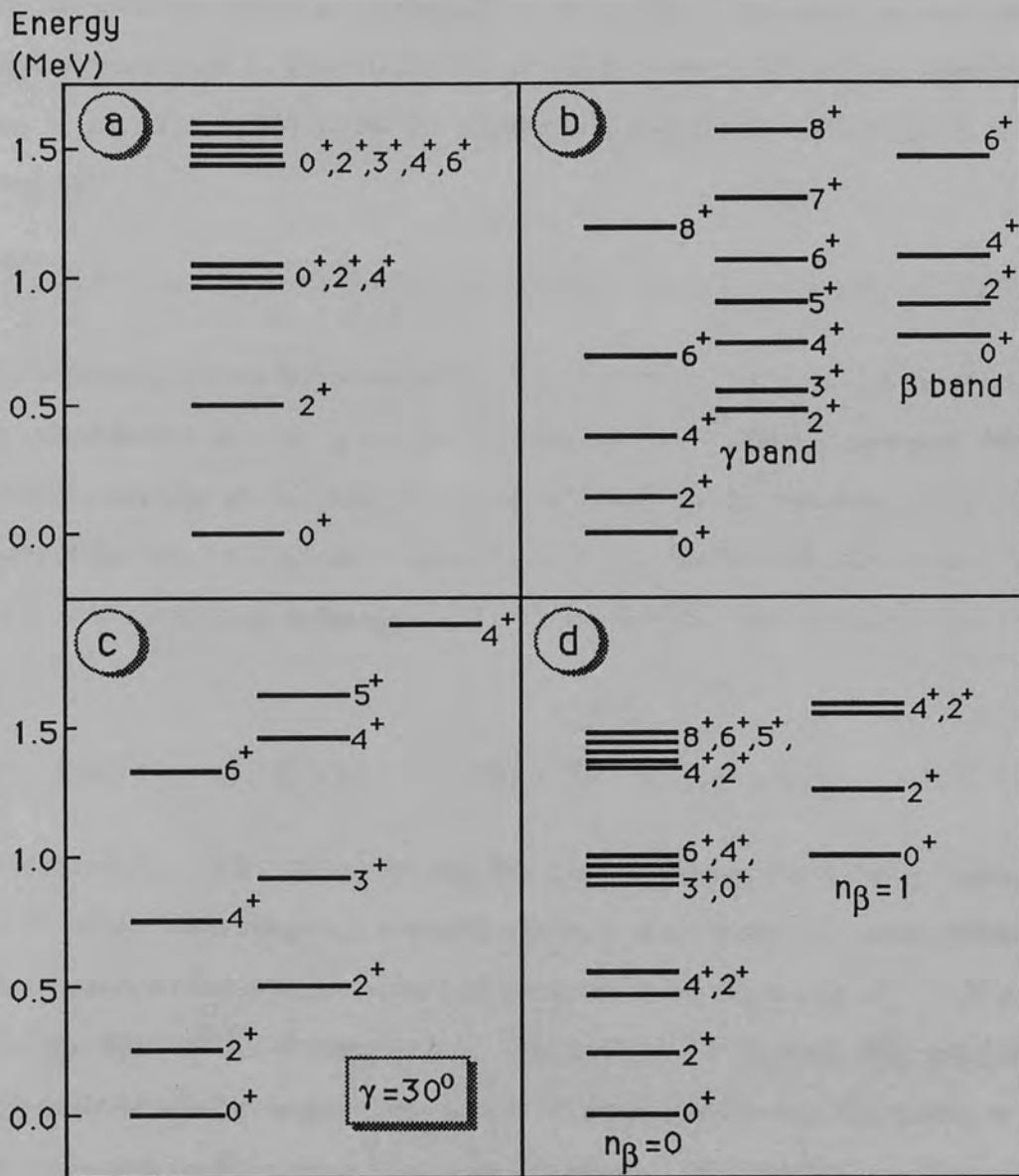
Fig (2.1) Representative energy spectra of collective excitations in collective Model. The states are labeled by their J^π values and characteristic quantum numbers. **(a)** Spectrum of a harmonic vibrator. The states are labeled by the phonon number n. **(b)** Spectrum of a symmetric rotor. The spectrum is divided into various bands: the ground band, γ band, and β band. **(c)** Spectrum of a rigid triaxial rotor with asymmetry γ =30° . **(d)** Spectrum of a γ-unstable oscillator. The states are labeled by n_β, which counts the number of β-vibrational quanta. *The figure is from Cizewiski* [74].

One can label the collective excitations by the number of phonons, n_λ, and the angular momentum L. Transitions will only occur between states connected by $\Delta n_\lambda = \pm 1$. The B(Eλ) values for allowed transitions between two levels are given by[10]

$$\sum B(E\lambda : n_\lambda \quad L_i \to n_\lambda - 1 \quad L_f) = n_\lambda B(E\lambda : n_\lambda = 1 \to n_\lambda = 0) \quad (2.2.1.6)$$

The summation of the left-hand-side of the equation is over all states to which the initial state can decay, given the selection rules of the B(Eλ) operator. For example, consider the 4_1^+ level (the subscript refers to the first occurrence of a 4^+ state) of the two $\lambda = 2$ phonon triplet. Here $n_2 = 2$ and the only state to which the 4_1^+ state can decay is the $n_2 = 1$ 2_1^+ state. Therefore Eq. (2.2.1.6) reduces to

$$B(E2 : n_2 = 2 \quad 4_1^+ \to n_2 = 1 \quad 2_1^+) = 2B(E2 : 2_1+ \to 0_1^+) \quad (2.2.1.7)$$

In addition, Eq. (2.2.1.6) implies that for any higher-lying state, for example, the 2^+ of the three-phonon quintuplet, the sum of all transition probabilities will be equal to the phonon number of the initial level times B(E2:$2_1^+ \to 0_1^+$), although the individual transition to the lower $n_2 = 2$ state will not be necessarily of equal strength. The actual branching ratios are determined by the respective coefficients of fractional parentage (CFP) for the coupling of particles with angular momentum λ. In particular, for $\lambda = 2, 3, 4$ these have been tabulated by Bayman and Laude[45]. Important branching ratios for some of the low-lying levels are presented in Table (2.1).

Apart from quadrupole oscillations, oscillations corresponding to $\lambda = 3$, known as octupole vibrations, may also occur at approximately the energy of the $\lambda = 2$ two-phonon triplet[43]. Again, an energy spectrum given by E $\propto \hbar\omega_3$ will occur, with the lowest state being a 3^- level. It should also be noted that

Table (2.1)

Branching ratios for γ-deexcitation of collective states in the collective model

$J_i \rightarrow J_f$ / $J_i \rightarrow J_f$	Vibrator[a]	Symmetric[b] Rotor	Asymmetric Rotor Triaxial[c]	Asymmetric Rotor γ-unstable[d]
$\dfrac{2_2 \rightarrow 0_1}{2_2 \rightarrow 2_1}$	0	0.70	0	0
$\dfrac{3_1 \rightarrow 2_1}{3_1 \rightarrow 4_1}$	0	2.50	0	0
$\dfrac{3_1 \rightarrow 4_1}{3_1 \rightarrow 2_2}$	0.40	*small* ~0.02	0.40	0.40
$\dfrac{4_2 \rightarrow 2_1}{4_2 \rightarrow 4_1}$	0	0.34	0	e
$\dfrac{4_2 \rightarrow 3_1}{4_2 \rightarrow 2_2}$	0	2.23	0	e
$\dfrac{0_2 \rightarrow 2_1}{0_2 \rightarrow 2_2}$	∞	∞	f	e
$\dfrac{0_3 \rightarrow 2_1}{0_3 \rightarrow 2_2}$	0	0	f	0

(a) The quantum number relevant to the vibrator model is N, the phonon number. The states listed correspond to the following values of N: $0_1 \rightarrow$ N=0; $2_1 \rightarrow$ N=1; $2_2, 0_2, 4_1 \rightarrow$ N=2; $4_2, 3_1, 0_3 \rightarrow$ N=3. The branching ratios have been calculated with the coefficients of fractional parentage[46].

(b) The relevant label for states in the symetric rotor is the band (i.e.,ground,γ or β band) and the K quantum number. The $0_1, 2_1, 4_1$ states are members of the K=0 ground band; $2_2, 3_1, 4_2$ states are members of the K=2, γ-band; 0_2 is the band-head of the K=0 β band; 0_3 is the band-head of the K=0 two-phonon γ band. Interband transitions are assumed to be ~1/50 of the intraband transitions. Where applicable, Eq. (2.2.2.8) has been used to determine the branching ratios.

(c) All of the states, except for the excited $0_2, 0_3$ states, are members of the same "band". The branching ratios have been obtained with the B(E2) values of Ref. (51,52)

(d) The relevant quantum number for a γ-unstable rotor is τ, (see Eq. 2.2.2.10). The states listed correspond to the following values of τ: $0_1 \rightarrow \tau$=0; $2_1 \rightarrow \tau$=1; $2_2, 4_1 \rightarrow \tau$=2; $4_2, 3_1, 0_3 \rightarrow \tau$=3. The 0_2 state has τ=0 but is the "head-band" of the first β vibration with n_β=1.

(e) These branching ratios are not avaliable.

(f) Excited 0 states do not occur for a rigid triaxial rotor.

negative-parity states characterized by a mixture of quadrupole and octupole vibration may occur. The lowest excitations of this type, namely with n_2 = 1 and n_3 = 1, will consist of five degenerate states with spin-parity $1^-, 2^-, 3^-, 4^-, 5^-$. However, because both the octupole vibration and any higher order coupling of vibrations occur relatively high in excitation energy, there is a greater probability that these states will mix with non-collective excitations, so that their simple structure may be obscured.

2.2.2 The Rotational Shape

A particular nuclear shape emerges as a result of the competition between long-range and short-range interactions. The particular effective interactions that are important to the BM description are the short-range monopole pairing interactions and the long-range quadrupole-quadrupole interaction between nucleons. A more detailed discussion of these interactions is presented in numerous review articles, in particular, Ref. (40). The pairing interaction tends to make the nucleus spherical, and the strength of this interaction is proportional to the number of particles, N, outside the closed shell. The quadrupole-quadrupole interaction, in contrast, tends to make the nucleus a non-spherical shape because of the characteristic range[40]; here the strength of the interaction is proportional to N^2. Near closed shells, the pairing interaction will dominate, but toward the middle of the shell, where $N^2 \gg N$, the quadrupole interaction will dominate the pairing force and, hence, the nucleus will assume a permanent deformation.

To describe the surface of a rotational nucleus, it is convenient to transform Eq. (2.2.1.1) into the coordinate system fixed with respect to the nucleus. Therefore,

for a quadrupole shape, Eq. (2.2.1.1) becomes[43]

$$R = R_\circ \big[1 + \sum_\mu a_{2\mu} Y_2^\mu(\theta', \phi')\big] \qquad (2.2.2.1)$$

where the $a_{2\mu}$ are related to earlier $\alpha_{2\mu}$ through[43]

$$a_{2\nu} = \sum_\mu \alpha_{2\mu} D_{\mu\nu}^2(\theta, \phi, \psi) \qquad (2.2.2.2)$$

where the $D_{\mu\nu}^2$ are the usual rotation matrices and θ, ϕ, ψ are the Euler angles, which are related to the body-fixed and space fixed axes. Since[43] $a_{21} = a_{2-1} = 0$ and $a_{22} = a_{2-2}$, only five parameters are needed to describe the system, namely the Euler angles θ, ϕ, ψ and a_{20} and a_{22}. For convenience, the parameters a_{20} and a_{22} are replaced by β and γ through the following relations[43]

$$a_{20} = \beta cos\gamma$$

$$a_{22} = \frac{1}{\sqrt{2}} \beta sin\gamma \qquad (2.2.2.3)$$

The parameter β is a measure of the degree of quadrupole deformation, while γ is a measure of the departure from axial symmetry.

The expression for the kinetic energy is given by[43]

$$T = -\frac{\hbar^2}{2B} \Big[\frac{1}{\beta^4} \frac{1}{\partial\beta} \beta^4 \frac{\partial}{\partial\beta} + \frac{1}{\beta^2} \frac{1}{sin3\gamma} \frac{\partial}{\partial\gamma} sin3\gamma \frac{\partial}{\partial\gamma}$$

$$-\frac{1}{4} \sum_K \frac{L_K^2}{sin^2(\gamma - \frac{2}{3}\pi K)} \Big] \qquad (2.2.2.4)$$

where the L_K are the angular momentum operators associated with the Euler angles. This kinetic energy, together with the appropriate potential energy, will be referred to as the Bohr Hamiltonian.

Three types of potentials will be discussed. The most familiar, which corresponds to the symmetrical rotor, occurs for $\beta \neq 0$, $\gamma = 0$. The other

two correspond to symmetrical rotor : the triaxial rotor, where V = V $(\beta, \gamma_\circ)$ for a specific $\gamma_\circ \neq 0$, and the γ-unstable rotor, where V = V (β) (i.e independent of γ).

The symmetrical rotor is characterized by a quadrupole deformation β which may be positive or negative, referring to prolate or oblate shapes, respectively. Empirically, most deformed nuclei are prolate. Two types of collective excitations may occur: the nucleus may rotate about an axis perpendicular to the axis of symmetry or the nucleus may oscillate about its equilibrium shape. These oscillations may be along the symmetry axis, β vibration, or such as to introduce symmetries, γ vibrations. In either case, rotations will again be built upon the intrinsic structure at excitation energy, E_{vib}. In all of these cases, the energy spectrum can be simply expressed as[47]

$$E = \frac{\hbar^2}{2\Im} \left[L(L+1) - K^2 \right] + E_{vib} \qquad (2.2.2.5)$$

where $\Im$ is is the moment of inertia and K is the projection of angular momentum on to the symmetry axis. For rotations building from the ground state and the β vibrations, k = 0 the spin sequence will be $0^+, 2^+, 4^+, \cdots$ while for the γ-vibrations k = 2 and the sequence of levels will be $2^+, 3^+, 4^+, \cdots$. (The derivation of these spin sequences may be found in numerous references such as Ref .(45)). However with decreasing deformation and increasing rotational frequency, the intrinsic nuclear structure is excited by rotational motion, and the quantum numbers K, τ are no longer exact constants of motion. This indicates a modification in the rotational spectrum of Eq. (2.2.2.5), which may often be described by a term proportional to $L^2(L+1)^2$ as is characteristic of the rotation vibration interaction in molecules. One can thus expand the rotational energy powers of angular momentum. This gives[4]:

$$E(L(L+1)) = E_k + A(L+1) + BL^2(L+1)^2 + \cdots \qquad (2.2.2.6)$$

where E_k is the intrinsic energy and is the same for members of the band. A and B are normalizing parameters which can be determined from the experimental values of energy levels. An example of a typical spectrum of positive-parity collective states in a deformed nucleus is shown in Fig. (2.1b). The transition probabilities again provide a convenient probe of the wave functions. For transitions between states belonging to the same rotational band labelled by K, one obtains[4]

$$B(E2 : L_i K \rightarrow L_f K) = \frac{5}{16\pi} e^2 Q_o^2 < L_i 2K0|L_f K >^2 \qquad (2.2.2.7)$$

where Q_o is the intrinsic quadrupole moment, and the right-hand-side contains the usual Clebsch-Gordan coefficient. For deformed nuclei Q_o is large,[43] thus, enhanced transitions occur within a band. In general, for transitions between bands K_i and K_f, the branching ratios are given by[48]

$$\frac{B(E2 : L_i K_i \rightarrow L_f K_f)}{B(E2 : L_i K_i \rightarrow L'_f K_f)} = \frac{< L_i 2K K_i - K_f|L_f K_f >^2}{< L_i 2K K_i - K_f|L'_f K_f >^2} \qquad (2.2.2.8)$$

where the matrix element $M(K_i, K_f)$ only depends on the intrinsic structure of the bands and not on the particular states in question. This means that the branching ratio, commonly referred to as the Alaga ratio, from an initial state to two levels of the same rotational band only depends on the L and K of the various states and not on the intrinsic structure, since the same matrix element M appears in both numerator and denominator of Eq. (2.2.2.8). Note: this description only holds for $2 \leq K_i + K_f$. The case when $K_i + K_f \leq 2$, or where multipolarities other than electric quadrupole are involved, are discussed in Ref. (48). Some characteristic E2 branching ratios are listed in Table (2.1).

Extensive investigations of the properties of nuclei with rigid asymmetric deformation have been performed by Davydov and coworkers[49−52]. In their model, which consists of the Bohr Hamiltonian with γ-dependent potential, the

nucleus is described by γ and β, where γ may be determined by the energy of 2_2^+ state. A sketch of the energy spectrum one expects for $\gamma = 30°$ is shown in Fig. (2.1c). Unlike the case for a symmetrical rotor, the 2_2^+ level and associated states are rotational excitations rather than members of a γ-vibration. The difference in behavior of these "anomalous" rotational states can be seen in Table (2.1), which presents some important branching ratios for states in a nucleus with $\gamma = 30°$, along with the predictions of the axial rotor. Vibrations can be added to this triaxial structure by introducing μ, the "non-adiabaticity" parameter[51]. This parameter μ is a measure of the importance of the rotation-vibration interaction. For $\mu < \frac{1}{3}$ the distinction between rotations and vibrations is clear, while for $\mu > \frac{1}{3}$, the nucleus is considered "soft" and the distinction is not obvious. The definition of μ and the value for many nuclei are presented in Ref. (51). It should be noted that only by introducing the non-adiabaticity parameter can excited 0^+ states be incorporated into the triaxial description.

A discussion of the Bohr Hamiltonian with a potential that is defined to be independent of γ was presented by Wilets and Jean[46]. A particular example of a γ-unstable potential is the displaced harmonic oscillator where[46]

$$V(\beta) = \frac{1}{2}C(\beta - \beta_\circ)^2 \qquad (2.2.2.9)$$

One result of the γ-independent potential is that the Bohr Hamiltonian can be expressed using two equations, one that depends only on β and one that depends on γ, for which the separation parameter Λ is given by[46]

$$\Lambda = \tau \ (\tau + 3) \qquad (2.2.2.10)$$

This increases the energy spectrum as shown in Fig. (2.1d). Also shown are the states which occur when β-vibrations are included.

44

In many ways, the spectrum is similar to that of the harmonic oscillator presented in Fig. (2.1a) where τ is analogous to a phonon number n. The energy spacings are proportional, however, to $\tau(\tau + 3)$ rather than linear in n.

In conclusion, the model of Bohr and Mottelson can be used to describe a variety of nuclear shapes: spherical, rotational, symmetric and asymmetric. Characteristic energy spectra are presented in Fig. (2.1) and branching ratios in Table (2.1). To these shapes odd nucleons may be coupled, as described in Ref. (53-55). As presented here, however, the Bohr and Mottelson description is strictly phenomenological.

2.3 The Interacting Boson Model

2.3.1. General

The Interacting Boson Model of Arima and Iachello[8-11,56-58] attempts to give a combined account of nuclear collective excitations except for those near closed shells. The particles outside of closed shells are treated as bosons, or pairs of particles, which can occupy one or two levels: a ground state with an angular momentum equal to zero (called s-bosons), and an excited state with two units of angular momentum (called d-bosons), higher angular momentum bosons may be introduced to improve the model predictions. In particular an L=3, f, boson is required to describe negative parity states and L=4, g, boson becomes important at higher excitation energies. The d-bosons have energy ε_d, the s-bosons ε_s; one can define a bosons energy $\varepsilon = \varepsilon_d - \varepsilon_s$. This model is called the Interacting Boson Model (IBM) because unlike the more familiar bosons, these particular

bosons may interact with one another. Two version of this model are avaliable: IBM-1 in which no distinction is made between proton and neutron bosons, IBM-2 includes four types of bosons, one set of (s_ν, d_ν) for nuetrons and the other (s_π, d_π) for protons. The number of d-bosons is added to the number of s-bosons, $N = n_d + n_s$ which is a constant in the IBM description for a given nucleus. N is the number of pairs of neutrons plus the number of pairs of protons, outside their respective nearest closed shells, without distinguishing between the particle or hole character of the pairs. For example, $^{182}_{74}W_{108}$ is characterized by N = 13, due to the 8 protons (4 proton pairs) + 18 neutrons (9 neutron pairs) away from the closed shell.

As previously, interactions may occur between the s- and d-bosons, and even among themselves. Therefore, in the simplest terms, the Hamiltonian of the system can be written as[59]

$$H = \varepsilon_s s^\dagger s + \varepsilon_d d_m^\dagger d_m + V \qquad (2.3.1.1)$$

where ε_s and ε_d are the s- and d-boson energies, $s^\dagger$ (s) is the creation (annihilation) operator for s-bosons, $d^\dagger$ (d) is the creation (annihilation) operator for d-bosons. The sum is taken over the 5 [2(L=2)+1] components of the d-boson state; and V is the interaction between the bosons.

In this description three natural limits occur. The first[8,56,57] occurs when $\varepsilon = \varepsilon_d - \varepsilon_s \gg V$, so that the energy spectrum is simply given by $E = \varepsilon n_d$, the ground state being a zero d-boson state. This first limit is similar to the harmonic oscillator of the geometrical picture described in section (2.2) of this Chapter. The IBM interpretation will be discussed later in section (2.3.2).

The other two limits occur when $V \gg \varepsilon$, and correspond to specific information. If V is a quadrupole-quadrupole interaction[9,57] between bosons, the system

obtained is very similar to a certain kind of deformed rotor. The IBM version will be presented in section (2.3.3). The third limit arises when a repulsive pairing interaction[10,58] exists between the bosons. As will be seen in the discussion in section (2.3.4), this limit is very similar to the geometrical description of the γ-unstable oscillator of Wilets and Jean[46].

The most general form of the IBM Hamiltonian, in which all possible boson-boson interactions up to the second order are explicitly included, is given by[8]

$$H = \varepsilon_s s^\dagger s + \varepsilon_d \sum_m d_m^\dagger d + \sum_{L=0,2,4} \frac{1}{2}(2L+1)^{\frac{1}{2}} C_L[(d^\dagger d^\dagger)^{(L)} \times (dd)^{(L)}]^{(0)}$$

$$+ \frac{1}{\sqrt{2}} v_2[(d^\dagger d^\dagger)^{(2)} \times (ds)^{(2)} + (s^\dagger d^\dagger)^{(2)} \times (dd)^{(2)}]^{(0)} \qquad (2.3.1.2)$$

$$+ \frac{1}{2} v_0[(d^\dagger d^\dagger)^{(0)} \times (ss)^{(0)} + (s^\dagger s^\dagger)^{(0)} \times (dd)^{(0)}]^{(0)}$$

$$+ u_2[(d^\dagger s^\dagger)^{(2)} \times (ds)^{(2)}]^{(0)} + \frac{1}{2} u_0(s^\dagger s^\dagger)^{(0)} \times (ss)^{(0)}]$$

where $d^\dagger$, d, $s^\dagger$, s are as described for Eq. (2.3.1.1) and the parentheses denote angular momentum couplings. The parameters C_L, v_L, u_L are related to the two-body matrix elements by[8]

$$C_L = <d^2 L \mid V \mid d^2 L>$$

$$v_2 = <ds2 \mid V \mid d^2 2> (5/2)^{\frac{1}{2}}$$

$$v_0 = <d^2 0 \mid V \mid s^2 0> (1/2)^{\frac{1}{2}} \qquad (2.3.1.3)$$

$$u_2 = <ds2 \mid V \mid ds2> 5^{\frac{1}{2}}$$

$$u_0 = <s^2 0 \mid V \mid s^2 0>$$

Eq. (2.3.1.2) appears formidable, especially given the explicit form of the parameters, as introduced in Eq. (2.3.1.3). However, the terms correspond to one of four types:

47

(1) $\varepsilon_s s^\dagger s + \varepsilon_d \sum_m d_m^\dagger d$ – simply counts the number of s-and d-bosons, respectively, and multiplies this number by the appropriate energy;

(2) the terms with coefficients C_L, u_2 and u_o represent interactions in which the total number of d-bosons and s-bosons, separately, are conserved, i.e., n_d remains the same;

(3) a term (with coefficient v_2) in which n_d is changed by unity;

(4) a term (with coefficient v_o) in which n_d is changed by two units.

With regard to the three limits referred to earlier, the vibrational limit will correspond to a Hamiltonian with only n_d-conserving terms, the rotational limit to a situation with one and two d-boson number changing terms, and the "γ-unstable" limit will represent the situation with two d-boson number changing terms included.

An alternate form, in which the general Hamiltonian may often be written, is in terms of the specific interactions between the bosons. In these cases[8,61]

$$H = \varepsilon \sum_m d_m^\dagger d_m - k\mathbf{Q}.\mathbf{Q} - k'\mathbf{L}.\mathbf{L} + k''\mathbf{P}.\mathbf{P} + k_3\mathbf{T_3}.\mathbf{T_3} + k_4\mathbf{T_4}.\mathbf{T_4} \quad (2.3.1.4)$$

where $\varepsilon = \varepsilon_d - \varepsilon_s$ is the boson energy. For simplicity, ε_s was set equal to zero only $\varepsilon = \varepsilon_d$ appears. The parameters k, k', k'', k_3 and k_4 designate the strengths of the quadrupole, angular momentum, pairing, octupole and hexadecapole interaction between bosons, respectively. The relation between k, k', k'' and the parameters of Eq. (2.3.1.2) are given in Table (2.2).

Associated with the collective states calculated using IBM are transition operators. In the most general form, the E0, M1, E2, M3, E4 transition operators are, to the leading order, given by[8,9,60]

$$T_m^{(\ell)} = \alpha_\ell \delta_{\ell 2}[d^\dagger \times s + s^\dagger \times d]_m^{(2)} + \beta_\ell (d^\dagger d)_m^{(\ell)} + \gamma_{\ell 0}\delta_{\ell 0}\delta_{m0}(s^\dagger s)_0^{(0)} \quad (2.3.1.5)$$

Table (2.2)

The relationship between the coefficients of equation (2.3.1.2), the coefficients of equation (2.3.1.4), which compared to the **Q.Q, L.L, P.P** and the parameters of computer code PHINT[62].

Equation	Equation (2.3.1.4)			PHINT
(2.3.1.2)	Q.Q k	L.L k'	P.P k''	
$E(2_1^+)$	$\epsilon + 9/2k$	$\epsilon - 6k'$	ϵ	
C_0	$-7k$	$12k'$	$5k''$	$C(1)$
C_2	$3/2k$	$6k\prime$	0	$C(2)$
C_4	$-2k$	$-8k\prime$	0	$C(3)$
v_2	$2\sqrt{35}k$	0	0	$F(one-phonon)$
v_0	$-2\sqrt{5}k$	0	$-\sqrt{5/2}k\prime\prime$	$G(two-phonon)$
u_0	0	0	1	$CH1$
u_2	$-4k$	0	0	$CH2$

Equation (2.3.1.4)	PHINT
ϵ	EPS
k	$-\dfrac{QQ}{4}$
k'	$-\dfrac{ELL}{2}$
k''	$PAIR$
k_3	$\dfrac{5}{\sqrt{7}}OCT$
k_4	$15HEX$

where ℓ denotes the multipolarity with projection m, and α, β, γ are the coefficients of the different terms of the operator. In particular for E2 transitions[8,9,60]

$$T_m^{(E2)} = \alpha_2[d^\dagger \times s + s^\dagger \times d]_m^{(2)} + \beta_2(d^\dagger \times d)_m^{(2)} \qquad (2.3.1.6)$$

This operator has two parts: $(d^\dagger s + s^\dagger d)$ which satisfies the selection rule $\Delta n_d = \pm 1$, and $(d^\dagger d)$ which satisfies the $\Delta n_d = 0$ selection rule. The coefficients α and β depend on the limit involved or the appropriate intermediate structure. The form of the operator that corresponds to the various limiting symmetries will be discussed later.

The Hamiltonian solution, in either Eq. (2.3.1.2) or the Eq. (2.3.1.4) form, can be attempted either analytically or numerically. Arima and Iachello[8-11,56-58] have been able to solve the three Hamiltonians analytically in the three limiting situations described earlier by employing the underlying group theory aspects of this system. As discussed in Ref. (8), the five components of the $L = 2$ d-boson state and the single component of the $L = 0$ s-boson state span a linear vector space which provides a basis for the totally symmetric representations of the group SU(6), the special unitary group in six dimensions. The group SU(6) is partitioned, with each totally symmetric representation labelled by [N]. When all boson states are degenerate and no boson-boson interactions exist, all states belonging to a particular partition [N] are degenerate. A defined energy spectrum will exist, however, given the energy diffrence $\varepsilon = \varepsilon_d - \varepsilon_s$ and an interaction between the bosons. The group SU(6) is characterized by nine parameters which correspond to the parameters of Eq. (2.3.1.2), i.e, N, ε and coefficients C_L(L=0,2,4), v_2, v_o, u_2, u_o.

If one can find a subgroup $G \subset SU(6)$ in which the Hamiltonian is invariant, then the diagonalization problem is simplified. Arima and Iachello, in particular,

have observed that there are three subgroups, namely SU(5)[8,56], SU(3)[9,57], and O(6)[10,58], the special unitary groups in five and three dimensions, and the orthogonal group in six dimensions. The solutions obtained correspond to the same three limits mentioned earlier, namely the vibrational, rotational, and "γ-unstable" limits.

When the subgroup G under which the Hamiltonian is invariant has been identified, the problem may often be written in terms of the forces as given in Eq. (2.3.1.4). Then the eigenvalue problem is reduced to finding the expectation value of the forces. This method of solution in the different limits will be discussed in its own section.

An alternative approach to the eigenvalue problem, presented in Eq. (2.3.1.2) or Eq. (2.3.1.4), is to solve the Hamiltonian numerically. The advantage of this that the entire Hamiltonian may be solved, not only in the limits for which analytic solutions are readily obtainable, but also in the intermediate cases. To this end, O.Scholten has written a computer code PHINT[62] which solves the entire IBM Hamiltonian in Eq. (2.3.1.2) or Eq. (2.3.1.4) parameterization, or a convenient mixture of the two forms. The relation between the parameters of Eq. (2.3.1.4) and Variable Names employed in PHINT program are given in Table (2.2).

The computer code presents the wave functions in the basis $L^{\pi}|n_d n_\beta n_\Delta >$, where L^{π} is the spin-parity, n_d is the number of d-bosons, n_β is the number of pairs of d-bosons coupled to angular momentum zero, and n_Δ is the number of boson triplets coupled to zero angular momentum. For example, the 2 d-boson 0^+ state would be denoted $0^+|210 >$; the 3 d-boson 0^+ state would be

$0^+|301>$; the 3 d-boson 2^+ state would be $2^+|310>$, because the "parentage" of this state is the $0^+|210>$.

Calculations have been performed with this code to reproduce a number of different situations: 1- calculations of the three limiting symmetries which recreate the analytic solutions; 2- calculations of symmetric deviations from these limiting cases; and 3- calculations of situations, not necessarily physical, to understand the operation and interplay of the different parameters belonging to the IBM. The first case will be discussed in section (2.3.2), (2.3.3) and (2.3.4), the second case in section (2.3.3.a). However, since an understanding of the effect of parameters is essential to further understanding, the third case must be tackled immediately.

The situation where only $\varepsilon \neq 0$ must first be considered. The resulting energy spectrum is illustrated in Fig. (2.2). It is characterized by a sequence of equally-spaced levels, with a number of degeneracies of states with different spin. Each set of degenerate states correspond to a value of n_d. This spectrum is exactly what one would expect for the coupling of particles with an angular momentum equal to two. A spectrum such as this could have been derived just as easily using the "Young tableaux" method or any other system for counting symmetric states. There is, though, one important difference, the finite dimensionality, given by N, of the IBM limits the number of states in any spectrum. The highest spin level will be $L = 2N$, and only one such state will occur. Similarly, electric quadrupole transitions will occur only between levels where $\Delta n_d = \pm$ 1. The branching ratios for allowed transitions will be as calculated from the coefficients of fractional parentage for $L = 2$ particles. This system will be looked at in more detail in section (2.3.2).

53
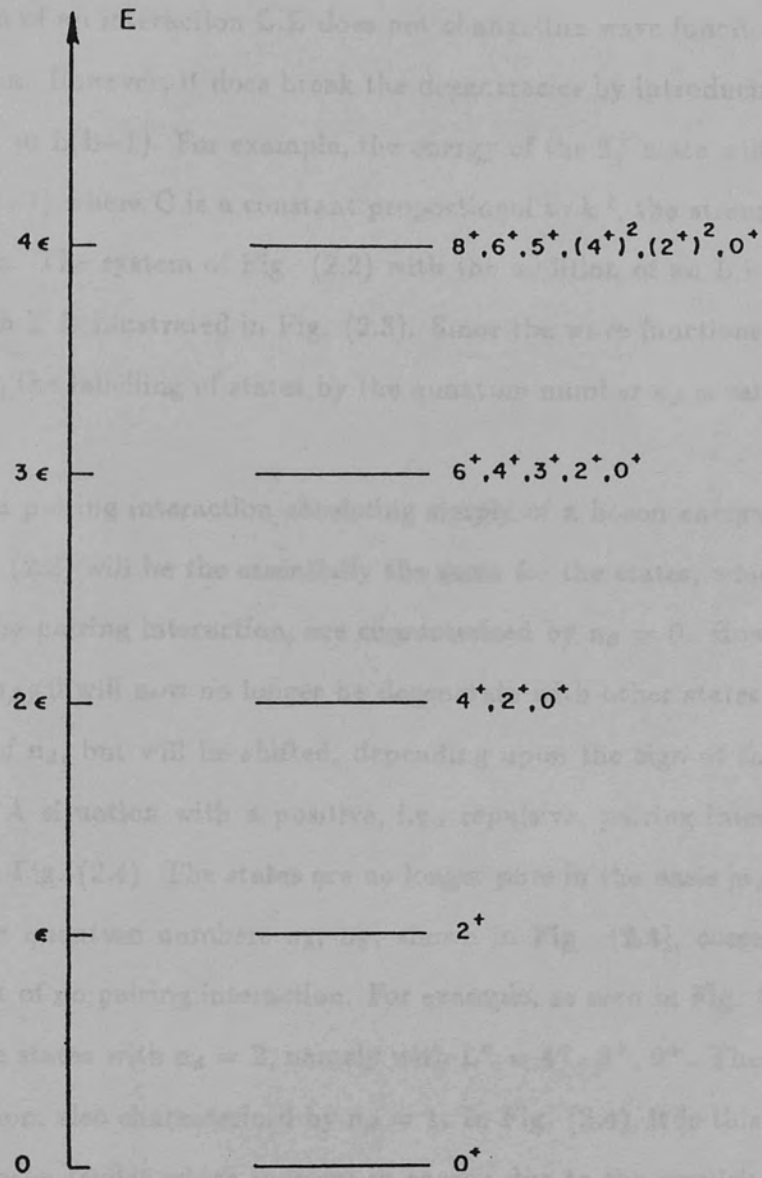
Fig. (2.2) Spectrum in the IBM with no interactions. This figure is from Iachello[60].

The addition of an interaction **L.L** does not change the wave functions of this simple system. However, it does break the degeneracies by introducing a term proportional to $L(L+1)$. For example, the energy of the 2_1^+ state will be given by $\varepsilon + C2(2+1)$ where C is a constant proportional to k ', the strength of the L interaction. The system of Fig. (2.2) with the addition of an L interaction with strength k' is illustrated in Fig. (2.3). Since the wave functions have not been altered, the labelling of states by the quantum number n_d is valid.

If one adds a pairing interaction consisting simply of a boson energy ε to the system, Fig. (2.2) will be the essentially the same for the states, which, in the absence of the pairing interaction, are characterized by $n_\beta = 0$. However, the states with $n_\beta \neq 0$ will now no longer be degenerate with other states with the same value of n_d, but will be shifted, depending upon the sign of the pairing interaction. A situation with a positive, i.e., repulsive, pairing interaction is illustrated in Fig. (2.4). The states are no longer pure in the basis $|n_d n_\beta n_\Delta >$. However, the quantum numbers n_d, n_β, shown in Fig. (2.4), correspond to those in limit of no pairing interaction. For example, as seen in Fig. (2.2), one expects three states with $n_d = 2$, namely with $L^\pi = 4^+, 2^+, 0^+$. The 0^+ state is, by definition, also characterized by $n_\beta = 1$. In Fig. (2.4), it is this 0^+ state of the two-boson triplet which increase in energy due to the repulsive pairing interaction. Similarly, the 2^+ state and other states with $n_\beta = 1$ are increased, as are the states corresponding to $n_\beta = 2,3$ in the limit of no pairing interaction.

Since the pairing interaction includes two d-boson number changing terms in the Hamiltonian (see Table 2.2), the wave functions are considerably altered compared to the pure $|n_d n_\beta n_\Delta >$ configuration. The transition probabilities are therefore, also affected, so that previously allowed transitions are now forbidden, and branching ratios altered. A more detailed study of the effects
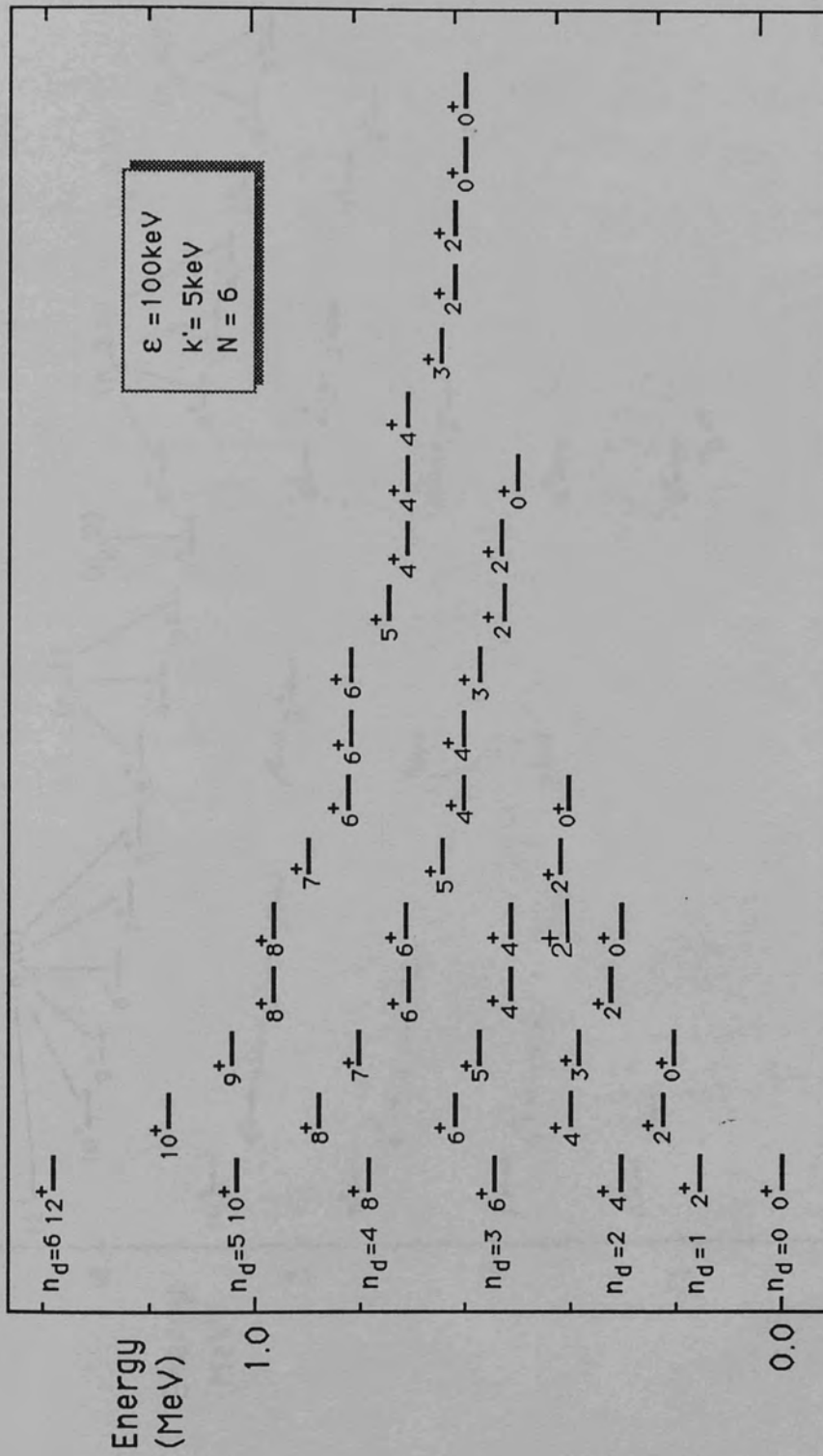
Fig (2.3)   Spectrum in the IBM for N=6 where ε=100 and with an L interaction of strength k'=5keV between bosons. The states are labeled by their J^π and n_d values. *This figure is from Cizewiski* [74].
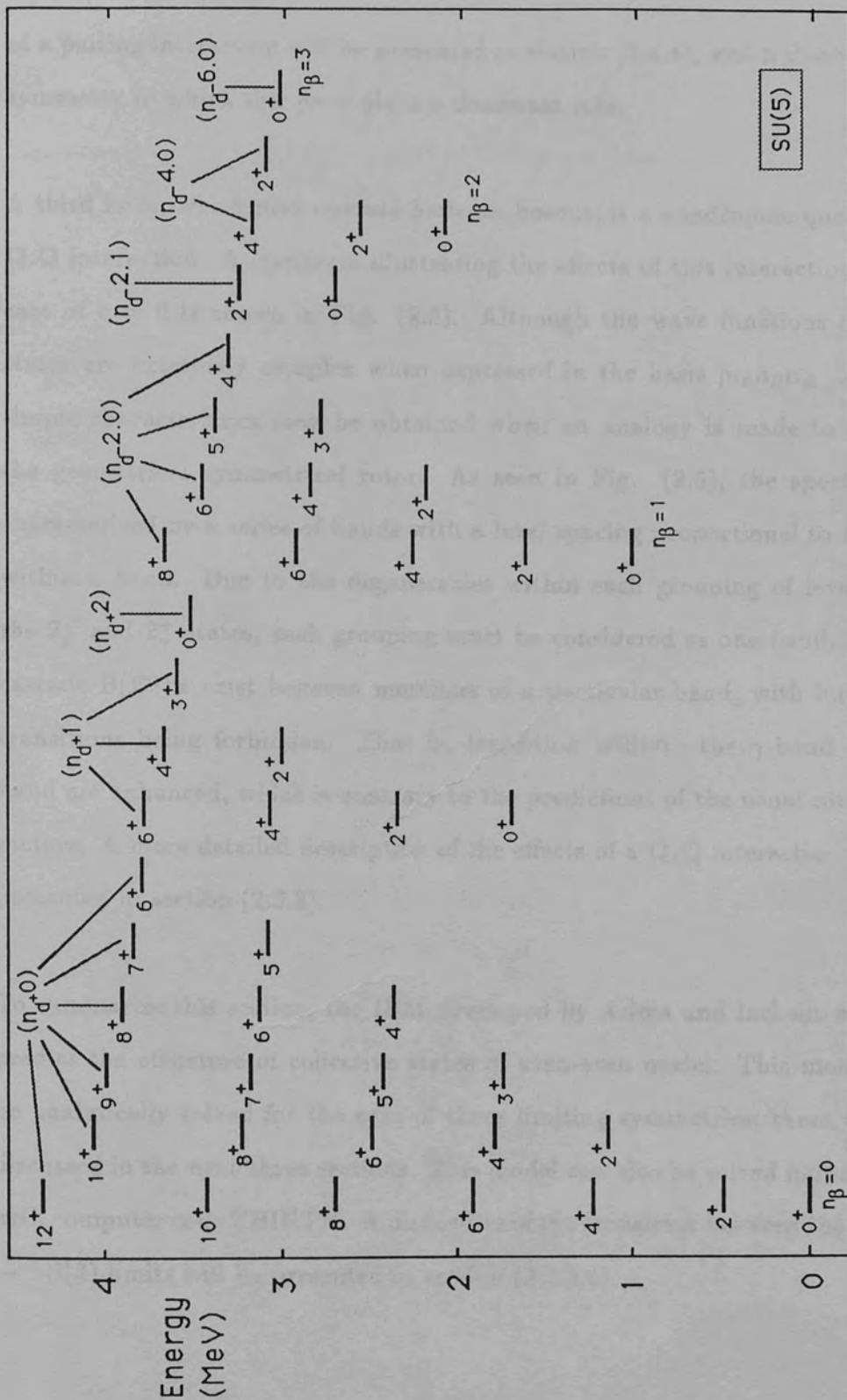
Fig (2.4) Spectrum in the IBM for N=6 where $\varepsilon \neq 0$ and with a repulsive pairing interaction between bosons. The states are labeled by the n_d and n_β quantum numbers that are valid in the limit of no pairing interaction. *This figure is from Arima* [59].

of a pairing interaction will be presented in section (2.3.4), which discusses the symmetry in which this force plays a dominant role.

A third force, which may operate between bosons, is a quadrupole-quadrupole **Q.Q** interaction. A spectrum illustrating the effects of this interaction in the case of $\varepsilon = 0$ is shown in Fig. (2.5). Although the wave functions of these states are extremely complex when expressed in the basis $|n_d n_\beta n_\Delta>$, some simple characteristics may be obtained when an analogy is made to that of the geometrical symmetrical rotor. As seen in Fig. (2.5), the spectrum is characterized by a series of bands with a level spacing proportional to L(L+1) within a band. Due to the degeneracies within each grouping of levels, e.g, the 2_β^+ and 2_γ^+ states, each grouping must be considered as one band. Strong cascade B(E2)'s exist between members of a particular band, with interband transitions being forbidden. That is, transition within the γ-band and β-band are enhanced, which is contrary to the predictions of the usual rotational picture. A more detailed description of the effects of a **Q.Q** interaction will be presented in section (2.3.3).

To summarize this section, the IBM developed by Arima and Iachello aims to predict the structure of collective states of even-even nuclei. This model can be analytically solved for the case of three limiting symmetries; these will be discussed in the next three sections. This model can also be solved numerically with computer code PHINT[62]. A discussion of the transition between the SU(5) $\rightarrow$ SU(3) limits will be presented in section (2.3.3.a).
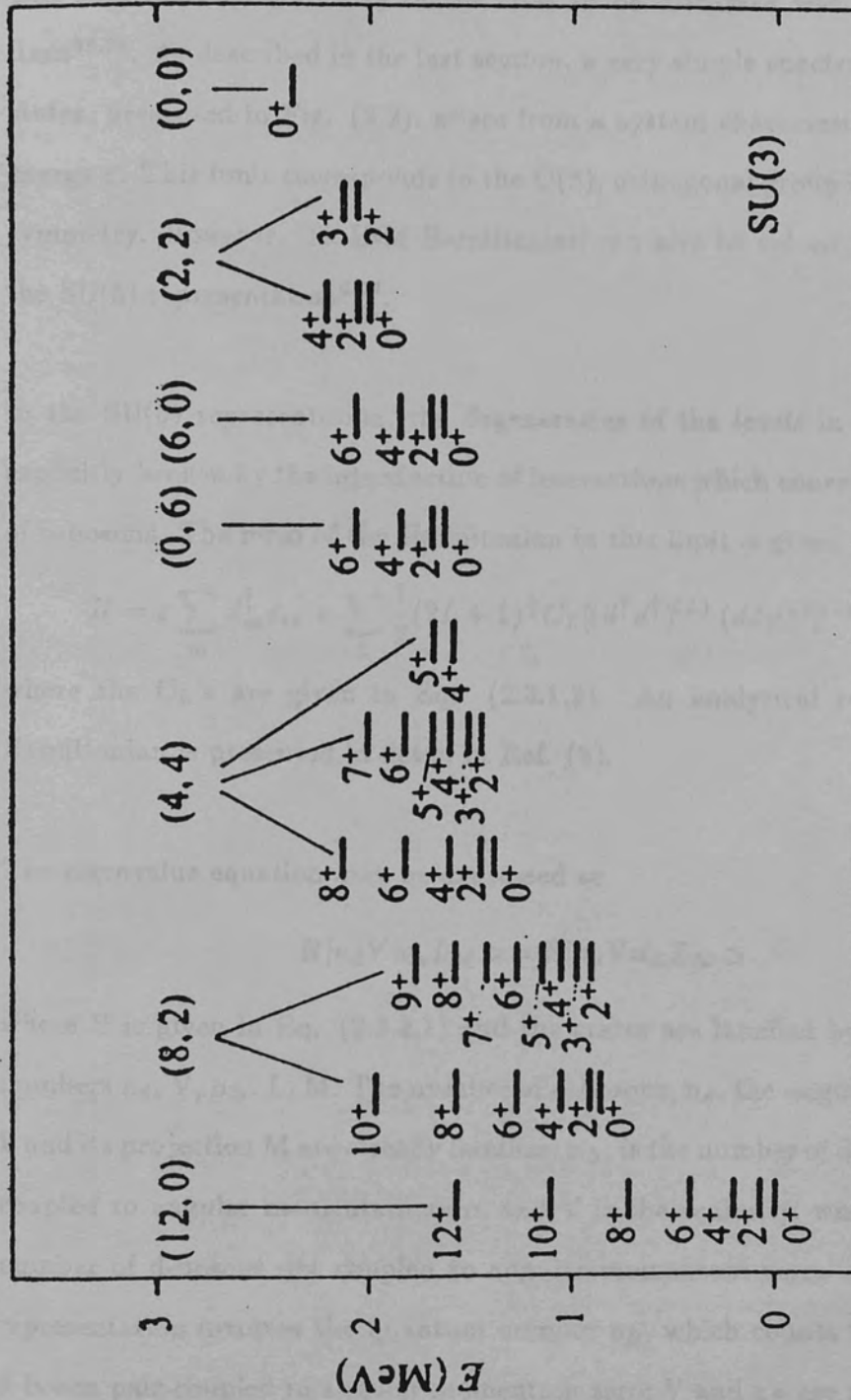
Fig. (2.5) Spectrum with N=6 where $\varepsilon=0$ and with a quadrupole-quadrupole interaction of strength k=2.5 keV between the bosons. This figure is from Iachello et al[73].

2.3.2 The Vibrational SU(5) limit

The first limiting symmetry of the IBM to be discussed was the vibrational limit[34,36]. As described in the last section, a very simple spectrum of collective states, presented in Fig. (2.2), arises from a system characterized by a boson energy ε. This limit corresponds to the O(5), orthogonal group in 5 dimensions symmetry. However, the IBM Hamiltonian can also be solved analytically for the SU(5) representation[8,56].

In the SU(5) representation, the degeneracies of the levels in Fig. (2.2) are explicitly broken by the introduction of interactions which conserve the number of d-bosons. The form of the Hamiltonian in this limit is given by[8,56]

$$H = \varepsilon \sum_m d_m^\dagger d_m + \sum_L \frac{1}{2}(2L+1)^{\frac{1}{2}} C_L [(d^\dagger d^\dagger)^{(L)}.(dd)^{(L)}]^{(0)} \qquad (2.3.2.1)$$

where the C_L's are given in Eq. (2.3.1.3). An analytical solution to this Hamiltonian is presented in detail in Ref. (8).

The eigenvalue equation may be expressed as

$$H|n_d V n_\Delta L_M >= E|n_d V n_\Delta L_M > \qquad (2.3.2.2)$$

where H is given in Eq. (2.3.2.1) and the states are labelled by the quantum numbers n_d, V, n_Δ, L, M. The number of d-bosons, n_d, the angular momentum L and its projection M are already familiar; n_Δ, is the number of d-boson triplets coupled to angular momentum zero, and V is the seniority, which counts the number of d-bosons not coupled to angular momentum zero. An alternative representation involves the quantum number n_β, which counts the number of d-boson pair coupled to angular momentum zero; V and n_β are related by[36] V = n_d - 2 n_β. The total number of bosons is partitioned as[8]

$$n_d = 2n_\beta + 3n_\Delta + \lambda \qquad (2.3.2.3)$$

where λ is the excess bosons and determines the angular momentum range[8]

$$L = \lambda, \lambda + 1, \lambda + 2, \cdots, 2\lambda - 2, 2\lambda \qquad (2.3.2.4)$$

The angular momentum $L = 2\lambda - 1$ is absent because of the requirement that bosons may only be coupled to form symmetric states[43].

An alternative method of solving the Hamiltonian in Eq. (2.3.2.1) is to rewrite it in terms of the forces presented earlier in Eq. (2.3.1.4). Only three parameters are necessary to describe the interaction between two d-bosons, because only three angular momentum couplings can occur[43]; $L = 0, 2, 4$. The coefficients $C_L(L = 0, 2, 4)$ in Eq. (2.3.2.1), or three alternate parameters α, β, γ, are therefore, necessary. The relation between the C_L's and α, β, γ are

$$\alpha = (1/14)(6C_4 + 8C_2)$$

$$\beta = (3/70)C_4 - (1/7)C_2 + (1/10)C_0$$

$$\gamma = (1/14)(C_4 - C_2)$$

Arima and Iachello have expressed the interaction as[8]

$$V = \sum_{i<j} V_{i,j} = \sum_{i<j}(\alpha I_{i,j} + \beta P_{i,j} + \gamma L_{i,j}) \qquad (2.3.2.5)$$

where $I_{i,j}$ is the unit operator, and $P_{i,j}$ and $L_{i,j}$ are the pairing and L interactions discussed earlier in section (2.3.1). The expectation values of these operators, as given in Ref. (8), are

$$< I > = \frac{1}{2}n_d(n_d - 1)$$

$$< L > = J(J + 1) - 6n_d \qquad (2.3.2.6)$$

$$< p > = (n_d - v)(n_d + v + 3)$$

The eigenvalues of the interacting d-boson Hamiltonian are therefore,[8,56]

$$E([N], n_d, v, n_\Delta, L, M) = \varepsilon n_d + \alpha \frac{1}{2} n_d(n_d - 1)$$

$$+\beta(n_d - v)(n_d + v + 3) \qquad (2.3.2.7)$$

$$+\gamma[L(L+1) - 6n_d]$$

A typical spectrum in the vibrational limit is shown in Fig. (2.6). The spectrum itself may be divided into several "bands"; this terminology is valid since large E2 matrix elements exist between adjacent members of the same band. The states in Fig. (2.6) are labeled by the quantum numbers: (n_d, v, n_Δ). The "bands" are very reminiscent of those occurring in rotational nuclei. The Y-band corresponds to the ground band, X and Z to a γ-vibrational band, β to a β-vibrational band and Δ to a 2-phonon γ-vibrational band. The energies of states in some of these bands are given by[8]

Y band $E_Y(n_d, n_d, 0, L = 2n_d, M) = \varepsilon n_d + \frac{1}{2} C_4 n_d(n_d - 1)$

X band $E_X(n_d, n_d, 0, L = 2n_d - 2, M) = \varepsilon n_d + \frac{C_4}{2} n_d(n_d - 1) - \gamma(8n_d - 2)$

Z band $E_Z(n_d, n_d, 0, L = 2n_d - 3, M) = \varepsilon n_d + \frac{C_4}{2} n_d(n_d - 1) - \gamma(12n_d - 6)$

β band $E_\beta(n_d, n_d - 2, 0, L = 2n_d - 4, M) = \varepsilon n_d + \frac{C_4}{2} n_d(n_d - 1)$

$+\gamma(12 - 16n_d) + \beta(4n_d + 1) \qquad (2.3.2.8)$

Δ band $E_\Delta(n_d, n_d, 1, L = 2n_d - 6, M) = \varepsilon n_d + \frac{C_4}{2} n_d(n_d - 1) - 6\gamma(4n_d - 5)$

The general form of the electric quadrupole transition operator T(E2) was given in Eq. (2.3.1.6). In the limits for which analytic solutions are obtainable, Arima and Iachello require the transition operator to be the generator of the underlying group. For the limit characterized by SU(5), T(E2) is given by[8]

$$T_m^(E2) = \alpha[d^\dagger s + s^\dagger d]_m^{(2)} \qquad (2.3.2.9)$$

for $\alpha = <d\|\vec{Q}\|s>(1/5)^{\frac{1}{2}}$, where $\vec{Q}$ is the quadrupole operator. This form of the operator leads to the selection rule $\Delta n_d = \pm 1$.
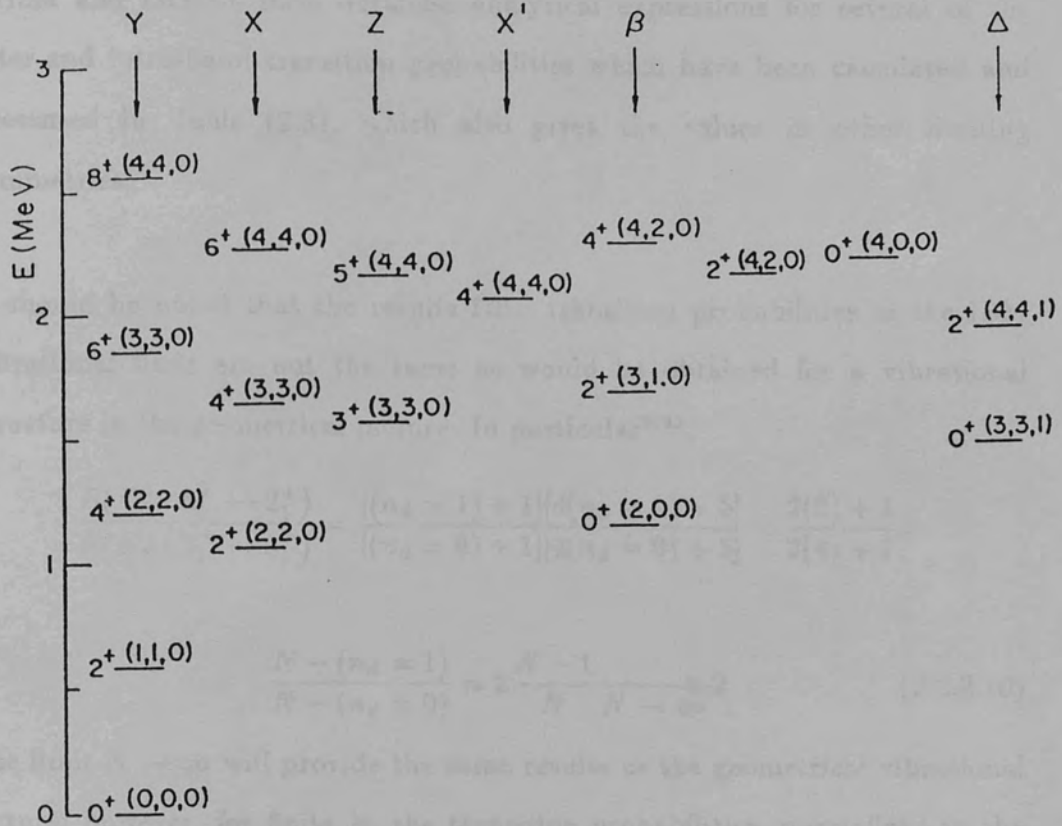
Fig. (2.6) Typical spectrum of a nucleus exhibiting the SU(5) symmetry. The states are labeled by the quantum numbers $J^\pi(n_d,v,n_\Delta)$. The spectrum is broken up into a number of bands, as further described in the text. This figure is from Arima et al[8].

Arima and Iachello have obtained analytical expressions for several of the inter-and intra-band transition probabilities which have been calculated and presented in Table (2.3), which also gives the values in other limiting symmetries.

It should be noted that the results for transition probabilities in the IBM vibrational limit are not the same as would be obtained for a vibrational structure in the geometrical picture. In particular[8,61],

$$\frac{B(E2 : 4_1^+ \rightarrow 2_1^+)}{B(E2 : 2_1^+ \rightarrow 0_1^+)} = \frac{[(n_d = 1) + 1][4(n_d = 1) + 5]}{[(n_d = 0) + 1][4(n_d = 0) + 5]} \times \frac{2(2) + 1}{2(4) + 1} \times$$

$$\frac{N - (n_d = 1)}{N - (n_d = 0)} = 2\frac{N - 1}{N} \xrightarrow{N \rightarrow \infty} 2 \qquad (2.3.2.10)$$

The limit $N \rightarrow \infty$ will provide the same results as the geometrical vibrational picture; however, for finite N, the transition probabilities, normalized to the $2_1^+ \rightarrow 0_1^+$ transition, will be reduced. The effects of this finite dimensionality are illustrated in Fig. (2.7). Experimentally it has been observed that the limiting B(E2) ratio of Eq. (2.3.2.10) is not realized, but is always found to be < 2, as required by the present finite dimensionality argument.

Nuclei which may be characterized by the vibrational limit are expected to occur near, but not precisely at, closed shells. An example is ^{110}Cd which has a triplet of states with spin 0^+, 2^+, 4^+ at approximately twice the energy of the first excited 2^+ state. Also for the 2_2^+ state the cascade to cross over to E2 the transition ratio is very large, as required by the E2 selection rule $\Delta n_d = \pm 1$. Details of the comparison between the SU(5) predictions and the empirical excitations of ^{110}Cd are presented in Ref. (8).

$$\dfrac{B(E2, L'=2n_d \rightarrow L=2n_d-2)}{B(E2, L'=2 \rightarrow L=0)}$$

Conventional Vibrational Model

N = 12

N = 6

n_d
L'
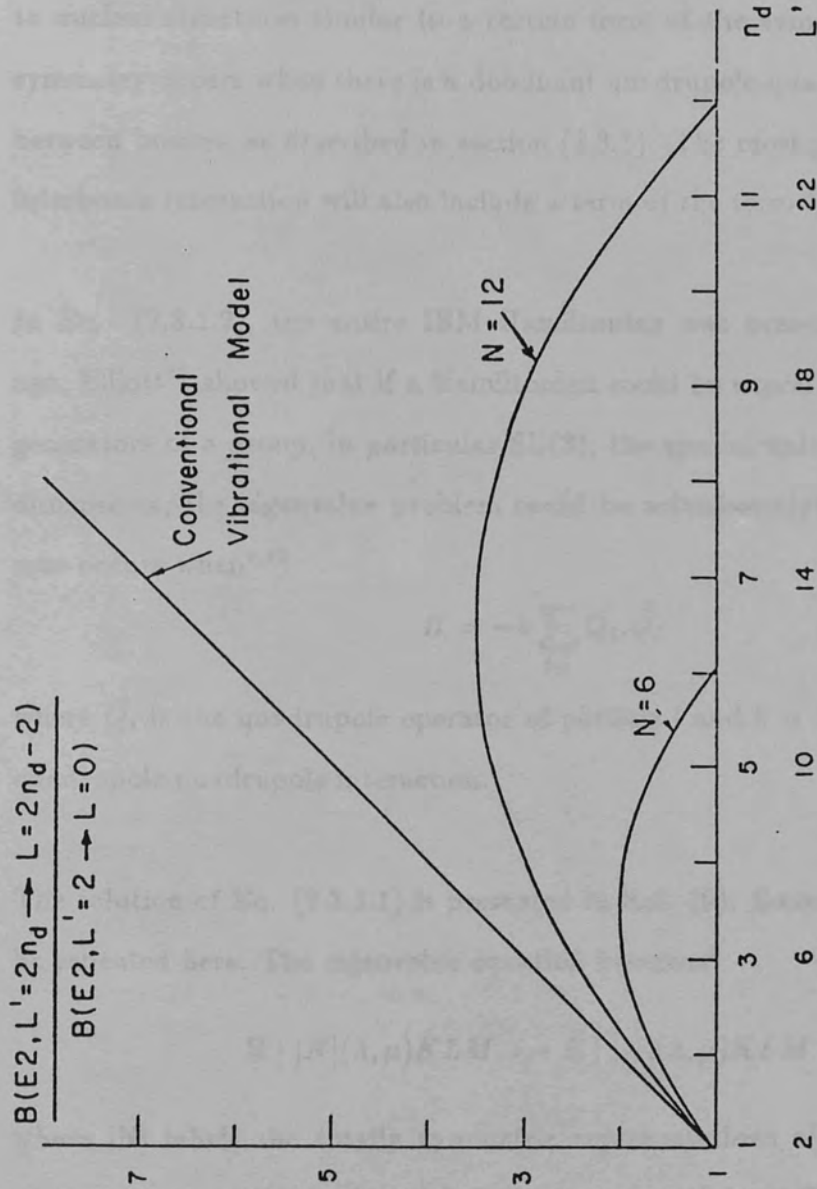
Fig. (2.7) Effect of the finite dimensionality of the IBM on the relative B(E2) values. The transition probabilities within the ground band B(E2: $L'=2n_d \rightarrow L=2n_d-2$) are normalised to the B(E2: $L' \rightarrow L=0$) value. This value is plotted as a function of L' and n_d for $n = 6$ and $n = 12$. The "Conventional Vibrational Model" is the result expected from Eq. (2.2.6). This figure is from Arima[8].

2.3.3 The Rotational SU(3) limit:

The second limit of the IBM model is based on the SU(3) group and gives rise to nuclear structures similar to a certain form of the symmetric rotor. This symmetry occurs when there is a dominant quadrupole-quadrupole interaction between bosons, as described in section (2.3.1). The most general form of the interboson interaction will also include a term of the form $\vec{l}_i.\vec{l}_j$.

In Eq. (2.3.1.2), the entire IBM Hamiltonian was presented. Many years ago, Elliott[37] showed that if a Hamiltonian could be expressed in terms of the generators of a group, in particular SU(3), the special unitary group in three dimensions, the eigenvalue problem could be solved analytically. The SU(3) case occurs when[9,63]

$$H = -k \sum_{i,j} \vec{Q}_i.\vec{Q}_j \qquad (2.3.3.1)$$

where $\vec{Q}_i$ is the quadrupole operator of particle i and k is the strength of the quadrupole-quadrupole interaction.

The solution of Eq. (2.3.3.1) is presented in Ref. (9). Some of the results will be repeated here. The eigenvalue equation becomes[4]

$$H \mid [N](\lambda,\mu)KLM >= E \mid [N](\lambda,\mu)KLM > \qquad (2.3.3.2)$$

where [N] labels the totally symmetric representations of SU(6); (λ,μ) are two quantum numbers which label the representations of SU(3); and L,M are the angular momentum and its projection along the z-axis, respectively. The additional quantum number k labels the states having the same λ, μ, L. In this basis, the eigenvalues can be written[9]

$$E \mid [N](\lambda,\mu)KLM >= K[L(L+1) - C(\lambda,\mu)] \qquad (2.3.3.3)$$

Table (2.3)

Branching ratios in the limiting symmetries of the IBM model.

$\dfrac{J_i \to J_f}{J_i \to J_f}$	SU(5)[a]	SU(3)[b]	O(6)[c]
$\dfrac{2_2 \to 0_1}{2_2 \to 2_1}$	0	*undef.* (0.70)	0
$\dfrac{3_1 \to 2_1}{3_1 \to 4_1}$	0	*undef.* (2.50)	0
$\dfrac{3_1 \to 4_1}{3_1 \to 2_2}$	0.40	0	0.40
$\dfrac{4_2 \to 2_1}{4_2 \to 4_1}$	0	*undef.* (0.34)	0
$\dfrac{4_2 \to 4_1}{4_2 \to 2_2}$	0.91	0	0.91
$\dfrac{4_2 \to 3_1}{4_2 \to 2_2}$	0	2.23	0
$\dfrac{0_2 \to 2_1}{0_2 \to 2_2}$	0	0	*undef.* (0)
$\dfrac{0_3 \to 2_1}{0_3 \to 2_2}$	0	*undef.* (0)	0

(a) The quantum number relevant to the SU(5) limit is n_d. The states listed correspond to the following values of n_d: $0_1 \to n_d = 0$; $2_1 \to n_d = 1$; $4_1, 2_2 \to n_d = 2$; $4_2, 3_1, 0_3 \to n_d = 3$.

(b) The quantum numbers relevant to the SU(3) limt are K and (λ, μ) for the total number of bosons N. The K = 0 (2N,0) states are $0_1, 2_1, 4_1$; the K = 0 (2N - 4,2) state is 0_2; the K = 2 (2N - 4,2) states are $2_2, 3_1, 4_2$; and the 0_3 state is K = 0 (2N - 8,4). When both transitions are forbidden, the branching ratio is undefined (undef). However, in parenthesis is given the ratio when a slight perturbation is introduced.

(c) The quantum numbers of the O(6) limit are $(\sigma, \tau, \nu_\Delta)$. The states correspond to the following quantum numbers: $0_1 \to$ (N, 0, 0); $2_1 \to$ (N, 1, 0); $4_1, 2_2 \to$ (N, 2, 0); $4_2, 3_1 \to$ (N, 3, 0); $0_3 \to$ (N, 3, 1); $0_2 \to$ (N - 2, 0). When both transitions are forbidden, the branching ratio is undefined (undef). However, the ratio when a slight perturbation is introduced is given in parenthesis.

where $C(\lambda, \mu)$ is the quadratic Casimir operator of SU(3)[9]

$$C(\lambda, \mu) = \lambda^2 + \mu^2 + \lambda\mu + 3(\lambda + \mu) \qquad (2.3.3.4)$$

As mentioned earlier,the addition of the L interaction does not change the diagonalization problem. In its most general form, the Hamiltonian therefore, becomes[9]

$$H = -k \sum_{i,j} \vec{Q}_i.\vec{Q}_j - k' \sum_{i,j} \vec{\ell}_i.\vec{\ell}_j \qquad (2.3.3.5)$$

with the eigenvalues[9]

$$E|[N](\lambda, \mu) K L M \rangle = \alpha L(L+1) - \beta C(\lambda, \mu) \qquad (2.3.3.6)$$

$$\alpha = \tfrac{3}{4} k - k' \qquad \beta = k$$

The parameters k and k' of Eq. (2.3.3.5) can be deduced in the following way:

$k = (E_{2_2^+} - E_{2_1^+})/6(\lambda - 1), \qquad k' = 0.75\, k - E_{2_1^+}/6$

where $E_{2_2^+}$ and $E_{2_1^+}$ are the energy values of first and second states, respectively.

Due to their importance in predicting the level spacings of deformed nuclei, the parameters (λ, μ) will be discussed here in terms of the Young tableaux[43] they represent. Each particle may be represented by a box, which can be coupled with another box to form symmetric or antisymmetric states. Examples of the different symmetries are

	Symmetric	Antisymmetric	Mixed symmetric

2 particles

3 particles
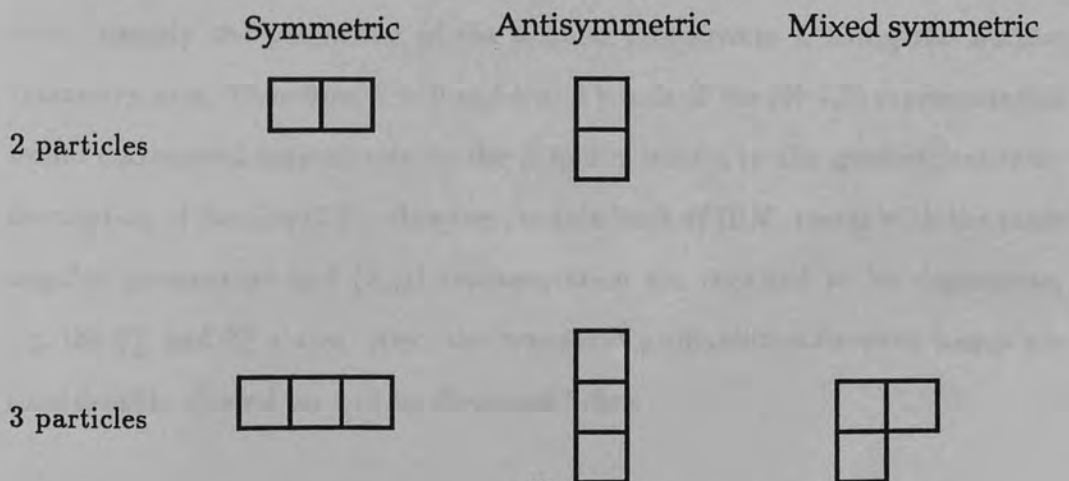
For bosons, antisymmetric couplings are not permitted. An N boson state will be of the form
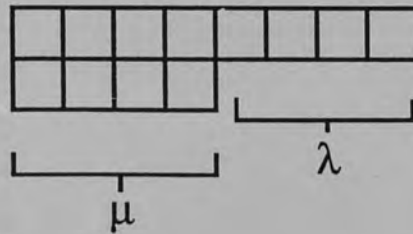
and will be labeled ($\lambda = 4, \mu = 4$), where λ is equal to the number of boxes remaining in the top row, and μ is the number remaining in the bottom row.

An example of the collective positive parity states characteristic of the SU(3) symmetry is shown in Fig. (2.8). The spectrum is divided into a number of bands according to the (λ, μ) value. The angular momenta L which may occur in each (λ, μ) group are given by[9]

$$L = k, (k+1), (k+2), \cdots (k + max\{\lambda, \mu\}) \qquad (2.3.3.7)$$

where k = integer = min $\{\lambda, \mu\}$, min $\{\lambda, \mu\}$ - 2,$\cdots$,1 or 0 unless k = 0. For k = 0, the allowed angular momentum values are[9]

$$L = max\{\lambda, \mu\}, max\{\lambda, \mu\} - 2, \cdots, 1 \quad or \quad 0 \qquad (2.3.3.8)$$

The quantum number k is analogous to the k quantum number of a symmetric rotor, namely the projection of the angular momentum L along the nuclear symmetry axis. Therefore, k = 0 and k = 2 bands of the (N-4,2) representation would correspond respectively to the β and γ bands, in the geometrical rotor description of Section (2.2). However, in this limit of IBM, states with the same angular momentum and (λ, μ) representation are required to be degenerate; e.g, the 2_β^+ and 2_γ^+ states. Also, the transition probabilities between bands are considerably altered, as will be discussed below.

68
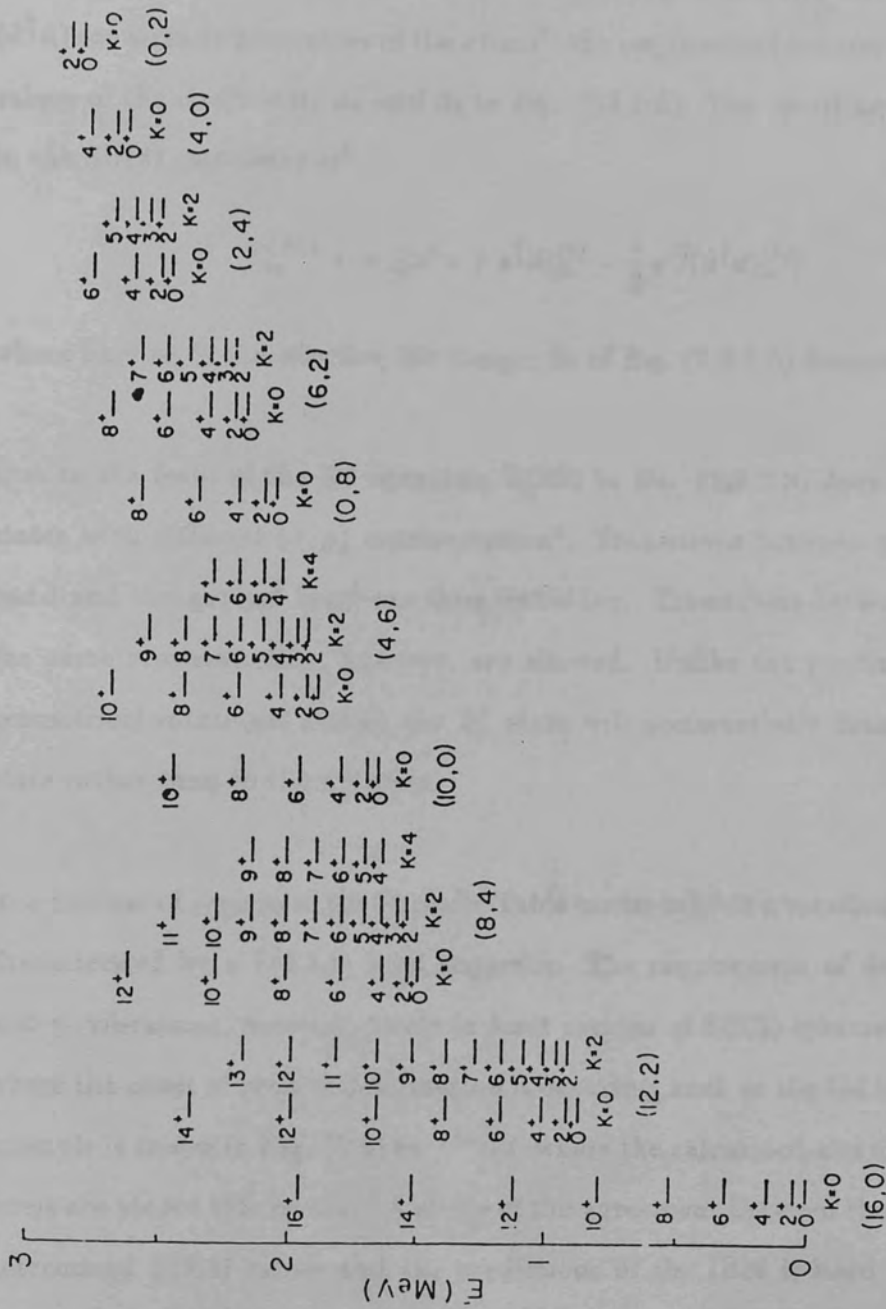
Fig. (2.8) Typical spectrum of a nucleus with N=8 exhibiting the SU(3) symmetry. The states are organized into "bands" labeled by the quantum numbers (λ, μ). The different states within each of these groupings are further distinguished by their J^π and K values. This figure is from Arima et al[57].

The most general form of the E2 transition operator T(E2) was presented in Eq. (2.3.1.6). As for the earlier SU(5) symmetry, Arima and Iachello require this operator to be a generator of the underlying group symmetry. For the case of SU(3) symmetry, since the operators of Eq. (2.3.1.6), namely $(d^\dagger s)$ and $(d^\dagger d)$ are already generators of the group[9], the requirement reduces to fixing the values of the coefficients α_2 and β_2 in Eq. (2.3.1.6). The resulting E2 operator in the SU(3) symmetry is[9]

$$T_m^{(E2)} = \alpha_2[(d^\dagger s + s^\dagger d)_m^{(2)} - \frac{1}{2}\sqrt{7}(d^\dagger d)_m^{(2)}] \qquad (2.3.3.9)$$

where here α_2 is the effective E2 charge; β_2 of Eq. (2.3.1.6) became $-\frac{1}{2}\sqrt{7}\alpha_2$.

Due to the form of the E2 operator, T(E2) in Eq. (2.3.3.9) does not connect states with different (λ, μ) representation[9]. Transitions between γ-band or β-band and the ground band are thus forbidden. Transitions between states of the same representation, however, are allowed. Unlike the predictions of the geometrical rotational model, the 2_γ^+ state will preferentially decay to the 0_β^+ state rather than to the 0_g^+ state.

In a number of regions of the Periodic Table nuclei exhibit a rotational structure characterized by a L(L+1) level sequence. The requirement of degenerate β- and γ- vibrations, however, tends to limit regions of SU(3) symmetry to those where the onset of prolate deformation is occuring, such as the Gd isotopes. An example is shown in Fig. (2.9) for ^{156}Gd, where the calculated and experimental levels are placed side by side. A study of the agreement between the empirically determined B(E2) values and the predictions of the IBM is hard to perform. Branching ratios for many "forbidden" compared to "allowed" transitions are difficult to measure. For example, B(E2: $2_\gamma^+ \to 0_g^+$) / B(E2: $2_\gamma^+ \to 0_\beta^+$) should be zero in SU(3) since the numerator is forbidden.

71

E
(MeV)

Exp   Th   Exp   Th   Exp   Th

1.5

4^+ — 1298 — 1317 4^+ — 1355 — 1316
3^+ — 1248 — 1210
2^+ — 1129 — 1129 2^+ — 1154 — 1129
0^+ — 1049 — 1049

1.0 8^+ — 965 — 965   K=2
                            K=0   (20,2)

6^+ — 585 — 563

0.5

4^+ — 288 — 268

2^+ — 89 — 80 $^{156}_{64}Gd_{92}$
0^+ — 0 — 0

K=0
(24,0)
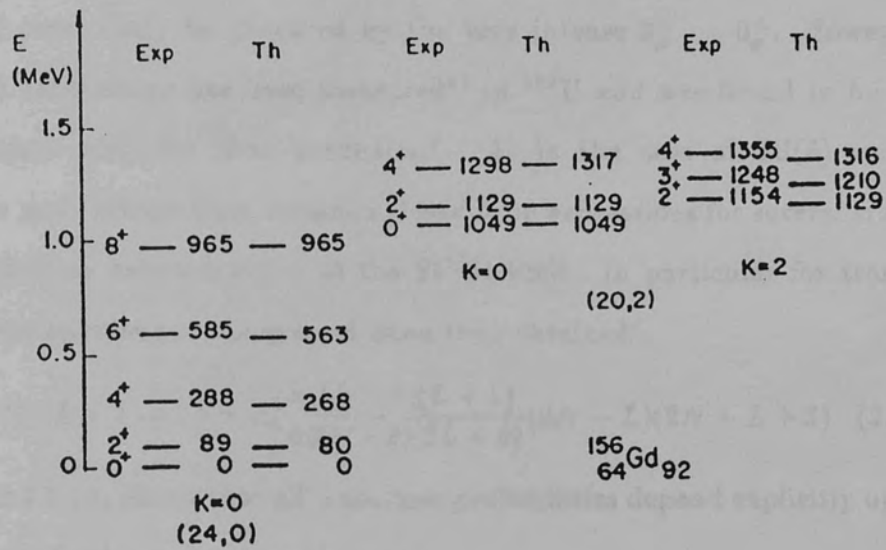
Fig. (2.9) Comparison between the experimental and theoretical SU(3) spectrum for ^{156}Gd where N=12. The experimental levels are to the left of the theoretical levels. The states are labeled by the appropriate J^π, K and (λ, μ) values. This figure is from Arima[9].

In a deformed nucleus near the SU(3) symmetry, the $2_\gamma^+ \to 0_\beta^+$ γ-ray transition would most likely be obscured by the very intense $2_g^+ \to 0_g^+$. However, the B(E2) ratio above has been measured[64] in ^{232}U and was found to be ~ 0.06 consistent with the IBM prediction[9]. As in the case of SU(5) symmetry Arima and Iachello have obtained closed form expressions for several transition probabilities between states of the SU(3) limit. In particular for transitions between members of the ground band they obtained[9].

$$B(E2 : L + 2 \to L) = \alpha_2^2 \frac{3}{4} \frac{(L+2)(L+1)}{2L+3)(2L+5)}(2N - L)(2N + L + 3) \quad (2.3.3.10)$$

Eq. (2.3.3.10) shows that all transition probabilities depend explicitly upon the number of valence nucleons.

2.3.3.a The Transitional Limit From SU(5) to SU(3)

The vibrator SU(5) $\to$ rotor SU(3) transition near A=150 was investigated by Scholten, Iachello and Arima[10]. In this investigation, they considered a simpler form of the IBM Hamiltonian in Eq. (2.3.1.2) namely[10,66,71,72]

$$H = \varepsilon n_d - k \sum_{i,j} \vec{Q}_i.\vec{Q}_j - k' \sum_{i,j} \vec{L}_i.\vec{L}_j - k'' \sum_{i,j} \vec{P}_i.\vec{P}_j \quad (2.3.3.a.1)$$

where ε, the bosons energy, and the quadrupole-quadrupole, L angular momentum and P pairing interactions are as previously described. To study a transitional region, they fixed k and k', allowing ε to decrease linearly as a function of the number of bosons[10];

$$\varepsilon = \varepsilon_c - \theta N_\nu$$

where ε_c is a constant and N_ν is the number of neutron bosons. This simulates the transition, since ε , near SU(5), is much greater than any interboson
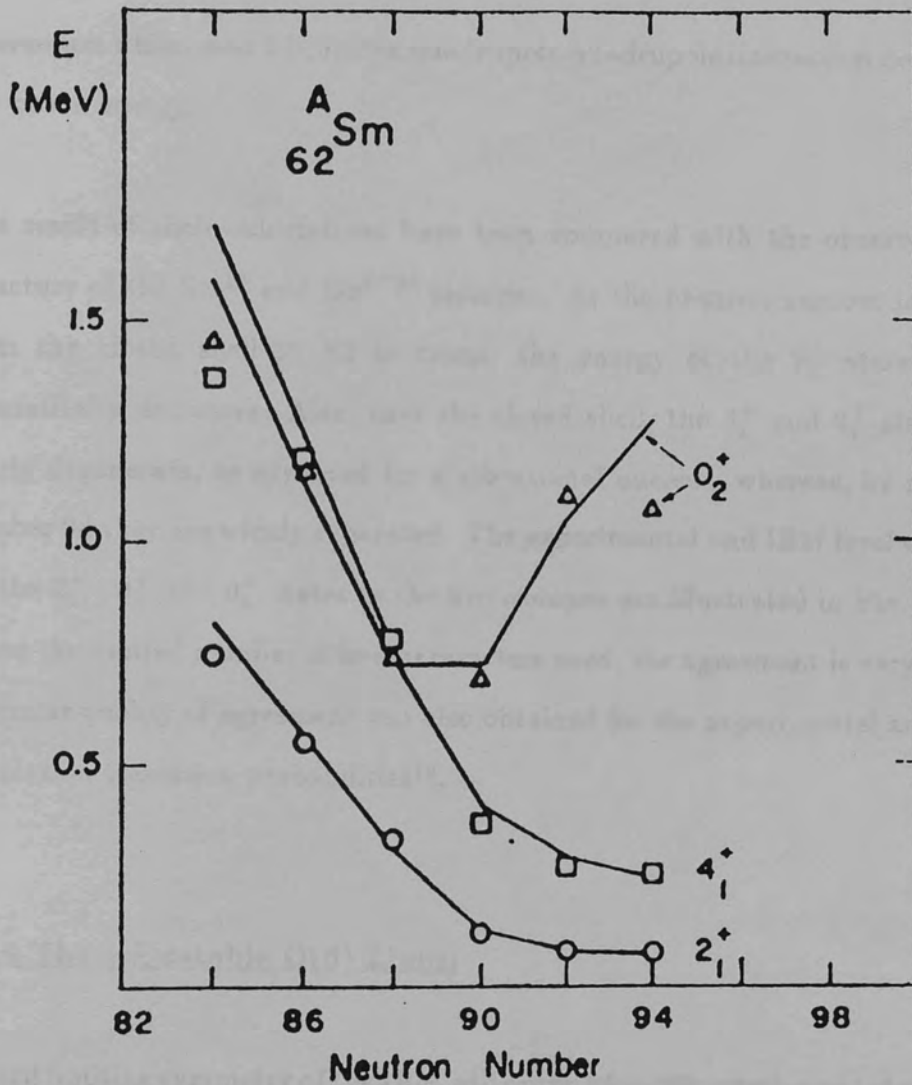
Fig. (2.10) Comparion between the calculated (solid line) and experimental (symbols) energies of the 2_1^+ (circles). 4_1^+ (squares) and 0_2^+ (triangles) states in the Sm isotopes. The calculations were chosen to simulate an SU(5) $\rightarrow$ SU(3) transition as described in more detail in Ref. (48). The emprical values were taken from Ref. (54). This figure is from Scholten et al[11].

73

interaction while, near SU(3), the quadrupole-quadrupole interaction dominates the boson energy.

The result of their calculations have been compared with the observed level structure of the Sm[10] and Gd[65,66] isotopes. As the neutron number increases from the closed shell of 82 neutrons, the energy of the 2_1^+ state in Sm dramatically decreases. Also, near the closed shell, the 4_1^+ and 0_2^+ states are nearly degenerate, as expected for a vibrational nucleus, whereas, by neutron number 94, they are widely separated. The experimental and IBM level energies for the 2_1^+, 4_1^+ and 0_2^+ states in the Sm isotopes are illustrated in Fig. (2.10). Given the limited number of free parameters used, the agreement is very good . A similar quality of agreement was also obtained for the experimental and IBM calculation transition probabilities[10].

2.3.4 The γ-Unstable O(6) Limit:

A third limiting symmetry of the IBM will occur when the interboson interaction is dominated by a pairing force[11,58]. The first empirical candidate for this O(6) limit was ^{196}Pt, and Fig. (2.11), shows a comparison of the predicted and observed positive parity levels for this nucleus.

Analogous to the SU(5) and SU(3) symmetries, Arima and Iachello have diagonalized the IBM Hamiltonian, generated by SU(6) Eq.(2.3.1.2), by identifying a subgroup of SU(6) under which the Hamiltonian is invariant. The particular subgroup in question is O(6), which happens to contain the other subgroups O(5) and O(3). By using the group chain SU(6)$\supset$ O(6)$\supset$ O(5)$\supset$

75
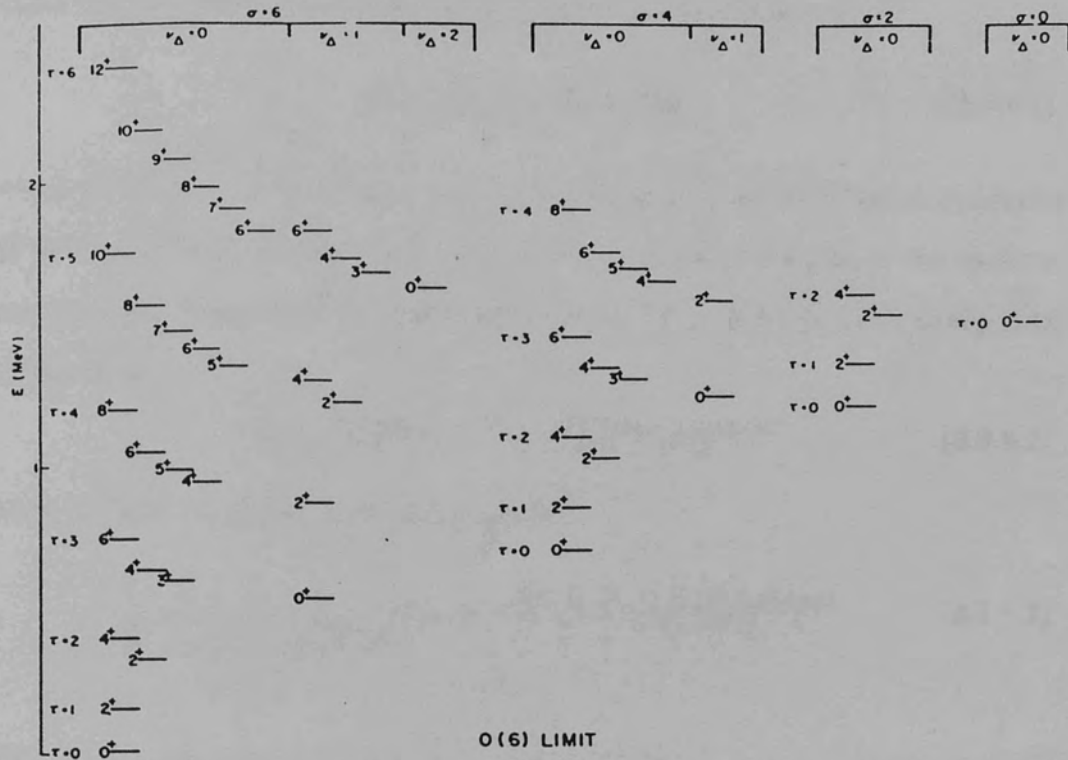
Fig. (2.11) A typical spectrum for a nucleus exhibiting the O(6) symmetry of the IBM. The energy levels are given by Eq. (2.3.4.8) where N=6, A=100 keV, B=30 KeV, and C=5 keV. This figure is from Casten et al[72].

O(3), the IBM Hamiltonian in the O(6) limit can be written as[11,58]

$$H = AP_6 + BC_5 + CC_3 \qquad (2.3.4.1)$$

where P_6 is the pairing operator in O(6) and C_5 and C_3 are the Casimir operators of O(5) and O(3), respectively. A, B, and C are the strengths of the various components. In terms of the IBM Hamiltonian of Eq. (2.3.1.2), P_6 corresponds to the term

$$v_0[(d^\dagger d^\dagger)^{(0)}(ss)^{(0)} + (s^\dagger s^\dagger)^{(0)}(dd)^{(0)}]^{(0)} \qquad (2.3.4.2)$$

while C_5 and C_3 correspond to the terms

$$\varepsilon \sum_m d_m^\dagger d_m + \sum_{L=0,2,4} \frac{1}{2}(2L+1)^{\frac{1}{2}} C_L [(d^\dagger d^\dagger)^{(L)}(dd)^{(L)}]^{(0)} \qquad (2.3.4.3)$$

The relation between the coefficients A,B,C and the parameters of Eq. (2.3.1.2) is presented in Table (2.4).

The symmetry of the irreducible representations of O(6) are labelled by a quantum number σ where[11,58]

$$\sigma = N, N - 2, N - 4, \cdots, 0 \quad or \quad 1 for \qquad (2.3.4.4)$$

$$N = even \qquad N = odd$$

The expectation value of the O(6) pairing operator, P_6, can be written in terms of σ as[11,58]

$$< P_6 > = \frac{1}{4}(N_\sigma)(N + \sigma + 4) \qquad (2.3.4.5)$$

A more detailed discussion of how Eq. (2.3.4.5) arises is given by Arima[11]. As stated, the quantum number τ is chosen to characterize the representation of O(5) where

$$\tau = \sigma, \sigma - 1, \cdots\cdots, 0 \qquad (2.3.4.6)$$

Table (2.4)

Values of the coefficients of equation (2.3.1.2) which correspond to the parameters of the O(6) limit[a].

Equation	O(6) Parameters		
(2.3.1.2)	**A**	**B**[b]	**C**
ε_s	0	0	0
ε_d	0	2/3B	6C
C_0	5/2A	−4/3B	−12C
C_2	0	1/3B	−6C
C_4	0	1/3B	8C
v_2	0	0	0
v_0	$-\sqrt{5/4}A$	0	0
u_0	1/2A	0	0
u_2	0	0	0

(a) Arima[11] noted that A = 2k″, where k″ is the strength of the pairing interaction.

(b) The effective boson energy $\varepsilon = 2B\,(N+1)$.

The expectation value of C_5 in the τ representation of O(5) is given by[11,58]

$$< C_5 >= \frac{1}{6}\tau(\tau + 3) \qquad (2.3.4.7)$$

Therefore, the eigenvalues of states corresponding to the Hamiltonian in Eq. (2.3.4.1) are[11,58]

$$E([N]\sigma\tau\nu_\Delta LM) = \frac{A}{4}(N - \sigma)(N + \sigma + 4) + B\tau(\tau + 3)$$

$$+CL(L + 1) \qquad (2.3.4.8)$$

where the $\frac{1}{6}$ in Eq. (2.3.4.7) has been incorporated into the constant B. The quantum number ν_Δ is useful in labelling the states; it is related to n_Δ which counts the number of boson triplets coupled to angular momentum zero. The quantum numbers τ and ν_Δ are related by $\tau = 3\nu_\Delta + \lambda$, for $\nu_\Delta = 0, 1, \cdots$. The value of λ determines the angular momentum of states through[11,58]

$$L = 2\lambda, 2\lambda - 2, 2\lambda - 3, \cdots \lambda + 1, \lambda \qquad (2.3.4.9)$$

Arima and Iachello have also been successful in acquiring analytical expressions for transition probabilities[11,58]. As in the SU(5) and SU(3) symmetries, they require the E2 transition operator, T(E2), to be a generator of the underlying group structure in this O(6) limit. The form of T(E2) satisfying this requirement is[11,58]

$$T(E2) = \alpha_2(d^\dagger s + s^\dagger d) \qquad (2.3.4.10)$$

Since T(E2) is a generator of O(6), it cannot connect states from different representations. Therefore, one selection rule is $\Delta\sigma = 0$. Also, due to the O(5) structure contained in O(6), the O(5) selection rule $\Delta\tau = \pm 1$ still holds. Some useful branching ratios are given in Table (2.3). In particular, it should be noted that, as in all IBM B(E2) values, the finite dimensionallity of the system

78

is automatically included. Due to the form of the transition operator, branching ratios occuring in the O(6) limit are independent of the parameters A, B, and C.

In Fig. (2.11), an example is presented of a spectrum characteristic of the O(6) symmetry. Each level can be uniquely identified by the quantum number L^π $(\sigma, \tau, \nu_\Delta)$, and the levels can be placed into groups characterized by a σ value. Each such group has identical energy spacings and spin levels, but with different cut-offs given by $\tau = \sigma$. The levels of the same σ are further subdivided by the quantum number ν_Δ. A characteristic feature of a level scheme within the O(6) limit is, therefore, a recurring 0^+-2^+-4^+ pattern of levels with the E2 selection rule $\Delta\tau = \pm 1$ predicting strong cascade γ-transitions within the sequence.

Within each σ grouping itself, the level spacing resembles a vibrational model, as described in Section (2.2), but with an energy spacing proportional to $\tau(\tau + 3)$ rather than simply to τ. This will give rise to the energy ratio $E(4_1^+)/E(2_1^+) = 2.5$ rather than 2, as expected in the vibrational picture. Also, as τ increases even larger energy differences will occur between states of different τ. Furthermore, the degeneracies of the geometrical vibrational phonon model are explicitly eliminated by the $L(L+1)$ term and certain states, e.g. the 0^+ states of the two phonon triplet, do not occur. As described earlier in section (2.3.1), the state which would correspond to this 0^+ state is "repelled" by the ground state, and energy is increased due to the repulsive pairing force which characterizes this limit. Branching ratios and absolute B(E2) values also differ significantly from the geometrical description.

In some ways the level scheme presented in Fig (2.12) is reminiscent of the phenomenological triaxial models, discussed in Section (2.2), which are
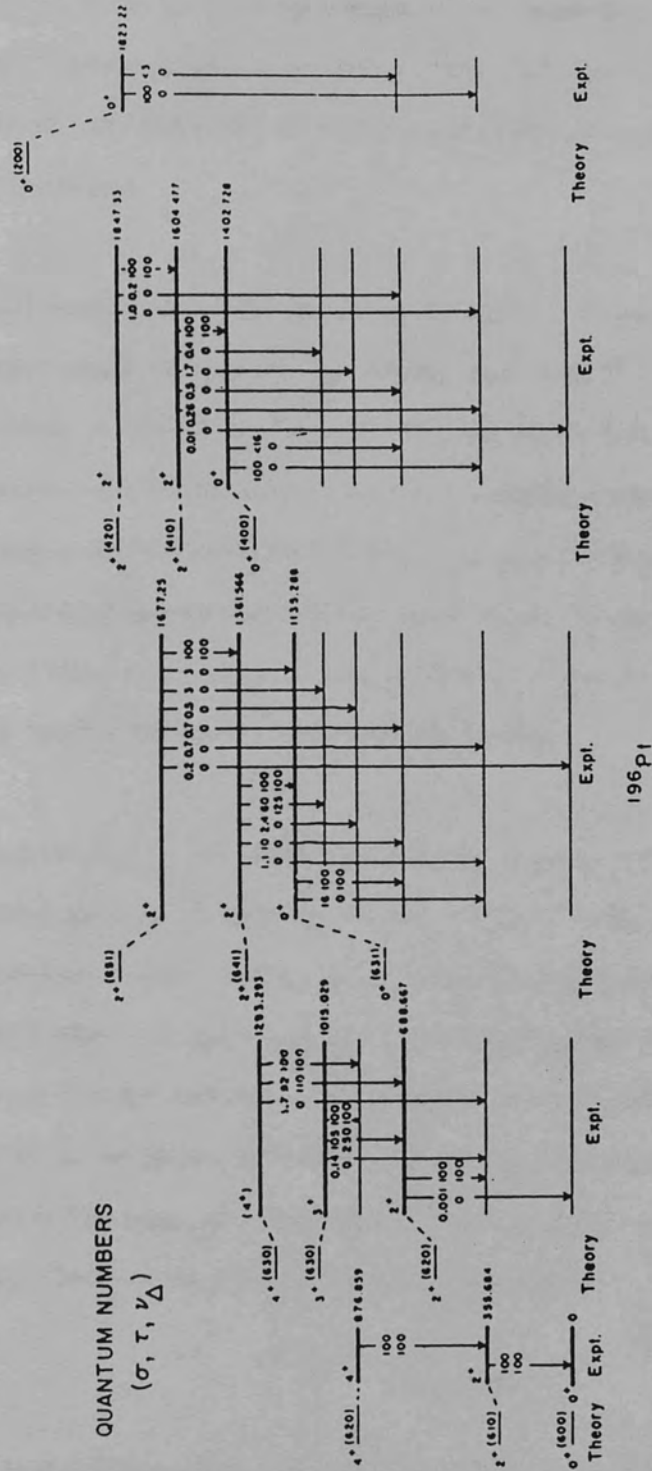
Fig. (2.12) A comparison of the positive parity levels in ^{196}Pt with the O(6) limit for N=6 and using A=185 keV, B=43 keV and C=23 keV. This figure is from Casten et al[72].

characterized by low-lying 2_2^+ states and "missing" 0^+ states. However, when Table (2.1) and Table (2.3) are compared, the branching ratios are not the same in the O(6) and triaxial limits. Also, in the O(6) limit, excited 0^+ states occur in a natural way, and many more levels are predicted because of the σ-generated recurring pattern.

The O(6) limit (especially for large N) seems to resemble most closely the γ-unstable model described by Wilets and Jean[46]. In such geometrical descriptions, as shown in Fig. (2.1.d), the levels follow a $\tau(\tau + 3)$ energy dependence. Also the same levels and level spacings that occur in the γ-unstable $n_\beta = 0$ group are repeated for the higher-lying $n_\beta \neq 0$ groups. In this way, the role of n_β is analogous to that of different σ values. In the O(6) scheme, however, the level degeneracies are no longer maintained, and there are spin cuttoffs, as well as a specific number of different σ groupings.

It is logical that the O(6) description corresponds to the γ-unstable geometrical models, in analogy to the SU(5)-vibrator and SU(3)-symmetric rotor correspondences. As described in section (2.2) the Hamiltonian of a γ-unstable oscillator is characterized by potential energy which is independent of γ, although γ-dependent terms are included in the kinetic energy. A link exists between the co-ordinates of the Bohr-Mottelson picture and the operators of the IBM. Arima has suggested the result of the γ-unstable potential corresponding to the O(6) limit of the IBM would be of the form[68]

$$V = -C\beta^2 + d\beta^4 \qquad (2.3.4.11)$$

where β is the deformation parameter and C and d are arbitrary constants. This form of potential arises from zero d-boson and two d-boson numbers changing the terms of the O(6) Hamiltonian. A γ-dependent term in the potential would

be of the form $\beta^3 \cos 3\gamma$, which corresponds to the one d-boson number changing to terms that are not included in this symmetry[68].

A convenient basis from which to describe the O(6) level wave functions is that of the vibrational limit, given by $L^\pi \mid n_d n_\beta n_\Delta >$ where n_d, n_β, n_Δ are, as usual, the number of d-bosons, number of d-boson pairs coupled to angular momentum zero, and the number of d-boson triplets coupled with an angular momentum of zero, respectively.

The relation between τ and the more familar phonon number is given by calculating the expectation value of n_d. Arima[11] has determined that, for the $\sigma = \sigma_{max} = N$ states, the expectation value of n_d in the O(6) limit is given by

$$< n_d > = \frac{N(N-1)}{2(N+1)} + \frac{\tau(\tau+3)}{2(N+1)} \qquad (2.3.4.12)$$

The origin of the characteristic $\tau(\tau + 3)$ energy spacing in the O(6) limit is now apparent, since the spacings depend on the boson energy times n_d, or the effective n_d given in Eq. (2.3.4.12).

Two types of perturbations may be added to the exact results of the O(6) limit. One which does not change the forces of the symmetry, and another which introduces a force from outside the limit. The former type can be accomplished, for example, by changing the boson energy from the value determined by section (2.2). This will alter the amplitudes of the non-zero components of all wavefunctions, but will not add new components. The result will be to break the selection rule $\Delta\sigma = 0$, but not to preserve the $\Delta\sigma = \pm 1$ E2 selection rule. The second type of perturbation can be accomplished, for example, by the introduction of a quadrupole-quadrupole interaction force. Since such an interaction contains one d-boson changing term, all wavefunction components

83

would be non-zero, though perhaps small, and the effect would be to break both O(6) E2 selection rules, as well as to alter all E2 branching ratios.

The O(6) symmetry is expected to be important near the end of shells. Fig. (2.12), however, shows that   overall there is a very good agreement between the empirical level scheme and that predicted by the O(6) limit of symmetry scheme. ^{196}Pt was the first empirical example of such a scheme, but Casten[69] has uncovered and showed near A=130, an extensive region of nuclei displaying O(6) symmetry.

CHAPTER III
EXPERIMENTAL ARRANGEMENT

3.1 Single Spectra Measurements

Since the advent of semiconductor radiation detectors, there has been a tremendous improvement in the quality of the γ-ray spectra obtainable from commercially produced radiation detection equipment. A pure germanium detector was used to measure gamma-ray energies up to about 200 keV, while the large volume true-coaxial Ge(Li) detectors were used for extensive measurements of higher energy gamma-rays[95]. The specifications of the above mentioned detectors are given in Table (3.1).

The simple pulse counting system of this work is illustrated in the block diagram of Fig. (3.1). The linear output pulses from the preamplifier were fed into a spectroscopy amplifier (Ortec-572) whose shape time constant of 2 μsec indicated a good signal-to-noise ratio. The signals were then fed through an Analog to Digital Converter (ADC) into a memory unit whose conversion gain was set at 4096 channels.

The source activity was chosen at about 10 μCi to achieve count rates below 2000 count/sec at 25 cm from the face of the detector. The dead time of the ADC was always below 10 %. As a result, pile-up effects[75] were avoided and coincidence summing corrections as suggested by Debertin and Schötzig[76] minimised.

Table (3.1)

Specification of the detectors used in this work.

Detector	Approximate Volume	Relative Efficiency	Resolution (keV) 1332.5 keV (^{60}Co)	Photopeak/compton 1332.5 keV (^{60}Co)
Ortec Ge(Li)	60 CC	10%	2.07 (16)	38
Ortec Ge(Li)	60 CC	9.6%	2.31 (19)	35
Ortec Ge	59.7 CC	31.3%	1.70 (11)	58.5

Ortec 572
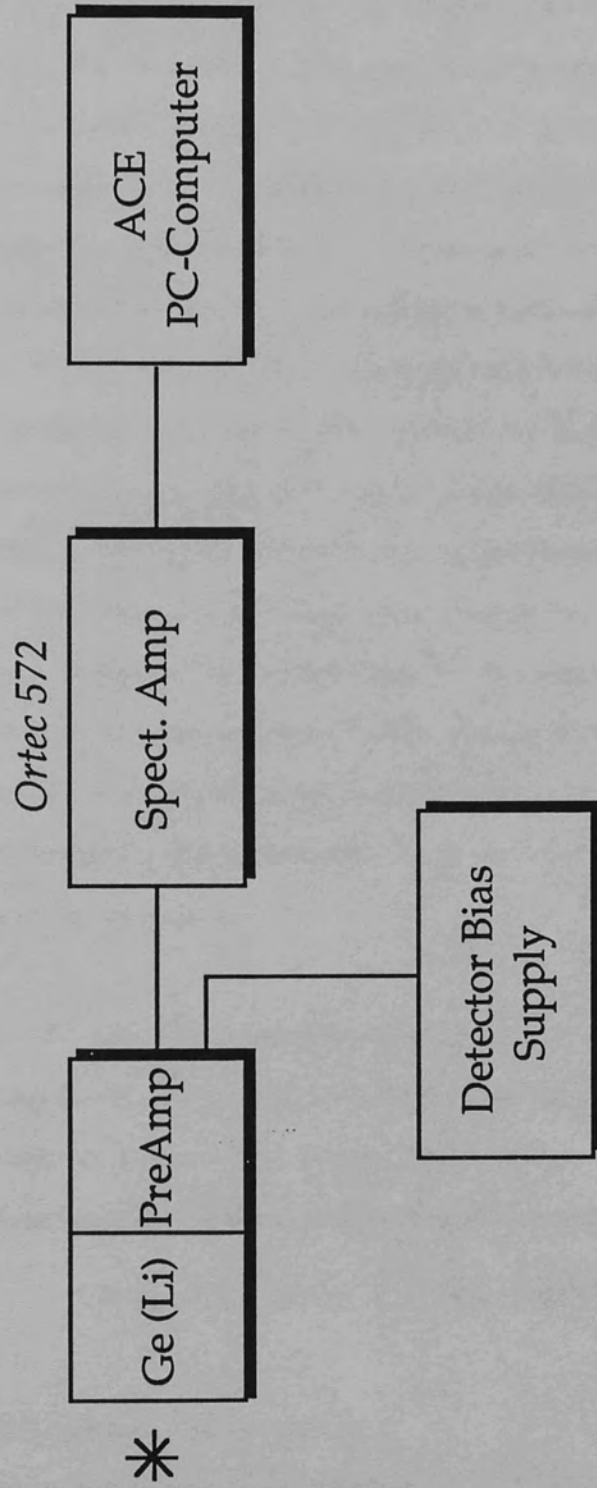
Fig (3.1) Block diagram of the single measurements arrangement.

3.2 Energy and Efficiency Calibration

Data from the analyzer used in the singles γ-ray experiments were first transferred to the computer. The gamma-ray energies were calculated by means of a computer program, SAMPO[77]. A least-squares fit to an Nth degree polynomial[77] is made for the calibration points. The coefficients of the polynomial are then used to calculate the energies of the remaining gamma-rays. The energies were taken from a set of calibrated sources[78] which include ^{241}Am, ^{57}Co, ^{22}Na, ^{137}Cs, ^{54}Mn and ^{60}Co. The program SAMPO fits a Gaussian curve to the experimental points after subtraction of the background. Although the program allowed the use of higher degree polynomials to fit the background under a peak, in nearly all cases a linear approximation was used. In some cases where the Gaussian fit of the data points was very poor, it was felt advisable to use channel by channel sum of the counts in each peak less the background to obtain the peak area[79]. The computer program also yields error estimates for the energies, based on uncertainties in the energy peak location of the calibration points, the goodness of the fit and the uncertainty in the peak locations of the data points.

In order to calculate the intensities of γ-rays from the photopeak areas of the singles spectrum, the photopeak efficiency of the detector must be known very accurately as a function of energy. The absolute efficiency of the Ge(Li) detectors were calculated with a set of calibrated sources[78] from the formula[80]

$$\varepsilon = N_p/3.7 \times 10^4 A_0 \quad I \quad texp(-0.693T/T_{1/2}) \qquad (3.2.1)$$

where

N_p number of count in the photopeak.

A_0 is the calibrated activity of the source .

I is the absolute intensity.

T is the time interval between the calibration of the source and the counting time.

$T_{1/2}$ is the half-life of the source.

t is the time measurement.

The program Sampo employs a functional representation of the efficiency curve[77]:

$$\varepsilon = P_1(E^{P_2} + P_3 \exp(P_4 E)) \tag{3.2.2}$$

Where the four parameters P_1, P_2, P_3 and P_4 are determined from the fit of the efficiency ε versus the energy expressed in keV. Fig. (3.2) illustrates the graph of Efficiency (ε) versus Energy (E) for the 10% Ge(Li) detector.

The numerous γ-ray spectra were analyzed off-line and searched for new peaks with an automatic peak fitting routine in Sampo, which required relatively little user input and produced very satisfactory and reliable results. The relative intensities of the gamma-rays were determined by measuring the number of counts in the peaks from Sampo and correcting for the efficiency of the detector deduced by Eq.(3.2.1). The area of well-separated peaks was determined by summing the counts in the peak and subtracting a linear background. There are several cases involving two or more overlapping peaks. The individual peaks were separated using the shape of nearby peaks. Sampo was used to calculate the relative intensities and error estimates. The error estimates include a contribution from the uncertainty in peak area and about 3% uncertainty in the detector efficiency calibration.
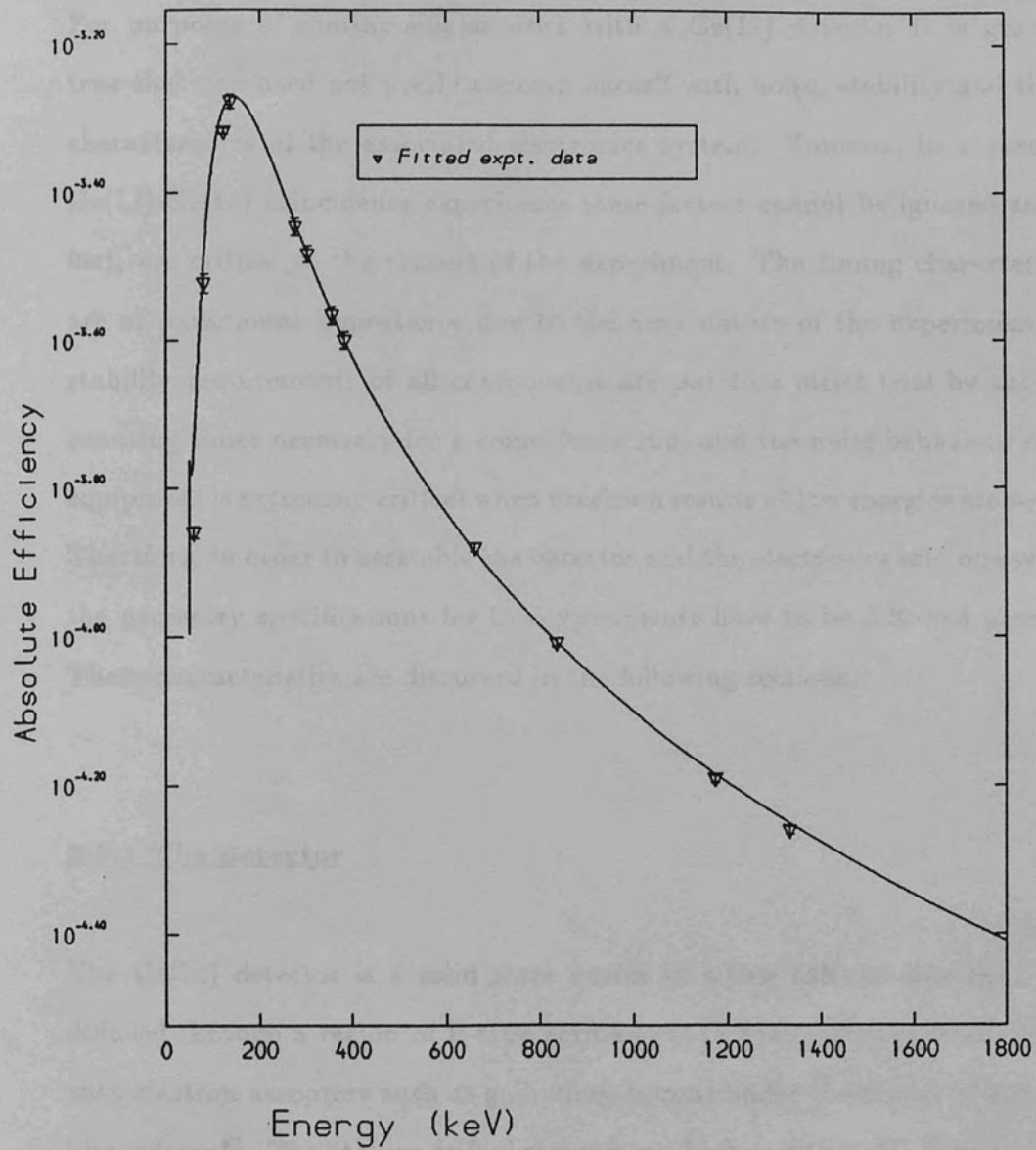
Fig. (3.2) Absolute efficiency curve of 10% detector as a function of γ-rays energy.

3.3 Detailed Description of Electronics

For purposes of routine singles work with a Ge(Li) detector it is generally true that one need not overly concern oneself with noise, stability and timing characteristics of the associated electronics system. However, in a precision Ge(Li)-Ge(Li) coincidence experiment these factors cannot be ignored and, in fact, are critical to the success of the experiment. The timing characteristics are of paramount importance due to the very nature of the experiment, the stability requirements of all components are put to a strict trial by the long counting times necessary for a coincidence run, and the noise behaviour of the equipment is extremely critical when precision results at low energies are sought. Therefore, in order to assemble the detector and the electronics into one system the necessary specifications for the experiments have to be followed precisely. These characteristics are discussed in the following sections.

3.3.1 The detector

The Ge(Li) detector is a solid state device in which lithium ions have been diffused through a region of P-type germanium (a germanium crystal dop ed with electron acceptors such as gallium or boron) under the action of a reverse bias voltage[81]. The lithium drifted region has a high resistivity[82]. When a γ-ray is stopped in this region, its energy is transferred to electrons which are excited into the conduction band (the band gap in germanium is 0.66 eV) were they are swept by the bias voltage. This produces a current which is proportional to the energy deposited by the γ-ray. To keep the lithium ions from diffusing out of the compensated region and to reduce the number of electrons which

90

are thermally excited into the conduction band producing noise, the detector is kept at liquid nitrogen temperature.

When a γ-ray enters the compensated region, any of three primary types of interactions can occur: a photoelectric interaction, a Compton collision, or pair-production. These processes are represented diagrammatically[83] in Fig. (3.3). In the photoelectric process, all of the energy of the γ-ray is transferred to the detector crystal through ionization to yield an electronic pulse which is proportional to the total energy of the original γ-ray. When a Compton collision occurs, the γ-ray interacts with an electron, depositing only part of the energy with the crystal through ionization. If another interaction does not occur before the degraded γ-ray escapes the detector, the resulting pulse will correspond to only a portion of the original γ-ray energy. When the incident γ-ray interacts through pair-production, its energy is absorbed in the creation of an electron-positron pair. This process requires that the γ-ray energy be at least 1.022 MeV (the energy equivalent of the rest mass of the electron-positron pair). The electron from the created pair loses its energy through the normal ionization process, but the positron, after coming to rest in the detector, annihilates another electron creating two γ-rays of 0.511MeV each. One or both of these γ-rays may escape from the detector before having been totally degraded. The resulting pulse then corresponds to an energy which is again less than that of the original γ-ray.

In the energy spectra which are obtained when the detector pulses from a particular source of γ-rays are processed, peaks occur for those γ-rays which have undergone total energy degradation in the detector. However, those pulses which result from partially degraded γ-rays which have undergone Compton collisions contribute to an unwanted background known as the

PAIR PRODUCTION

NUCLEUS

E_γ

POSITRON ELECTRON PAIR

COMPTON SCATTERING

ATOMIC ELECTRON

E_γ

θ

SCATTERED GAMMA

E'_γ

PHOTOELECTRIC EFFECT

ATOM

E_e

INCIDENT GAMMA

E_γ

PHOTOELECTRON
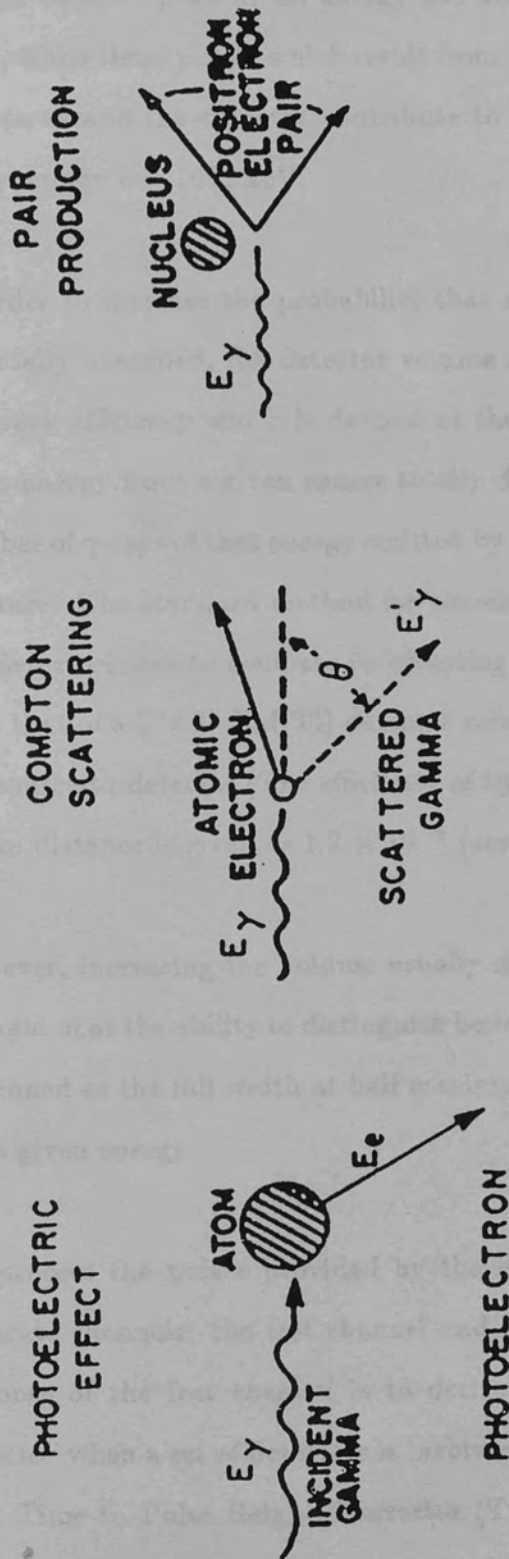
Fig. (3.3) Illustration of major gamma-ray interaction processes.

compton background. Those pulses which result from pair-production with the escape of one of the 511 keV γ-rays from the detector contribute to a "single escape" peak at an energy 511 keV less than that of the full energy peak, while those pulses which result from pair-production where both 511 keV quanta escape the detector contribute to a "double escape" peak at the full γ-ray energy less 1022 keV.

In order to increase the probability that a γ-ray which enters a detector will be totally absorbed, the detector volume must be increased[84]. This improves the peak efficiency which is defined as the ratio of the number of γ-rays of a given energy from a given source totally degraded in the detector to the total number of γ-rays of that energy emitted by the source for a given source detector distance. The standard method for obtaining the relative efficiency of each of the detectors was to compare its counting rate for the 1.332 MeV line of ^{60}Co with that of a 3"$\times$3" NaI(Tl) detector using a standard distance of 25 cm from the source-to-detector (The efficiency of the above size NaI(Tl) detector for the 25 cm distance is given as 1.2×10^{-3} (see Ref. 85)).

However, increasing the volume usually degrades the resolution which can be thought of as the ability to distinguish between close lying peaks. The resolution is defined as the full width at half maximum (FWHM) for the full energy peak for a given energy.

To process the pulses provided by the detector, a system composed of two separate channels: the fast channel and the slow channel must be used. The purpose of the fast channel is to derive the best possible signal from each detector when a set of detectors is involved, and to change the time information in a Time to Pulse Height Convertor (TPHC). The time spectrum from the

93

output of the TPHC is essentially of Gaussian shape. For measuring time differences, the timing peak must be narrow, that is the timing resolution must be good. It is important that the narrow peak be maintained down to a small fraction of the total peak height to make certain that all true coincident events are recorded (the figure of merit is the FW(1/10)M).

3.3.2 Preamplifier

The detector was equipped with a factory mounted Ortec 120 preamplifier having a charge-sensitive field effect transistor (FET) for the first stage input[81]. The detector was DC coupled to the preamplifier for low noise operation[86,87] (the noise rating was 700 eV at 0 picofarad (PF) capacitance and the slope was 17 eV/pf). Typical output pulses from the preamplifier have rise-times of 100 nsec or less and decay time 200 μsec. In order that the pulses do not overlap (at 5000 cps the average time between pulses in just 200 μsec) the pulse must be reshaped by the amplifier to reduce the long decay time.

3.3.3 Amplifier

In addition to amplifying the signal received from the preamplifier, the amplifier removes the slow, exponential decay of these pulses and filters the high frequency noise from the signal. Simplified versions of a differentiating and an integrating pulse shaping circuit which may be employed in typical amplifiers are shown in Fig. (3.4). In a typical unipolar pulse shaping network, the long pulse tail undershoots the baseline as illustrated by the CR-RCcircuit in Fig. (3.4). At a rate above 2000 count/sec, an incoming pulse may be superimposed on the tail
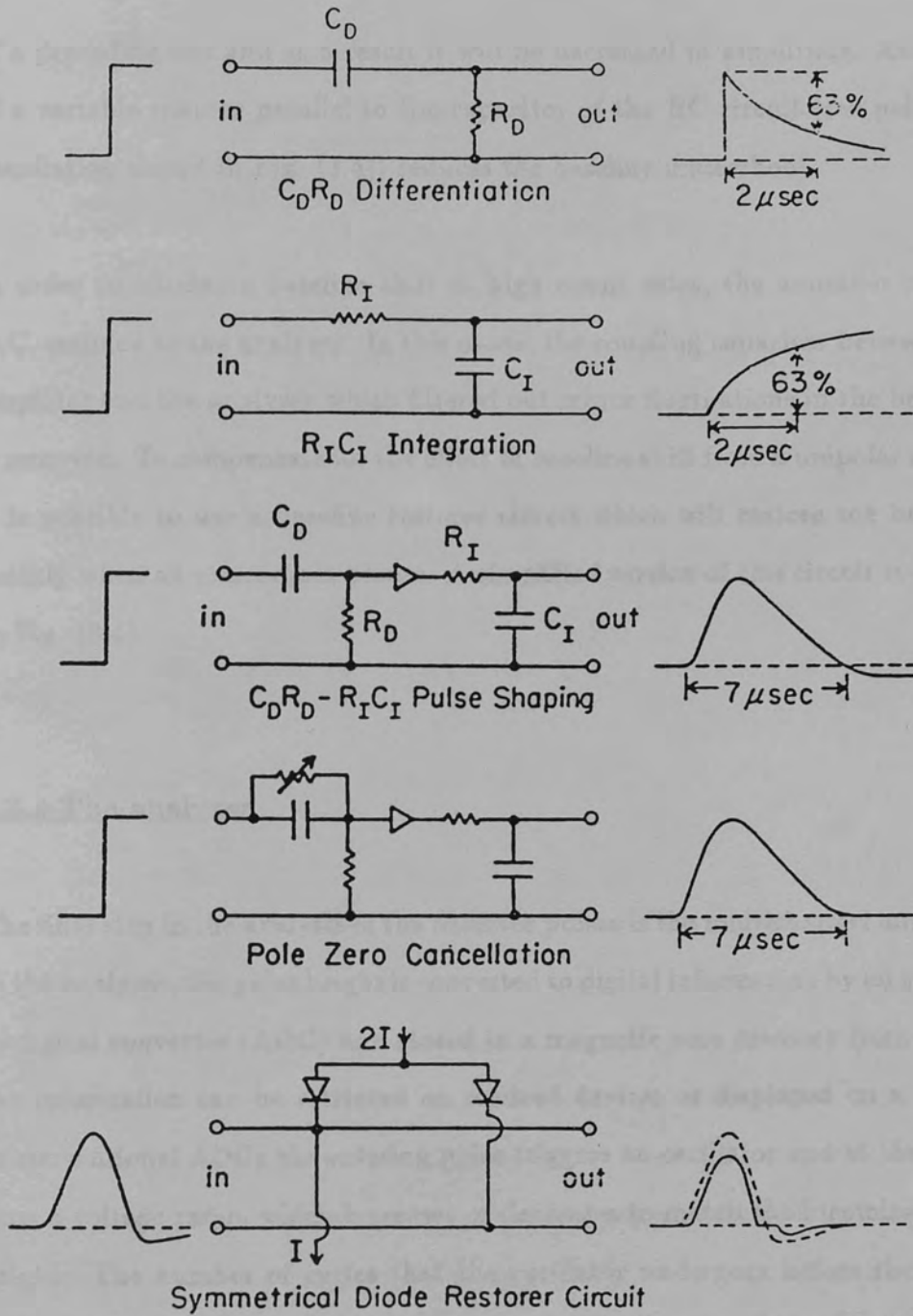
Fig. (3.4) Pulse shaping circuits used in the amplifiers for the singles and coincidence γ-ray experiments.

of a preceding one and as a result it will be decreased in amplitude. Addition of a variable resistor parallel to the capacitor of the RC circuit (see pole-zero cancellation circuit in Fig. (3.4)) reduces the baseline undershoot.

In order to eliminate baseline shift at high count rates, the amplifier can be D.C. coupled to the analyzer. In this mode, the coupling capacitor between the amplifier and the analyzer which filtered out minor fluctuations in the baseline is removed. To compensate for the effect of baseline shift from a unipolar signal, it is possible to use a baseline restorer circuit which will restore the baseline quickly when an undershoot occurs. A simplified version of this circuit is shown in Fig. (3.4).

3.3.4 The analyzer

The final step in the analysis of the detector pulses is the multichannel analyzer. In the analyzer, the pulse height is converted to digital information by an analog-to-digital convertor (ADC) and stored in a magnetic core memory from which the information can be retrieved on readout devices or displayed on a scope. In conventional ADCs the entering pulse triggers an oscillator and at the same time a voltage ramp, which increases or decreases to match the incoming pulse height. The number of cycles that the oscillator undergoes before the ramp voltage matches the pulse height is utilized digitally as a channel location in which the event is recorded. When one pulse is being analyzed no other pulses can enter the ADC. The length of time required to digitize a pulse is dependent both on the pulse height and the frequency of the oscillator. For a 50 mega Hertz oscillator, the time required to digitize a pulse is 20 nsec/channel plus an initial dead time of about 10-20 μsec.

3.4 Timing Spectroscopy

Time spectroscopy involves the measurements of the time relation between the occurrence of two events[88−90]. The source of events is frequently a pair of γ-rays or a combination of γ-rays and /or charge particles in cascade, which de-excite some level in the nucleus.

The most important consideration in timing measurement is the specifications of the detectors involved, such as electric field strength in the detector, efficiency, peak-to-compton ratio and resolution [see Section 3.3.1]. It is important to understand some of the characteristics that affect the time resolution of the system in the following sections.

3.4.1 Walk and Jitter

Characteristics that strongly affect timing in germanium are the walk due to amplitude variations or rise time changes and the intrinsic time jitter of the detector signal [91]. These effects are shown by an ideal discriminator with threshold V_T operating on detector signals, see Figs. (3.5a, 3.5b and 3.5c). The discriminators used in properly designed timing electronics have minimized the charge necessary to trigger an output, and most of the apparent walk is contributed by variation in pulse amplitudes and rise times. Fig. (3.5c) shows the effect of the system noise on the timing accuracy. The width of the timing uncertainty which is statistical in its nature is given by the triangle rule:

$$\sigma_T = \frac{\sigma_v}{\frac{dV(t)}{dt}\big|_{t=T}}$$

Fig.(3.5a). Time
walk caused by
the amplitude
variation and
the charge
sensitivity
of the discriminator.

Fig.(3.5b). Time
walk caused by
the rise time
effect and the
charge sensiti-
vity of the
discriminator.

Fig.(3.5c). Time
jitter due to
noise.
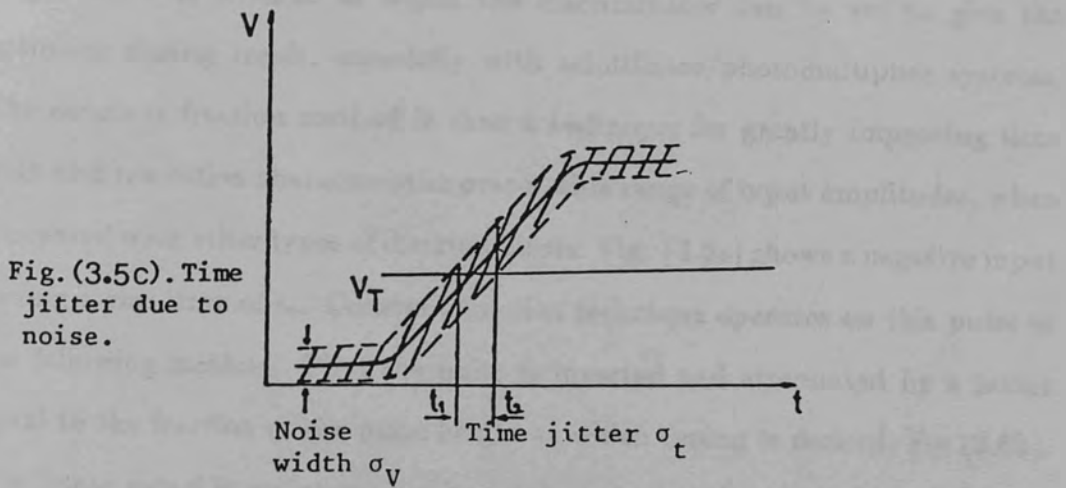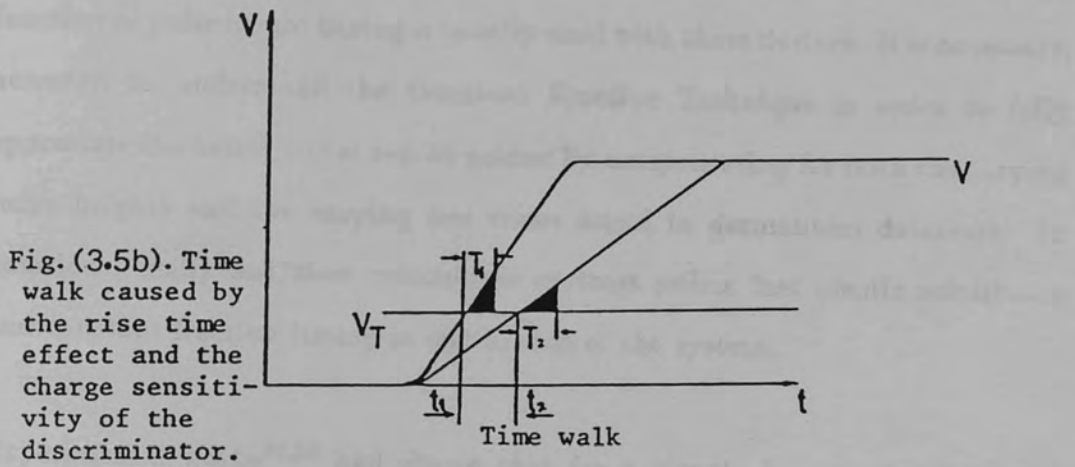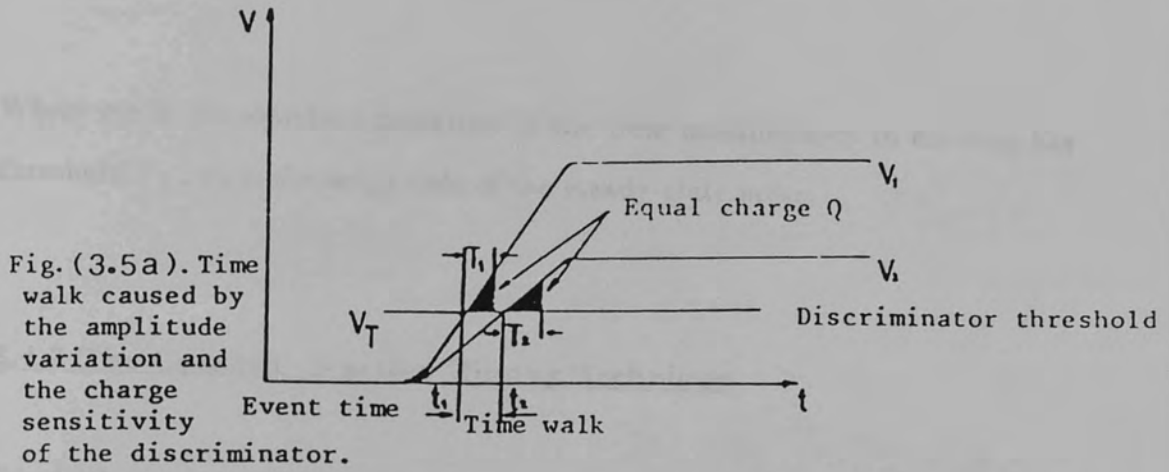
Where σ_T is the standard deviation in the time measurement in crossing the threshold V_T, σ_v is the amplitude of the steady-state noise.

3.4.2 The Constant Fraction Timing Technique

Due to the varying rise times of germanuim detector signals, a modified constant function of pulse height timing is usually used with these devices. It is necessary, however, to understand the Constant Fraction Technique in order to fully appreciate the benefits that can be gained by compensating for both the varying pulse heights and the varying rise times found in germanuim detectors. In addition , many fast/slow coincidence systems utilize fast plastic scintillator and constant fraction timing in one branch of the system.

Experimental works[92,93] had shown that for a signal of given rise time and height there is a value at which the discriminator can be set to give the optimum timing result, especially with scintillator/photomultiplier systems. The constant fraction method is then a technique for greatly improving time walk and resolution characteristics over a wide range of input amplitudes, when compared with other types of discriminators. Fig. (3.6a) shows a negative input having a rise time of t_r. Constant fraction technique operates on this pulse in the following method. First the pulse is inverted and attenuated by a factor equal to the fraction of the pulse height at which timing is desired, Fig (3.6b). The linear signal is maintained in its original slope and amplitude and delayed for a period of time somewhat greater than the rise time Fig. (3.6c). The signals are then added together as shown in Fig. (3.6d), and the timing output is taken at the zero crossing point. All signals will cross zero at the same time, independent of rise times and amplitudes. With fast plastic scintillator, this

99

(a)
Input signal

T_r
Rise time

(b)
Inverted and
attenuated signal

(c)
Delayed signal

T_d
Delay time

(d)
Shaped signal
for timing

Zero crossing time
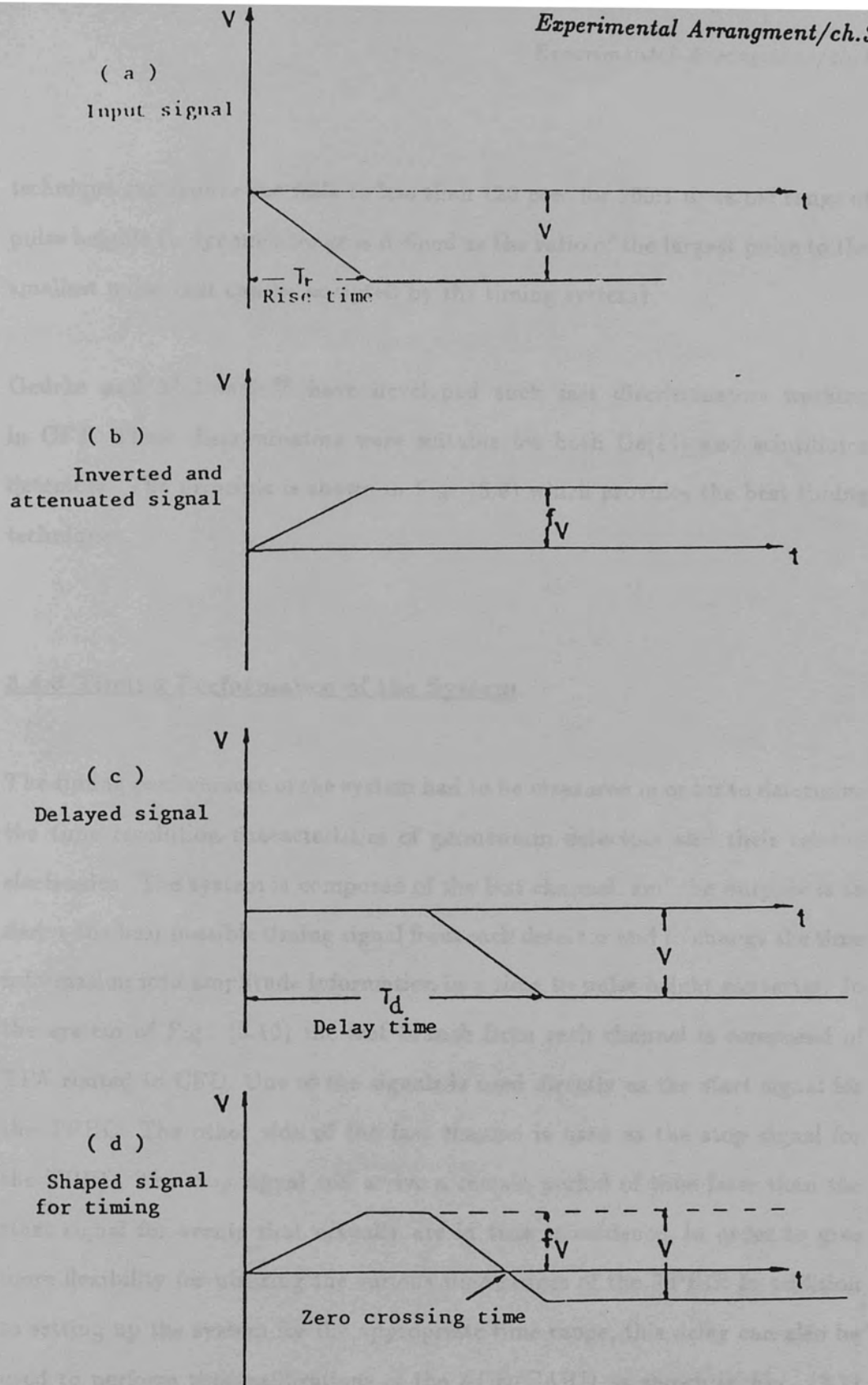
Fig. (3.6) Pulse shape and time considerations for the constant fraction timing technique.

technique can reduce the walk to less than 120 psec for 100:1 dynamic range of pulse heights (a dynamic range is defined as the ratio of the largest pulse to the smallest pulse that can be accepted by the timing system).

Gedrke and McDonald[92] have developed such fast discriminators working in CFT. These discriminators were suitable for both Ge(Li) and scintillator detectors. The principle is shown in Fig. (3.6) which provides the best timing techniques.

3.4.3 Timing Performance of the System

The timing performance of the system had to be measured in order to determine the time resolution characteristics of germanuim detectors and their related electronics. The system is composed of the fast channel, and the purpose is to derive the best possible timing signal from each detector and to change the time information into amplitude information in a time to pulse height converter. In the system of Fig. (3.10) the fast branch from each channel is composed of TFA routed to CFD. One of the signals is used directly as the start signal for the TPHC. The other side of the fast channel is used as the stop signal for the TPHC. The stop signal will arrive a certain period of time later than the start signal for events that actually are in true coincidence, in order to give more flexibility for utilizing the various time ranges of the TPHC. In addition to setting up the system for the appropriate time range, this delay can also be used to perform time calibrations of the ACE/CARD as shown in Fig. (3.7) while Fig. (3.8) illustrates the result.

REFERENCE PULSER   Canberra 1407

Ortec 473A   Ortec 463

CFD   CFD

Ortec 425A

DELAY

Ortec 467

Start   TPHC   *Stop*

NS 710

MCA
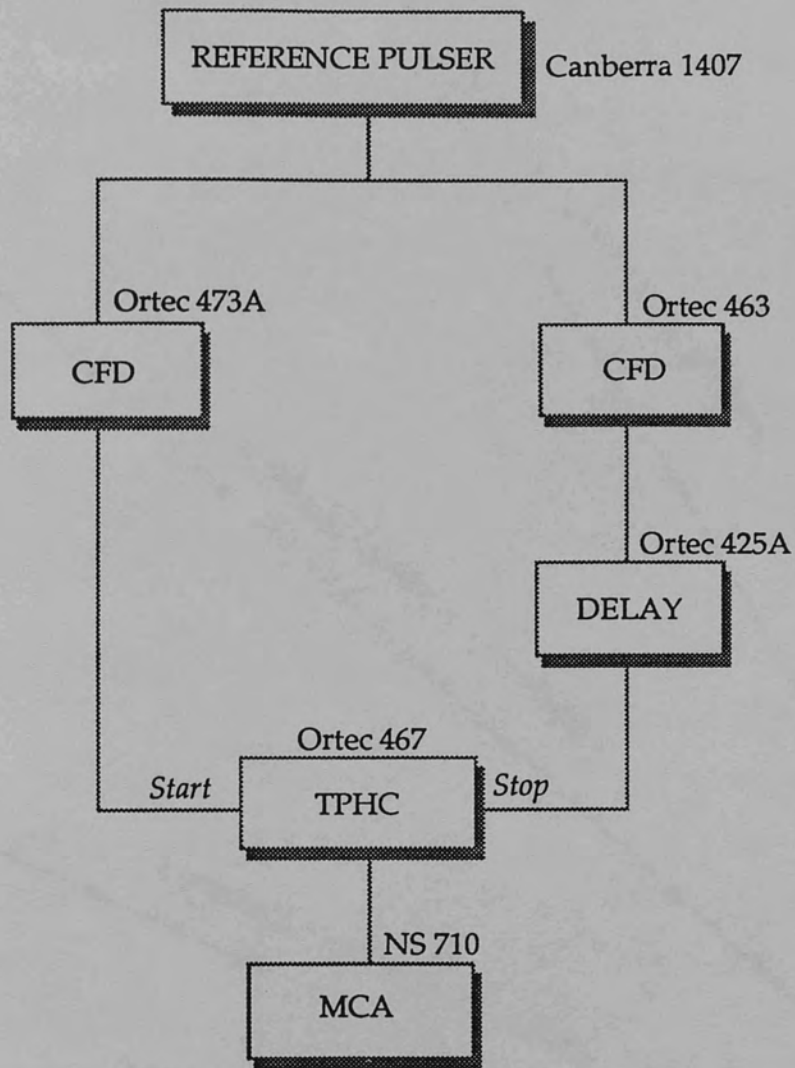
Fig (3.7)   Block diagram of the time calibration of the MCA
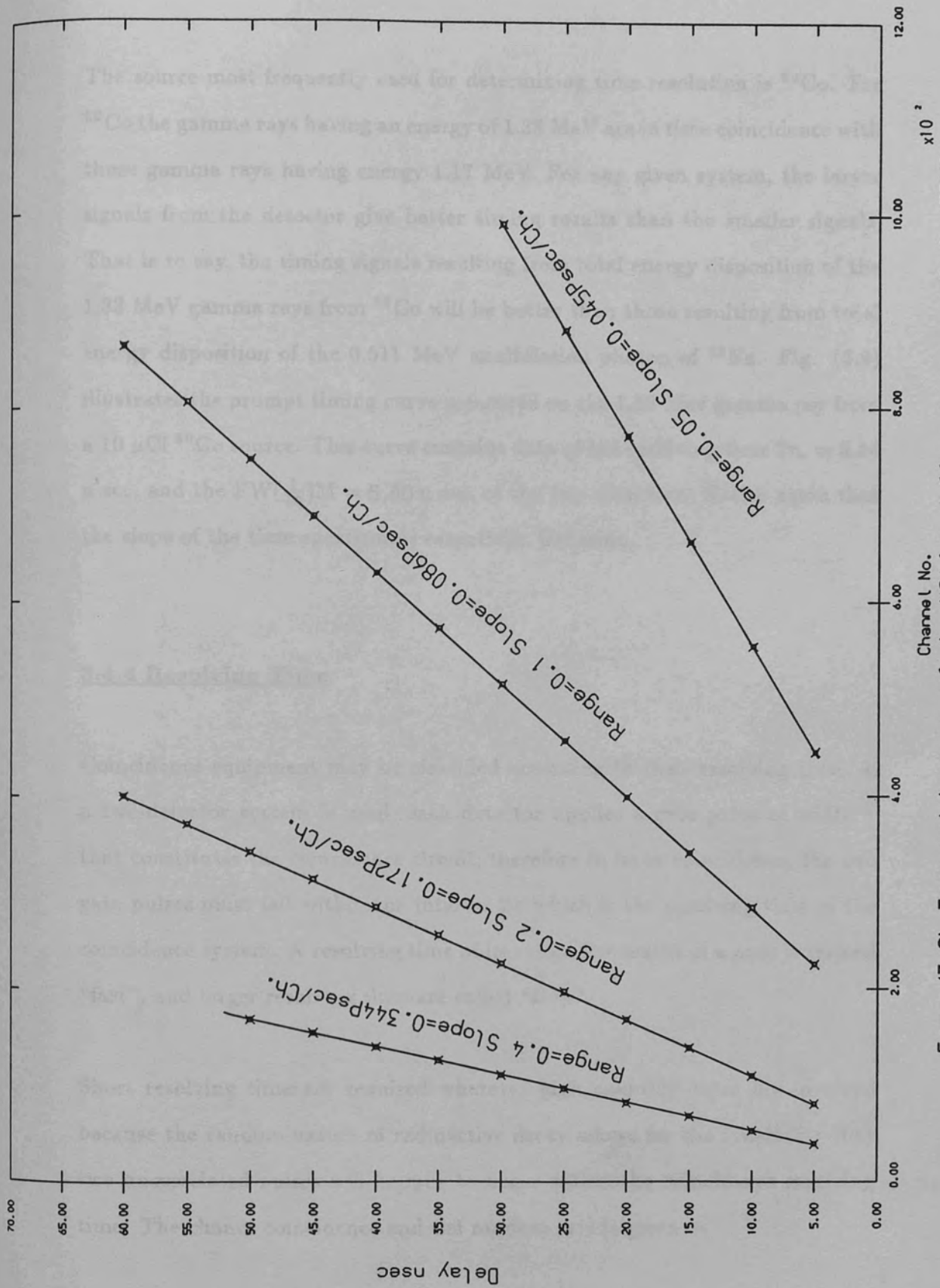
Fig. (3.8) Time calibration of the MCA for different ranges of the TPHC

The source most frequently used for determining time resolution is ^{60}Co. For ^{60}Co the gamma rays having an energy of 1.33 MeV are in time coincidence with those gamma rays having energy 1.17 MeV. For any given system, the larger signals from the detector give better timing results than the smaller signals. That is to say, the timing signals resulting from total energy disposition of the 1.33 MeV gamma rays from ^{60}Co will be better than those resulting from total energy disposition of the 0.511 MeV annihilation photon of ^{22}Na. Fig. (3.9) illustrates the prompt timing curve measured on the 1.33 Mev gamma ray from a 10 μCi ^{60}Co source. This curve contains data of the resolving time $2\tau_o = 3.44$ n sec, and the FW($\frac{1}{10}$)M $= 6.40$ n sec, of the two detectors. Notice again that the slope of the time spectrum is essentially Gaussian.

3.4.4 Resolving Time

Coincidence equipment may be classified according to their resolving time. If a two-detector system is used, each detector applies a gate pulse of width τ that constitutes the coincidence circuit; therefore to be in coincidence, the two gate pulses must fall within the interval 2τ which is the resolving time of the coincidence system. A resolving time of less than few tenths of a μsec is termed "fast", and larger resolving times are called "slow".

Short resolving times are required wherever high counting rates are involved because the random nature of radioactive decay allows for the possibility that two uncorrelated pulses will happen to occur within the coincidence resolving time. The chance coincidence and the random rate is given as

$$N_{chance} = 2\tau N_o^2 \varepsilon_1 \varepsilon_2 \qquad (1)$$
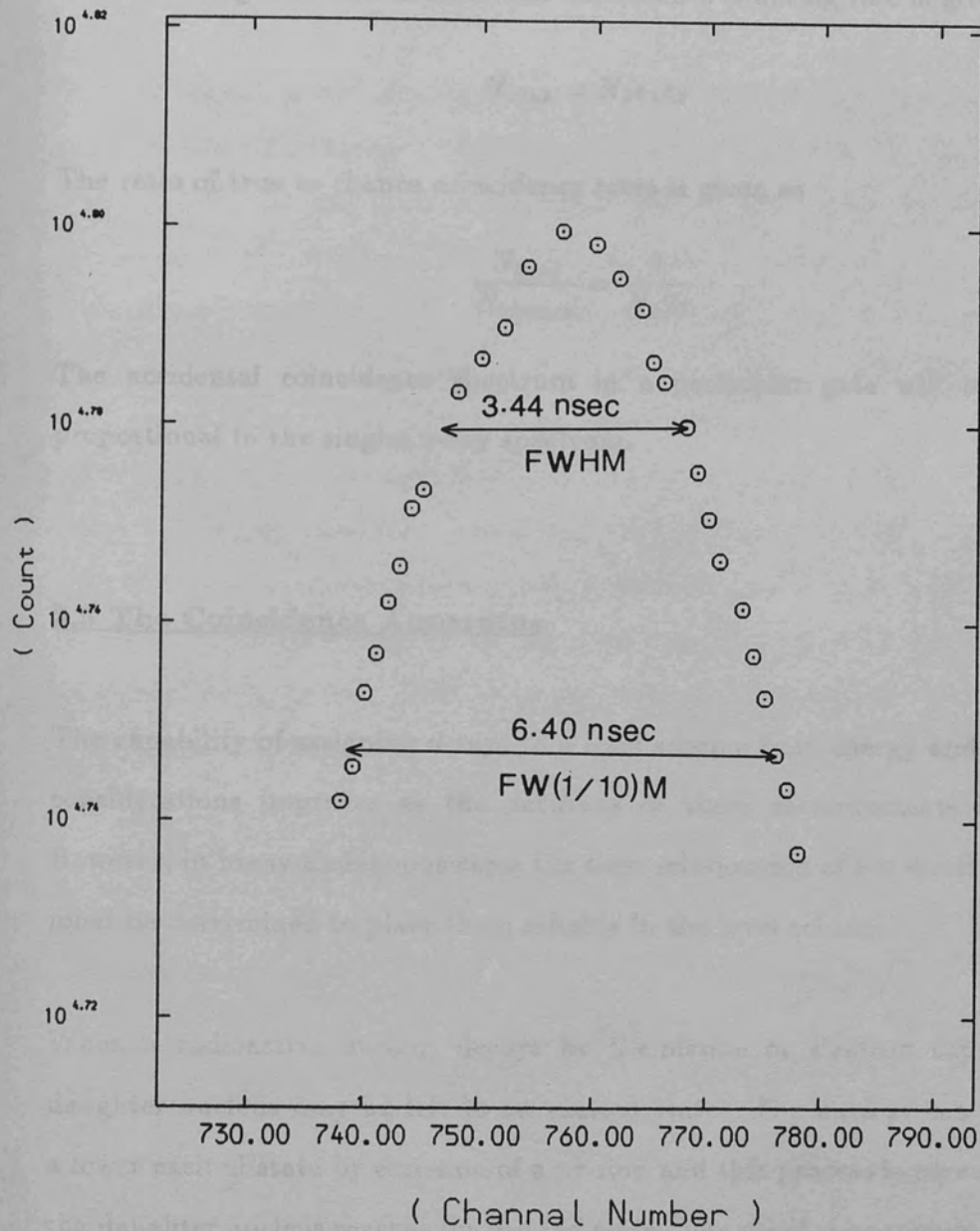
Fig. (3.9) Prompt time distribution curve CO-60.

Where 2τ is the resolving time, N_o is the source strength and ϵ_1 and ϵ_2 are the absolute efficiencies of the respective detectors. It thus appears that the best way to reduce chance coincidences is to make 2τ as small as possible. However, 2τ cannot be reduced below the interval of the time jitter in the detector pulses without losing true coincidence. The coincidence counting rate is given as

$$N_{true} = N_o \epsilon_1 \epsilon_2 \tag{2}$$

The ratio of true to chance coincidence rates is given as

$$\frac{N_{true}}{N_{chance}} = \frac{1}{N_o 2\tau} \tag{3}$$

The accidental coincidence spectrum in a particular gate will be exactly proportional to the singles γ-ray spectrum.

3.5 The Coincidence Apparatus

The capability of assigning γ-rays to a level scheme from energy and intensity considerations improves as the accuracy of these measurements increases. However, in many ambiguous cases the time relationship of the emitted γ-rays must be determined to place them reliably in the level scheme.

When a radioactive nucleus decays by β-emission or electron capture, the daughter nucleus may be left in an excited state. The nucleus can decay to a lower excited state by emission of a photon and this process is repeated until the daughter nucleus reaches the ground state. The usual time required for this cascade process to occur is of the order of 10^{-8} to 10^{-16} sec, and the emitted γ-rays are said to be in prompt coincidence with one another.

Coincident γ-rays can be recorded with two detection systems which have the requirement that they only analyze γ-rays which enter the detectors within a certain preselected time interval known as the resolving time. The coincidence requirement is met by "gating" the recording ADC with a pulse which results only if a γ-ray enters each detector within the resolving time of the system.

Fig. (3.10) shows a block diagram of the Fast-Slow coincidence system[94] which was used in coincidence experiments on ^{182}W, ^{152}Gd and ^{152}Sm. One of the Ge(Li) detectors was used in the singles experiment. The two detectors are set at an angle of 90° to each other, as shown in Fig. (3.11), to minimize coincidences arising from the Compton scattering of high energy gamma rays from one detector to the other. Each detector was mounted with an Ortec 120 preamplifier. The output signal from each preamplifier was sent to the Ortec 572 amplifier and to the Ortec 474 timing filter amplifier where it was used for timing purposes. The Ortec 572 amplifier was used to amplify the signal for energy measurements and to improve resolution at high count rates a pile-up rejection was operated. The unipolar output pulse from the spectrum detector (detector No.1, Table 3.1) was delayed and routed to the high level of the ACE/PC-Computer.

Another branch of the output (the energy gating by detector No.2, Table 3.1) was amplified by Ortec 572 amplifier and routed to an Ortec 551 timing single channel analyzer (No.1, slow) set to select a particular energy.

The timing branch of the signal from either preamplifier was sent to an Ortec 474 timing filter amplifier which shaped the pulses for use by the Ortec 583 constant fraction discriminator unit. In the Ortec 583 constant fraction discriminator unit, the technique of amplitude and rise time compensation is used to the original pulse peak, regardless of its amplitude (see Section 3.4.2). The output
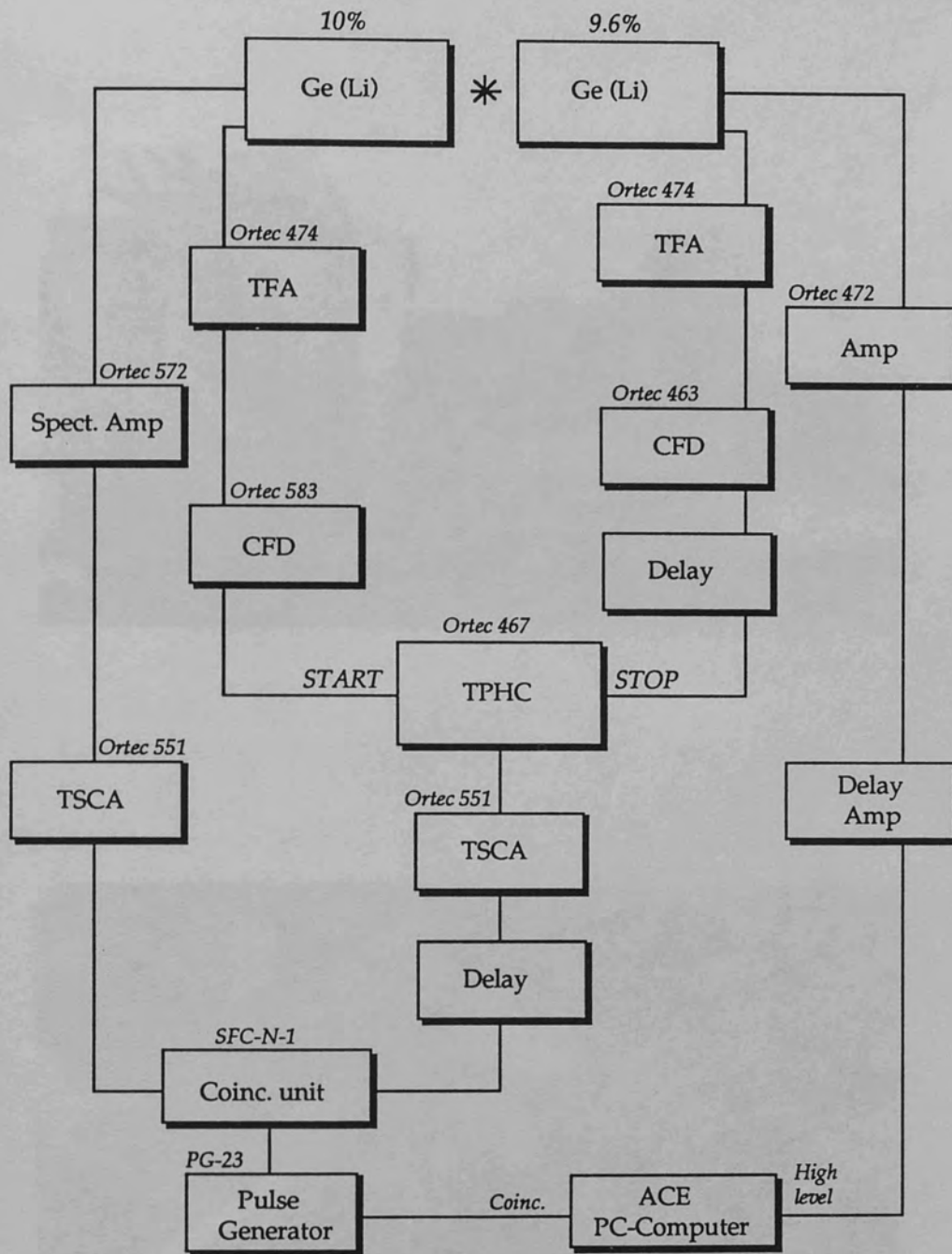
Fig (3.10)   Block diagram of conventional Fast – Slow coincidence system.

108
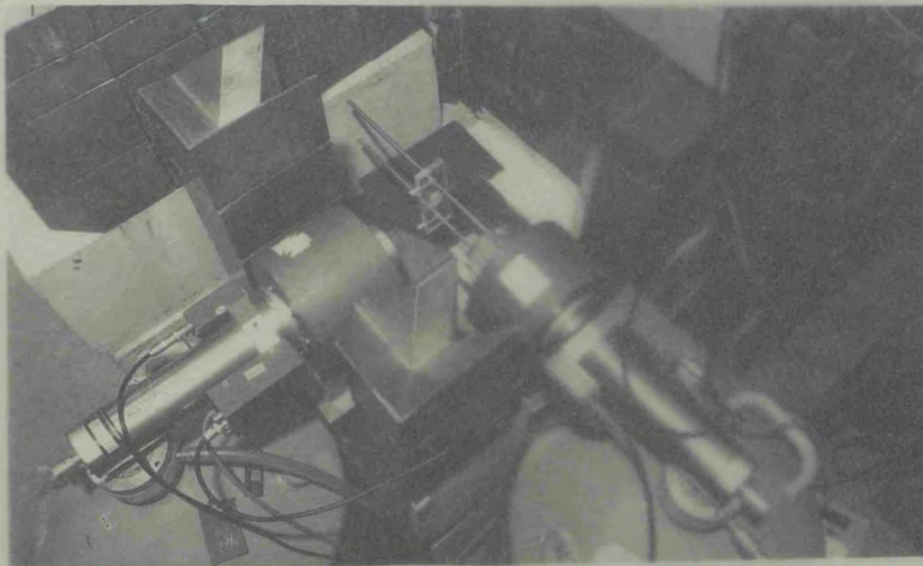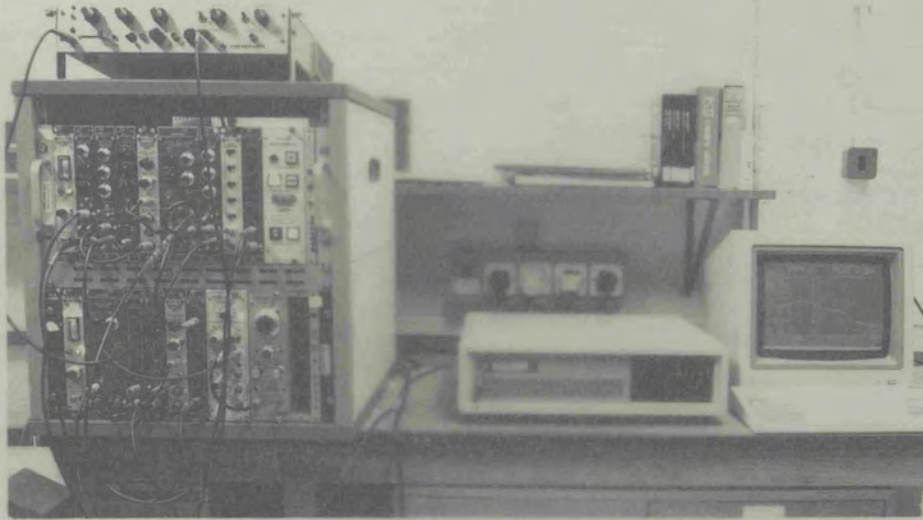
Fig. (3.11) A view of the experimental arrangement
of the Fast-Slow Coincidence System.
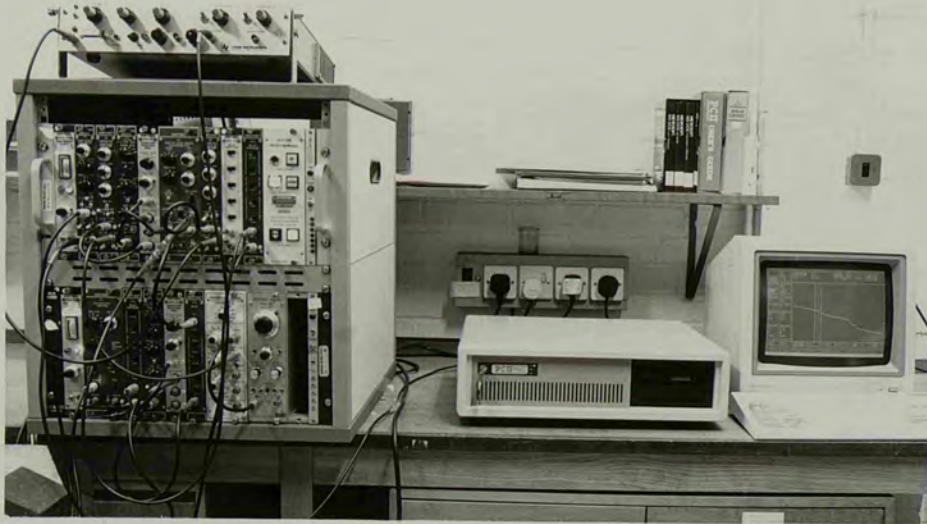
trigger pulses from the constant fraction discriminator units were used as start and stop pulses for the Ortec 467 Time-to Pulse-High-Convertor (TPHC). In the TPHC the start pulse initiates the charging of a capacitor which is discharged by the stop pulse, creating a pulse whose height is proportional to the time duration between the start and the stop pulses. The TPHC output pulses were routed to a Timing Single Channel Analyzer (TSCA, fast No. 2) in which a window was set to select the proper pulse amplitude which corresponded to pulses originating from coincidence events (when in this condition, the TSCA window is said to be set on the "prompt peak"). The pulse was delayed and routed to the Elsint coincidence unit.

The TSCA (No. 1) connected to an Elsint coincidence unit which required that these signals lie above the noise region. The coincidence logic pulse was routed to the gate pulse generator to shape the width and the amplitude. Finally, the logic pulse triggered a gate and gating pulse to the ADC of the ACE/PC-Computer.

CHAPTER IV

PROPERTIES OF THE ^{152}Gd ISOTOPE STATES

POPULATED IN THE DECAY OF ^{152}Eu

4.1 Introduction

The level structure of ^{152}Gd which lies in the beginning of a transitional region between spherical and deformed[11,66,72,96] nuclei may be studied either from the decay of ^{152}Eu or ^{152}Tb . The first decay has some experimental advantage because of its long half-life (13.33 y). On the other hand, ^{152}Tb does present some experimental problems due to its rather short half-life (17.5 h) but the β^+-and the the EC decays of its spin 2 ground state populate strongly the quadrupole and octupole quasi-vibrational bands of ^{152}Gd .

The level structure of ^{152}Gd has been investigated before. Barrette et al[97] considered that the spectra of this nucleus show more rotational than vibrational characteristics, i.e, it can be described as a deformed nucleus. Riedinger et al[98] preferred to consider the low lying states as resulting from quasi-rotations and quasi-vibrations than to treat them as members of one, two, and three-phonon vibrational excitations about spherical equilibrium shapes. Toth et al[99] classified a second 2^+ state at 930.58 keV, and another 0^+ state a 1408 keV, as members of a three-phonon vibrational band. Gromov et al[100] treated the third 2^+ state at 1108.97 keV, the second 0^+ state, and a possible 4^+ level, as members of a three-phonon band. On the other hand, the works of Gino et al[101], and Zolnowski et al[102] on the conversion electrons emitted in the ^{150}Sm $(\alpha,2n)$ and ^{152}Sm $(\alpha,4n)$ ^{152}Gd reactions, indicate the rotational nature of the levels in ^{152}Gd . The results of that work indicate the presence of a rotational

111

band up through spin 10, with the 344.25 and 755.39 keV states taken as the first and second members of this band. Another β-band of levels built on the 615 keV state was reported. Bloch et al[103] found that the inelastic scattering cross-sections of 12 MeV deuterons for the 615.54, 930 and 1280 keV levels are similar to those for the 0^+, 2^+ and 4^+ respectively, member of β-bands in deformed nuclei, thus, describing this band as a quasi-β band. Baker et al[104] calculated a ratio of B(E2) values for interband transitions in ^{152}Gd by considering it as an adiabatic rotor.

Conflicting values for energies and intensities emitted by ^{152}Eu were reported by many workers[97,98,104−112], and at the same time new transitions were suggested. Sharma et al[105] gave a complete list of energies and intensities including those transitions seen by Riedinger et al[98] and Barrette et al[97]. Both workers reported new transitions, but they did not agree with each other. Baker et al[112] reported another fourteen new transitions, some of which were determined from coincidence data. None of these were seen by other workers, while some of the transitions seen by Sharma et al[105] were missing from Baker's et al[104] list. Whilst Yoshizawa et al[106] have reported a set of data starting from energies above 270 keV with a cutoff energy at 1528 keV.

In this work, all the energies reported by Sharma et al[105] were observed; three new energy levels and eight possible new transitions   have been placed in the decay scheme. These were confirmed from the coincidence data and energy sum relations. Relative intensities and logft values were calculated and multipolarities, spin and parities deduced.

4.2 Experimental Procedure and Results

4.2.1 Source Preparations

The ^{152}Eu source was prepared by thermal-neutron capture (n,γ) reaction irradiation of europium oxide enriched to 97% for the mass 151 isotope, at the University of London Reactor Centre (ULRC) following the method described in section (1.2). The source was left for two weeks after irradiation before taking any measurements. This allows any short life activity to be eliminated. The source was packed in a polythene thin tube. A source activity of 10 μCi is sufficient to give about 1500 counts/sec with a source to detector distance of 25 cm.

^{152}Eu undergoes two branches of decays. It decays by β^- to ^{152}Gd and by, EC and β^+, to ^{152}Sm [Chapter V]. Thus, the singles spectra of the decay of ^{152}Eu contains the transitions of the two nuclei. However, it is difficult to distinguish between these transitions, but the coincidence technique was used to separate the transition belonging to each nucleus.

4.2.2 Singles Spectra

For the gamma-ray energy and intensity measurements of ^{152}Eu , three sufficiently long run spectra from Ge(Li) detector (No. 1, in Table 3.1) were analysed and the final results weighted and the average was taken. Determination of the energy and efficiency calibration was fully described in section (3.2). The spectrum includes a number of additional peaks; escape and background. Fig. (4.1) shows a typical gamma-ray spectrum of ^{152}Eu . The background spectrum, shown in Fig. (4.1a), collected for the same time period helped in the analysis of the singles spectra. Since the ^{152}Gd nucleus arises from β^--decay

113

of ^{152}Eu , whilst ^{152}Sm arises mainly from the electron capture (EC) and some β^+-decay of ^{152}Eu , a column in this Table was introduced to specify the transition corresponding to a certain nuclei. Some of these transitions are found to be belonging to both nuclei, these transitions are given to ^{152}Sm and ^{152}Gd .

The energies and relative intensities of all transitions from present work are listed in Table (4.1). One could not be uniquely assigned to either ^{152}Sm or ^{152}Gd : thirteen transitions were new and observed for the first time in this work. The intensity results of Sharma et al[105] and Baker et al[104] are also given in this Table for comparison.

4.2.3 Coincidence Spectra

The ^{152}Eu gamma-gamma coincidence experiment were performed with the two Ge(Li) detectors arranged in a 90° geometry throughout the experiments. The 12% efficient detector was used as the spectrum detector, while the 10% efficient detector [see Table (3.1) for specifications] provided the gate in a Fast-Slow coincidence system as shown in Fig. (3.10). Four gamma-rays 344, 411, 586 and 779 keV were taken to establish the decay scheme on the basis of the coincidence between these gates and the rest of the spectrum. In these studies chance contributions to the coincidence intensities were estimated at less than one percent, and, therefore, have been neglected.

Figs. (4.3-6) illustrate the coincidence spectra, while Fig. (4.2) shows the total spectrum, which is obtained by spreading the gating window along the whole
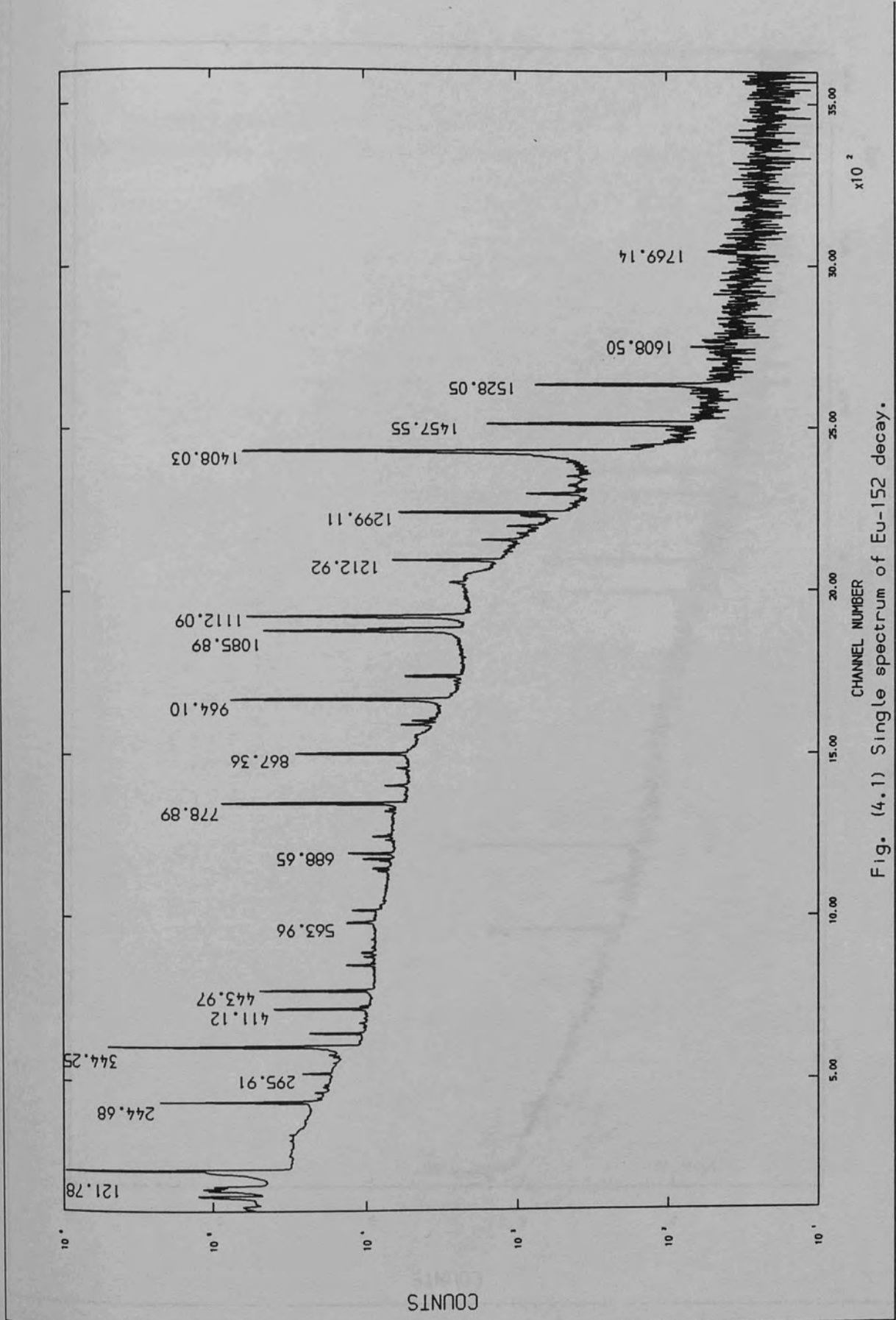
Fig. (4.1) Single spectrum of Eu-152 decay.

115
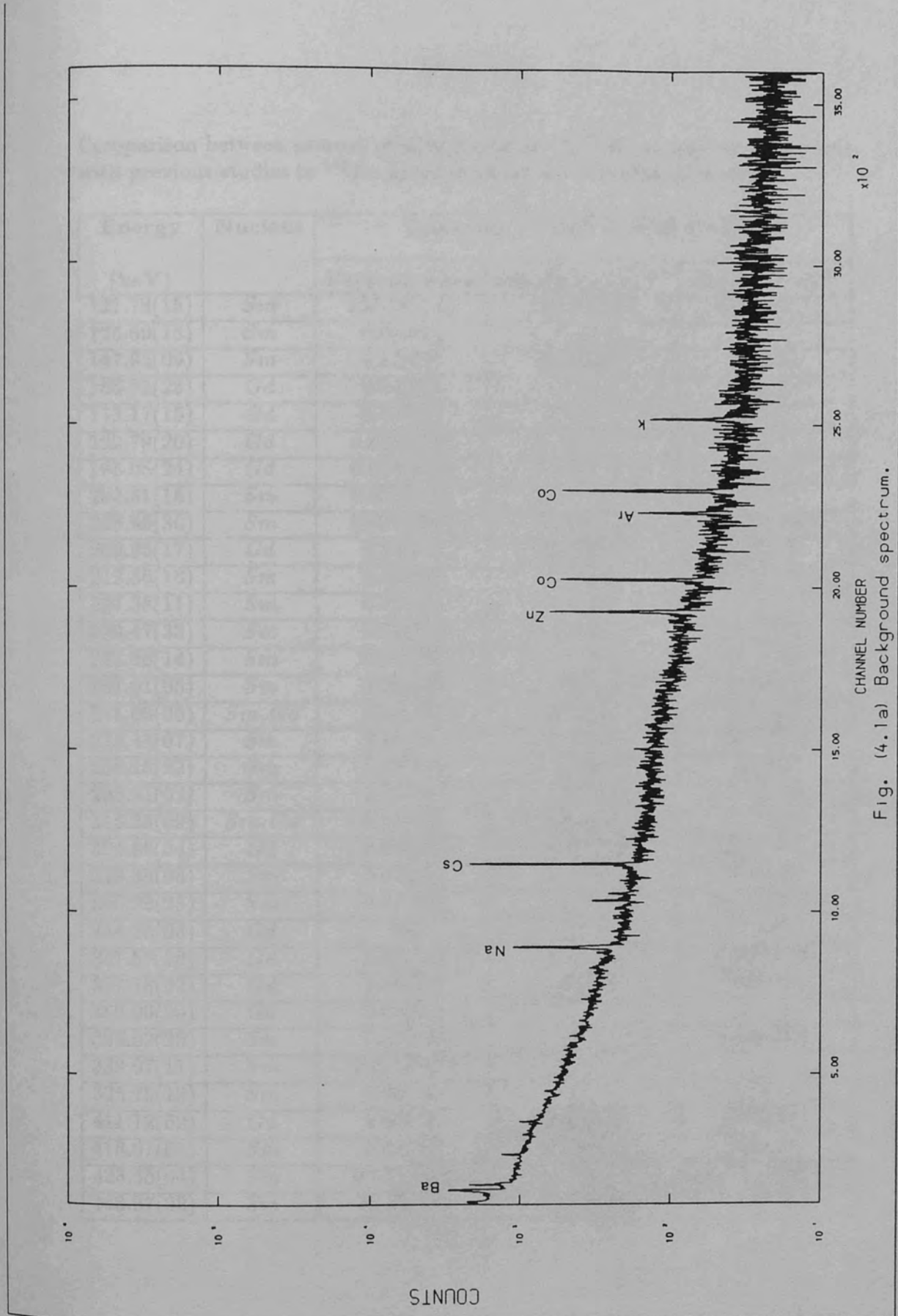
Fig. (4.1a) Background spectrum.

Table (4.1)

Comparison between present relative intensities (I_γ) of gamma-ray transitions with previous studies in ^{152}Eu decay (normalized to $I_\gamma(344.25 = 100)$).

Energy	Nucleus	Intensity related to I(344)=100		
(keV)		Present work	Sharma et al[105]	Baker et al[104]
121.78(15)	Sm	106.58(1.4)	109.70(2.2)	112.79(3.7)
125.69(15)	Sm	0.09(01)	–	–
147.94(09)	Sm	0.17(02)	0.12(01)	≤ 0.02
166.91(25)	Gd	0.04(01)	–	–
173.17(15)	Gd	0.03(01)	–	–
192.79(20)	Gd	0.018(005)	–	–
195.05(24)	Gd	0.023(005)	–	–
202.61(15)	Sm	0.022(005)	–	–
206.95(36)	Sm	0.024(005)	0.03(01)	0.027(009)
209.35(17)	Gd	0.03(01)	0.02(01)	0.03(02)
212.50(18)	Sm	0.09(02)	0.08(02)	0.076(023)
237.38(11)	Sm	0.05(02)	≤ 0.01	–
239.47(33)	Sm	0.04(01)	≤ 0.01	0.025(12)
244.68(14)	Sm	29.66(39)	27.91(50)	28.38(93)
251.61(05)	Sm	0.25(02)	0.28(01)	0.28(04)
271.00(06)	Sm, Gd	0.29(02)	0.32(02)	0.28(03)
275.43(07)	Sm	0.16(02)	0.17(02)	0.12(01)
286.15(22)	Sm	0.05(02)	≤ 0.01	≤ 0.025
295.91(02)	Sm	1.72(05)	1.61(04)	1.59(05)
315.25(09)	Sm, Gd	0.18(03)	0.24(02)	0.16(03)
324.86(04)	Gd	0.27(01)	0.28(02)	0.27(04)
329.35(06)	Sm	0.47(02)	0.49(03)	0.45(05)
340.23(25)	Sm	0.11(03)	–	0.091(009)
344.25(03)	Gd	100	100	100
351.57(18)	Gd	0.07(02)	0.08(02)	0.067(014)
367.78(02)	Gd	3.16(05)	3.24(07)	3.18(11)
380.06(20)	Gd	0.04(01)	–	–
385.92(20)	Sm	0.21(02)	–	0.085(038)
389.07(11)	Sm	0.013(005)	–	–
395.75(19)	Sm	0.03(01)	–	–
411.12(02)	Gd	8.44(12)	8.23(17)	8.26(21)
416.01(03)	Sm	0.41(02)	0.40(02)	0.39(04)
423.45(04)	Sm	0.021(005)	–	≤ 0.02
443.97(02)	Sm	11.75(17)	11.66(06)	10.60(60)

Table (4.1) (continued)

Energy	Nucleus	Intensity related to I(344)=100		
(keV)		Present work	Sharma et al[105]	Baker et al[104]
482.41(09)	Sm, Gd	0.12(02)	0.13(01)	0.10(02)
488.69(03)	Sm	1.57(03)	1.52(02)	1.49(05)
493.56(05)	Sm, Gd	0.14(02)	0.14(02)	0.17(03)
496.57(16)	Gd	0.05(02)	0.04(01)	0.02(01)
503.46(06)	Gd	0.61(04)	0.56(02)	0.55(03)
520.26(07)	Gd	0.18(02)	0.22(02)	0.20(03)
523.11(18)	Sm	0.08(03)	≤ 0.01	0.024(008)
526.76(14)	Gd	0.06(02)	0.05(02)	0.036(011)
534.25(10)	Gd	0.15(03)	0.18(02)	0.14(04)
556.48(14)	Sm	0.06(01)	0.04(02)	0.07(02)
557.76(18)	Gd	0.04(01)	−	0.02
563.96(03)	Sm	1.81(04)	1.80(05)	1.86(07)
566.50(21)	Sm	0.43(02)	0.53(03)	0.45(04)
586.31(03)	Gd	1.75(04)	1.77(04)	1.73(07)
595.61(12)	Sm	0.12(04)	−	−
615.83(29)	Sm, Gd	0.04(01)	0.03(02)	0.04(02)
644.29(29)	Sm	0.04(01)	0.03(02)	0.023(007)
656.47(06)	Sm	0.56(03)	0.51(03)	0.53(04)
664.83(15)	Sm	0.05(02)	0.03(02)	0.013(006)
671.21(15)	Sm	0.06(03)	0.05(02)	0.085(030)
674.66(03)	Sm, Gd	0.73(04)	0.74(03)	0.48(05)
678.62(02)	Gd	1.88(06)	1.80(05)	1.71(11)
688.65(03)	Sm	3.17(06)	3.18(08)	3.13(20)
696.87(19)	Gd	0.06(03)	−	−
703.46(24)	Gd	0.08(03)	−	0.06(02)
712.75(09)	Gd	0.37(03)	0.38(03)	≤ 0.05
719.32(07)	Sm	1.26(03)	1.30(04)	0.97(10)
727.42(16)	Sm	0.05(02)	0.04(01)	0.034(007)
764.87(05)	Gd	0.75(04)	1.12(03)	0.69(09)
768.98(06)	Sm	0.39(03)	0.32(03)	0.27(03)
778.89(03)	Gd	48.43(69)	48.74(90)	46.76(53)
794.84(20)	Gd	0.15(03)	0.15(02)	0.11(07)
805.39(15)	Sm	0.07(02)	−	0.06(02)
810.45(08)	Sm	1.21(03)	1.21(04)	1.17(05)
838.84(50)	Sm	0.05(01)	≤ 0.01	0.062(035)
841.61(10)	Sm	0.60(03)	0.61(03)	0.60(09)
867.36(05)	Sm	15.84(28)	15.83(40)	15.06(27)

Table (4.1) (continued)

Energy	Nucleus	Intensity related to I(344)=100		
(keV)		Present work	Sharma etal[105]	Baker et al[104]
896.59(09)	*	0.21(04)	–	–
901.20(10)	*Sm*	0.31(03)	0.27(03)	0.28(06)
919.34(08)	*Sm*	1.59(04)	1.67(05)	1.47(05)
926.28(07)	*Sm*	1.05(05)	1.04(04)	0.95(09)
930.67(15)	*Gd*	0.30(03)	0.28(03)	0.27(04)
937.11(23)	*Gd*	0.04(02)	–	0.046(015)
958.55(50)	*Sm*	0.08(03)	0.05(02)	0.06(03)
964.10(08)	*Sm*	54.34(74)	54.95(1.1)	53.08(1.4)
974.23(30)	*Gd*	0.07(02)	0.05(01)	0.04(01)
989.99(18)	*Gd*	0.13(03)	0.14(02)	0.12(04)
1005.22(11)	*Sm*	2.70(10)	2.80(10)	2.34(16)
1085.89(06)	*Sm*	38.37(52)	38.7(1.0)	37.12(67)
1090.05(08)	*Gd*	6.22(40)	6.70(20)	6.16(29)
1112.09(02)	*Sm*	50.88(77)	51.2(1.0)	49.28(67)
1170.56(24)	*Sm*	0.18(03)	0.20(02)	0.13(03)
1206.28(38)	*Gd*	0.05(02)	0.03(02)	0.03(01)
1212.92(07)	*Sm*	5.44(14)	5.24(11)	5.26(20)
1249.92(08)	*Sm*	0.72(04)	0.75(03)	0.65(05)
1261.33(20)	*Gd*	0.15(02)	0.15(02)	0.13(03)
1292.84(15)	*Sm*	0.50(05)	0.39(02)	0.37(06)
1299.11(04)	*Gd*	6.19(15)	6.22(15)	6.15(34)
1315.32(23)	*Sm*	0.03(01)	0.03(01)	–
1348.23(19)	*Gd*	0.07(01)	0.07(01)	0.063(008)
1363.72(22)	*Sm*	0.10(01)	0.11(01)	0.098(012)
1390.30(27)	*Sm*	0.024(008)	≤ 0.01	0.015(005)
1408.03(03)	*Sm*	77.36(89)	77.9(1.5)	76.20(2.2)
1457.55(07)	*Sm*	1.86(08)	1.92(04)	1.87(10)
1485.94(30)	*Gd*	0.021(009)	–	–
1528.05(08)	*Sm*	0.98(08)	0.99(03)	1.14(07)
1605.57(27)	*Gd*	0.03(01)	0.04(01)	0.029(006)
1608.50(27)	*Sm*	0.021(005)	≤ 0.02	0.021(005)
1647.42(14)	*Sm*	0.032(005)	0.03(01)	0.024(005)
1698.13(37)	*Gd*	0.022(007)	–	–
1769.14(22)	*Sm*	0.03(01)	0.03(01)	0.033(004)

* cannot be placed in the decay scheme.

pulse height spectrum. A summary of the coincidence results is given in Table (4.2).

4.3 Decay Scheme

The decay scheme of ^{152}Gd , established from the coincidence results of four gates (Table 4.2) and energy sum relations (Table 4.3), is shown in Fig. (4.7). The logft values, spin and parity assignments, together with the β^- energies and its feeding branching ratios for each level, are given in Table (4.4). The B.R's were evaluated from the balance between the decay and the feeding γ-rays for each level. The logft was calculated using the Moszowski monograms [Section 1.3]. The Q_β value of 1819.2 keV used was taken from Baglin[113]. The new levels and transitions observed in this work are shown as dotted lines in Fig. (4.7).

Table (4.4) shows the B.R's, logft values for the β^--decay of ^{152}Eu , and the deduced spins and parities. The values of B.R's reported here agree with those reported by Barratte et al[97], Riedinger et al[98] and Baglin[113] (within the reported errors). The value reported Barratte et al[97] and Baglin[113] for the 1108.97 (2_2^+) keV level was as twice the value reported here. The value reported by Riedinger et al[98] was (0.097%) which is close to the value given in this work (Table 4.4). In this study as well as Riedinger et al[98], the 1108.97 keV transition was not seen. If it exists it will be masked by the strong peak at 1112.09 keV. Hence, the B.R of this work is low. However, this difference in B.R. did not affect the logft value very much and the deduced spin and parity are not affected. The energy level at 615.54 (0^+) keV could not be given a B.R from direct balance between decay and feeding γ-rays, but the spin and parity of this level are

120

Table (4.2)

Summary of gamma-gamma coincidence results following the decay of ^{152}Eu to levels in ^{152}Gd.

Energy	Gates (keV)			
(keV)	344	411	586	779
166.91	x	x	x	x
173.71	x	—	—	—
192.79	x	—	x	—
195.05	x	x	x	x
209.35	x	x	x	—
271.00	x	—	—	—
315.25	x	—	—	—
324.86	x	—	—	—
344.25	—	x	x	x
351.57	x	—	x	—
367.78	x	x	—	—
380.06	x	x	x	x
411.12	x	—	—	—
482.41	x	x	x	x
493.56	x	—	—	—
496.57	x	—	—	—
503.46	x	—	x	—
520.26	x	x	x	x

Table (4.2) (continued)

Energy	Gates (keV)			
(keV)	344	411	586	779
526.76	x	x	—	—
534.25	x	—	—	—
557.76	x	—	—	—
586.31	x	—	—	—
674.66	x	—	x	—
678.62	x	x	—	—
696.87	x	—	—	—
703.46	x	—	—	—
712.75	x	—	x	—
764.87	x	—	—	—
778.89	x	—	—	—
794.84	x	x	—	—
937.11	x	x	—	—
974.23	x	—	—	—
989.99	x	—	—	—
1090.05	x	—	—	—
1206.28	x	—	—	—
1261.33	x	—	—	—
1299.11	x	—	—	—
1348.23	x	—	—	—
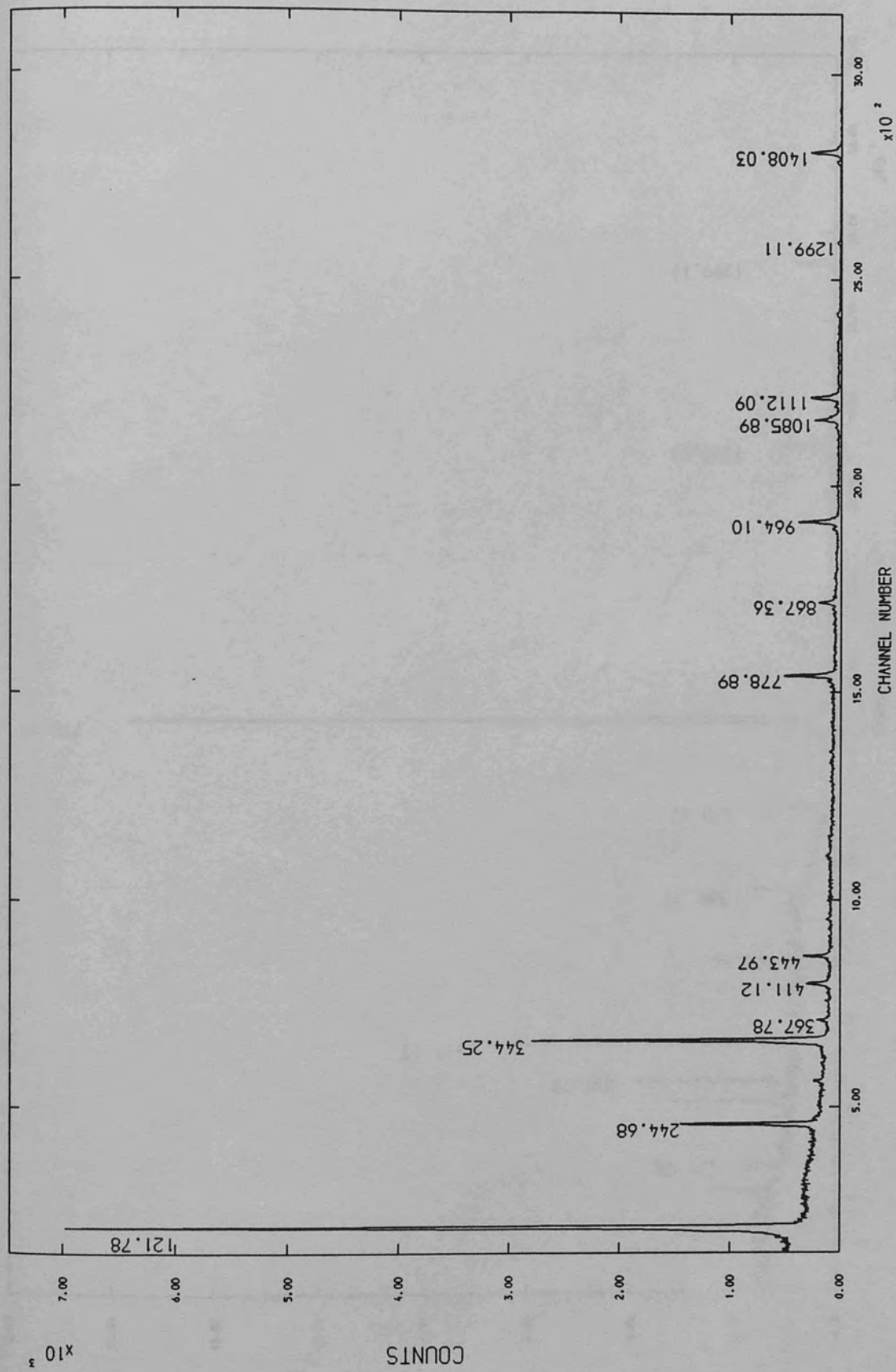
Fig. (4.2) Total spectrum of Eu-152 decay.
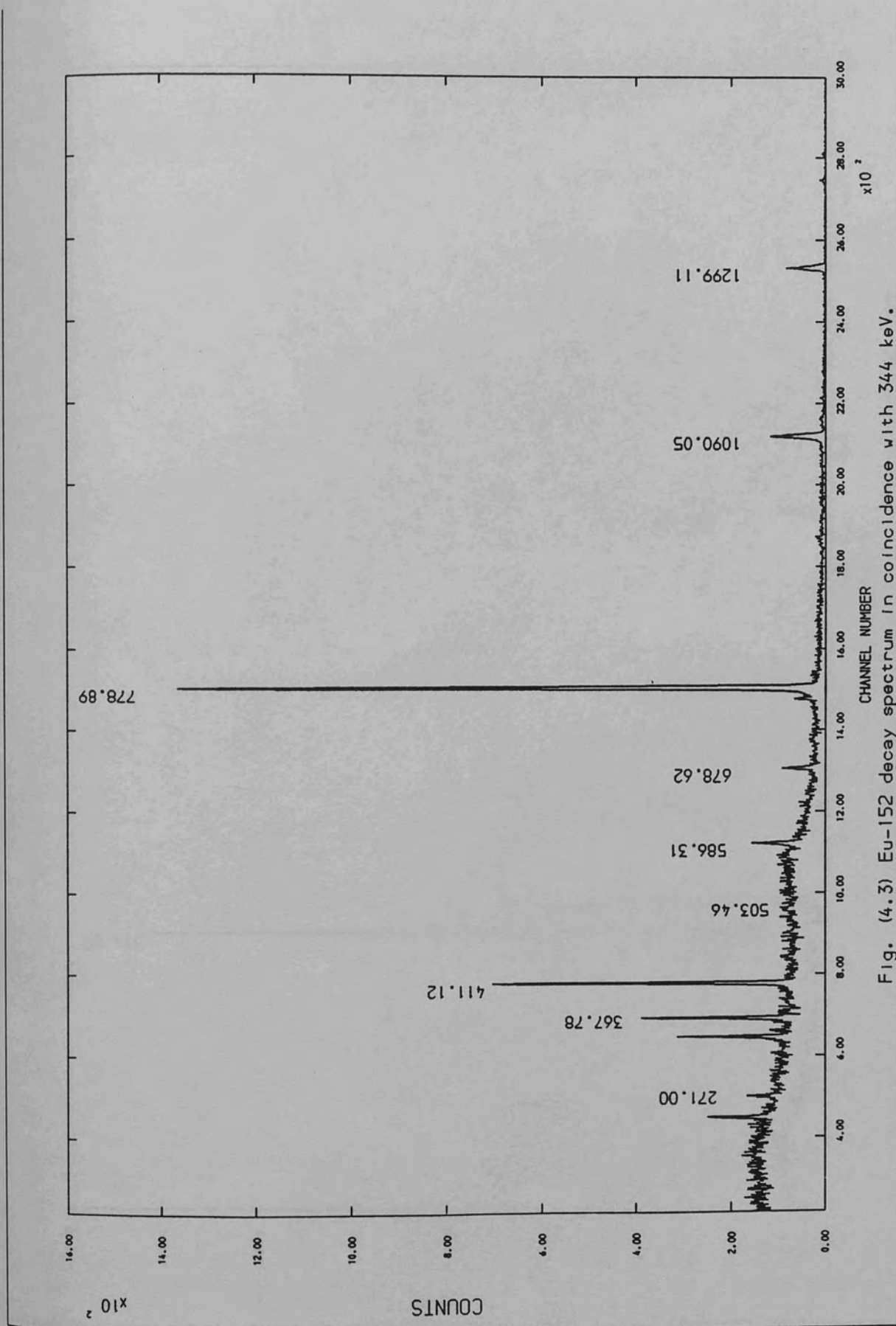
Fig. (4.3) Eu-152 decay spectrum in coincidence with 344 keV.
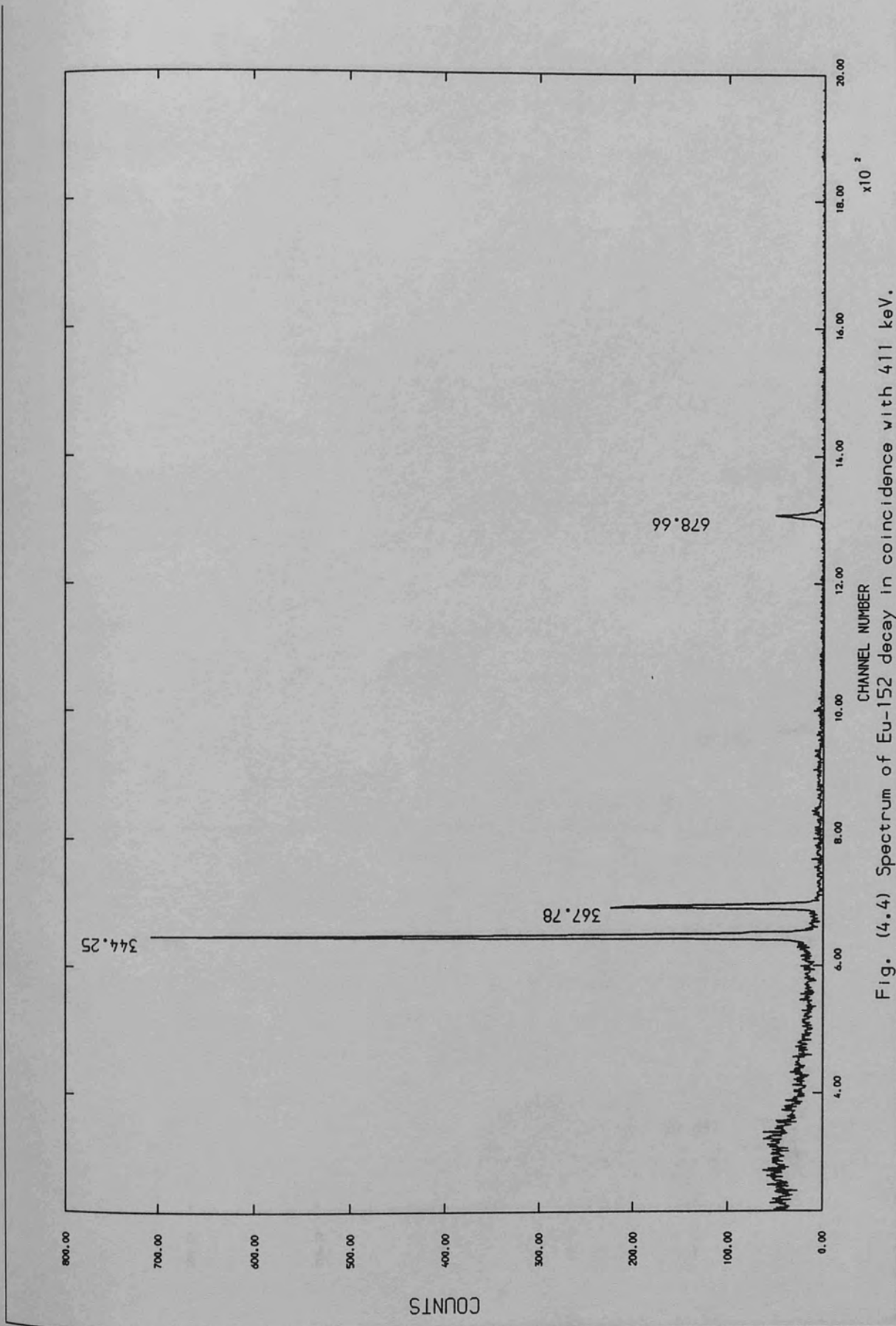
Fig. (4.4) Spectrum of Eu-152 decay in coincidence with 411 keV.
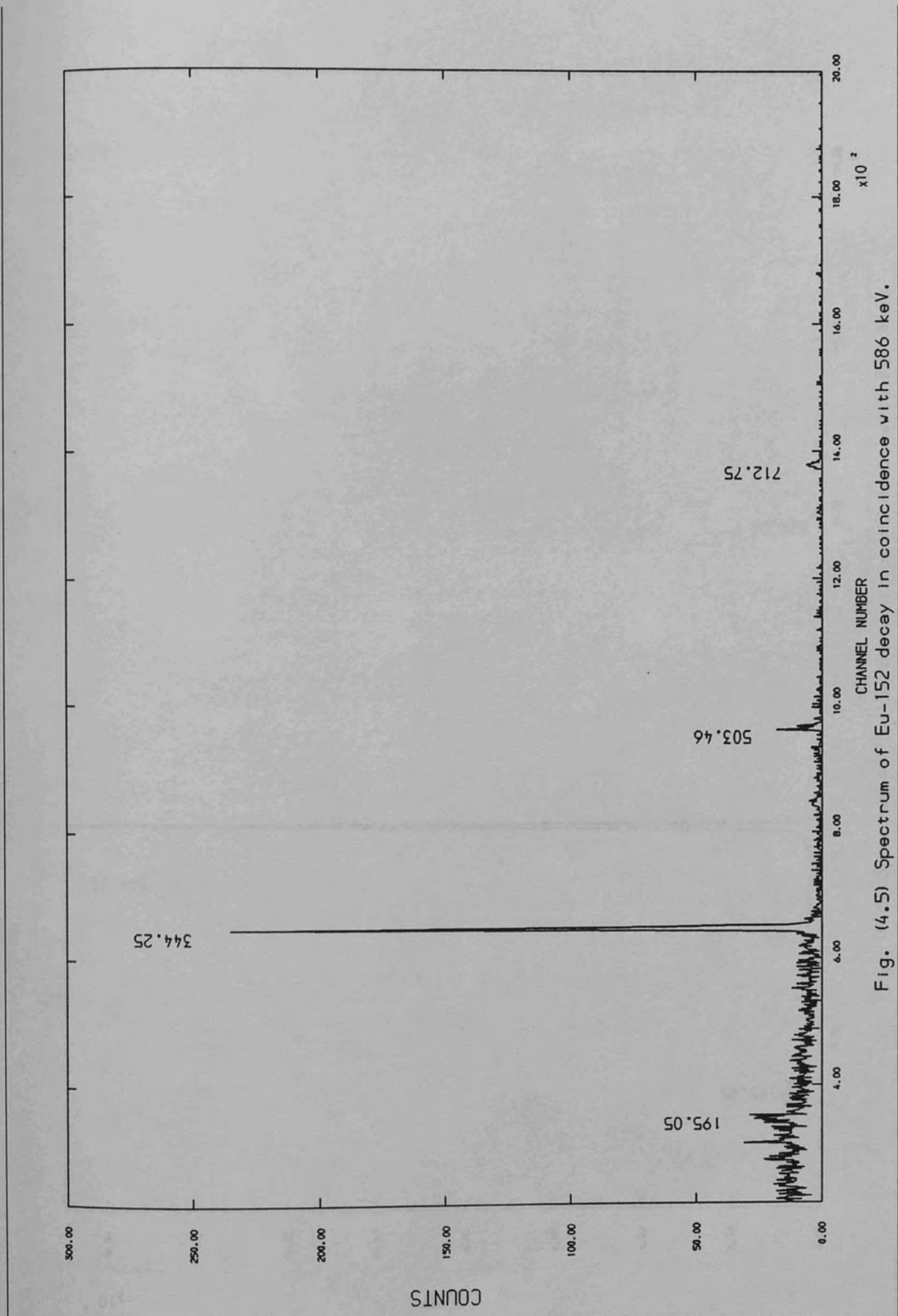
Fig. (4.5) Spectrum of Eu-152 decay in coincidence with 586 keV.
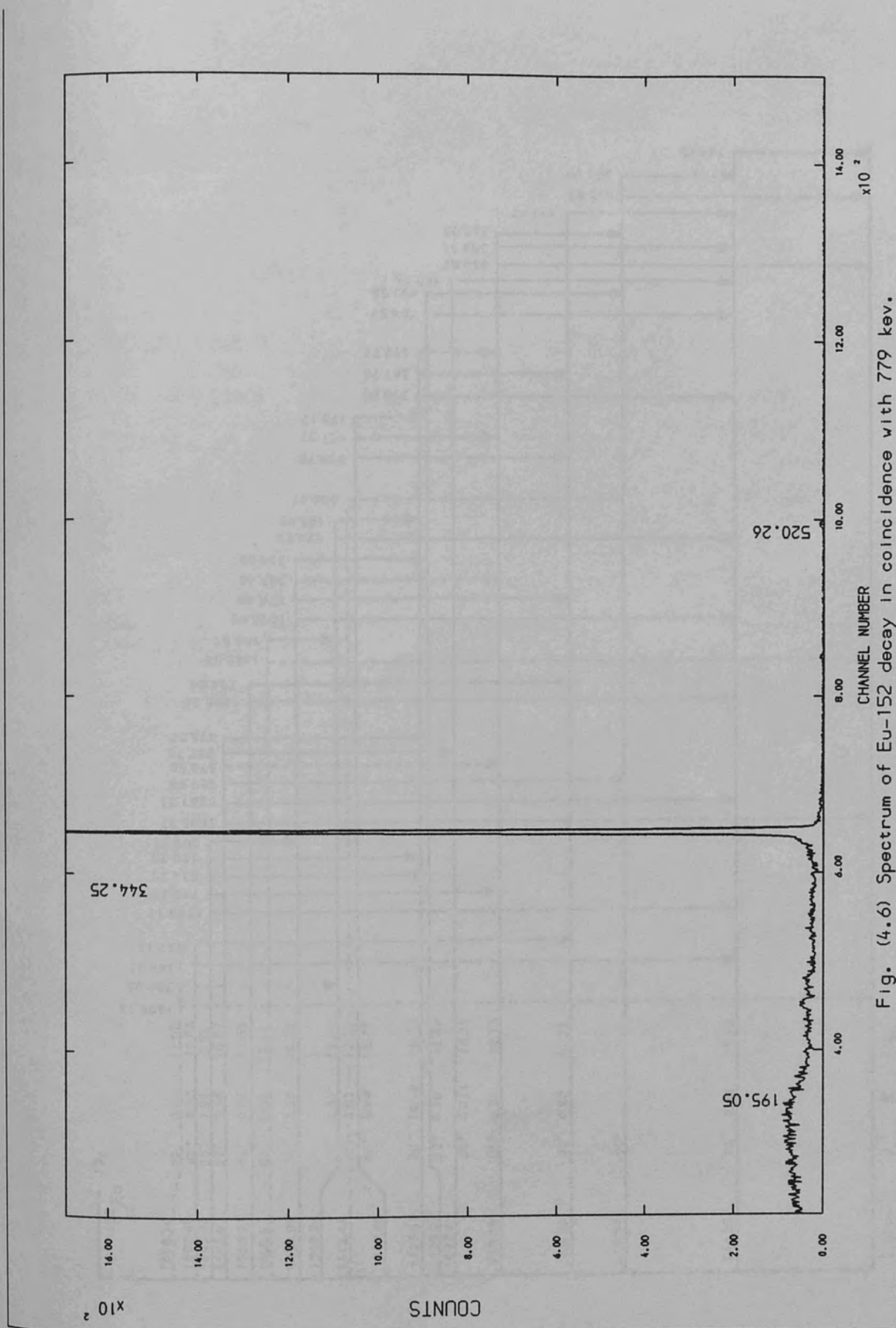
Fig. (4.6) Spectrum of Eu-152 decay in coincidence with 779 kev.
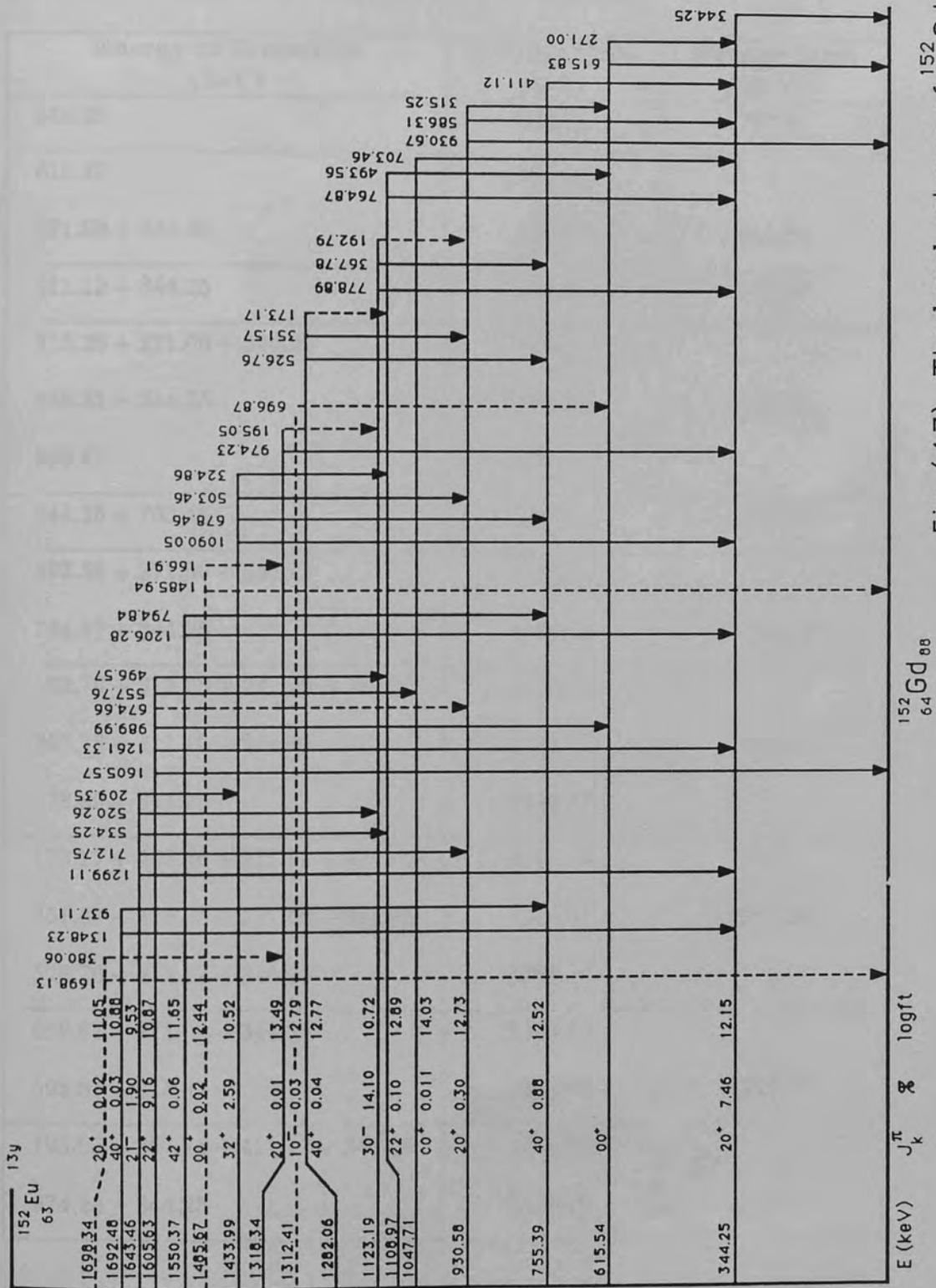
Fig (4.7) The level scheme of ^{152}Gd

Table (4.3)

Summary of energy (keV) sum relations in ^{152}Gd nucleus.

Energy of Transition (keV)	Energy Sum (keV)	Energy Level (keV)
344.25	344.25	344.25
615.83	615.83	
271.00 + 344.25	615.25	615.54
411.12 + 344.25	755.39	755.39
315.25 + 271.00 + 344.25	930.50	
368.31 + 344.25	930.56	930.58
930.67	930.67	
344.25 + 703.46	1047.71	1047.71
493.56 + 271.00 + 344.25	1108.81	
764.87 + 344.25	1109.12	1108.97
192.79 + 315.25 + 271.00 + 344.25	1123.29	
367.78 + 411.12 + 344.25	1123.15	1123.19
778.89 + 344.25	1123.14	
173.17 + 493.56 + 271.00 + 344.25	1281.98	
351.57 + 315.25 + 271.00 + 344.25	1282.07	1282.06
526.76 + 411.12 + 344.25	1282.13	
696.87 + 271.00 + 344.25	1312.12	
696.87 + 615.83	1312.70	1312.41
195.05 + 367.78 + 411.12 + 344.25	1318.20	
974.23 + 344.25	1318.48	1318.34

Table (4.3) (continued)

Energy of Transition (keV)	Energy Sum (keV)	Energy Level (keV)
324.86 + 493.56 + 271.00 + 344.25	1433.67	
503.46 + 586.31 + 344.25	1434.02	
678.62 + 411.12 + 344.25	1433.99	1433.99
1090.05 + 344.25	1434.30	
166.91 + 974.23 + 344.25	1485.39	
1485.94	1485.94	1485.67
794.84 + 411.12 + 344.25	1550.21	
1206.28 + 344.25	1550.53	1550.37
496.57 + 493.56 + 615.83	1605.96	1605.58
557.76 + 703.46 + 344.25	1605.47	
674.66 + 930.67	1605.33	
1605.57	1605.57	
209.35 + 503.46 + 315.25 + 271.00 + 344.25	1643.56	
520.26 + 192.79 + 586.31 + 344.25	1643.61	
534.25 + 764.87 + 344.25	1643.37	1643.46
712.75 + 930.67	1643.42	
1643.32	1643.32	
937.11 + 411.12 + 344.25	1692.48	
1348.23 + 344.25	1692.48	1692.48
380.06 + 974.23 + 344.25	1698.54	
1698.13	1698.13	1698.34

well determined to be 0^+. This means that the B.R. of this level must be $\ll 0.01$ because this figure will give a logft value of about 16, which agrees with the deduced spin and parity.

Table (4.5) shows experimental and theoretical K-shell conversion coefficients for β^--decay of ^{152}Eu (α_k). The electron intensities are according to Malmsten et al[22] and the relative intensities of the γ-transitions were taken from the singles measurements reported in this study. The experimental (α_k) values were normalized to the 344.25 keV transition, which is considered to be a pure E2 transition. Good agreement between theoretical and experimental (α_k) values is shown in Table (4.5). This enables correct multipolarity for the given transitions to be assigned, these deduced multipolarities were written in the last column of Table (4.5).

4.3.1 Discussions of Individual Levels in ^{152}Gd

4.3.1.1 The 344.25, 615.54 and 755.39 keV levels

These are the well-known first (2^+), second (0^+), and third (4^+) excited states in ^{152}Gd , which have been studied in the past through the ^{152}Eu decay[113,115,116], deuteron inelastic scattering experiments[11], and the decay of ^{152}Tb by Gromov et al[100]. The 615.54 keV 0^+ level has also been excited in the decay of ^{152}Eu in this study since the 271.00 keV transition deexciting this state to the 344.25 keV level has clearly been seen in coincidence with the 344.25 keV gated spectrum. The spin of the 755.39 keV level was confirmed from the α_k value of the 411 keV transition depopulating this level (Table 4.5) to the first excited state. The calculated logft value for this level gives another support for the 4^+ assignment

131

Table (4.4)

Summary of the levels properties in ^{152}Gd.

Energy level (keV)	Q_{value} $\varepsilon_\beta = 1819.2$	$\sum I_\gamma$ feed	$\sum I_\gamma$ decay	$\sum I_\gamma$ decay $-I_\gamma$ feed	B.R %	$\log ft$
344.25	1474.95	72.86	100	27.14	7.46	12.15
615.54	1203.66	0.47	0.3	–	–	–
755.39	1063.81	5.23	8.44	3.21	0.88	12.52
930.58	888.62	1.15	2.22	1.07	0.30	12.73
1047.71	771.49	0.04	0.08	0.04	0.01	14.03
1108.97	710.23	0.50	0.86	0.36	0.10	12.89
1123.19	696.01	0.32	51.61	51.29	14.10	10.72
1282.06	537.14	0.02	0.16	0.14	0.04	12.77
1312.41	506.79	–	0.12	0.12	0.03	12.79
1318.34	500.86	0.08	0.10	0.02	0.01	13.49
1433.99	385.21	0.03	9.45	9.42	2.59	10.52
1485.67	333.63	–	0.06	0.06	0.02	12.44
1550.37	268.83	–	0.20	0.20	0.06	11.65
1605.58	213.55	–	0.56	0.56	0.15	10.87
1643.46	175.74	–	6.90	6.90	1.90	9.53
1692.48	126.72	–	0.11	0.11	0.03	10.88
1698.34	120.86	–	0.06	0.06	0.02	11.05

Table (4.5)

Comparison between experimental and theoretical α_k conversion coefficients. The deduced multipolarities are shown in the last column.

Energy (keV)	$J_i^\pi \to J_f^\pi$	Experimental $\alpha_k(\times 10^4)$	Theoretical $\alpha_k(\times 10^4)$			Deduced Multi-polarity
			E1	E2	M1	
271.00	$0^+ \to 2^+$	302 (118)	207	764	1299	$E2$
315.25	$2^+ \to 0^+$	218 (141)	125	419	759	$E2$
344.25	$2^+ \to 0^+$	300 (17)	104	341	628	$E2$
367.78	$3^- \to 4^+$	60.08 (8.6)	93.07	300	556	$E1$
411.12	$4^+ \to 2^+$	173 (18)	72	225	423	$E2$
503.46	$3^+ \to 2^+$	103 (35)	43	123	239	$E2$
586.31	$2^+ \to 2^+$	262 (50)	33	174	291	$M1$
615.83	$0^+ \to 0^+$	8333 (2421)	29	80	152	$E0$
678.62	$3^+ \to 4^+$	46 (16)	21	54	103	$E2$
764.87	$2^+ \to 2^+$	50 (17)	18	46	86	$E2$
778.89	$3^- \to 2^+$	16.31 (1.9)	17	45	82	$E1$
1299.11	$2^- \to 2^+$	8.04 (2.06)	6.7	16	25	$E1$

for it (Table 4.5). The IBM calculations of the ground state band 2^+ and 4^+ are found to be in poor agreement with the experimental values, while the 615.25 keV (0^+) is in very good agreement.

4.3.1.2 The 930.58 keV (2^+) level

The existence of this level was established by Toth et al[99] and Dzhelepov et al[115] in the decay of ^{152}Eu . Furthermore, Gromov et al[100] have reported the population of this state in the decay of ^{152}Tb and Bloch et al[103] found that this level had a rather large cross section in their ^{152}Gd (d,d′) experiments. The presence of the 586.31 and 315.25 keV transitions in the 344 keV gated spectrum totally verifies the existence of this level. The conversion coefficient of the 315.25 keV transition is consistent with the E2 character that is expected. The 930.67 keV transition is the crossover decaying to the ground state of ^{152}Gd . The angular correlation by Barratte et al[119] showed that the 586.31 keV transition ($2_\beta \rightarrow 2_g$) has a relatively large M1 mixing [see Table (4.5) and Ref. (117)]. The IBM prediction gave a lower value of energy for this level than the experimental.

4.3.1.3 The 1047.71 keV (0^+) level

The existence of this level was established by Gromov et al[100] who in their electron conversion measurements on the ^{152}Tb decay placed two E0 transitions as de-exciting this level to 615.54 keV (0^+) level and to the ground state. It is believed that the presence of this level in ^{152}Gd has been detected in this work. In fact, in the ^{152}Eu decay the 703.46 keV transition was found to be in coincidence with the 344 keV[97,104,111,118]. Since no other sum-peaks involves the 703.46 transition, this γ-ray must decay directly to the 344.25 keV level from the 1047.71 keV (0^+) state. The 1047.71 keV level does not seem to be detected in the work of Bloch et al[103] and Sharma et al[105]. This is a probable indication that this state does not have collective characteristics. The IBM calculation

[Section 4.5.2] suggests that there should be an 0^+ level, but is higher value than the experimental [Table 4.6].

4.3.1.4 The 1108.97 keV (2^+) level

This level is assigned as 2^+ on the basis of the 764.87 keV and supported by Gromov et al[100]. Coincidence measurements also established this level which is depopulated by the 493.56 and the 192.79 keV transitions to the 0^+ and 2^+ respectively. The IBM predicted a value as 2^+, which agrees with the experimental.

4.3.1.5 The 1123.19 keV (3^-) level

This state is the lowest negative-parity level established in the past[100,113,119]. The 3^- assignment follows from the E1 character of the 778.89 and 367.78 keV transitions [Table 4.5], and agrees with that made previously by Bloch et al[103]. The spin and parity were also confirmed from logft values [Table 4.4].

4.3.1.6 The 1282.06 keV (4^+) level

Bloch et al[103] observed this level in (d,d') reaction and proposed the 4^+ assignment. It has been observed by Gono et al[117], who was able to excite several states in ^{152}Gd by the ^{150}Sm (α,2n) ^{152}Gd and ^{153}Eu (p,2n) ^{152}Gd reactions. The coincidence experiments show that 526.76 and 351.57 keV transitions feed the 755.39 and 930.58 keV levels respectively. It is believed that the presence of this level in ^{152}Gd has also been envisaged in this investigation since two weak transitions 526.76 and 351.57 keV have been detected in the decay of ^{152}Eu . These two gamma-rays could not be placed elsewhere in the decay scheme of both ^{152}Sm and ^{152}Gd except by involving the existence of a level at 1282.06 keV in ^{152}Gd , in agreement with previous result[113]. The spin and parity are

confirmed as well from logft value and our IBM calculations [see Tables 4.5 and 4.6].

4.3.1.7 The 1312.41 keV (1⁻) level

This level is suggested by the new transition at 696.87 keV which is in weak coincidence with the 344 keV gate. Such a level was inferred by early work[103,118,120]. on the decay of ^{152}Tb ($t_{\frac{1}{2}}$ =17.5 h). The present logft value of 12.8 is consistent with a spin parity of 1⁻ as suggested by theoretical studies[121] on the negative parity states of ^{152}Gd .

4.3.1.8 The 1318.34 keV (2⁺) level

The existence of this state in ^{152}Gd levels structure is inferred from de-exciting of the 195.05 and 974.23 keV to the 3⁻ and 2⁺ levels respectively. This is in agreement with the Gromov et al[100] and Zolnowski et al[118]. The spin and parity of this level is supported from logft values and the IBM calculation.

4.3.1.9 The 1433.99 keV (3⁺) level

The existence of a state at 1433.99 keV is confirmed by the observance of the 1090.05, 678.62, and 503.46 transitions in coincidence with the 344.25, 411.12 and 586.31 keV transitions, respectively. Varnell et al[116] placed this level correctly, which is in good agreement with the present result. The angular correlation experiments[119,122] established the spin value of this state as 3⁺, which the IBM predicted as a lower value. This assignment is also consistent with the fact that the 1433.99 keV level is not observed in (d,d') experiments[103].

4.3.1.10 The 1485.67 keV (0⁺) level

The new level at 1485.67 keV is suggested by the observance of two new transitions at 166.91 and 1485.94 keV. The 1485.94 keV transition goes direct to the

ground state, and is seen in the singles only, but as the 166.9 keV gamma-ray is in strong coincidence with the 779 keV gate, it is considered to populate the level at 1318.3 keV. The present study of the IBM calculations do suggest that these should be an 0^+ level between 1460 and 1490 keV. This assignment is supported by the decay of ^{152}Tb , Zolnowski et al[118]

4.3.1.11 The 1550.37 keV (4^+) level

This level has been found by Barratte et al[97]. Coincidence measurements confirm the existence of the level 1550.37, keV since the 1206.28 and 794.84 keV transitions de-exciting this state have been detected in the 344.25 and 411.12 keV gated spectrum, respectively. The spin and parity of this level is supported from the logft values [Table 4.5] and the IBM calculation.

4.3.1.12 The 1605.58 keV (2^+) level

The E2 character of the 989.99 keV transition decaying to the 0^+ state at 615.25 keV suggests the 2^+ assignment for this level[100,118]. This assignment is confirmed by the decay characteristics of this level, as envisaged in this study of the ^{152}Eu decay. The 1605.58 keV transition is placed to the ground state. The 1261.33, 674.66, 557.76 and 496.57 keV transitions de-exciting to the 2^+ first excited state, fourth excited state (2^+), fifth excited state (0^+) and sixth excited state (2^+) in ^{152}Gd , respectively, have been detected in the gating spectra . The 674.66 γ-ray is a composite transition, and it was found, in this study, by the coincidence measurements, and therefore can be placed in the ^{152}Gd level structure. That is supported by other works[100,123]. There is a good agreement with the IBM prediction.

4.3.1.13 The 1643.46 keV (2⁻) level

The 1643.46 keV level has been assigned spin and parity 2⁻ on the basis of directional correlation[122,124] and conversion coefficient measurements[125-127]. The 712.75 keV transition as de-exciting the 1643.46 state to the 930.67 keV (2⁺) is detected in the 586 keV gated spectrum, which would be very reasonable on the basis of spin consideration[116]. Futhermore, the 1299.11, 534.25, 520.26, and 209.35 keV transitions are placed between this level and 344.25 (2⁺), 1108.97 (2⁺), 1123.19 (3⁻) and 1433.99 (3⁺) keV states, respectively. The placing of these transitions are supported by the present coincidence measurements [Table 4.2] and energy sum relations. The present logft value of 9.53 is consistent with a spin and parity of 2⁻, as suggested earlier.

4.3.1.14 The 1692.48 keV (4⁺) level

The existence of the 1692.48 keV level is supported by the coincidence measurements and decays via 1348.23 and 937.11 keV which were detected in coincidence with the 344.25 and 411.12 keV transitions. The absence of a transition to the ground state and the E2 nature[118] of the 1348.23 keV transition make the 4⁺ assignment most likely. This assignment is supported by the logft value and the IBM calculation is in very good agreement.

4.3.1.15 The 1698.34 keV (2⁺) level

The new level at 1698.34 keV is suggested by the transition at 380.06 and 1698.13 keV: the former is in weak coincidence with the 344 and 586 keV gates, so it can go to the well established level at 1318.34 keV; the latter is seen in singles only, as it is direct to the ground state. The logft value of 10.6 is consistent with a spin and parity of 2⁺, which would be required of a second

level in a third β-band starting with the 0^+ state at 1485.89 keV. Such a β-band is found in the IBM calculations, but the 2^+ state is raised higher in energy.

4.4 Nuclear Model Calculations

4.4.1 Collective Model

The ^{152}Gd nucleus with 64 protons and 88 neutrons (as well as the ^{150}Sm nucleus with 62 protons and 88 neutrons) lies at the edge of the so-called transitional region, namely the region where the level properties of the nuclei having N≤88 seem to be drastically different from those of nuclei having N≥90. In the usual simple picture, the nuclei with N≤88 are said to belong to the "vibrational region", whereas the nuclei with N≥90 form a "rotational region". Shiline et al[128] was the first to propose the existence of a correlation in the level structure of the "transitional" nuclei. Sakai et al[129] suggest that the so-called "vibrational" nuclei should be regarded more in a framework of a rotational picture than a vibrational one. In this respect, following Sakai's idea, ground-state rotational, β- and γ-bands should be present also in ^{152}Gd . This suggestion, as far as the ^{152}Gd nucleus is concerned, is supported by other work[11,66,96,97,103,117]. The ^{152}Gd is considered as a deformed nucleus and calculation based on rotational theory will be applied to it. The two parameters A and B from Eq. (2.2.2.6) where determined by fitting the experimental energies of the first two excited states of the bands. Table (4.6) shows together the energies found experimentally and also the theoretical calculations. Fig. (4.8) shows the experimental and theoretical (rotational) energy levels as determined in this work.

The experimental results · in this work for ^{152}Gd , and the data obtained in a previous investigation[97,117,118], show in a neat and dramatic manner that the ^{152}Gd displays a rotational nature, and not a vibrational one as previously suggested[8,100]. This is shown in Figs. (4.8, 4.9), where the experimental states in ^{152}Gd and theoretical calculation are presented for comparison.

4.4.1.1 The ground state band

A ground state band has been proposed with levels at 344.25 (2$^+$) and 755.39 (4$^+$) in ^{152}Gd and is also observed in the ^{152}Tb (17.5 h) decay.

4.4.1.2 The β-band

The 0$^+$, 2$^+$ and 4$^+$ levels of this band are observed in this work and have energies of 615.54, 930.58 and 1282.06 keV. Several workers supported the interpretation of these levels as members of a β-band (k$^\pi$=0)[11,66,97,103-105,113,118,136,137].

If these levels are indeed analogous to β-vibrational levels in deformed nuclei, one would expect the relative B(E2) ratios for these levels to be similar to those for the β-bands in the nearby deformed nuclei ^{154}Gd and ^{152}Sm, as can be seen from Table (4.7). Another piece of evidence is found in (d,d') reaction studies[103], where the excitation cross sections for these β-bands levels resemble those found for β-bands in deformed nuclei. The fact that the level spacing is less than that found in the ground state band also indicates a more collective nature for these levels.
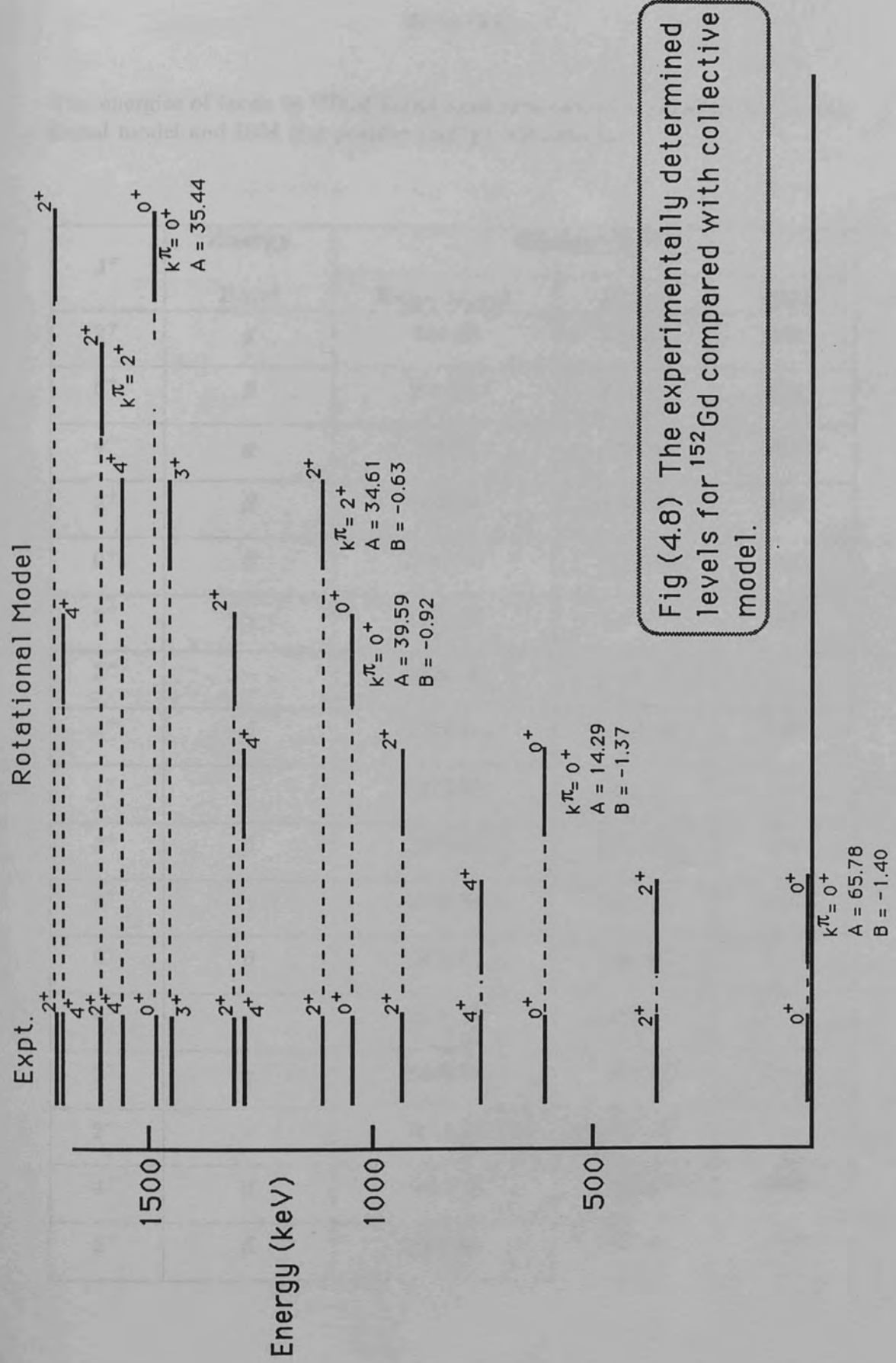
Fig (4.8) The experimentally determined levels for ^{152}Gd compared with collective model.

Table (4.6)

The energies of levels in ^{152}Gd found experimentally compared with the rotational model and IBM (for positive parity) calculations.

J^π	Energy Band	Energy (keV)		
		Experiment	Rotor	IBM
2^+	g	344.25	344.25	399
0^+	β	615.54	615.25	619
4^+	g	755.39	755.39	792
2^+	β	930.58	930.58	828
0^+	β	1047.71	1047.71	1081
2^+	γ	1108.97	1108.97	1027
3^-	$-$	1123.19	1123.19	$-$
4^+	β	1282.06	1282.06	1195
1^-	$-$	1312.41	1312.41	$-$
2^+	β	1318.34	1318.36	1344
3^+	γ	1433.99	1433.99	1347
0^+	β	1485.67	1485.67	1461
4^+	γ	1550.37	1632.88	1459
2^+	γ	1605.58	1605.58	1595
2^-	$-$	1643.46	1643.46	$-$
4^+	β	1692.48	1692.48	1689
2^+	β	1698.34	1698.34	1832

4.4.1.3 The second β-band

At approximately twice the energy of the β-vibrational band in deformed nuclei, one would expect to find a rotational band (k=0) corresponding to the coupling of two β-vibrational phonons. It is expected that the members of such a band would decay preferentially to one-phonon states rather than to the members of the ground state rotational band.

A group of levels analogous to such a band is observed in ^{152}Gd with energies 1047.71 (0^+), 1318.34 (2^+), and 1692.48 (4^+). A similar one has been observed in ^{154}Gd by Meyer et al[39], who describes it as a second β band.

4.4.1.4 The third β-band

The level at 1485.67 is assigned as the band-head of the third k=0 band[117], since such a band is expected to be located in ^{152}Gd at about 2 MeV. This is supported by our IBM calculations for this assignment and the 1698.34 keV (2^+) is a first excited state for this band.

4.4.1.5 The γ-band

The $2^+, 3^+$ and 4^+ levels of this band are observed at 1108.97, 1433.99, and 1550.37 keV, respectively. The apparent absence of any E0 admixture in the 764.87 keV $2_\gamma^+ \rightarrow 2_g^+$ transition supports a "k=2" designation. Both the 1108.97 and 1550.37 keV levels are seen in (d,d') reaction studies and hence are probably collective states. The experimental B(E2) ratios for the members of this band are given in Table (4.8) and are compared to other transitional nuclei and the theoretical prediction of the IBM.

Table (4.7)

Experimental B(E2) branching ratios for transitions from positive parity states in ^{152}Gd compared with adiabatic rotor[104].

Transition $\mathbf{E_\gamma / E'_\gamma}$	Energy level (kev)	$\mathbf{J_i \to J_f}$ $\overline{\mathbf{J_i \to J_f}}$	B(E2) Ratio		
			Experimental	Theory	IBM
$\dfrac{315.25}{586.31}$	930.58	$\dfrac{2_\beta \to 0_\beta}{2_\beta \to 2_g}$	2.29 (0.39)	0.70	0.807
$\dfrac{930.67}{586.31}$	930.58	$\dfrac{2_\beta \to 0_g}{2_\beta \to 2_g}$	0.017 (0.002)	0.70	0.049
$\dfrac{351.57}{526.76}$	1282.06	$\dfrac{4_\beta \to 2_\beta}{4_\beta \to 4_g}$	10.07 (4.2)	1.1	3.419
$\dfrac{1206.28}{794.84}$	1550.37	$\dfrac{4_\gamma \to 2_g}{4_\gamma \to 4_g}$	0.042 (0.018)	1.1	0.067

4.4.1.6 The second γ-band

It is possible to have a two-phonon state resulting from the coupling of one β-vibrational phonon and one γ-vibrational phonon. The band-head energy of such state would be expected to be approximately the sum of β-and γ-band-heads. The 1605.58 (2$^+$) keV level in ^{152}Gd is predicted as a member of the second γ-band in the present IBM calculations. The assignment of this level, supported by studies of the decay of the 496.57 keV transition between the 2$^+$ level at 1605.58 and the 2$^+$ state of the γ-band at 1108.97 keV, has a large internal conversion coefficient[118], thus indicating the likelihood of some E0 admixture. Anderson and Ewan[131] have reported large E0 components in the transitions between 2$^+$ and 3$^+$ levels of a second k=2 band and the corresponding 2$^+$ and 3$^+$ level of the k=2 γ-vibrational band for the case of ^{154}Gd. They have suggested that the upper k=2 band may be a β-virational band built on the γ-vibrational band.

4.4.1.7 The Negative Parity States

In the transition to a deformed equilibrium shape the octupole states found in spherical nuclei are expected to separate into K = 0$^-$,1$^-$,2$^-$ and 3$^-$ components. The k=0 band is predicted to be the lowest in energy, and to be the most collective in character[132].

In ^{152}Gd 3$^-$ and 1$^-$, levels were observed at 1123.19 keV and 1312.41 keV, respectively. The B(E1) ratios for transitions from these levels are given in Table (4.9), and are compared to the ratios for k=0 octupole states in other transitional nuclei. The inverted order of the 1$^-$ and 3$^-$ states may be due to a Δk=1 coupling with the k=1 band and possibly other negative bands nearby.

Table (4.8)

B(E2) Ratio for γ-bands.

Energy level (keV)	$J_i \rightarrow J_f$	B(E2) Ratios		
		^{152}Gd	^{154}Gd (a)	^{152}Sm (b)
1108.97	$\dfrac{2_\beta \rightarrow 0_g^+}{2_\beta \rightarrow 2_g}$	1.31(0.25)	0.14(0.05)	–
1433.99	$\dfrac{3_\gamma \rightarrow 2_g}{3_\gamma \rightarrow 4_g}$	1.00(0.09)	1.26(0.04)	1.19(0.03)
1433.99	$\dfrac{3_\gamma \rightarrow 2_\gamma}{3_\gamma \rightarrow 2_g}$	18.46(0.69)	18.74(1.56)	80.20(3.24)
1550.29	$\dfrac{4_\gamma \rightarrow 2_\gamma}{4_\gamma \rightarrow 4_g}$	0.04(0.01)	0.15(0.02)	0.09(0.06))

(a) Calculated from the intensities given in Ref. [13]. The level energies in ^{154}Gd are 996.3 (2^+), 1127.8 (3^+) and 1263.8 keV (4^+).

(b) Calculated from the intensities given in Table (4.1). The level energies in ^{152}Sm are 1086.10 (2^+), 1234.15 (3^+) and 1371.71 keV (4^+).

Because this coupling would shift the odd-spin members of k=1 band to higher energies, the lowest observed member of the k=1 band is the 2⁻ state at 1643.46 keV. A similar inversion of levels is observed in the neighboring, nucleus ^{154}Gd. The B(E1) ratios for transitions from the 1643.46 keV are also given in Table (4.9).

4.4.2 The IBM Calculations and Result

The ^{152}Gd was considered as a deformed nucleus, showing rotational spectra as reported [97,98,102,118]. However, rotational theory expects R= 3.33 by Bloch et al[103], whereas the experimental value is 2.2, closer to the value of 2.0 as expected for a vibrational nucleus. Since a spherical nucleus should exhibit vibrational characteristics, Casten et al[96] suggested that ^{152}Gd should exist in a region where a spherical-deformed phase transition is occurring. It is to be expected that such a nucleus should be described in terms of the IBM, as transitional between the SU(5) vibrational, and SU(3) rotational, limits.

The calculations were done using the IBM computer codes PHINT for energies and FBEM for B(E2) values[62]. The number of bosons implied by the number of valence neutrons and protons in ^{152}Gd is 10. The inclusion of an F boson, to generate negative parity states, then produces a severe computational problem in terms of the dimensions of the matrices, which must be diagonalized. For this reason, the calculations have been limited to the positive parity bands.

With the framework of the IBM[8,10], the ^{152}Gd is considered as transitional nucleus between SU(5) and SU(3)[11,66,72,96], and calculations were made with transitional Hamiltonian [Eq. (2.3.3.a.1)].

147

Table (4.9)

B(E1) Ratios for transitions from negative-parity states.

Energy level (keV)	$\dfrac{J_i \rightarrow J_f}{J_i \rightarrow J_f}$	B(E1) Ratios		
		^{152}Gd	^{154}Gd (a)	^{152}Sm (b)
1123.19	$\dfrac{3^- \rightarrow 4_g^+}{3^- \rightarrow 2_g}$	0.62(0.01)	1.27(0.38)	1.51(0.25)
1643.46	$\dfrac{2^- \rightarrow 2_\beta}{2^- \rightarrow 2_g}$	0.36(0.03)	0.26(0.01)	0.31(0.07)
1643.46	$\dfrac{2^- \rightarrow 2_\gamma}{2^- \rightarrow 2_g}$	0.35(0.07)	0.18(0.03)	36.74(1.31)
1643.46	$\dfrac{2^- \rightarrow 3_\gamma}{2^- \rightarrow 2_\gamma}$	3.32(1.29)	0.04(0.01)	0.59(0.03))

(a) Calculated from the intensities given in Ref. [105]. The level energies in ^{154}Gd are 1251.6 (3^-) and 1397.53 keV (2^-).

(b) Calculated from the intensities given in Table (4.1). The level energy in ^{152}Sm are 1041.12 (3^-) and 1529.86 keV (2^-) [see Fig. (5.8)].

In the calculation of B(E2) values, the two parameters α_2 and β_2 of Eq. (2.3.1.6) were adjusted to approximately reproduce the measured B(E2, $2_1 \to 0_1$) for excitations of 2_1^+ members of the ground state and gamma-vibrational bands, respectively.

The present IBM calculation predicts the new β-band with the new levels at 1485.67 and 1698.34 keV. The assignment of the 1485.67 keV level is 0^+, which is reported by Zolnowiski et al[118] and is predicted in the present IBM calculation. The 1698.34 keV level is considered to be 2^+, and is predicted in the IBM calculations, although the latter gives a higher values than the experimental energy level. The result of the calculations for the energy levels are shown in Fig. (4.9) and compared with the experiment, while Table (4.6) listed the energy levels.

The values of the parameters used are the first four of the Table (4.10), whereas the remaining two were needed for the calculation of the B(E2) values presented in Table (4.11), which is compared with the data from Gupta[133]. All experimental transitions shown in Table (4.11) are assumed to be pure E2, and the corresponding B(E2) values were deduced[134].

$$B(E2) = \frac{56.3}{E_\gamma^5 t_{\frac{1}{2}}(expt)(1 + \alpha_T)}(e^2 b^2) \tag{4.4.2.1}$$

The above Eq. (4.4.2.1) was used, where E_γ is the gamma ray transition in keV, $t_{\frac{1}{2}}$(expt) is the half life of a given transition whose value is obtained from Baglin[113] and α_T is the total conversion coefficient.

It can be seen from Fig. (4.9) that the entire theoretical sequence of states has been well reproduced, and is in agreement with the experimental results. Table (4.11) shows a remarkable agreement between theory and experiment for transitions originating within the ground state.

4.5 Conclusion

The nuclear structure of the more "spherical" ^{152}Gd nuclei seems to show a rotational nature more than a "vibrational" one as previously suggested[8,100]. In fact, following a suggestion put forth by Séline[128], and reported in more detail in previous works[97,103,118,126,129], states that groups of levels, which can be labelled as ground state, β-and γ-vibrational bands, seem to be present in ^{152}Gd . The observation of band structure in ^{152}Gd is similar to that observed in ^{154}Gd as a weakly deformed nucleus[99,118]. The rotational theory expects R=3.33 (Bloch et al[103]) for the first two excited states (2^+ and 4^+) of the ground state band, whereas the experimental value is 2.2, is closer to the value 2.0 as expected for a vibrational nucleus. Since a spherical nucleus should exhibit vibrational characteristics, Casten[96] suggested that ^{152}Gd should exist in a region where a spherical to deformed phase transition is occurring. It is to be expected that such a nucleus should be described in term of the IBM as transitional between the SU(5) vibrational, and SU(3) rotational limits. Recently[66,126] ^{152}Gd has also been compared with such transitional IBM calculations. The experimental results agree remarkably with the IBM calculations are listed in Table (4.6) and shown in Fig. (4.9). The parameters used in the IBM calculation are listed in Table (4.10). The IBM calculation predicts a third β-band using Eq. (2.3.3.a.1). Full Hamiltonian and pure SU(5) [Eqs. (2.3.1.4), (2.3.2.7)] were used to compare them with the transitional result, but gave poor agreement and could not explain the ^{152}Gd in terms of transitional nucleus.
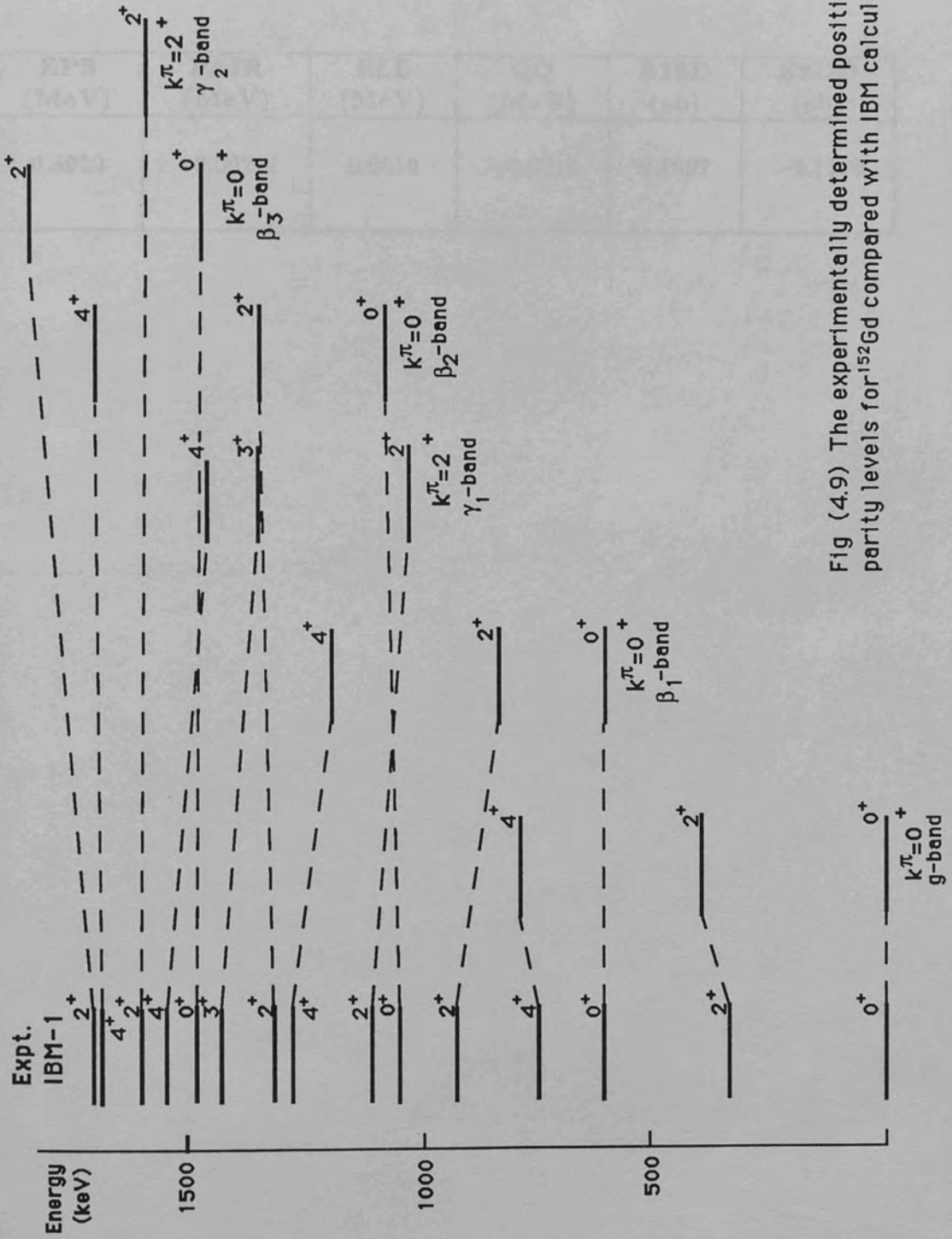
Fig (4.9) The experimentally determined positive parity levels for ^{152}Gd compared with IBM calculations.

Table (4.10)

Parameters used in programs PHINT and FBEM to calculate positive parity states and absolute B(E2) values.

EPS (MeV)	PAIR (MeV)	ELL (MeV)	QQ (MeV)	E2SD (eb)	E2DD (eb)
0.3910	−0.00221	0.0010	−0.0210	0.1897	−0.1190

Table (4.11)

Experimental absolute B(E2) values (e^{2}b^2) in comparison with IBM prediction.

Energy	Transition	B(E2) Values		
(keV)	$J_i \to J_f$	Experiment	Gupta [45]	IBM
344.25	$20^+ \to 00^+$	0.327	0.330	0.327
411.12	$40^+ \to 20^+$	0.643	0.640	0.647
586.31	$20^+ \to 20^+$	0.110	0.077	0.371
271.00	$00^+ \to 20^+$	0.958	0.850	0.841

Table (4.7) shows the B(E2) ratios from some positive parity states. The theoretical values[97] were calculated using the adiabatic rotor model[104]. While the experimental values for the transitional nucleus were in full agreement with the IBM prediction, there was a significant departure with the rotor model theory. This indicated that these states are quasi-rotational. The ratio of B(E2,494)/B(E2,765) from the γ-band at level 1108.97 keV to β-band at level 615.54 keV and to level 344.25 keV ground band is 0.45 ± 0.06. The experimental B(E2) values were in full agreement with IBM prediction (Table 4.11).

The decay scheme of ^{152}Gd has been studied on several occasions[97,98,104−112], and were mostly singles measurements. Sharma[105] provided the most complete list of energies and intensities, but, however, missed many. In this study using singles and coincidence techniques, the analysis has shown eight new transitions. There are several differences in many of the intensity and energy values previously reported[97,98,104−112]. However, a remarkable agreement is observed with Baker et al[104] and Sharma et al[105] [Table (4.1)].

The Ge(Li)-Ge(Li) coincidence measurements carried out in this study and the energy values of the γ-rays do not allow any other placing of the transitions except that established in Fig. (4.7).

Ismail[111] has proposed a new level at 1381 keV (4$^+$), which depopulates via the 258 keV transition. This level has not been reported in previous works[97,98,104−112]. In this study it could neither be supported experimentally, nor predicted by the IBM calculations. It is therefore believed that the 258 keV transition is background from the ^{214}Pb in the reactor.

The transition 1643.60 keV, which was detected by Sharma et al[105], who could not place it in the decay scheme, has also been observed in this investigation in Singles, but not in coincidence, is considered as due to summing effects

(1643.36 = 344.25 + 1299.11). The placement of the 674.66 keV transition between level 1605.58 keV (2$^+$) and level 930.58 keV (2$^+$) in ^{152}Gd is supported by other works[98,123].

Three new levels have been introduced together with eight new transitions. The existence of these levels has been confirmed from coincidence data and theoretical calculations. The spins and parities for these levels have been assigned from logft values and other possible information. For level at 1550.37 keV the spin was confirmed as 4$^+$, the spin of the level 1692.48 keV was confirmed to be the new value 4$^+$. The spin of the level 1605.58 keV is confirmed to be 2$^+$. The new levels at 1485.67 and 1698.34 keV were assigned spin and parity values of 0$^+$ and 2$^+$, respectively, for the third β-band. The new level at 1312.41 keV was assigned to be (1$^-$), this level forms together with the level 1123.19 keV (3$^-$) an octupole band. The new energy 195.05 keV was placed in the decay scheme according to the coincidence data.

CHAPTER V
STUDIES OF THE LOW-LYING STATES
IN ^{152}Sm ISOTOPE

5.1 Introduction

^{152}Eu has a very long half life ($t_{\frac{1}{2}}$=13.33 y). It decays by EC and β^+ to establish the decay scheme of ^{152}Sm . Nuclei with N=90 are belived to be slightly deformed, and therefore show rotational-like spectra. The even-even ^{152}Sm nucleus lies on the edge of this deformation region[4,98]. This left many authors to consider it as transitional between spherical and deformed nuclei. The region of deformed nuclei extends from A=150 to 190. As a consequence of the nuclear "softness", the β and γ-vibrational bands lie at lower excitation energies than the corresponding states of more rigid nuclei in the middle of the deformed rare-earth region[97].

The B(E2) branching ratios show disagreement with rotation theory even if the mixing of β and γ bands into ground state band (first order effect) or the mixing of the β and γ bands into each other (second order effect) are allowed. This is a general feature of all the rotational nuclei clustering around the "transitional region"[138] and cannot be explained by the simple collective model of Bohr and Mottelson[3]. The level at 1293 keV is of special interest. Schick[139] suggested that this level may be the 2^+ member of the two phonon β-vibrational band. The result from the two nucleon transfer reaction supports this approach[140,154]. In the (t,p) reaction on ^{150}Sm leading to states in ^{152}Sm , Hinds et al[140] and Passoja et al[141] found evidence for the 0_3^+ states; the ground state, the β

vibrational band-head and the 1082 keV (unseen). This suggests that there is "spherical" excitation coexisting with rotational excitation. Therefore, an interaction between spherical and deformed states in ^{152}Sm is expected to happen. In this work, the rotational collective model was applied to calculate the energy spectra, which were compared with the experimental results. Comparisons were made with predictions of the IBM calculation on the basis of transitional[11,142] nucleus between the SU(5) vibrational and the SU(3) rotational limits.

The results of this study of the intensities of the γ-rays emitted in the decay of ^{152}Eu were given in the previous chapter. Table (4.1) shows that five new transitions were observed in case of ^{152}Sm (one of these confirmation of a transition reported only by Baglin[113]). The existence of two new energy levels was confirmed from coincidence and energy band calculations. The logft values and multipolarities were calculated, spins and parities deduced.

5.2 Singles and Coincidence Spectra

In chapter IV, the method of measuring the singles spectra following the decay of ^{152}Eu was described. These spectra were shown in Fig. (4.1) and the results were tabulated in Table (4.1). Although the most extensive coincidence measurements on the ^{152}Sm isotope were carried out by Baker et al[104], the most complete analysis were reported by Barratte et al[97] who only took two gates (122 and 689 keV) to establish the decay scheme. During the course of this study the seven gates at 122, 244, 444, 686, 842, 919, 964 keV were chosen to provide sufficient coincidence data to establish the decay scheme. These gates provide a large amount of coincidence data and are well separated from other

Table (5.1)

Summary of the γ-γ coincidence results from the decay of the ^{152}Eu.

Energy	Gates (keV)						
(keV)	122	245	444	689	842	919	964
121.78	−	x	x	x	x	x	x
125.69	x	−	x	−	−	−	−
147.94	x	x	x	x	−	−	x
202.61	x	x	x	x	x	−	x
206.95	x	x	−	−	−	−	−
212.50	x	x	x	x	x	x	x
237.38	x	x	x	x	x	x	−
239.47	x	x	x	x	x	x	x
244.68	x	−	x	−	−	−	−
251.61	x	−	−	−	−	x	−
271.00	x	−	−	−	x	−	−
275.43	x	x	x	x	−	−	−
286.15	x	x	x	x	−	−	x
295.91	x	x	x	x	x	−	x
315.25	x	x	−	−	−	−	−
329.35	x	−	−	−	x	x	x
340.23	x	x	−	−	−	−	−
385.92	x	x	−	−	−	−	−
389.07	x	x	x	x	x	x	−
395.75	x	−	−	−	−	x	−
416.01	x	x	x	x	x	−	x
423.45	x	x	x	x	−	−	−
443.97	x	x	−	x	−	−	x
482.41	x	x	x	x	−	−	−
488.69	x	−	−	−	−	x	−
493.56	x	x	x	x	−	−	x
523.11	x	x	x	x	x	−	x
556.48	x	x	−	−	−	−	−
563.96	x	x	x	x	−	−	x
566.50	x	−	−	−	x	−	−
595.61	x	x	x	x	−	−	x
615.83	x	−	−	−	x	−	−

Table (5.1) (continued)

Energy	Gates (keV)						
(keV)	122	245	444	689	842	919	964
644.29	x	x	x	x	—	—	x
656.47	x	x	—	—	—	—	—
664.83	x	x	—	—	—	—	—
671.21	x	x	x	x	—	—	x
674.66	x	x	—	—	—	—	—
688.65	x	—	x	—	—	—	—
719.32	x	x	x	x	—	—	—
727.42	x	—	—	—	—	x	—
768.98	x	x	x	x	—	—	—
805.39	x	—	—	—	x	—	—
810.45	—	—	x	—	—	—	—
838.84	x	x	x	x	—	—	—
841.61	x	—	—	—	—	—	—
867.36	x	x	—	—	—	—	—
901.20	x	—	—	—	—	—	—
919.34	x	—	—	—	—	—	—
926.28	x	x	—	—	—	—	—
958.55	x	x	x	x	—	—	—
964.10	x	—	x	—	—	—	—
1005.22	x	x	—	—	—	—	—
1085.89	—	—	x	—	—	—	—
1112.09	x	—	—	—	—	—	—
1170.56	x	—	—	—	—	—	—
1212.92	x	x	—	—	—	—	—
1249.92	x	—	—	—	—	—	—
1315.32	x	x	—	—	—	—	—
1363.72	x	x	—	—	—	—	—
1390.30	x	x	—	—	—	—	—
1408.03	x	—	—	—	—	—	—
1457.55	x	—	—	—	—	—	—
1528.05	x	—	—	—	—	—	—
1608.50	x	—	—	—	—	—	—
1647.42	x	—	—	—	—	—	—

transitions in the spectrum of ^{152}Eu , and at the same time are quite strong peaks. The 121.78 keV transition depopulates the first excited state to the ground state. This means that most of the transitions are in coincidence with this energy. Hence, the first step in coincidence investigations is to take this transition as a gating energy, especially as it leads to a very prominent and well-separated peak. The 443.97 keV transition was suggested to be doublet[113,123], thus this gate provides vital coincidence data to investigate this suggestion, in addition to the fact that this line is a well-separated peak (Fig. 4.1). The two gates 689 and 842 keV provide useful coincidence information for the levels which lie in the middle of the decay scheme. The 919 keV gives coincidence data for the existence of the new transition 395.75 keV and the new energy level at 1436.65 (2^{+}) keV which decays by 395.75 keV transition to the level at 1041.17 (3^{-}) keV. The 964 keV gate gives coincidence data for the existence of the new transition 595.61 keV and the new level at 1681.56 (4^{-}) keV which decays by the new transitions 389.07 and 595.61 keV to the levels 1371.71 (4^{+}) and 1086.10 (2^{+}) keV respectively. The results of these measurements were given in Table (5.1). The coincidence spectra are shown in Figs. (5.1-7).

5.3 Decay Scheme and Level Properties

The decay scheme was established on the basis of the coincidence results of the seven gates (Table 5.1) and the energy sum relations as given in Table (5.2). The decay scheme is shown *in Fig. (5.8) and includes* the logft values, the electron capture (E.C) feeding branching ratios (I$_{EC}$), the spins, the K quantum numbers, the parities and finally, the energy levels in keV. The number at the base of the arrow indicates the energy of the transition. The new transitions and levels reported in this study are shown as dotted lines.
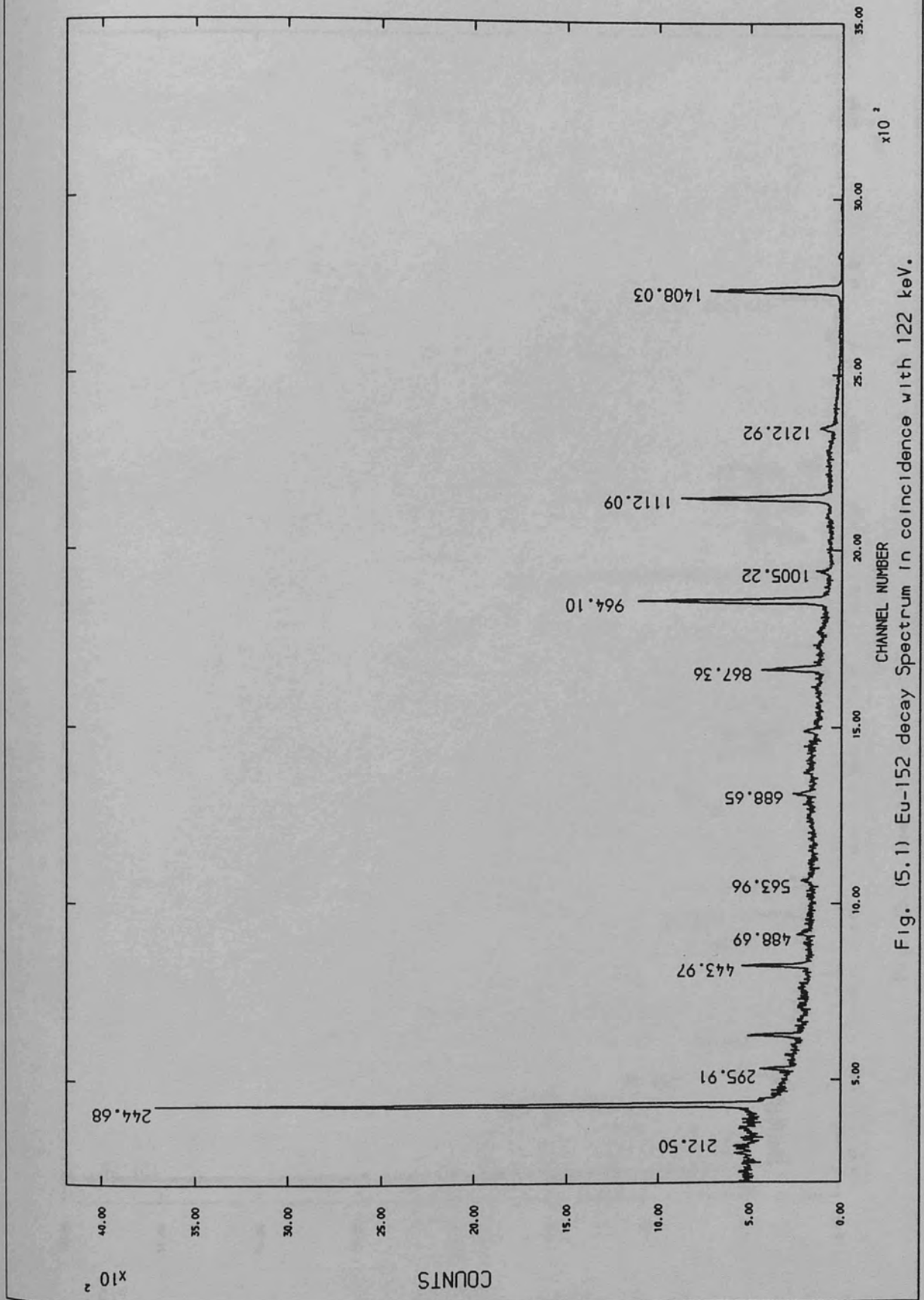
Fig. (5.1) Eu-152 decay Spectrum in coincidence with 122 keV.
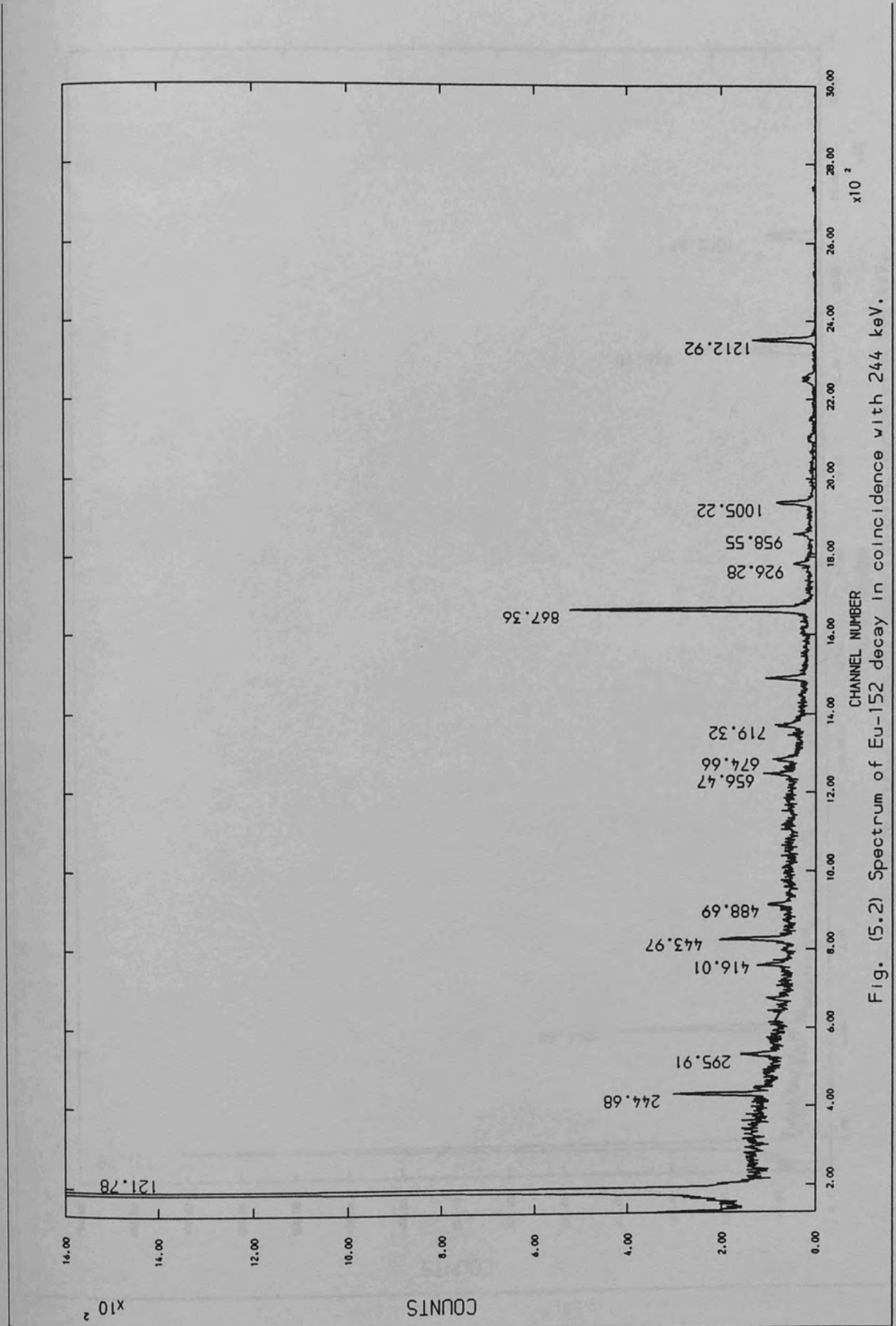
Fig. (5.2) Spectrum of Eu-152 decay in coincidence with 244 keV.
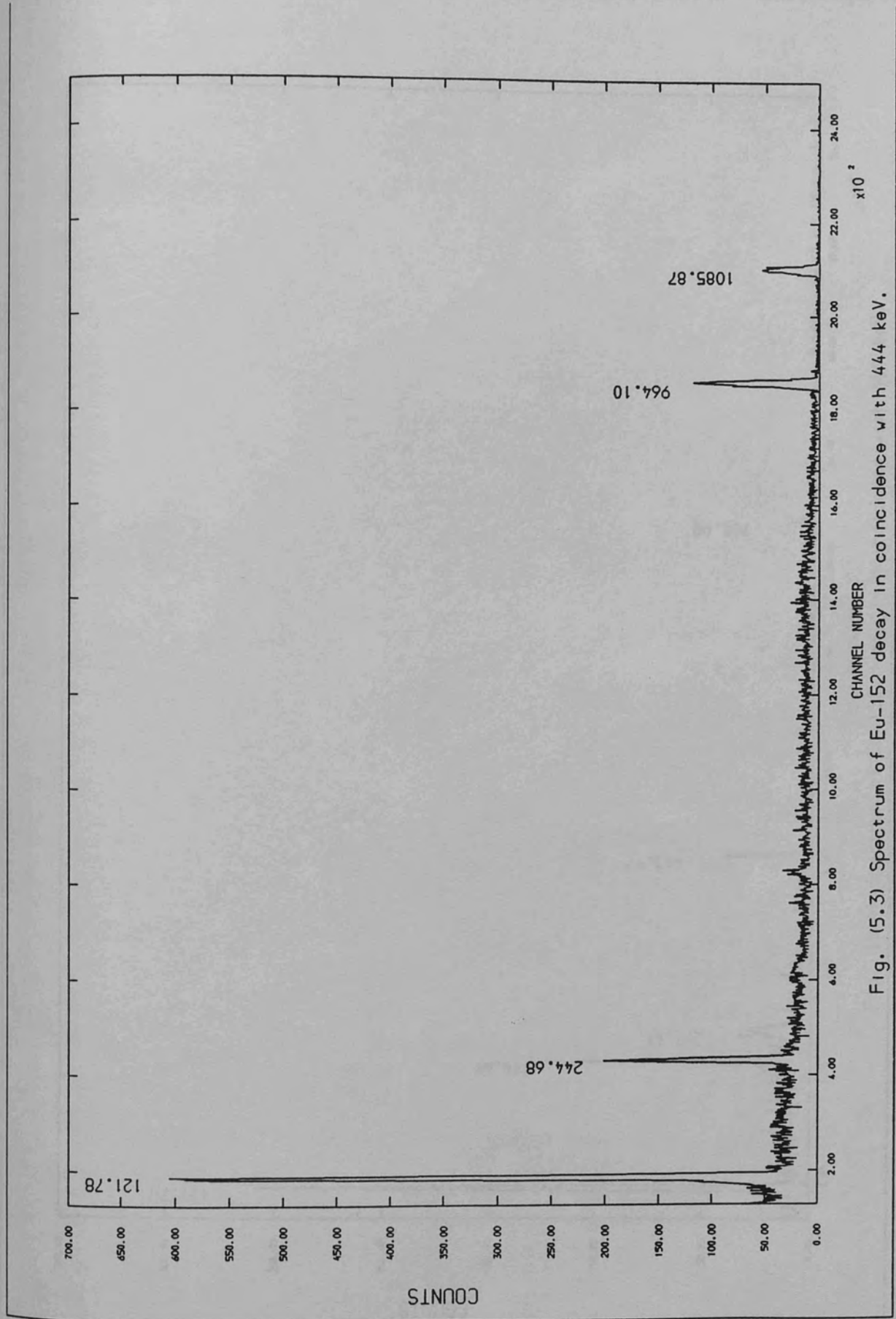
Fig. (5.3) Spectrum of Eu-152 decay in coincidence with 444 keV.
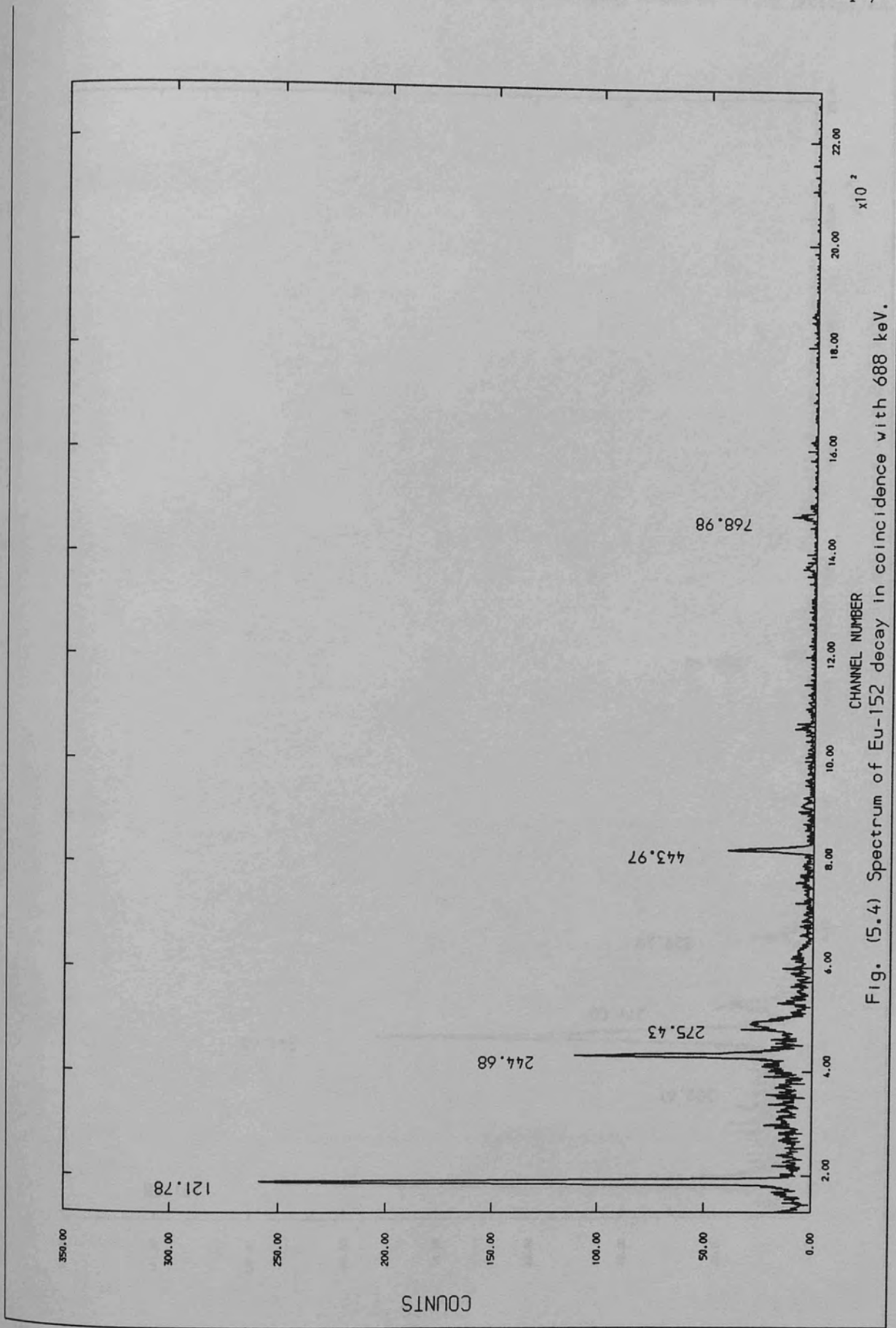
Fig. (5.4) Spectrum of Eu-152 decay in coincidence with 688 keV.
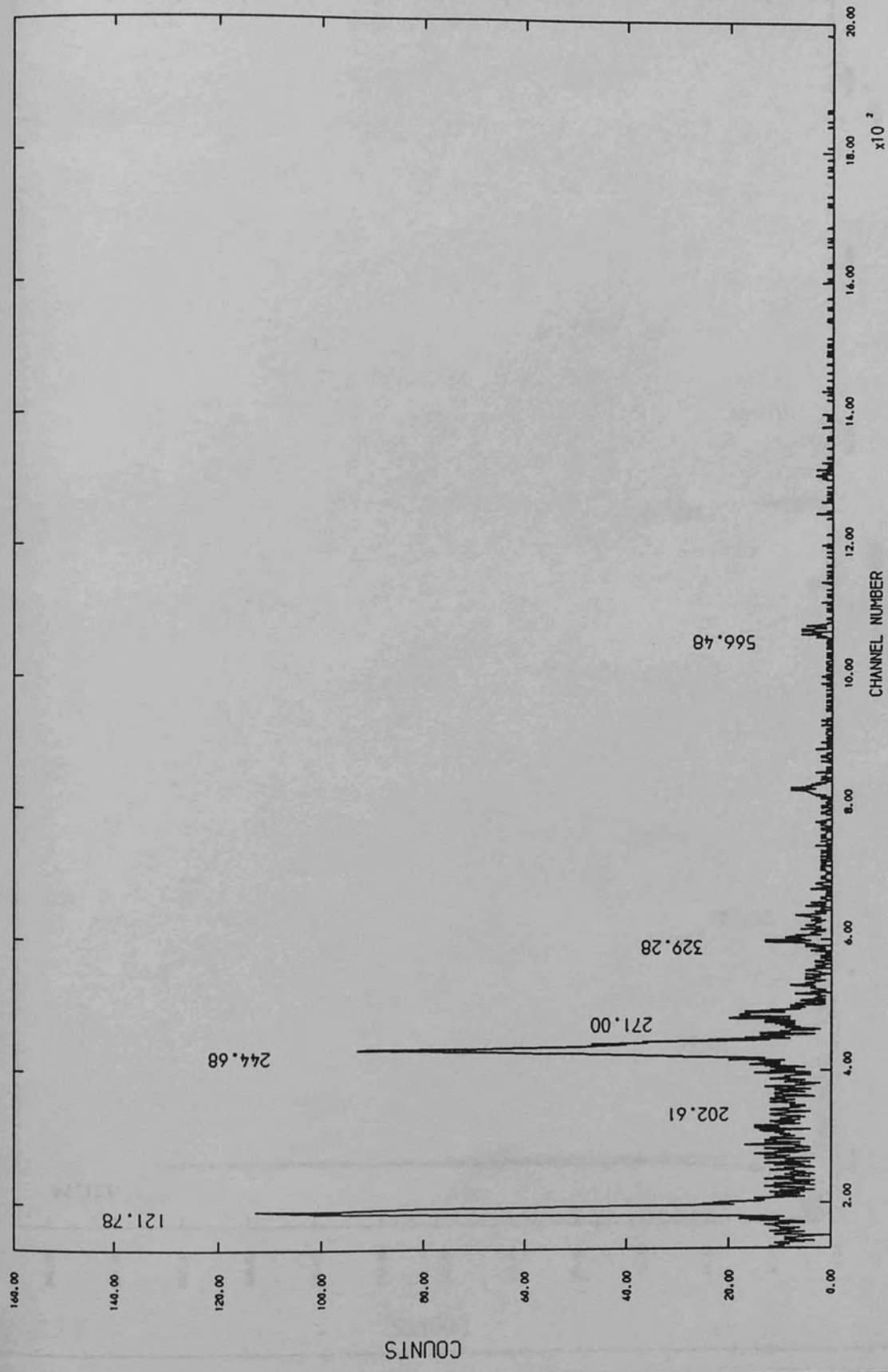
Fig. (5.5) Spectrum of Eu-152 decay in coincidence with 842 keV.
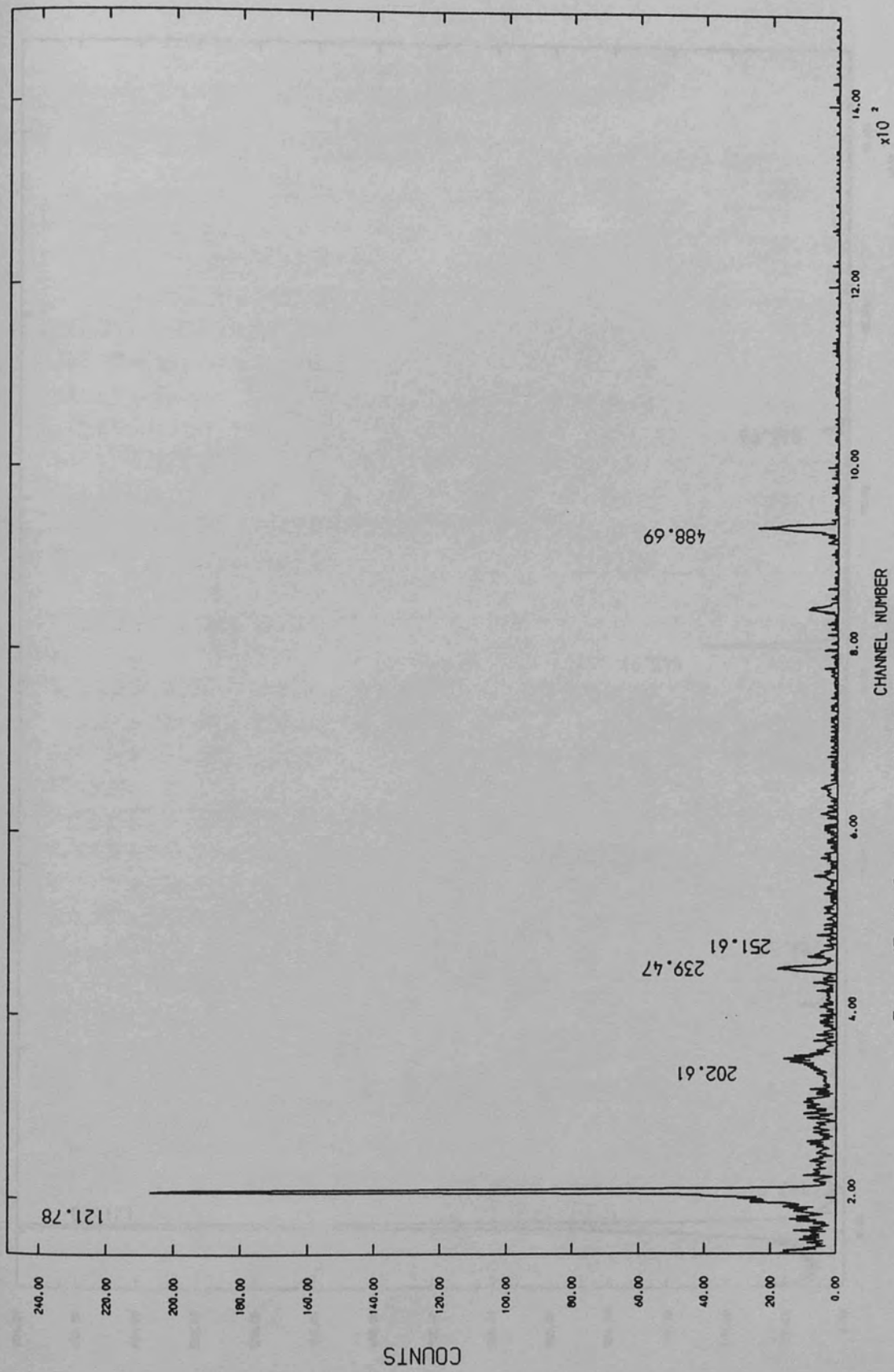
Fig. (5.6) Spectrum of Eu-152 decay in coincidence with 919 keV.
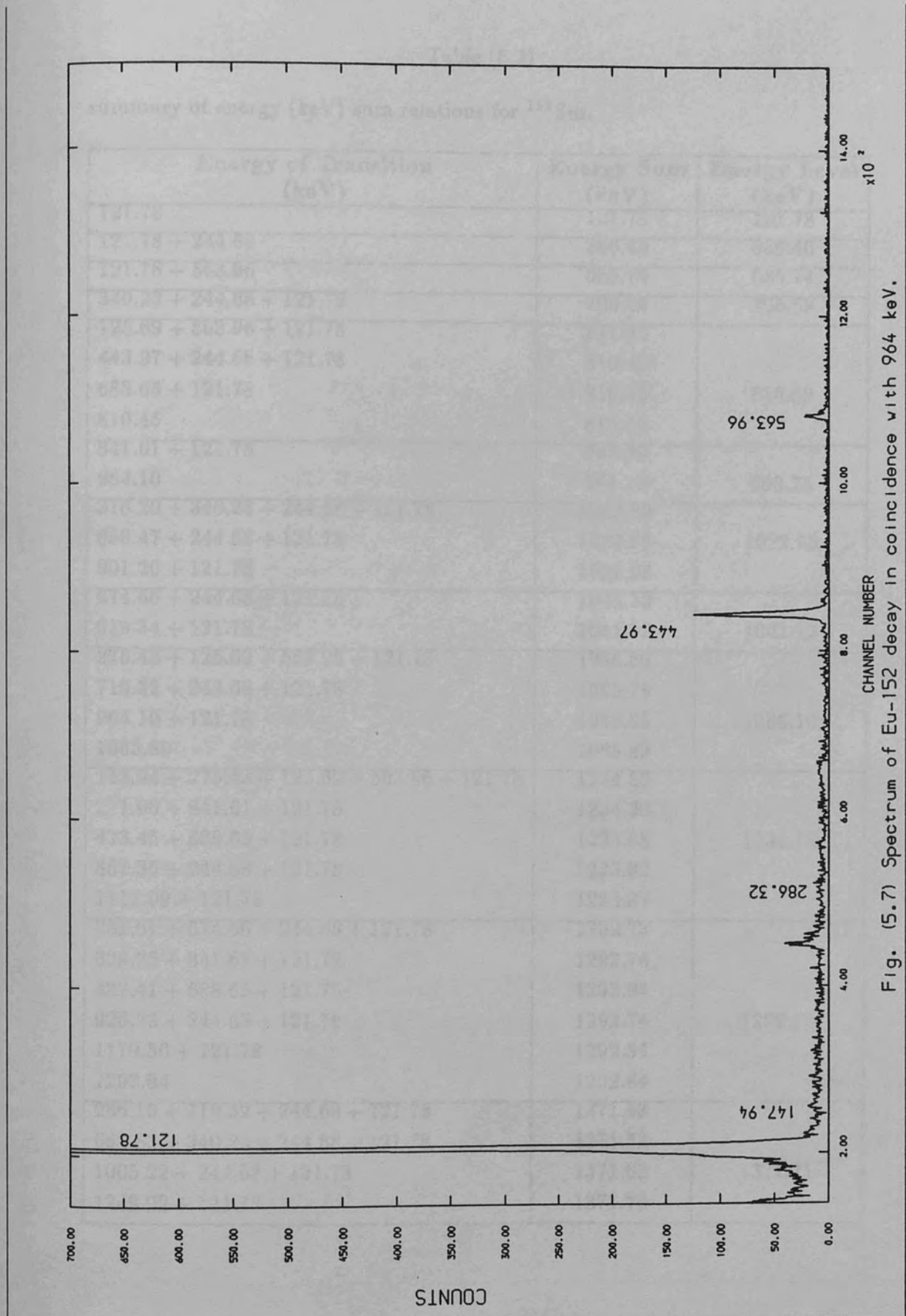
Fig. (5.7) Spectrum of Eu-152 decay in coincidence with 964 keV.

Table (5.2)

summary of energy (keV) sum relations for ^{152}Sm.

Energy of Transition (keV)	Energy Sum (keV)	Energy Level (keV)
121.78	121.78	121.78
121.78 + 244.68	366.46	366.46
121.78 + 563.96	685.74	685.74
340.23 + 244.68 + 121.78	706.69	706.69
125.69 + 563.96 + 121.78	811.43	
443.97 + 244.68 + 121.78	810.42	
688.65 + 121.78	810.43	810.69
810.45	810.45	
841.61 + 121.78	963.39	
964.10	964.10	963.75
316.20 + 340.23 + 244.68 + 121.78	1022.89	
656.47 + 244.68 + 121.78	1022.93	1022.93
901.20 + 121.78	1022.98	
674.66 + 244.68 + 121.78	1041.12	
919.34 + 121.78	1041.12	1041.12
275.43 + 125.69 + 563.96 + 121.78	1086.86	
719.32 + 244.68 + 121.78	1085.78	
964.10 + 121.78	1085.88	1086.10
1085.89	1085.89	
147.94 + 275.43 + 125.69 + 563.96 + 121.78	1234.80	
271.00 + 841.61 + 121.78	1234.39	
423.45 + 688.65 + 121.78	1233.88	1234.15
867.36 + 244.68 + 121.78	1233.82	
1112.09 + 121.78	1233.87	
251.61 + 674.66 + 244.68 + 121.78	1292.73	
329.35 + 841.61 + 121.78	1292.74	
482.41 + 688.65 + 121.78	1292.84	
926.28 + 244.68 + 121.78	1292.74	1292.71
1170.56 + 121.78	1292.34	
1292.84	1292.84	
286.15 + 719.32 + 244.68 + 121.78	1371.93	
664.83 + 340.23 + 244.68 + 121.78	1371.52	
1005.22 + 244.68 + 121.78	1371.68	1371.71
1249.92 + 121.78	1371.70	

Table (5.2) (continued)

Energy of Transition (keV)	Energy Sum (keV)	Energy Level (keV)
202.61 + 867.36 + 244.68 + 121.78	1436.43	
395.75 + 919.34 + 121.78	1436.87	1436.65
237.38 + 926.28 + 244.68 + 121.78	1530.12	
295.91 + 867.36 + 244.68 + 121.78	1529.73	
443.97 + 964.10 + 121.78	1529.85	
566.50 + 841.61 + 121.78	1529.89	1529.86
719.32 + 688.65 + 121.78	1529.75	
1408.03 + 121.78	1529.81	
207.31 + 286.15 + 719.32 + 244.68 + 121.78	1579.24	
493.56 + 275.43 + 688.65 + 121.78	1579.42	
556.48 + 316.20 + 340.23 + 244.68 + 121.78	1579.37	
615.83 + 841.61 + 121.78	1579.22	1579.34
768.98 + 443.97 + 244.68 + 121.78	1579.41	
1212.92 + 244.68 + 121.78	1579.38	
1457.55 + 121.78	1579.33	
212.50 + 395.75 + 919.34 + 121.78	1649.37	
416.01 + 867.36 + 244.68 + 121.78	1649.83	
563.96 + 964.10 + 121.78	1649.84	1649.63
838.84 + 688.65 + 121.78	1649.27	
1528.05 + 121.78	1649.83	
389.07 + 1170.56 + 121.78	1681.41	
595.61 + 964.10 + 121.78	1681.49	1681.56
1315.32 + 244.68 + 121.78	1681.78	
644.29 + 964.10 + 121.78	1730.17	
1363.72 + 244.68 + 121.78	1730.18	1730.21
1608.50 + 121.78	1730.28	
385.92 + 1005.22 + 244.68 + 121.78	1757.60	
523.11 + 867.36 + 244.68 + 121.78	1756.93	
671.21 + 964.10 + 121.78	1757.09	1757.10
1390.30 + 244.68 + 121.78	1756.76	
239.47 + 719.32 + 688.65 + 121.78	1769.22	
727.42 + 919.34 + 121.78	1768.54	
805.39 + 841.61 + 121.78	1768.78	
958.55 + 688.65 + 121.78	1768.98	1768.98
1647.42 + 121.78	1769.20	
1769.14	1769.14	

Table (5.3) shows the EC+β^+ branching ratios (B.Rs) of the decay of ^{152}Eu , the logft values and the deduced spins and parities for the energy levels. The B.Rs were calculated from the balance between the decay and the feeding of the γ-rays for each level . The results match well with the values reported previously[33,97,143,144]. The value for 121.78 keV could not be obtained in this study, neither from Barratte et al[97]. Therefore, the value provided by Baglin[113] was adopted here. For the 366.46 keV level the reported values are variable; 1.7% Riedinger et al[98], 0.76% Barratte et al[97], 0.8% Baglin[113]. In this study a value of 0.13% was calculated. The level at 685.74 (0^+) and 1436.65 (2^+) keV could not be assigned a B.R in same way as the other levels because the intensities of the feeding γ-rays were greater than the decay ones. The logft values were calculated according to Lederer et al[143] as well as the endpoint energy of the conversion electrons (Q_β=1876.9 keV). The spins and parities of the levels were deduced according to the selection rules[144]. The theoretical α_k, Rosel et al[33], were compared with the experimental values in Table (5.4). The experimental values were obtained using the conversion electron intensities[114] and the calculated γ-rays relative intensities (I_γ). The experimental α_k were normalized to the pure E2 multipolarity of the first excited state (344 keV) in ^{152}Gd (see chapter IV). In most cases there is full agreement with the predicted values of α_k, and hence the multipolarity for the transition can be assigned with confidence. Thus, the spins and parities of the levels depopulated by these transitions can be compared with those deduced from logft values.

Table (5.3)

The beta branching ratios, log*ft* values, spins and parities assignments for levels in ^{152}Sm nucleus.

Energy level (keV)	Q_{value} $\varepsilon_\beta = 1819.2$	$\sum I_\gamma$ feed	$\sum I_\gamma$ decay	$\sum I_\gamma$ decay $-I_\gamma$ feed	B.R %	log*ft*
121.78	1758.12	223.01	106.58	–	1.62	11.39
366.46	1513.44	28.91	29.64	0.73	0.20	12.24
685.74	1194.16	0.09	0.09	–	–	–
706.69	1173.21	0.06	0.08	0.02	0.01	14.48
810.69	1069.21	1.61	5.82	4.66	1.28	11.23
963.75	916.15	1.04	1.10	0.04	0.02	13.75
1022.93	8576.97	0.06	0.88	0.82	0.23	11.82
1041.12	838.78	0.76	2.24	1.48	0.41	11.57
1086.10	793.80	12.61	93.24	80.63	22.17	9.81
1234.15	645.75	2.23	66.96	64.73	17.79	9.77
1292.71	587.19	0.06	2.57	2.51	0.69	11.10
1371.71	508.14	0.23	3.57	3.34	0.92	10.89
1436.65	443.25	0.09	0.05	–	–	–
1529.86	350.04	0.04	91.81	91.77	25.23	9.25
1579.34	299.93	–	7.85	7.85	2.16	10.24
1649.63	230.27	–	3.34	3.34	0.92	10.37
1681.56	198.34	–	0.16	0.16	0.05	11.55
1730.21	149.69	–	0.16	0.16	0.05	11.36
1757.10	122.80	–	0.38	0.38	0.11	10.83
1768.98	110.92	–	0.36	0.36	0.10	10.78

Table (5.4)

Deduced multipolarities from k-shell internal conversion coefficients for ^{152}Sm.

Energy (keV)	$J_i^\pi \to J_f^\pi$	Experimental $\alpha_k(\times 10^4)$	Theoretical $\alpha_k(\times 10^4)$			Deduced Multi-polarity
			E1	E2	M1	
121.78	$2^+ \to 0^+$	6098 (414)	1391	6856	8507	$E2$
244.68	$4^+ \to 2^+$	748 (51)	238	933	1367	$E2$
295.91	$2^- \to 3^+$	85 (18)	148	545	842	$E1$
443.97	$2^- \to 2^+$	43 (46)	52	159	275	$E1$
488.68	$2^- \to 3^-$	117 (22)	42	121	214	$E2$
563.97	$2^- \to 2^+$	35 (16)	33	93	164	$E1$
566.50	$2^- \to 1^-$	119 (50)	32	92	162	$E2/M1$
656.47	$4^+ \to 4^+$	431 (87)	22	59	103	$E0/E2$
674.66	$3^- \to 4^+$	11 (19)	20	52	91	$M1$
688.65	$2^+ \to 2^+$	347 (33)	18	49	86	$E0/E2$
719.32	$2^- \to 2^+$	40 (17)	18	46	81	$E2$
810.45	$2^+ \to 0^+$	30 (13)	15	38	66	$E2$
867.36	$3^+ \to 4^+$	26 (3)	18	33	57	$E2$
964.10	$2^+ \to 2^+$	22 (2)	10	24	40	$E2$
1005.22	$4^+ \to 4^+$	22 (7)	9	21	35	$E2$
1085.89	$2^+ \to 0^+$	18 (2)	8	19	31	$E2$
1112.09	$3^+ \to 2^+$	16 (2)	8	18	30	$E2$
1212.92	$3^- \to 4^+$	22 (6)	7	16	26	$E2/M1$
1408.03	$2^- \to 2^+$	4.2 (0.4)	5	12	18	$E1$

5.3.1 Discussion of Individual Levels in ^{152}Sm

5.3.1.1 The 121.78 , 366.46, 706.69 keV levels

These levels have well-known spin and parity of $2^+, 4^+$ and 6^+, respectively in view of the logft values (Table 5.3) and from the α_k coefficients (Table 5.4). The levels belong to the ground-state rotational band of ^{152}Sm where a large amount of information has been accumulated from the decay of the ^{152}Eu [97,98,104,105,111] and other reactions studied [71,145−149]. Remarkable agreement between experimental and theoretical value of α_k of the 121.78 keV transitions supportsthe 2^+ assignment of the 121.78 keV level. The experimental α_k for the 244.68 keV transition is in full agreement with the theoretical α_k. This support the E2 multipolarity of this transition, hence, the 4^+ assignment for the 366.46 keV level. The 706.67 keV level was assigned 6^+ since all theories (Table 5.5) predict a level of about 700 keV with $J^\pi = 6^+$.

The experimental values of the 6^+ level were compared with the predicted values from rotational theory and Kumar [150]. The agreement is poor with the rotational, and poorer with Kumar [150]. However, the experimental values are remarkably agreeing with the present IBM predictions.

5.3.1.2 The 685.74, 810.69 and 1022.93 keV

These levels are the $0^+, 2^+$ and 4^+ members of the first β-vibrational band respectively. It has been reported that the transition 563.96 keV is masked by the transition 564.01 keV in the decay of ^{152}Eu , and both considered as doublet [113]. This also was confirmed in this study. The transition 563.96 keV is deexcited from the 685.74 keV level which is shown very weakly as it is

173

Table (5.5)

The energy of level in ^{152}Sm found experimentally compared with rotation calculations and with values from other nuclear models.

J_k^{π}	Energy (keV)					
	Experiment	Rotor	IBM	IBM[11]	PPQM[150]	BET[152]
20^+	121.78	121.78	117	110	114	121
40^+	366.46	366.46	362	340	314	346
00^+	686.74	686.74	663	−	−	−
60^+	705.69	639.74	715	681	585	706
20^+	810.69	810.69	791	854	855	835
10^-	963.75	963.75	−	990	−	−
40^+	1022.93	1022.93	1037	1172	1039	1082
30^-	1041.12	1041.12	−	1030	−	−
22^+	1086.10	1086.10	1011	1039	1397	1050
32^+	1234.15	1234.15	1213	1214	1559	1353
20^+	1292.71	1292.71	1348	−	−	−
42^+	1371.71	1363.66	1344	1357	1705	1441
22^+	1436.65	1436.65	1507	−	−	−
21^-	1529.86	1529.86	−	1450	−	−
31^-	1579.34	1579.34	−	−	−	−
22^-	1649.93	1649.63	−	−	−	−
41^-	1681.56	1649.68	−	−	−	−
30^-	1730.21	1730.21	−	−	−	−
32^-	1757.10	1757.10	−	−	−	−
20^+	1768.98	1768.98	1769	−	−	−

considered as a doublet, because the transition 563.96 is deexcited from 1649.63 keV level and is stronger though the energy different with transition 563.96 keV is insignificant. This indicates the existence of the 685.74 (0^+) keV level in the decay of ^{152}Eu , and is in agreement with results other reactions[71]. Varnell et al[116] found a 400.1 keV transition deexciting the 2^+ at 1086.10 keV (which belongs to the γ-vibrational band). This γ-ray was not observed in either the singles or coincidence spectra of the present work.

The intensity value of the 443.97 keV transition deexciting the 810.69 (2^+) level to the 366.46 keV (4^+) level (G.S.B) is deduced essentially from Baglin[113] since this transition is masked by other stronger 443.97 keV transition deexciting the level (Fig. 5.8). Barratte et al[97] confirmed the assignment of the 901.20 keV γ-ray as a transition between 4^+_β and 2^+_g level as inferred by Riedinger et al[151] by energy fit. Furthermore, the 315.25 keV weak γ-ray was seen in coincidence with the 244.68 keV gated spectrum. This transition can be fitted between 4^+_β and 6^+_g levels. The stronger member of this doublet (315.25 keV) is placed in ^{152}Gd .

The new transition at 125.69 keV is placed between the 810.69 keV (2^+) and the 685.74 keV (0^+) levels. It has been seen in singles, although masked by the very intense121.78 keV transition. It was also seen in weak coincidence with the 122 and 245 keV gates spectra. This placement of the 125.69 keV transition is supported by the ^{152}Tb decay[113].

The spins and parities of these levels were confirmed from logft values (Table 5.3) and from α_k coefficients (Table 5.4). The 656.47 keV transition has high experimental α_k value, this suggested E0 multipolarity for this transition, since it depopulatesthe 1022.93 (4^+_β) keV level to the 366.46 (4^+_g) keV level. This
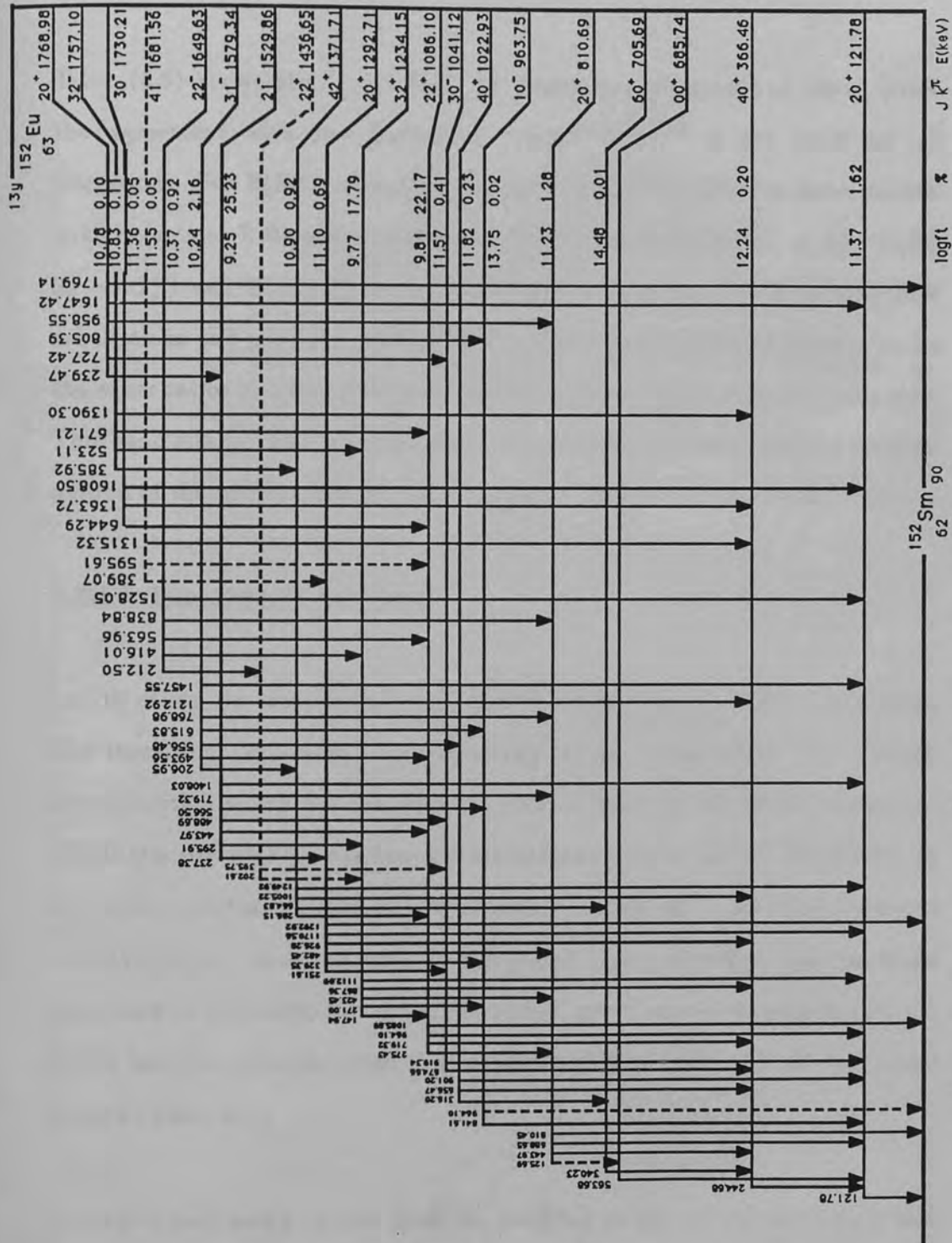
Fig (5.8) Decay scheme of ^{152}Sm. New transitions and levels are presented by dashed lines.

supports the 4^+ assignment to the 1022.93 keV level. The rotational theory calculations (Table 5.5, Fig. 5.9) show agreement as well as with the experimental for this band.

Table (5.6) shows the B(E2) B.R. for transitions depopulating these levels, the agreement with the theoretical values[6,11,150,152] is not good for all transitions. For B(E2) ratios involving interband transition, the experimental and theoretical B.Rs are in agreement, i.e the ratios B(E2, $2^+_\beta \to 4^+_g$)/ B(E2, $2^+_\beta \to 2^+_g$) and B(E2, $2^+_\gamma \to 2^+_g$)/$B(E2, 2^+_\gamma \to 0^+_g)$ agree with present IBM calculations and previous results[26,29,30]. When band mixing is present as for the other ratios in Table (5.6) poor agreement between experiment and theory was seen. This band mixing could arise from coupling between the rotational and intrinsic motion of the nucleus, which would support a transitional nature of ^{152}Sm .

5.3.1.3 The 1292.71 keV level

In this study six transitions were detected deexciting the 1292.71 keV state. The transition 1292.71 keV was deexciting to the ground-state. The 1170.56 keV transition which was found in coincidence with the 121.78 keV γ-ray, the 926.28 transition which was found in coincidence both in the 121.78 and 244.68 keV gated spectra, the 482.41 keV transition which was found in coincidence with 121.78, and, above all, with the 688.65 keV γ-ray, the 329.35 keV transition was found in coincidence with the 121.78 keV gated spectrum, and finally, the 251.61 keV transition detected in coincidence with the 122 and 245 keV gated spectra (Table 5.1).

The spins and parity of the level is confined to (2^+) from these data and the logft value (Table 5.3). It appears that this level decays preferentially to

Table (5.6)

Experimental B(E2) ratios for transitions depopulating positive parity states in ^{152}Sm compared with different nuclear model.

Transition E_γ/E'_γ	Energy Band	$J_i \to J_f$ $J_i \to J_f$	B(E2) Ratio						
			Present Work	IBM	IBM [11]	PPQM [150]	BET [A^{152}]*	BET [B^{152}]*	BET [160]
$\dfrac{443.97}{688.65}$	β	$2^+ \to \dfrac{(4)^+}{(2)_g}$	2.12 (09)	4.67	0.41	4.90	3.08	3.35	2.80
$\dfrac{810.45}{688.65}$	β	$2^+ \to \dfrac{(0)^+}{(2)_g}$	0.17 (01)	1.76	0.08	0.11	0.23	0.12	0.26
$\dfrac{901.20}{656.47}$	β	$4^+ \to \dfrac{(2)^+}{(4)_g}$	0.11 (01)	3.22	–	0.01	0.21	0.15	0.32
$\dfrac{964.10}{1085.89}$	γ	$2^+ \to \dfrac{(2)^+}{(0)_g}$	2.55 (05)	3.15	1.00	2.33	1.06	0.79	1.06
$\dfrac{964.10}{719.32}$	γ	$2^+ \to \dfrac{(2)^+}{(4)_g}$	17.78 (27)	15.27	1.60	19.70	5.26	2.39	9.14
$\dfrac{275.43}{964.10}$	γ	$2^+ \to \dfrac{(2_\beta)^+}{(2_g)}$	1.55 (19)	0.23	–	0.96	2.78	7.00	2.64
$\dfrac{1112.09}{867.36}$	γ	$3^+ \to \dfrac{(2)^+}{(4)_g}$	0.72 (02)	0.84	1.00	1.42	2.30	2.32	2.68
$\dfrac{1249.92}{1005.22}$	γ	$4^+ \to \dfrac{(2)^+}{(4)_g}$	0.09 (01)	0.06	–	0.16	0.46	0.50	0.34

* A and B represent two different cases and correspond to adjusting parameters best fit to the (2^+) excited state.
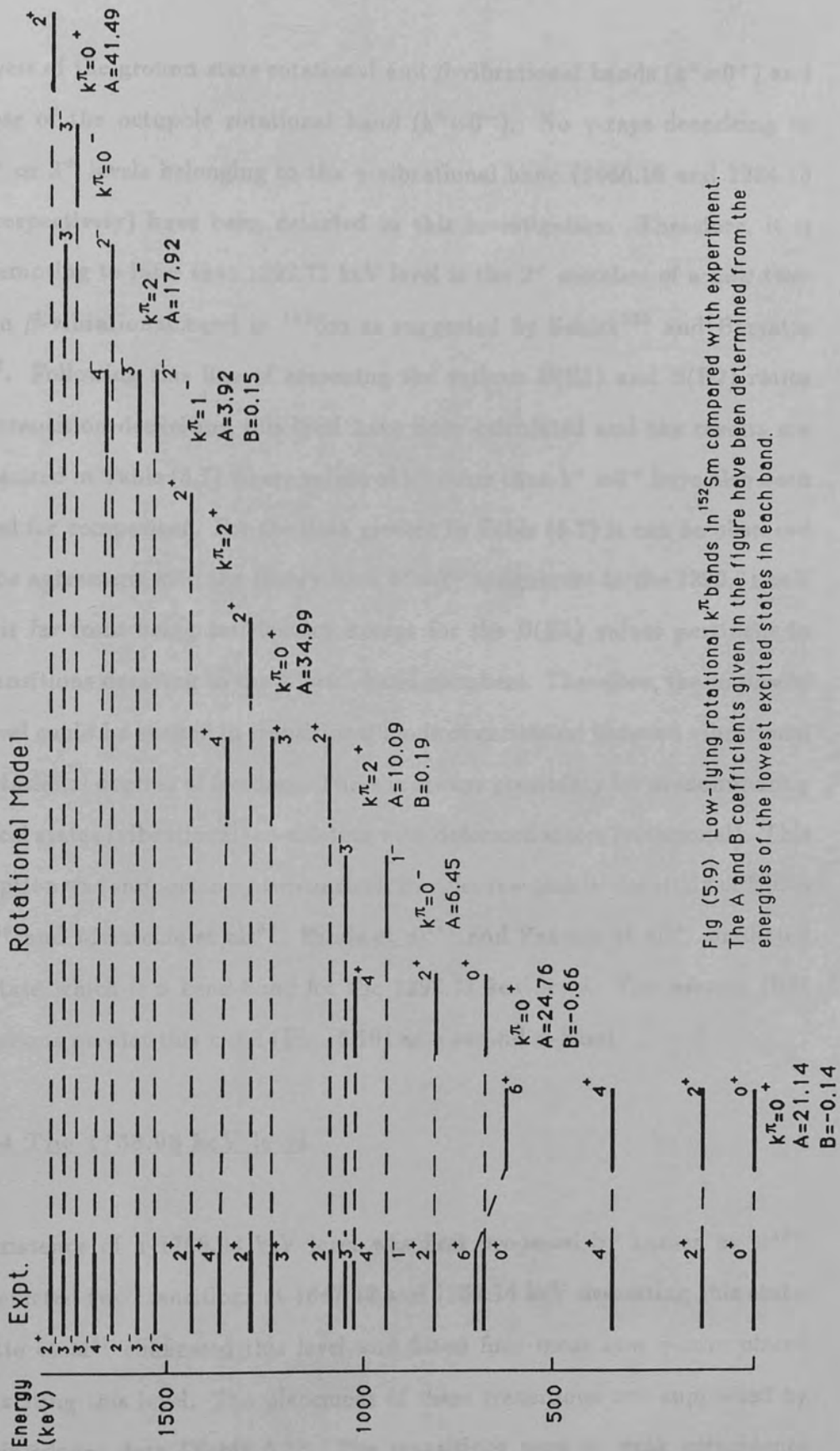
Fig (5.9) Low-lying rotational k^π bands in ^{152}Sm compared with experiment. The A and B coefficients given in the figure have been determined from the energies of the lowest excited states in each band.

the levels of the ground-state rotational and β-vibrational bands ($k^\pi=0^+$) and to those of the octupole rotational band ($k^\pi=0^-$). No γ-rays deexciting to the 2^+ or 3^+ levels belonging to the γ-vibrational band (1086.10 and 1234.15 keV, respectively) have been detected in this investigation. Therefore, it is very tempting to infer that 1292.71 keV level is the 2^+ member of a new two-phonon β-vibrational band in ^{152}Sm as suggested by Schick[139] and Barratte et al[97]. Following this line of reasoning the various B(E1) and B(E2) ratios of all transitions deexciting this level have been calculated and the results are summarized in Table (5.7) where values of k^π other than $k^\pi =0^+$ have also been inserted for comparison. For the data present in Table (5.7) it can be observed that the agreement with the theory for a $k^\pi=0^+$ assignment to the 1292.71 keV levels is far from being satisfactory except for the B(E1) values pertinent to the transitions decaying to the $k^\pi=0^-$ band members. Therefore, the nature of this level could be excited in transitional mode of excitation between vibrational and rotational degrees of freedom. There is always possibility for predominantly spherical states (vibrational) co-existing with deformed states (rotational). This assumption was supported by two nucleon transfer reaction in the study of Hinds et al[140] and Mclatchie et al[154]. Hinds et al[140] and Passoja et al[141] predicted a 0_3 state which is a head-band for the 1292.71 keV level. The present IBM calculations predict this band (Fig. 5.10) as a second β-band.

5.3.1.4 The 1768.98 keV level

The existence of a 1768.98 keV level was first proposed by Larsen et al[126], who detected two transitions at 1647.42 and 1769.14 keV deexciting this state. Barratte et al[97] confirmed this level and fitted four more new γ-rays placed as deexciting this level. The placement of these transitions was supported by the coincidence data (Table 5.1). The transitions were in weak coincidence

Table (5.7)

Relative experimental B(EL) ratios transitions from positive parity states in ^{152}Sm compared with theory[97].

Transition (keV)	Energy level (keV)	$J_i^\pi \to J(K)_f^\pi$	EL	Experiment	B(EL) Values for different K_i				Deduced K_i
					0	1	2		
1292.84	1293	$2 \to 00^+$	$E2$	0.009(002)	0.012	0.048	0.012		0,2
1170.56		$2 \to 20^+$	$E2$	0.018(004)	0.017	0.017	0.017		0
926.28		$2 \to 40^+$	$E2$	0.335(058)	0.031	0.054	0.008		0
482.41		$2 \to 20^+$	$E2$	1.000	1.000	1.000	1.000		0
329.35		$2 \to 10^-$	$E1$	0.838(076)	0.670	1.500	–		0
251.61		$2 \to 30^-$	$E1$	1.00	1.00	1.00	–		0
1769.14	1769	$2 \to 00^+$	$E2$	0.757(262)	0.700	0.280	0.700		0,2
1647.42		$2 \to 20^+$	$E2$	1.000	1.000	1.000	1.000		

181
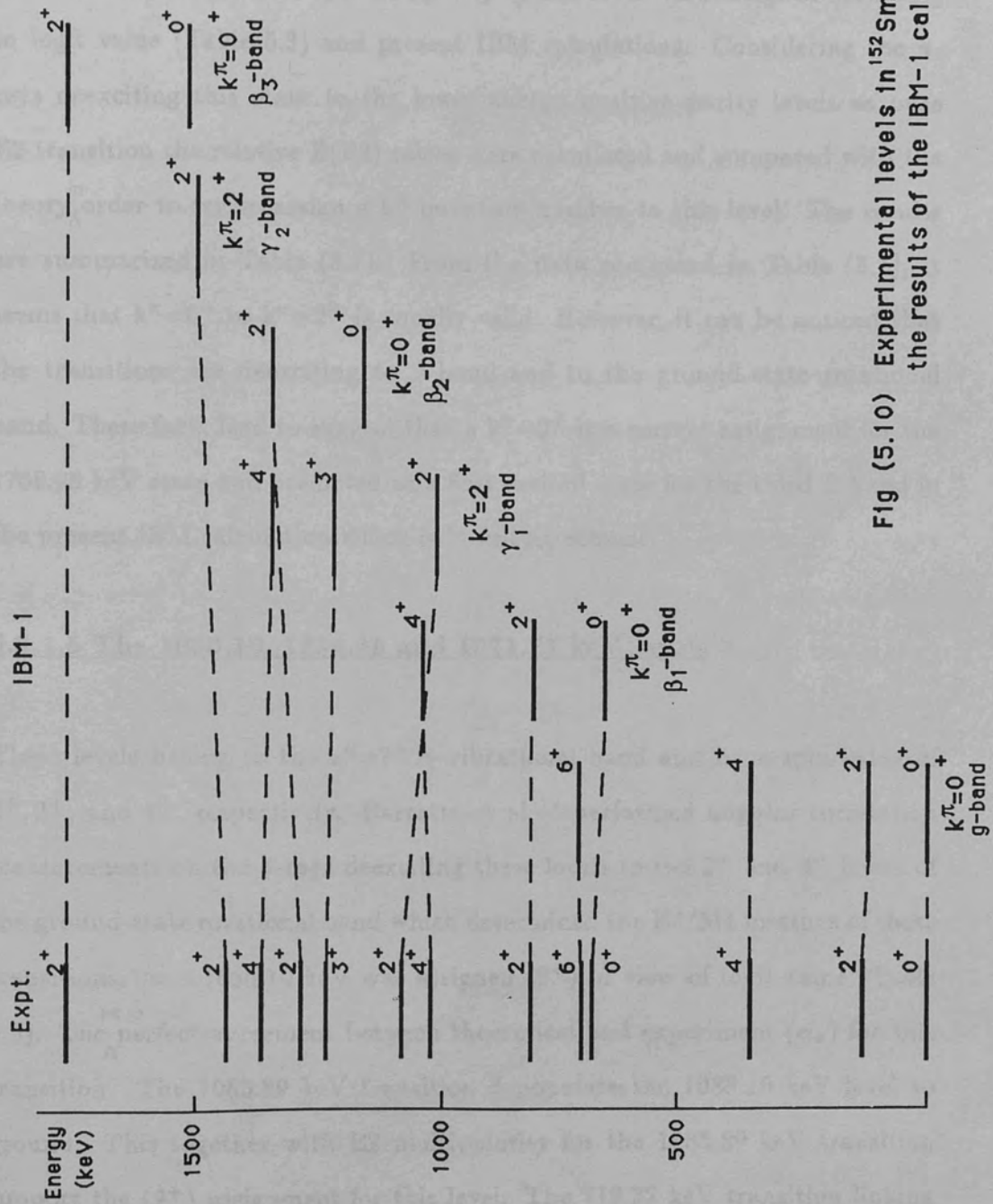
Fig (5.10) Experimental levels in ^{152}Sm compared with the results of the IBM-1 calculations.

with gates 122, 245, 444, 689, 919 keV. The energy balance was used to insert the transitions. The decay characteristics of the 1768.98 keV level leads to assignment of 2^+ for this state which is in agreement with the probable multipole order E2 measured by Larsen et al[126] for the 1768.98 and 1647.42 keV transitions, and also supported by Hinds et al[140] from the angular distribution of the emitted protons. The spin and parity of this level were assigned according to logft value (Table 5.3) and present IBM calculations. Considering the γ-rays deexciting this state to the lower energy positive parity levels as pure E2 transition the relative B(E2) ratios were calculated and compared with the theory in order to try to assign a k^π quantum number to this level. The results are summarized in Table (5.7). From the data presented in Table (5.7), it seems that $k^\pi = 0^+$ or $k^\pi = 2^+$ is equally valid. However, it can be noticed that the transitions are deexciting to β-band and to the ground-state rotational band. These facts lead to suggest that a $k^\pi = 0^+$ is a correct assignment for the 1768.98 keV state and predicted as a first excited state for the third β-band in the present IBM calculation which is in full agreement.

5.3.1.5 The 1086.10, 1234.15 and 1371.71 keV levels

These levels belong to the $k^\pi = 2^+$ γ-vibrational band and have spin value of $2^+, 3^+$, and 4^+, respectively. Barratte et al[119] performed angular correlation measurements on the γ-rays deexciting these levels to the 2^+ and 4^+ levels of the ground-state rotational band which determined the E2/M1 mixture of these transitions. The 1086.10 keV was assigned (2^+) in view of logft value (Table 5.3). The perfect agreement between theoretical and experiment (α_k) for this transition. The 1085.89 keV transition depopulates the 1086.10 keV level to ground. This together with E2 multipolarity for the 1085.89 keV transition support the (2^+) assignment for this level. The 719.32 keV transition linking

the 2_γ^+ level at 1086.10 keV to the 4^+ ground-state rotational level (at 366.46 keV) is a composite transition which is E2 multipole (Table 5.4). Barratte et al[3] found that 15% of the 719.32 keV transition deexcites the 1529.86 keV level to the 810.69 (2^+) keV β-vibrational level. The 275.43 keV transition is placed between the 2_γ^+ and 2_β^+ level since its presence was observed in the coincident 121.78, 244.68 and 443.97 keV gated spectra.

The spin and parity of the level 1234.15 keV was considered from logft value (Table 5.3) and from the α_k values of the two transitions 867.36 and 1112.09 keV. The first transition depopulatingthis level to the 366.46 (4^+) keV level. This transition is E2 multipole (Table 5.4), while the second transition depopulating this level to the 121.78 (2^+) keV level is another E2 multipole (Table 5.4, Fig. 5.8). Furthermore, the 147.94 keV γ-ray was seen in coincidence with the 964.10 keV gate spectra and confirmed between $3_\gamma^+ \to 2_\gamma^+$.

The third level at 1371.71 keV is assigned according to logft value (Table 5.3) and supported by the α_k value of the transition 1005.22 keV which depopulates this level to the state 366.46 (4^+) keV, since full agreement between theoretical and experimental α_k value (Table 5.4) indicates that this transition is E2 multipole. The 286.15 keV transition is seen very weak in coincidence with the 964.10 keV gated spectrum. Even though the placing of these transitions are done from the coincidence (Table 5.1) and energy sum relations (Table 5.2), since the intensity of these transitions are very weak. Table (5.7) shows the B(E2) B.Rs for transitions depopulating these levels in the above band which is taken as γ-band.

The theoretical expectations (Table 5.5) give another support for the spin sequence of these levels (2^+, 3^+ and 4^+). The best theoretical values are given by present IBM calculation and by rotational theory calculated in this work.

5.3.1.6 The 1436.65 keV level

The level at 1436.65 keV is suggested as being depopulate by the two new transitions at 202.61 and 395.75 keV to the levels at 1234.15 and 1041.12 keV respectively. The intensities of these transitions are weak, and also seen in weak coincidence with the 964.10 and 919.34 keV gates. The level 1649.63 keV could be depopulate by the 212.50 keV transition to the new level at 1436.65 keV which is supported by the weak coincidence with the 964.10 keV gate and energy sum relations (Table 5.2). The logft value cannot be determined for this level because the decay-feeding γ-rays rule cannot be applied here, but the IBM calculation would allow a 2^+ γ-band member in this energy region (Table 5.5).

5.3.1.7 The 963.75 and 1041.12 keV levels

The two levels at 963.75 (1^-) and 1041.12 (3^-) keV are known from the decay and reaction work[71,97,149,155]. These two levels belong to the $k^\pi=0^-$ octupole band as established in the work of Veje et al[149]. Barratte et al[119] studies the angular correlation between 919.34 and 121.78 keV γ-rays to confirm the E1 nature of this transition. Thus, using the very reasonable assumption that the γ-rays deexciting these two levels are E1 in nature, the relative B(E1) values to the ground-state rotational band were calculated, and the results are presented in Table (5.8). The rotational theory values are similar to experimental values at both levels. However, there is discrepancy between the IBM calculation and the experimental values for the two levels. It could be explained by the fact

Table (5.8)

Relative experimental B(E1) ratios for transitions depopulating the negative parity states in ^{152}Sm compared with theory.

Transition (keV)	Energy level (keV)	$\dfrac{J_i^\pi \to J(K)_f^\pi}{J_i^\pi \to J(K)_f^\pi}$	Present Experiment	B(E1) Values for different K_i^{97}			Deduced K_i
				IBM[11]	0	1	
$\dfrac{919.43}{674.66}$	1041.12	$\dfrac{3^- \to 2_g^+}{3^- \to 4_g^+}$	0.85 (01)	0.86	0.75	1.33	0

that symmetry breaking such as caused by Coriolis coupling can easily arise for negative parity bands.

5.3.1.8 The 1529.86, 1579.34 and 1681.56 keV Levels

A second state (3^-) in ^{152}Sm , which was described to a $k^\pi=1^-$ band, was observed in the study of Bisgaard et al[125], Veje et al[149] and Konijn et al[71]. These data showed that this level has a strong collective character. The 2^- and 4^- rotational states of this band are found at 1529.86 and 1681.56 keV, respectively. The collective nature of the 2^- level at 1529.86 keV, which has been extensively investigated in the past[113], is supported by Barratte et al[119]; it was found the 488.69 keV transition deexciting the 3^- collective level at 1041.12 keV essentially has an E2 nature (Table 5.4). The new level at 1681.56 keV is suggested by the observation of a new transition at 389.10 keV and 595.61 which go to the 1292.71 and 1086.10 keV levels respectively. Also 1315.32 keV transition, previously reported by Sharma et al[105] and Baker et al[104] but unplaced in their decay schemes, could be placed between the level 1681.56 keV and the level at 366.46 keV. Konijn et al[71] had suggested in his study a spin parity of 4^- and in present logft value is 11.6 which is consistent with this assignment.

Through coincidence measurements (Table 5.1) and by energy sum relations, several transitions could be placed between these levels and lower-energy states belonging to the ground-state rotational band, β-γ vibrational bands, and the $k^\pi=0^-$ octupole band. The relative B(Eλ) values of these transitions were calculated and compared with those expected in the rotational model. The results are summarized in Table (5.9). The theoretical branching ratios for

Table (5.9)

Relative experimental B(EL) ratios for transitions from negative parity states in ^{152}Sm compared with theory[97].

Transition (keV)	Energy level (keV)	$J_i^\pi \rightarrow J(K)_f^\pi$	EL	Experiment	B(EL) Values for different K_i				Deduced K_i
					0	1	2		
566.50	1530	$2 \rightarrow 10^-$	E2	0.13 (01)	–	0.25	4.00		1
488.64		$2 \rightarrow 30^-$	E2	1.00	–	1.00	1.00		1,2
443.97		$2 \rightarrow 22^+$	E1	1.00	–	1.00	1.00		1,2
295.91		$2 \rightarrow 32^+$	E1	0.56 (02)	–	2.00	0.50		2
1457.55	1579	$3 \rightarrow 20^+$	E1	0.20 (01)	0.75	1.33	–		0
1212.92		$3 \rightarrow 40^+$	E1	1.00	1.00	1.00	–		0,1
768.98		$3 \rightarrow 20^+$	E1	0.28 (02)	0.22	0.22	–		0,1
556.48		$3 \rightarrow 40^+$	E1	0.11 (02)	0.29	0.16	–		1
563.96	1650	$2 \rightarrow 22^+$	E1	1.76 (09)	–	0.50	2.00		2
416.01		$2 \rightarrow 32^+$	E1	1.00	–	1.00	1.00		2
1608.50	1730	$3 \rightarrow 20^+$	E1	0.13 (02)	0.75	1.33	–		0
1363.72		$3 \rightarrow 40^+$	E1	1.00	1.00	1.00	–		0
671.21	1757	$3 \rightarrow 22^+$	E1	0.36 (04)	–	0.11	0.71		2
523.11		$3 \rightarrow 32^+$	E1	1.00	–	1.00	1.00		2

other possible values of K which can be attached to each level of this band are also included merely for comparison.

The determined B(E1) ratios for the levels belonging to $k^\pi = 1^-$ band are still in poor agreement with those given by the symmetric-rotor model which could indicate that the couplings of this band with bands other than the $k^\pi = 0^-$ are important. This may suggest that ^{152}Sm is rather transitional nucleus than rotational.

5.3.1.9 The 1649.53 and 1757.10 keV levels

The existence of the 1649.63 level in ^{152}Sm was proposed for the first time by Larsen et al[126], and confirmed by Barratte et al[97]. The spin and parity of this level are assigned from both logft values (Table 5.3) and α_k coefficient of the 563.96 keV transition which depopulate from 1649.53 keV to the 1086.10 keV level (Table 5.4). The placing of the 563.96 and 838.84 keV γ-rays as deexciting the 1649.63 keV level to the 1086.10 and 810.69 keV states, respectively, is supported by the 964.10 and 688.65 keV gated spectra.

The existence of a level 1757.10 keV in ^{152}Sm is established from the coincidence and energy sum relations. The transitions which deexcited this level to 366.46 (4_g^+), 1086.10 (2_γ^+), 1292.71 (2_β^+)and 1371.71 (4_γ^+) keV are 1390.30, 671.21, 523.11 and 385.92 keV respectively. The decay characteristics of this state support a 3^- spin which is assigned in view of logft value (Table 5.3). Since the spin value of the 1649.63 keV state is now well established as 2^-, this level might be considered as the band-head of the octupole band with $k^\pi = 2^-$, and this assignment is supported by the relative B(E1) values pertinent to the transitions deexciting these levels as is shown in Table (5.9).

5.3.1.10 The 1730.21 keV level

The existence of the 1730.21 keV level is shown in the decay of ^{152}Eu . The 1608.50, 1363.72 and 644.29 keV transitions were seen in weak coincidence with the 121.78, 244.46 and 964.10 keV gates spectra. The decay characteristics of the 1730.21 keV level support a 3⁻ spin and in accordance with logft values (Table 5.3). Larsen et al[126] suggest that the 1608.50 keV is an E1 transition which supports the assignment of this level. Since the 1608.50 keV transition decays to the 2⁺ first excited state in ^{152}Sm , the spin of the 1730.21 keV level cannot be 5⁻ as suggested in previous studies[98,104,111]. In Table (5.9) notice that this level is is agreement with a k$^\pi$=0⁻ assignment, and can be supposed to form a new octupole rotational band k$^\pi$=0⁻ built on the β-vibrational band.

5.4 Nuclear Model Calculation

5.4.1 Collective Model

Deformed nuclei can exhibit rotational spectra, which depend on the nuclear equilibrium shape. for symmetric nuclei, the energy spectrum is given by Eq. (2.2.2.6)[103,156]. The parameters A and B are determined by fitting to the energies of the first two experimental levels in the GSB. Such a relation implies that the ratios between the energies of the excited states in the GSB is

$$E(4^+)/E(2^+)=10/3, \text{ and } E(6^+)/E(2^+)=7/1.$$

In this section, ^{152}Sm with N=90 is considered as a deformed nucleus, and calculations based on rotational theory will be applied to it. The two parameters

A and B were determined as described above for the GSB. The values calculated are: A=21.14 and B=0.14 keV. The values of the parameters of the other rotational bands are given in Fig. (5.9).

The energy spectrum calculated using these values is given in Table (5.5), together with the energies values obtained experimentally, and from the IBM model. Fig. (5.9) shows the comparison between experimentally determined energy levels and those calculated by rotational theory. In general, there is agreement. However, the bands consisting of negative parity levels show more discrepancies from theory than the positive parity bands. This might be due to the existence of configurations of the nucleus differing from axial symmetry, or arising from coupling between vibrational and rotational interactions.

The difference for the positive parity levels could also be due to departures from axial symmetry, indicating some vibrational characteristics which is turn suggest a transitional nature of the ^{152}Sm nucleus. The energy level ratio for the ground state band supports a mainly rotational character, but could allow some vibrational degrees of freedom since experimental $E(4^+)/E(2^+)$ is 3.02 and $E(6^+)/E(4^+)$ is 5.8 compared to the purely rotational values of 3.33 and 7.0 respectively.

5.4.2 The IBM Calculations and Result

The↓ ^{152}Sm was considered as a deformed nucleus, showing rotational spectra[11,61,157]. The calculations based on the transitional region between spherical and deformed nuclei. In the SU(5) vibrational limit, the ratio $E(4^+)/E(2^+)$ is 2.0 while in SU(3) rotational limit, $E(4^+)/E(2^+)$ is 3.33 and

$E(6^+)/E(4^+)$ is 7.0. In case of ^{152}Sm , $E(4^+)/E(2^+)$ is 3.02 and $E(6^+)/E(4^+)$ is 5.79. These values lie between the two limits; the SU(5)and the SU(3), and are closer to SU(3) limit.

The IBM calculations were done using the IBM computer codes PHINT for energies and FBEM for B(E2) values[61]. The number of bosons implied by the number of valance neutron and proton in ^{152}Sm is 10. The truncated multipole expansion of the IBM Hamiltonian for the transitional ^{152}Sm nucleus from SU(5) to SU(3) were used in the calculations[11,71][Eqs. (3.3.3.a.1)]. In the present IBM calculations the multipole Hamiltonian Eq. (2.3.1.4) gives the fitting to the experimental level, and is in agreement with Suhonen[157] and also supported by VanIsacker[158]. The full Hamiltonian predicts the second β-band at 1072 (0^+) keV band-head, in agreement with Passisga[141], and also predicts 1292.71 keV at 2^+ (Table 5.5) as a level value for this band, which could not be explained before in this model. The parameters used in this calculation are listed in Table (5.10).

Fig. (5.9) show a closer agreement between theory and experiment for energy levels of the bands. Since these calculations were based on rotational theory, then one assumes that these bands have more tendency towards rotational properties than vibrational ones. The two levels at 964.10 and 1041.12 keV show poor agreement with the rotational theory, but closer agreement is achieved with the transitional limit[11]. It is possible to conclude that this band possesses more vibrational properties than rotational ones.

For the B(E2) calculation, the two parameters α_2 and β_2 (Eq. 2.3.1.6) were approximately adjusted to the experimental B(E2, $2_g^+ \rightarrow 0_g^+$) and B(E2, $2_\gamma^+ \rightarrow 0_g^+$) values for the 2^+ of the ground state, and γ-vibrational bands,

Table (5.10)

Values of the parameters corresponding to the variable names in programs PHINT and FBEM; these are applicable to the case of ^{152}Sm with N=10.

EPS (MeV)	PAIR (MeV)	ELL (MeV)	QQ (MeV)	OCT (MeV)	HEX (MeV)	E2SD (eb)	E2DD (eb)
0.0275	0.0070	0.0084	−0.0211	0.0156	−0.0025	0.1753	−0.0076

respectively. Table (5.11) shows the experimental values and the different theoretical values for the B(E2) of the 121.78 keV transition. Good agreement between theory and experiment is achieved. Table (5.12) gives the electric quadrupole moment Q experimental values. When compared to the theoretical values a good agreement was seen. Table (5.13) gives all the experimental transitions which are assumed to be pure E2 and the corresponding compared with present IBM calculation. The results of the B(E2) ratios are given in Table (5.6) and compared with those predicted in IBM and other models.

The branching ratio B(E2: $2^+_\gamma \rightarrow 0^+_g$)/$B(E2 : 2^+_\gamma \rightarrow 0^+_\beta$) was calculated for the β-band transitions to the GSB was found to be 0.17 $\pm$(0.01) (Table 5.6), while, again, shows the transitional nature of ^{152}Sm between the two limits, vibrational with (R=0) and rotational with (R=7/10).

5.5 Conclusion

The ^{152}Sm nucleus has been considered as a deformed nucleus showing rotational characteristics but allowing some vibrational degrees of freedom. The expectations of the rotational theory for the energy levels show reasonable agreement with the experimental, Fig. (5.9). The transitional calculations of the IBM[11,71] show smaller values for the GSB than the experimental, while for the β-band the experimental values are lower than the theoretical values. For γ-band, these predictions are lower than the experimental values. The present IBM calculations using the full Hamiltonian, and hence having some O(6) characteristic predict the second and third β-band which were missing from previous studies[11,71] for the 1292.71 (2^+) keV, and 1768.98 (2^+) keV respectively. This calculation produces better agreement than recent

Table (5.11)

Experimental reduced transition probability B(E2) for the 122 keV transitions in ^{152}Sm compared with theory.

$J_i \rightarrow J_f$	B(E2) Value					
	Present Work	IBM	IBM[11]	PPQM[150]	BET[160]	BET[152]
$2^+ \rightarrow 0^+$	0.678	0.678	0.596	0.648	0.651	0.673

Table (5.12)

Electric quadrupole moment Q for the first excited state in ^{152}Sm compared with theory.

Energy level (keV)	Q (e.b)				
	Experiment	IBM	IBM [11]	PPQM[150]	BET[160]
121.78	-1.66	-1.61	-1.56	-1.64	-1.68

Table (5.13)

Experimental B(E2) values (e^2b^2) in ^{152}Sm compared with IBM predictions.

Energy	Transition	B(E2) Values		
(keV)	$J_i \rightarrow J_f$	Experiment	Suhonen[157]	IBM
121.78	$20^+ \rightarrow 00^+$	0.678	0.680	0.678
244.68	$40^+ \rightarrow 20^+$	0.999	1.020	0.962
340.23	$60^+ \rightarrow 40^+$	1.176	1.120	1.041
810.45	$20^+ \rightarrow 00^+$	0.022	0.005	0.011
1085.89	$22^+ \rightarrow 00^+$	0.044	0.018	0.057
1005.22	$42^+ \rightarrow 40^+$	0.049	0.034	0.174

studies[141,157,158], which indicated that ^{152}Sm is a transitional nucleus between SU(5) and SU(3). The present results of the IBM calculations are listed in Table (5.5) and shown in Fig. (5.10). There is a good agreement between the GSB and the experimental values. The experimental values of the first and third β-band are in good agreement, while for the second β-band the experimental value is lower than the theory. For the first γ-band, predictions are lower than the the experimental values, but for the second γ-band the IBM prediction is higher than the new established level at 1436.65 keV which is assigned to be 2^+. In the negative parity band (k^π=1^-), the two experimental values lie in between the theoretical value[11]. Many models, including the Variable Moment of Inertia (VMI)[159], Pairing Plus Quadrupole Model (PPQM)[133,150], Boson Expansion Technique (BET)[152,160] and Rotation Vibration Model (RVM)[161], have been used to calculate both the band energy and the B(E2) ratios for ^{152}Sm with varying degree of success. The results of these studies indicated that there is a coupling between the rotational and intrinsic motions of the nucleus, suggesting a transitional nature of ^{152}Sm . From those considerations, it is clear that the ^{152}Sm nucleus is transitional, but the energy spectrum is more rotational than vibrational

In the case of B(EL) ratios, the agreement between the experimental and theory is poor and no correction is made for possible rotation-vibration interactions. For an axially symmetric rotor, the intrinsic and the rotational motions of the nucleus do not disturb each other[162]. Therefore no correction should be made and no vibrational and rotation coupling is present. If the band mixing is allowed between the β-or the γ-vibrational bands into the GSB, the B(EL) ratios can be corrected. These reactions were presented by Lipas[163] and Mikhailove[164]. Table (5.14) shows the B(EL) ratios for the transitions for β-or γ-bands to the GSB. Bohr and Mottelson[3] gave the predictions of the adiabatic symmetric rotor

Table (5.14)

Experimental B(E2) ratios for transitions from β and γ ratios to ground band in ^{152}Sm compared with theory.

Transition E_γ/E'_γ	Energy Band	$J_i \to J_f$ $J_i \to J_f$	B(E2) Ratio				
			Present Work	IBM	Bohr et al[3]	Reidinger et al[153]	Barrette et al[97]
$\dfrac{443.97}{688.65}$	β	$2^+ \to \dfrac{(4)^+}{(2)_g}$	2.12 (09)	4.67	1.80	5.36	2.14
$\dfrac{810.45}{688.65}$	β	$2^+ \to \dfrac{(0)^+}{(2)_g}$	0.17 (01)	1.76	0.70	0.33	0.25
$\dfrac{443.97}{810.45}$	β	$2^+ \to \dfrac{(4)^+}{(0)_g}$	12.57 (65)	2.65	2.60	16.20	8.49
$\dfrac{901.20}{656.47}$	β	$4^+ \to \dfrac{(2)^+}{(4)_g}$	0.11 (01)	3.22	1.10	–	0.11
$\dfrac{964.10}{1085.89}$	γ	$2^+ \to \dfrac{(2)^+}{(0)_g}$	2.55 (05)	3.15	1.43	–	1.69
$\dfrac{964.10}{719.32}$	γ	$2^+ \to \dfrac{(2)^+}{(4)_g}$	17.78 (27)	15.27	20.00	–	0.57
$\dfrac{1085.89}{719.32}$	γ	$2^+ \to \dfrac{(0)^+}{(4)_g}$	6.69 (11)	4.86	14.00	–	0.34
$\dfrac{867.42}{1112.09}$	γ	$3^+ \to \dfrac{(4)^+}{(2)_g}$	0.84 (02)	1.19	0.40	–	2.70
$\dfrac{1005.22}{1249.92}$	γ	$4^+ \to \dfrac{(4)^+}{(2)_g}$	11.35 (68)	18.15	2.94	–	3.54

A without band mixing
B with band mixing.

model without mixing between the bands, while Riedinger et al[153] showed the predictions of Bohr and Mottelson model (assuming a symmetric rotor[3,162]), but with mixing corrections. Barratte et al[3] gave the predictions of the rotor model using the corrections made by Mikhailove[164]. It is seen that when mixing corrections are made, the theoretical values get closer to experimental.

In general, it is difficult to evaluate the band mixing, especially for nuclei clustering around the transitional region[138]. It was noticed that there is a general disagreement between the experimental and the theoretical B.Rs for the member of $k^{\pi}=1^{-}$ band (Table 5.9) which could be due to Coriolis Coupling between these negative parity bands.

The 1292.71 keV level could be a member of $k^{\pi}=0^{+}$ band (Table 5.7). The ratio B(E2, 482)/B(E2, 1170) is 56 ±13 supports this assumption, therefore this level could be a member of another β-band. The present IBM calculations predicted the second β-band, and the 0^{+} band-head for this level was also located at 1072 keV in full agreement with Passiga[141]. The K-quantum numbers of the other levels were confirmed by comparing the experimental and theoretical B.Rs of transitions depopulating them.

Two new levels have been proposed, together with five new transitions, and the existence of the levels are supported by theoretical calculations (Table 5.5). The spin and parities of these levels were assigned in view of their logft values, and from α_k and IBM calculations in this study and from previous works[11,97,98,104,113,139−142]. The assignment of the new level at 1436.65 keV (2^{+}) is supported by the present IBM calculation which is predicted as band-head for the second γ-band in ^{152}Sm. The new level at 1681.56 keV is suggested according to singles and coincidence data (Tables 5.1, 5.2). The spin and parities

4^- are assigned to this level in view of logft value, and this is in agreement with the prediction of Konijn et al[71] for this level from $(\alpha, 2n)$ reaction. The 1315.32 keV transition, previously reported by Sharma et al[105] and Baker et al[104] but unplaced in their decay scheme, could be placed between 1681.56 keV level and the level 366.46 keV. The 964.10 keV transition is considered to be a doublet by Baglin[113] and Warburton et al[123] which is confirmed in this work.

CHAPTER VI
STUDIES OF THE EXCITED STATES
IN ^{182}W ISOTOPE

6.1 Introduction

The decay of 115 d ^{182}Ta to ^{182}W and the excitation of several levels of this nucleus have been investigated. One aim of the present work is to confirm the decay scheme with high resolution detectors in order to establish more firmly many facets of the level structure. The level scheme of the even even nucleus ^{182}W has been theoretically and experimentaly investigated by many workers[3,9,12,167−170,174,175,193−196,201]. Most of the levels have been successfully interpreted[162,165−167] as belonging to different rotational bands according to the unified nuclear model developed by Bohr and Mottelson[3]. Recent theoretical studies, such as Duval et al[168], have focussed attention on the Interacting Boson Model (IBM)[9,12] as applied to the isotopes of tungsten.

^{182}Ta is widely used as a calibration source for Ge(Li) detectors since it emits two sets of gamma energies; a low energy portion (<300 keV) and the high energy portion (>900 keV). Considerable data on γ-ray transition in the β-decay of ^{182}Ta is available[110,170−173]. The earliest results are summarised in Schmorak[169]. Subsequently, energies and intensities have been reported from singles measurements[109,110,170−174]. A level scheme has been investigated by Murrey et al[166], Sapyta et al[167], recently by Rikovska et al[175] and Jilong[174]. Sapyta et al[167] have carried out singles and coincidence measurements using planar and coaxial Ge(Li) detector. Their list started from 85 keV transition

with a cutoff at 1453 keV and some transitions were missed from their list. The reported errors in relative intensities were 10% for energies <400 keV and 7% for energies >400 keV. In their coincidence experiment, only two energy gates (100 and 229 keV) were taken to establish the decay scheme. A complete list of their γ-rays and intensities was reported.

In the present study γ-ray energies and intensities in the decay of ^{182}Ta have been obtained with Ge(Li) detectors. Because Ge(Li) detectors are not so sensitive to low energies a pure Ge detector was also used. The $\gamma-\gamma$ coincidence data removed earlier ambiguities and allowed an accurate level scheme for ^{182}W to be built up for reliable comparison with current nuclear models[9,168]. Calculation have been carried out based on the symmetric rotor introduced by Bohr and Mottelson[4], and the IBM[9,168,176,177]. The ^{182}W isotope is a strongly deformed nucleus giving rise to rotational bands. Two new energy levels and five possible new transitions, have been placed in the decay scheme. These were confirmed from the coincidence data and energy sum relations. The spins and parities were assigned from logft values and confirmed from the other levels.

The negative parity states were investigated in view of residual interaction arising from pairing plus a modified octupole-octupole force. The microscopic theoretical calculation using residual pairing plus multipole forces performed by Neergard and Vogal[184] well reproduced the $k^{\pi}=2^{-}$ state at 1289 keV. Although these calculations were more realistic in explaining the band mixing between octupole vibrational multiplet states, the experimental evidence found by Herzog et al[185] suggested that the band mixing between $k^{\pi}=2^{-}$ and $k^{\pi}=3^{-}$ bands was not so strong as expected. A disputed configuration, Herzog et al[185], predicted a more collective structure at this state. Neergard and Vogal[184] predicted a low-lying octupole vibration in this energy region with $k^{\pi}=2^{-}$

and a rather strong Coriolis coupling of this band to the $k^\pi=3^-$ member of the octupole multiplet. The inelastic scattering cross section of deuterons measurements indicate that the $k^\pi=2^-$ rotational band in ^{182}W is rather more pure than predicted theoretically[186]. It was suggested that there is some configuration mixing with $k^\pi=2^-$ band.

6.2 Experimental procedure and Results

6.2.1 Source Preparations

The ^{182}Ta source was prepared by the (n,γ) capture reaction after thermal neutron irradiation of natural ^{181}Ta (99.99% purity) in a form of thin wire, at the university of London Reactor Centre (ULRC) following the method described in Section (1.2). The source was left for two weeks after irradiation before taking any measurements. This allows any short life activity to be eliminated. A source activity of 10 μCi is sufficient to give about 1500 counts/sec with a source to detector distance of 25 cm.

6.2.2 Single Spectra

The single spectra were measured using the 10% Ge(Li) efficient detector and also the Germanium detector to confirm the low energy peaks observed in this region, and to complement the use of the Ge(Li) detector near 100 keV region.

Fig. (6.1) shows the singles spectrum obtained from 10% Ge(Li) detector. The analyses of singles spectra enabled a total of 43 γ-rays to be identified
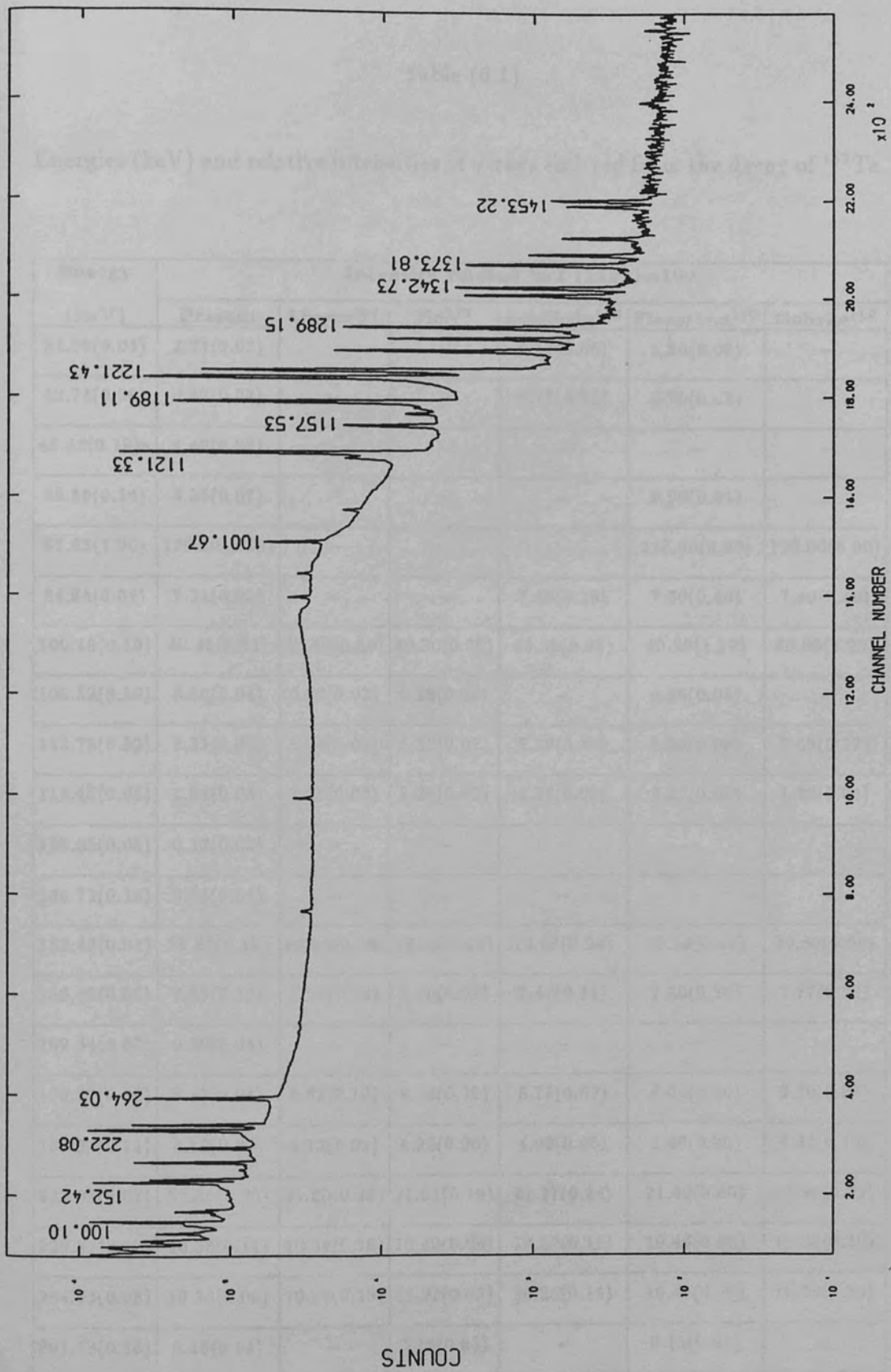
Fig. (6.1) Single Spectrum of Ta-182 decay.

Table (6.1)

Energies (keV) and relative intensities of γ-rays emitted from the decay of ^{182}Ta.

Energy	Intensity related to I (1121)=100					
(keV)	Present	Meyer[109]	Jin[174]	Schöhzig[173]	Firestone[170]	Gehrke[110]
31.69(0.04)	2.21(0.02)	–	–	2.53(0.06)	1.80(0.09)	–
42.74(0.06)	0.82(0.03)	–	–	0.75(0.02)	0.70(0.02)	–
49.43(0.19)*	4.49(0.08)	–	–	–	–	–
65.58(0.14)	8.55(0.07)	–	–	–	8.00(0.04)	–
67.83(1.00)	120.00(1.10)	–	–	–	118.00(6.00)	122.00(6.00)
84.64(0.04)	7.31(0.05)	–	–	7.45(0.16)	7.60(0.40)	7.80(0.40)
100.10(0.10)	40.45(0.51)	40.40(0.50)	40.30(0.60)	40.33(0.95)	40.20(1.10)	40.80(1.20)
109.52(0.19)	0.30(0.04)	0.30(0.02)	0.25(0.06)	–	0.26(0.05)	–
113.75(0.52)	5.31(0.08)	5.34(0.05)	5.36(0.07)	5.29(0.19)	5.50(0.09)	5.43(0.17)
116.43(0.05)	1.28(0.06)	1.26(0.02)	1.26(0.03)	1.26(0.05)	1.27(0.08)	1.26(0.04)
136.65(0.05)	0.12(0.03)	–	–	–	–	–
146.72(0.18)	0.04(0.01)	–	–	–	–	–
152.42(0.04)	19.86(0.17)	19.95(0.18)	19.94(0.18)	19.69(0.24)	20.50(0.40)	20.50(0.60)
156.46(0.05)	7.59(0.12)	7.59(0.10)	7.60(0.07)	7.46(0.11)	7.80(0.20)	7.77(0.23)
169.34(0.07)	0.20(0.04)	–	–	–	–	–
179.27(0.08)	8.83(0.08)	8.82(0.10)	8.84(0.09)	8.75(0.09)	9.00(0.30)	9.10(0.28)
198.34(0.11)	4.12(0.05)	4.19(0.09)	4.22(0.06)	4.09(0.05)	4.40(0.20)	4.31(0.13)
222.08(0.07)	21.80(0.20)	21.60(0.30)	21.61(0.19)	21.27(0.24)	21.60(0.60)	21.90(0.70)
229.33(0.12)	10.38(0.11)	10.39(0.18)	10.49(0.09)	10.32(0.11)	10.40(0.30)	10.60(0.30)
264.03(0.08)	10.14(0.09)	10.26(0.18)	10.37(0.06)	10.26(0.14)	10.40(0.30)	10.50(0.30)
891.73(0.18)	0.15(0.04)	–	0.16(0.05)	–	0.15(0.02)	–

Table (6.1) (Continued)

Energy	Intensity related to I (1121)=100					
(keV)	Present	Meyer[109]	Jin[174]	Schöhzig[173]	Firestone[170]	Gehrke[110]
927.90(0.07)	1.77(0.06)	1.73(0.03)	1.76(0.04)	–	1.79(0.09)	–
959.69(0.07)	1.01(0.03)	0.98(0.03)	0.98(0.05)	–	1.02(0.06)	–
1001.67(0.12)	6.01(0.05)	5.87(0.06)	5.85(0.10)	–	5.98(0.03)	–
1044.39(0.09)	0.70(0.8)	–	0.72(0.07)	–	0.69(0.08)	–
1113.50(0.12)	1.35(0.15)	1.32(0.03)	1.30(0.03)	–	1.13(0.01)	–
1121.33(0.11)	100	100	100	100	100	100
1157.53(0.07)	2.71(0.20)	2.92(0.03)	2.88(0.23)	–	2.83(0.63)	–
1180.88(0.14)	0.23(0.09)	–	0.21(0.04)	–	0.26(0.04)	–
1189.11(0.07)	47.37(0.29)	47.10(0.80)	46.40(0.14)	46.59(0.33)	47.00(0.50)	46.50(0.50)
1221.43(0.13)	77.48(0.34)	77.80(0.60)	76.80(0.60)	76.96(0.54)	78.30(0.10)	78.31(0.79)
1224.00(0.40)	55(0.12)	0.30(0.10)	0.53(0.24)	–	0.60(0.10)	–
1231.03(0.09)	33.85(0.22)	33.10(0.50)	32.72(0.10)	32.81(0.23)	33.1(0.40)	32.96(0.33)
1257.43(0.07)	4.35(0.6)	4.36(0.08)	4.27(0.02)	4.25(0.02)	4.33(0.07)	4.26(0.04)
1273.75(0.5)	1.90(0.04)	1.95(0.03)	1.87(0.01)	–	1.90(0.40)	1.86(0.02)
1289.15(0.11)	3.90(0.05)	4.29(0.08)	3.80(0.03)	3.86(0.02)	4.04(0.70)	3.86(0.05)
1294.57(0.13)	0.03(0.01)	–	–	–	–	–
1342.73(0.06)	0.76(0.04)	0.74(0.01)	0.72(0.01)	–	0.75(0.02)	–
1373.81(0.07)	0.65(0.02)	0.68(0.01)	0.63(0.01)	–	0.66(0.02)	–
1387.41(0.09)	0.24(0.03)	0.27(0.01)	0.20(0.01)	–	0.21(0.01)	–
1410.15(0.11)	0.14(0.02)	0.12(0.01)	0.11(0.01)	–	0.11(0.01)	–
1453.22(0.14)	0.11(0.02)	0.12(0.01)	0.09(0.01)	–	0.12(0.01)	–

* cannot be placed in the decay scheme.

with the computer program SAMPO for the purposes of peakfitting and energy calibration as described in Chapter III.

Table (6.1) shows the relative intensities of γ-rays resulting from the β^- decay of ^{182}Ta . A total of five transitions were identified for the first time in the decay of ^{182}Ta to ^{182}W . The energies are: 49.43, 136.65, 146.72, 169.34 and 1294.57 keV. The intensities are normalized to 100; the intensity of 1121.33 keV in ^{182}W . The intensities of the γ-rays were compared with Meyer[109], Jin et al[174], Schöhzig et al[173] and Gehrke et al[110]. There was a good agreement between the values reported in the present work and previous works[109,110,172−175] especially for the high energy portion. The uncertainties in the intensities of present work are about 3%.

6.2.3 Coincidence Spectra

The coincidence data were collected in the ACE buffer and stored in the PC-computer to accumulate sufficient counts for the gating spectrum. The analysis were performed offline by SAMPO on the VAX-computer in order to identify the strength of the observed line in the coincidence with each gate. A typical total spectrum of the ^{182}Ta decay is shown in Fig. (6.2).

In constructing the decay scheme of ^{182}W , five energy gates were taken. The energies were 100, 229, 1002, 1122 and 1289 keV. Selected in this manner these energy gates are well defined and clear of neighbouring peaks, they form good reasons for their choices.

The gate at 100 keV is important since such a transition depopulates the first excited state of ^{182}W and most transitions will be in cascade with it, therefore showing up in the coincidence spectra. The second gate was taken to provide more coincidence data for transitions depopulating the second excited state (4^+) in the ground state band to the 100.10 keV level. This gate gives support to some of the new transitions observed in the singles measurements during this study. The coincidence between the high energy transitions and the rest of the spectrum were studied by considering the last three gates 1002, 1122 and 1289 keV. The 1121.33 keV transition depopulates the first excited state in the γ-band to the 100.10 keV level, thus this gate provides the coincidence data which allows us to study the transitions between the members of this band and the members of other bands. The 1289.15 keV transition depopulates the first member of octupole band ($k^\pi=2^-$) to the ground state, and choosing this transition as energy gate enables us to study the transition from other bands to this band and supporting the new transition at 136.65 keV. The coincidence data taken in these five gates provide a required evidence for the existence of the new energy levels and transitions. The summary of the coincidence results are shown in Table (6.2). The energy gates are shown on the upper row while the entire (x) refer to the coincidence. The Coincidence spectra for all the energy gates are shown in Fig. (6.3 - 6.7).

6.3 Decay Scheme

The decay scheme of ^{182}W was established on the basis of the coincidence results of five energy gates (Table 6.2), and the energy sum relations as given in Table (6.3). The decay scheme is shown in Fig. (6.8). On the left side of the figure are shown the energy levels, the branching ratios (B.Rs), the logft values, spins,

Table (6.2)

Summary of the γ-γ coincidence results from the decay of the ^{182}Ta.

Energy	Gates (keV)				
(keV)	100.10	229.33	1001.67	1121.33	1289.15
42.74	x	x	x	x	x
65.58	x	x	x	x	x
67.83	x	x	—	x	—
84.64	x	x	—	x	x
100.10	—	x	x	x	—
109.52	x	x	—	—	—
113.75	x	x	x	x	x
116.43	x	x	—	—	—
136.65	x	x	x	x	x
146.72	x	x	x	x	x
152.42	x	x	—	x	—
156.46	x	x	x	x	x
169.34	x	x	x	x	x
179.34	x	x	x	x	x
198.34	x	x	—	x	x
222.08	x	x	x	x	x

Table (6.2) (Continued)

Energy	Gates (keV)				
(keV)	100.10	229.33	1001.67	1121.33	1289.15
229.33	x	—	x	—	—
264.03	x	x	—	x	x
891.73	x	x	—	—	—
927.90	x	x	—	—	—
959.69	x	x	—	—	—
1001.67	x	x	—	—	—
1044.39	x	x	—	—	—
1121.33	x	—	—	—	—
1157.53	x	x	—	—	—
1180.88	x	x	—	—	—
1189.11	x	—	—	—	—
1224.00	x	x	—	—	—
1231.03	x	—	—	—	—
1273.75	x	—	—	—	—
1294.57	x	x	—	—	—
1342.73	x	—	—	—	—
1387.41	x	—	—	—	—
1410.15	x	—	—	—	—
1453.22	x	—	—	—	—
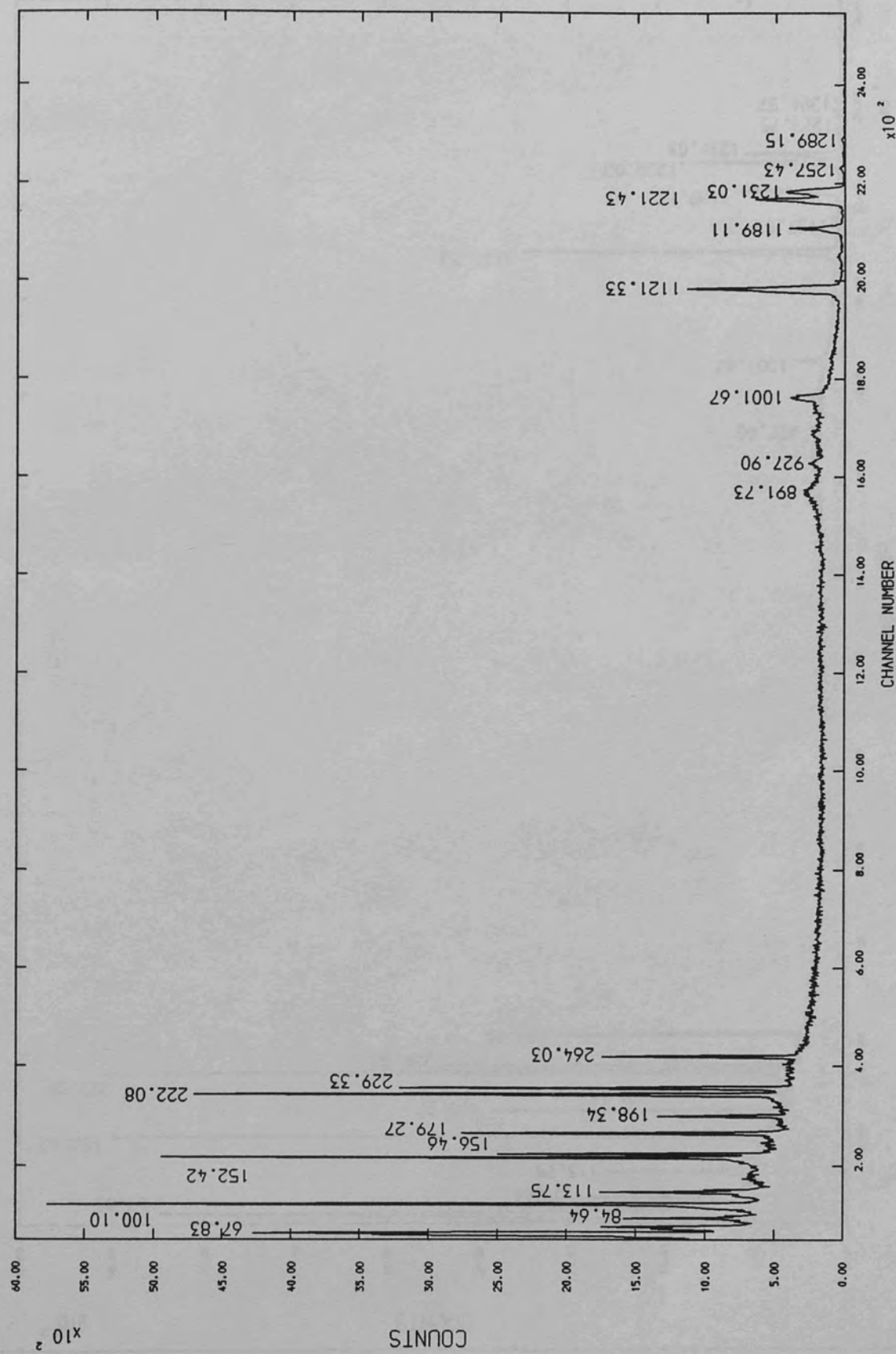
Fig. (6.2) Total Spectrum of Ta-182 decay.
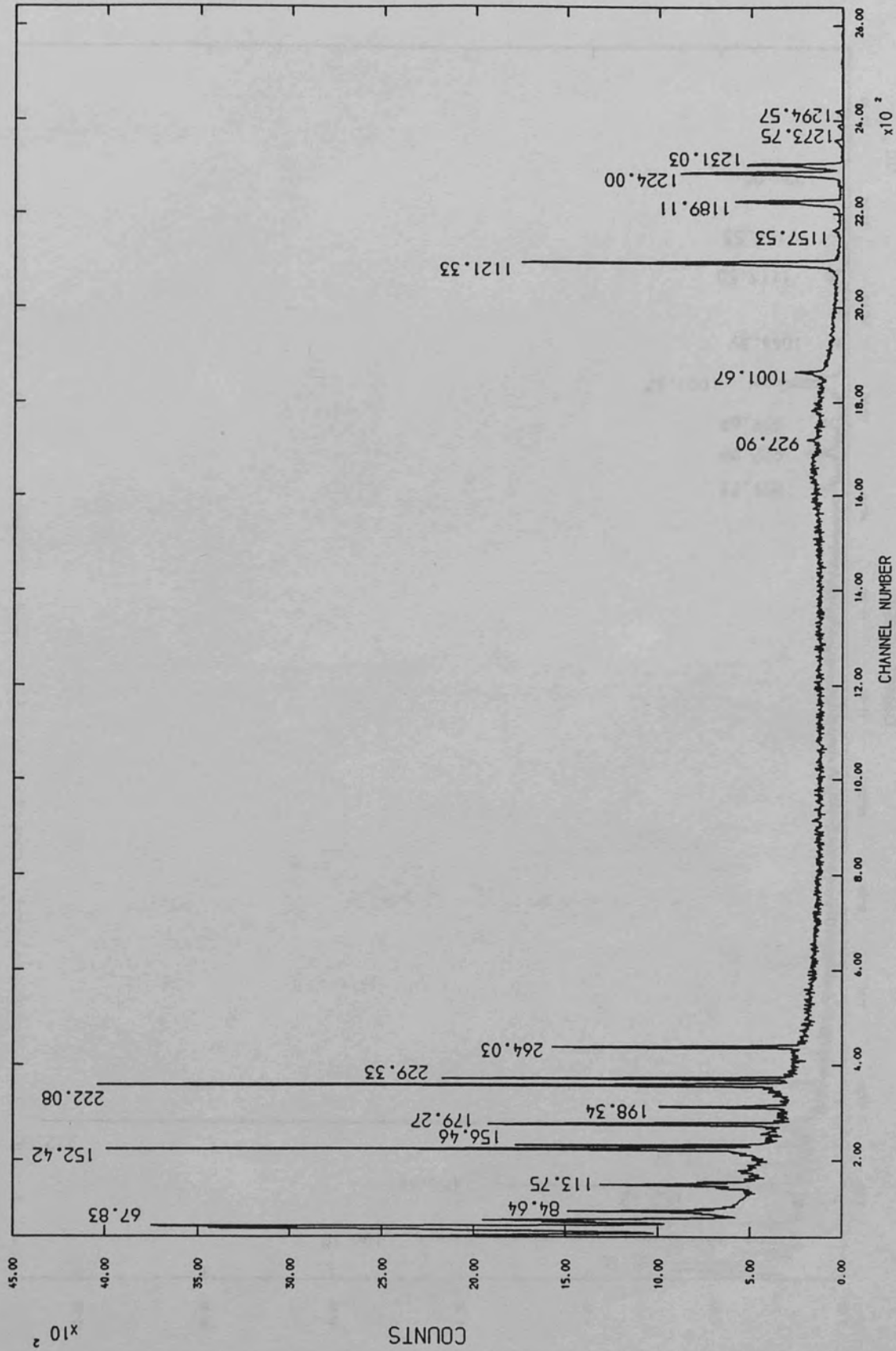
Fig (6.3) Spectrum of Ta-182 decay in coincidence with 100 keV.
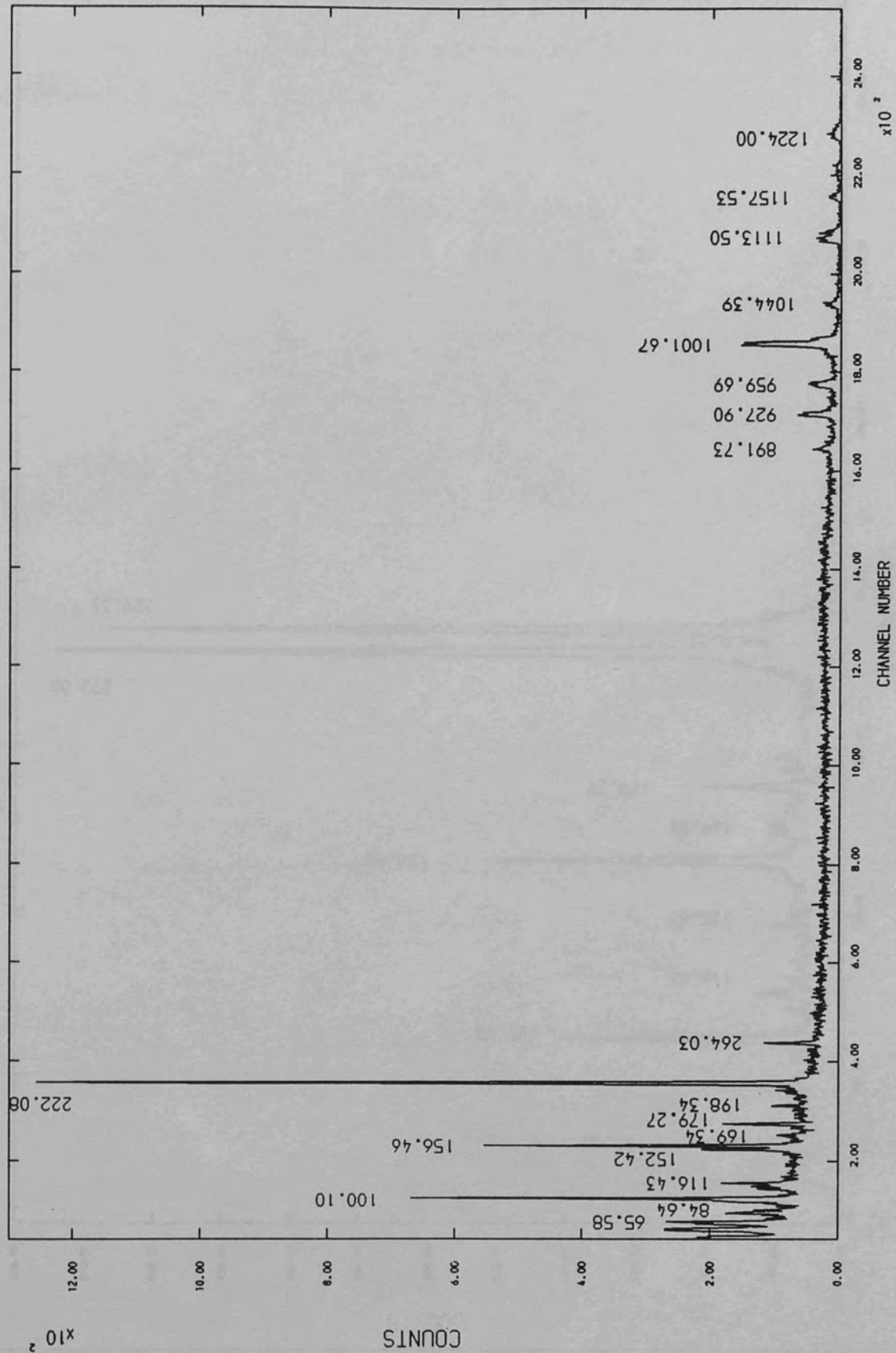
Fig (6.4) Spectrum of Ta-182 decay in coincidence with 229 keV.
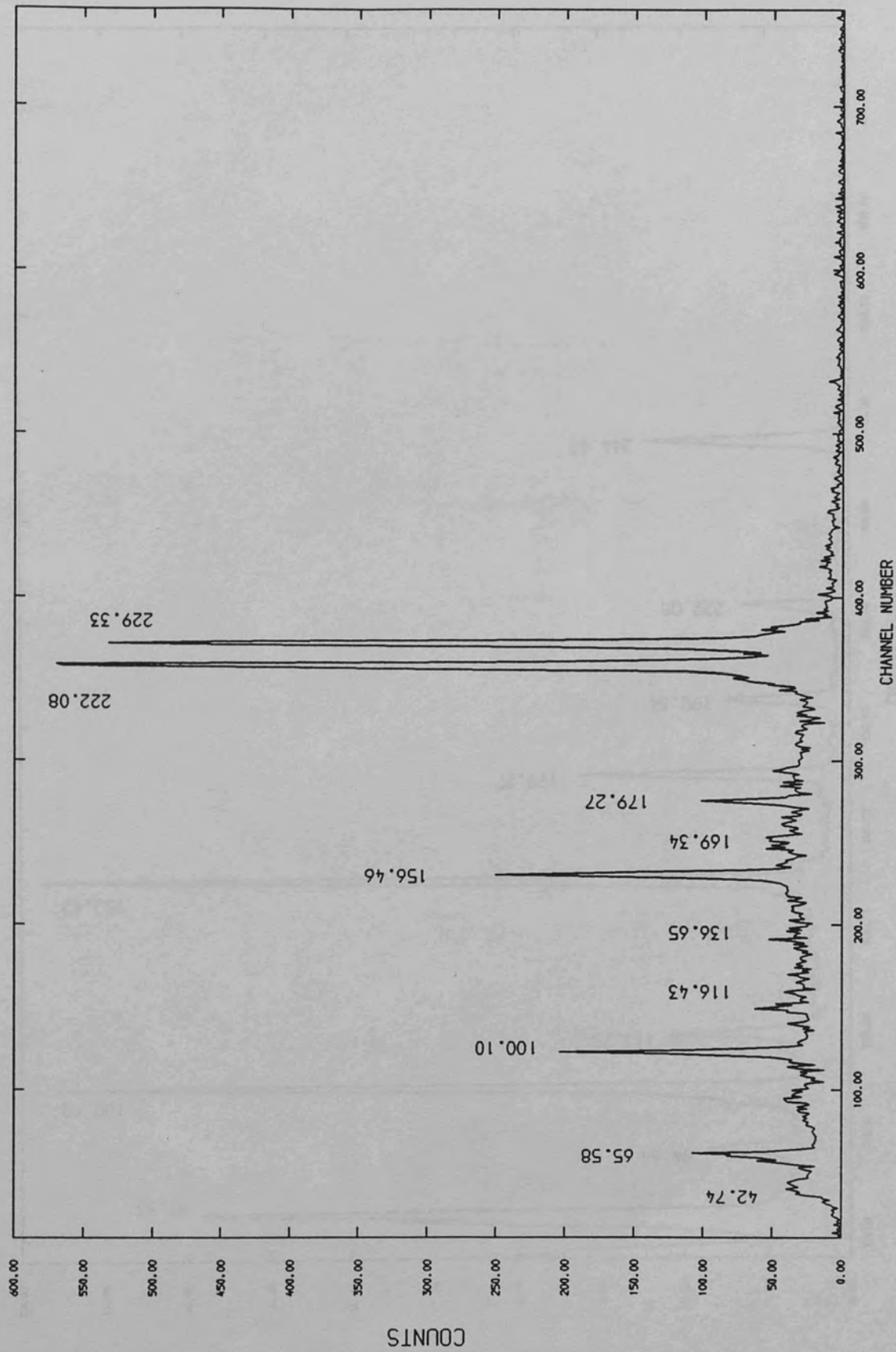
Fig (6.5) Spectrum of Ta-182 decay in coincidence with 1002 keV.
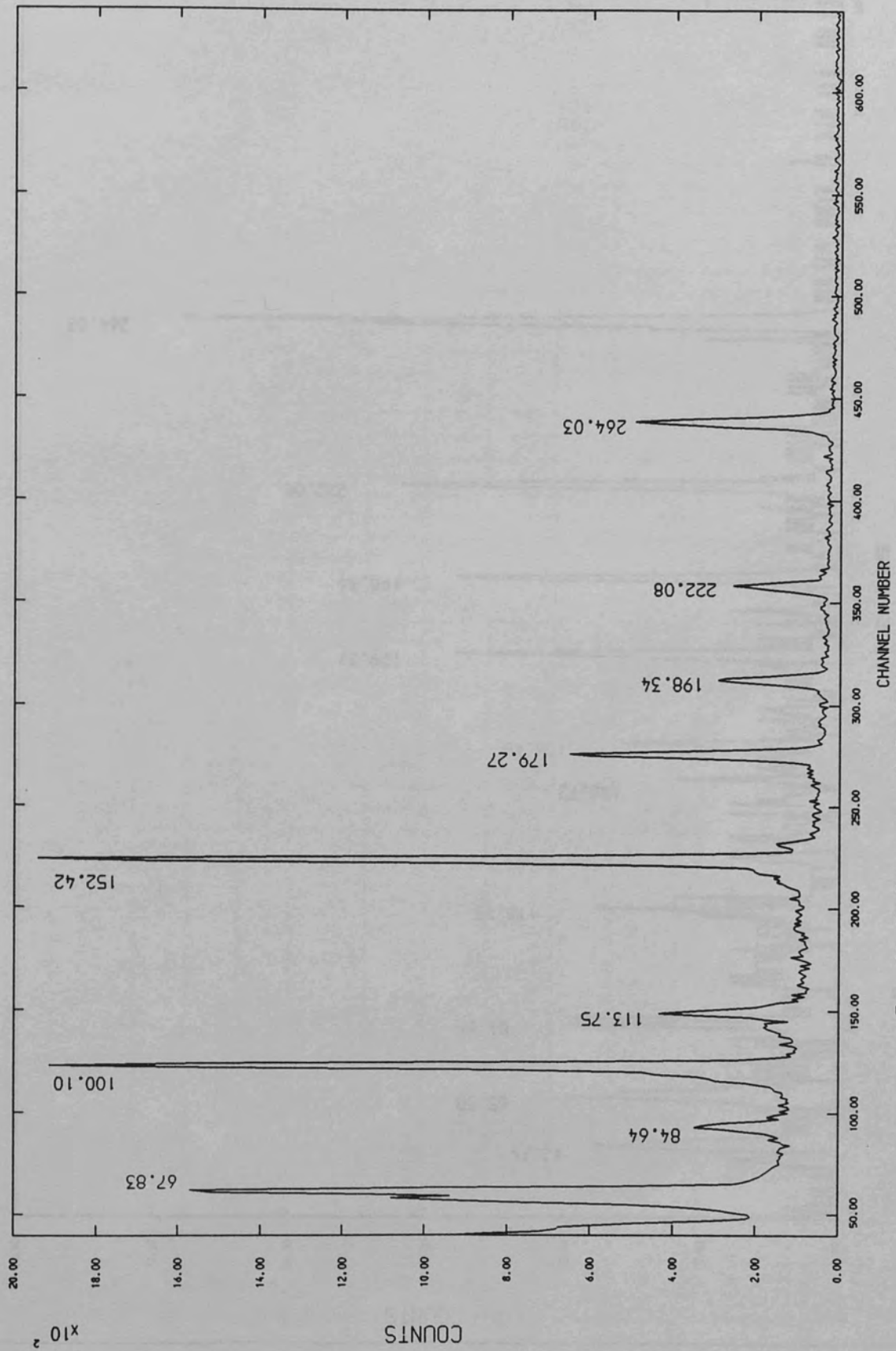
Fig (6.6) Spectrum of Ta-182 decay in coincidence with 1122 keV.
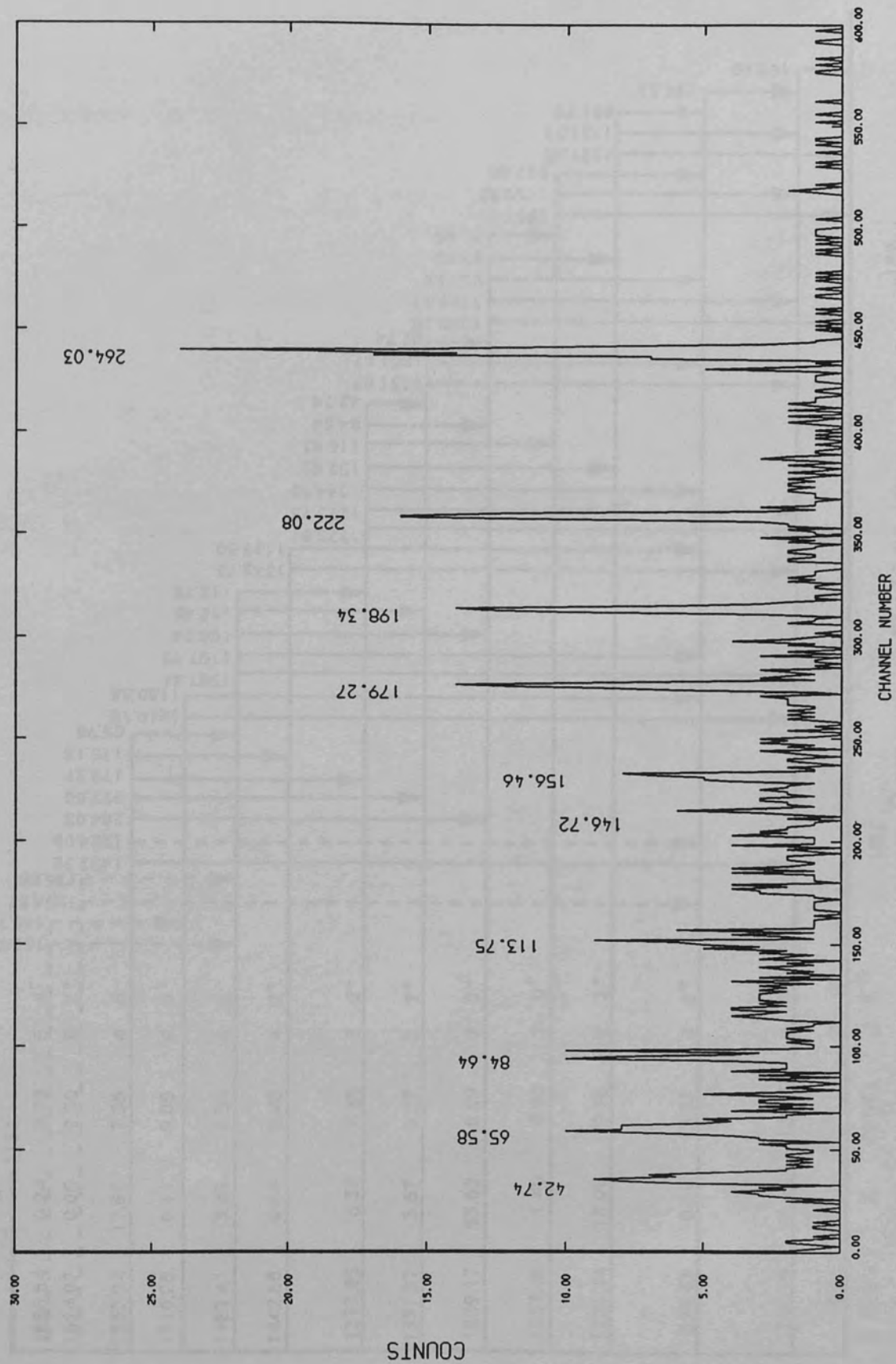
Fig (6.7) Spectrum of Ta-182 decay in coincidence with 1289 keV.
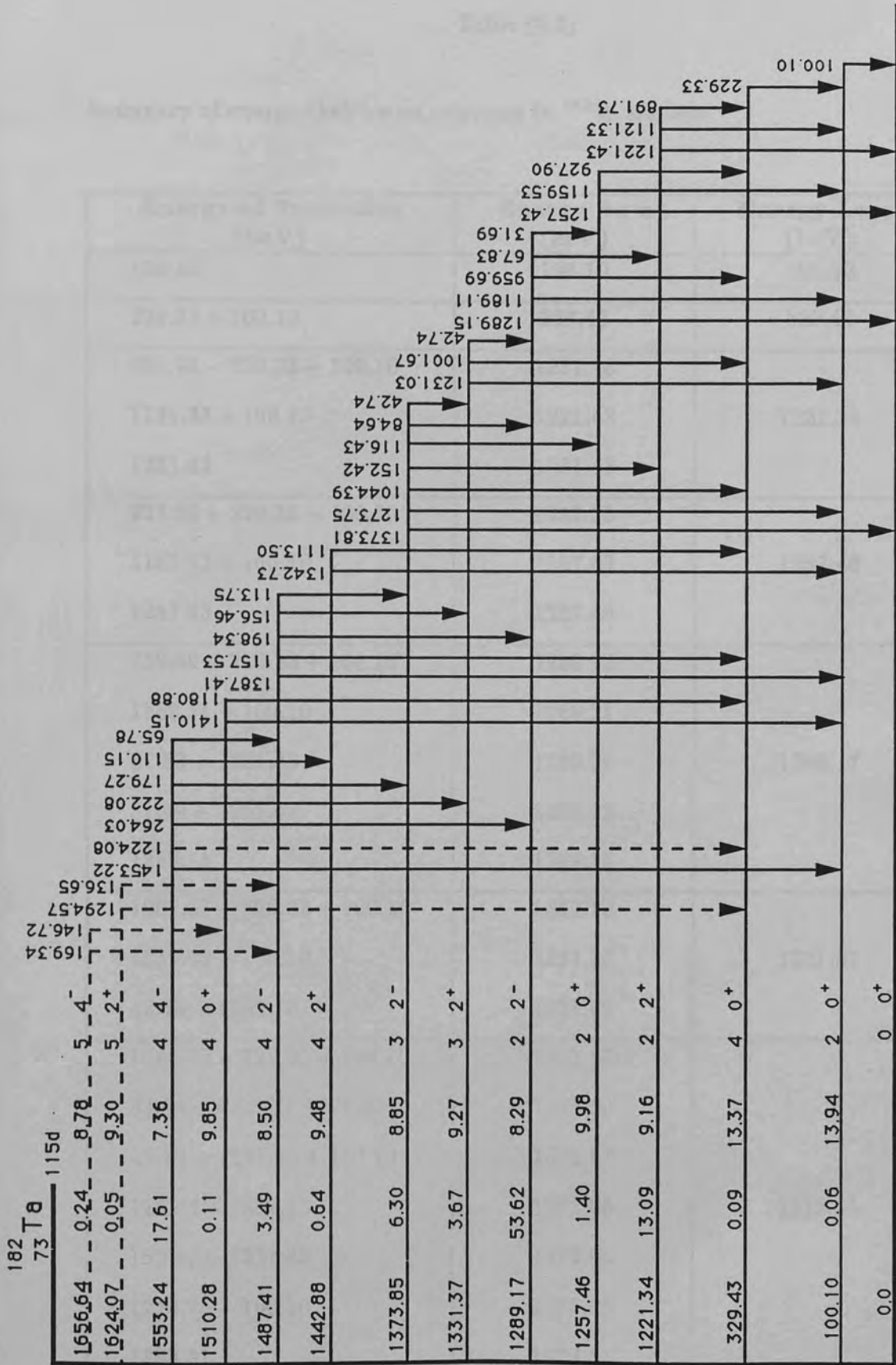
Fig (6.8)   Decay scheme of ^{182}W

Table (6.3)

Summary of energy (keV) sum relations in ^{182}W nucleus.

Energy of Transition (keV)	Energy Sum (keV)	Energy Level (keV)
100.10	100.10	100.10
229.33 + 100.10	329.43	329.43
891.73 + 229.33 + 100.10	1221.16	
1121.33 + 100.10	1221.43	1221.34
1221.43	1221.43	
927.90 + 229.33 + 100.10	1257.33	
1157.53 + 100.10	1257.63	1257.46
1257.43	1257.43	
959.69 + 229.33 + 100.10	1289.12	
1189.11 + 100.10	1289.21	
67.83 + 1221.43	1289.26	1289.17
31.69 + 1257.43	1289.12	
1289.15	1289.15	
1001.67 + 229.33 + 100.10	1331.10	
1231.03 + 100.10	1331.13	1331.37
42.74 + 1289.15	1331.89	
1044.39 + 229.33 + 100.10	1373.82	
84.64 + 67.83 + 1221.43	1373.90	
42.74 + 1231.03 + 100.10	1373.87	
116.43 + 1257.43	1373.86	1373.85
152.42 + 1221.43	1373.85	
1273.75 + 100.10	1373.85	
1383.81	1373.81	

Table (6.3) (Continued)

Energy of Transition (keV)	Energy Sum (keV)	Energy Level (keV)
1113.50 + 229.33 + 100.10	1442.93	
1342.73 + 100.10	1442.83	1442.88
1157.53 + 229.33 + 100.10	1486.96	
156.46 + 1231.03 + 100.10	1487.49	
198.34 + 1289.15	1487.49	1487.41
113.75 + 1373.81	1487.56	
1387.41 + 100.1	1487.51	
1180.88 + 229.33 + 100.10	1510.31	
1410.15	100.10	1510.28
110.15 + 1113.50 + 229.33 + 100.10	1553.08	
65.58 + 113.75 + 1373.81	1553.14	
179.27 + 116.43 + 1257.43	1553.13	
222.08 + 1231.03 + 100.10	1553.21	1553.24
264.03 + 67.83 + 1221.43	1553.29	
1224.00 + 229.33 + 100.10	1553.29	
1453.22 + 100.10	1553.32	
136.65 + 198.34 + 1289.15	1624.14	
1294.57 + 229.33 + 100.10	1624.00	1624.07
169.34 + 1157.53 + 229.33 + 100.10	1656.30	
146.72 + 1410.15 + 100.10	1656.97	1656.64

parities and the K-quantum numbers. The numbers at the base of the arrow indicate the energy of the transition. The new transitions and levels are shown as dotted lines.

The experimental and theoretical K-shell internal conversion coefficients α_k are shown in Table (6.4). The conversion electron intensities (I_β) were taken from Helmer[171] and Nilsson et al[182], while the γ-ray intensities (I_γ) were calculated (Table 6.1). In the low energy portion of the spectrum, the experimental α_k of the 100.10 keV transition from the first excited state to ground state was normalized to the theoretical α_k for pure E2 multipolarity.

In the high energy portion, the experimental α_k of the 1222 keV lines was normalized to the theoretical α_k for pure E2 multipolarity, since this state forms the first excited state of the γ-rotational band. The theoretical values were taken from Rosel[33]. The comparison between theoretical and experimental α_k values enables us to deduce the transition multipolarity, hence it is possible to assign spins and parities to the concerned levels. Good agreement between the experimental and theoretical α_k is seen in Table (6.4).

The logft values were calculated according to the relations given by Mozskowski[22]. The β^- B.R were calculated from the balance between the decay and feeding of the γ-rays for each level. The end point energies of the β^- electron were taken from Lederer et al[143] (Q value is 1811.3 keV). The spins and parities of the levels were deduced according to the β^- selection rules as given by Friedlander[144] and are shown in Table (6.5).

Table (6.4)

Deduced multipolarities from k-shell internal conversion coefficients for ^{182}W.

Energy (keV)	$J_i^\pi \to J_f^\pi$	Experimental		Theoretical α_k					Deduced Multi-polarity
				E1	E2	M1	E3	M2	
84.64	$32^- \to 22^-$	5.43	(0.84)	0.47	1.07	6.66	1.54	55.53	$M1$
100.10	$20^+ \to 00^+$	0.78	(0.08)	0.31	0.87	4.10	1.88	30.41	$E2$
113.75	$42^- \to 32^-$	2.42	(0.27)	0.22	0.69	2.87	1.71	19.56	$M1$
116.43	$32^- \to 20^+$	0.17	(0.02)	0.21	0.65	2.69	1.66	18.03	$E1$
152.42	$32^- \to 22^+$	0.11	(0.01)	0.11	0.35	1.25	1.01	7.02	$E1$
156.46	$42^- \to 32^-$	0.09	(0.02)	0.10	0.33	1.18	0.96	6.56	$E1$
179.27	$44^- \to 32^-$	0.52	(0.05)	0.07	0.23	0.79	0.68	3.96	$E2/M1$
198.34	$42^- \to 22^-$	0.18	(0.02)	0.06	0.18	0.62	0.54	3.00	$E2$
222.08	$42^- \to 32^+$	0.04	(0.01)	0.04	0.13	0.44	0.38	1.93	$E1$
229.33	$40^+ \to 20^+$	0.13	(0.01)	0.04	0.12	0.42	0.36	1.83	$E2$
264.03	$44^- \to 22^-$	0.08	(0.01)	0.03	0.09	0.32	0.28	1.35	$E2$
*891.73	$22^+ \to 40^+$	4.31	(0.78)	0.02	5.24	13.17	11.66	33.56	$E2$
927.90	$20^+ \to 40^+$	4.05	(0.65)	1.89	4.74	10.41	11.61	29.20	$E2$
959.69	$22^- \to 40^+$	8.99	(1.45)	1.73	4.30	10.24	9.31	25.36	$E3$
1001.67	$32^+ \to 40^+$	3.48	(0.55)	1.52	3.73	8.48	7.90	20.46	$E2$
1044.39	$32^- \to 40^+$	4.23	(0.68)	1.45	3.56	8.02	7.51	19.32	$E1/M2$
1113.50	$42^+ \to 40^+$	2.86	(0.55)	1.35	3.29	7.28	6.88	17.48	$E2$

Table (6.4) (Continued)

Energy (keV)	$J_i^\pi \to J_f^\pi$	Experimental		Theoretical α_k					Deduced Multi-polarity
				E1	E2	M1	E3	M2	
1121.33	$22^+ \to 20^+$	2.99	(0.47)	1.33	3.26	7.20	6.81	17.27	$E2$
1157.53	$20^+ \to 20^+$	4.81	(0.84)	1.28	3.11	6.81	6.48	16.31	$E2/M1$
1189.11	$22^- \to 20^+$	3.82	(0.61)	1.23	2.98	6.47	6.19	15.47	$E1/M2/E3$
1221.43	$22^+ \to 00^+$	2.53	(0.40)	1.18	2.85	6.13	5.90	14.61	$E2$
1224.00	$44^- \to 40^+$	2.74	(0.71)	1.17	2.84	6.10	5.88	14.54	$E1$
1231.03	$32^+ \to 20^+$	2.44	(0.39)	1.16	2.82	6.02	5.81	14.35	$E2$
1257.43	$20^+ \to 00^+$	2.43	(0.39)	1.12	2.71	5.74	5.57	13.65	$E2$
1273.75	$32^- \to 20^+$	2.86	(0.45)	1.10	2.65	5.57	5.42	13.22	$E1/M2$
1289.15	$22^- \to 00^+$	10.61	(1.71)	1.07	2.58	5.40	5.29	12.81	$M2$
1342.73	$42^+ \to 20^+$	2.17	(0.35)	0.99	2.37	4.82	4.80	11.38	$E2$
1373.81	$32^- \to 00^+$	3.95	(0.63)	0.94	2.25	4.49	4.52	10.56	$E3$
1387.41	$42^- \to 20^+$	3.84	(0.63)	0.92	2.19	4.35	4.39	10.19	$E3$
1410.15	$40^+ \to 20^+$	2.10	(0.39)	0.89	2.10	4.10	4.19	9.59	$E2$
1453.22	$44^- \to 20^+$	3.21	(0.61)	0.82	1.93	3.64	3.80	8.44	$E3$

*For the reminder of the Table all α_k values are to be multiplied by 10^3.

Table (6.5)

The beta branching ratios, logft values, spins and parities assignments for levels in ^{182}W nucleus.

Energy level (keV)	Q_{value} $\varepsilon_\beta = 1811$ (keV)	$\sum I_\gamma$ feed	$\sum I_\gamma$ decay	$\sum I_\gamma$ decay $-I_\gamma$ feed	B.R %	logft
100.10	1710.90	196.14	40.45	–	0.058	13.94
329.43	1481.57	13.13	10.38	–	0.096	13.37
1221.34	589.67	140.30	177.63	37.33	13.09	9.16
1257.46	553.54	3.49	7.48	3.99	1.397	9.98
1289.17	521.83	21.98	174.93	152.95	53.62	8.29
1331.37	479.63	29.80	40.27	10.47	3.670	9.27
1373.85	437.15	14.14	32.11	17.97	6.299	8.85
1442.88	368.12	0.30	2.11	1.81	0.635	9.48
1487.41	323.59	8.67	18.62	9.945	3.486	8.50
1510.28	300.78	0.05	0.37	0.32	0.112	9.85
1553.24	257.76	0.04	50.28	50.24	17.61	7.36
1624.07	186.93	–	0.15	0.15	0.053	9.30
1656.64	154.36	–	0.24	0.24	0.084	8.78

6.3.1 Discussion of Individual Levels in ^{182}W

6.3.1.1 The 100.10 keV (2^+) level

This is a well-known first (2^+) excited state in ^{182}W which has been studied in the past through the ^{182}Ta decay[169], deuteron inelastic scattering experiments[186] and the decay of ^{182}Re by Sapyta[167]. Remarkable agreement between experimental and theoretical value of α_k for the 100.10 keV transitions supports the 2^+ assignment (Table 6.4). The calculated logft value for this level gives another support for the 2^+ assignment (Table 6.5). The IBM calculation of this level is in full agreement with the experimental value (Table 6.6).

6.3.1.2 The 329.43 keV (4^+) level

The existence of this level was previously reported in the decay of ^{182}Ta . The spin of the 329.43 keV level was confirmed from the α_k value of the 229.33 keV transition depopulating this level (Table 6.4) to the first excited state. The spin and parity were also confirmed from logft values (Table 6.5). The IBM calculations of this level is in very good agreement with the experimental value.

6.3.1.3 The 1221.34 keV (2^+) level

This level is assigned as a 2^+ on the basis of its deexcitation to the ground state. The 1121.33 and 891.73 keV transitions deexcited from 1221.43 keV and were found in coincidence with 100.10 and 229.33 keV gated spectra respectively. The spin of the 1221.43 keV level was confirmed from the α_k values of the 1221.43, 1121.33 and 891.73 keV transitions depopulating this level (Table 6.4) to the ground, first and second ground state band respectively. The spin and

Table (6.6)

The energies of levels in ^{182}W found experimentally compared with rotational and IBM (for positive parity) and with values from other model.

J_k^π	Energy (keV)						
	Experiment	Rotor	IBM	GCM[54]	PPQM[53]	BET[6]	BET[42]
20^+	100.1	100.1	100.1	111	104	100	100
40^+	329.43	329.43	333.7	346	314	328	329
22^+	1221.34	1221.34	1222.6	1164	936	1210	–
20^+	1257.46	1257.46	1259.9	1359	1063	1260	–
22^-	1289.17	1289.17	–	–	–	–	–
32^+	1331.37	1331.37	1322.7	1298	1231	1320	–
32^-	1373.85	1373.85	–	–	–	–	–
42^+	1442.88	1442.88	1456.1	1442	–	1456	–
42^-	1487.41	1487.41	–	–	–	–	–
40^+	1510.28	1510.28	1493.5	1870	–	1543	–
44^-	1553.24	1553.24	–	–	–	–	–
52^+	1624.07	1625.84	1622.9	1637	–	–	–
54^-	1656.64	1656.64	–	–	–	–	–

parity were confirmed from logft values (Table 6.5). Full agreement between theoretical IBM, rotor model calculations and the experimental values (Table 6.6) was found.

6.3.1.4 The 1257.46 keV (2^+) level

Günther et al[186] observed this level in (d,d') reaction and proposed the 2^+ assignment. Sapyta et al[4] had proposed that 1157.53 keV transition depopulates from this level to the 100.10 keV (2^+) state, and the other transition proceeding from 4^- 1487.41 keV state state to 4^+, 329.43 keV state. This is confirmed by present coincidence spectra. The spin of the 1257.46 keV level was confirmed from α_k values of the 1257.46, 1157.53 and 927.90 keV transitions depopulating this level (Table 6.4) to the 0^+, 2^+ and 4^+ ground state band respectively. The spin and parity were confirmed from logft values (Table 6.5). Good agreement between theoretical IBM calculations and experimental values was found (Table 6.6).

6.3.1.5 The 1289.17 keV (2^-) level

The 1289.15 keV level has been assigned spin and parity 2^- by Sapyta et al[167] and Herzog et al[185]. The 31.69, 67.83, 959.69 and 1189.11 keV transitions as deexciting the 1289.17 keV state to the 20^+, 22^+, 42^+ and 20^+ states respectively were detected in the 100.1 and 229.33 keV gated spectra, which would be very reasonable on the basis of spin consideration (Tables 6.2 and 6.4). The present logft value of 8.29 is consistent with a spin and parity of 2^-, as suggested earlier.

6.3.1.6 The 1331.37 keV (3$^+$) level

The existence of a state at 1331.37 keV is confirmed by the observation of the 1231.03, 1001.67 and 42.74 keV transitions in coincidence with the 100.10, 229.33 and 1121.33 keV, respectively. This is in good agreement with Sapyta et al[167]. The angular correlations experiment[175] supported the spin value of this state as 3$^+$, while the IBM prediction is in agreement with the experimental value. This assignment is also consistent with the fact that 1331.37 keV level is not observed in (d,d') experiment[186].

6.3.1.7 The 1373.85 keV (3$^-$) level

This state is a member of the octupole rotational band established by Herzog et al[185] and Sapyta et al[167]. The 3$^-$ assignment follows from the E1 character of the 1273.75, 1044.39, 152.42 and 116.43 keV transitions (Table 6.4), and agrees with that made by Jilong et al[174] and Rikovska et al[175]. The spin and parity were also confirmed from logft values (Table 6.5).

6.3.1.8 The 1442.88 keV (4$^+$) level

Sapyta et al[167] observed this level by the decay of ^{182}Ta and ^{182}Re and proposed 4$^+$ assignment. This assignment was supported by the angular correlations experiment[175] and the (d,d') reaction[186]. The coincidence experiment show that 1342.73 and 1113.50 keV transitions feed the 100.10 and 329.43 keV states respectively. The spin and parity were confirmed as well from α_k (Table 6.4) and logft values (Table 6.5). There is an agreement between the IBM prediction and the experimental values (Table 6.6).

6.3.1.9 The 1487.41 keV (4⁻) level

This level belongs to the $k^\pi = 2^-$ octupole rotational band and has spin value 4^- as suggested by Sapyta et al[167] and Herzog et al[185] a member of rotational band. Coincidence measurements confirm the existence of the level 1487.41 keV, since the 1387.41, 1157.53, 198.34, 156.46 and 113.75 transitions deexciting this state have been detected in the 100.1, 229.33, 1121.33 and 1289.15 keV gated spectrum. The spin and parity of this level are supported from α_k (Table 6.4) and logft values (Table 6.5).

6.3.1.10 The 1510.28 keV (4⁺) level

This level was observed in previous works[167,170,174]. Güther et al[186] and Rikovska et al[175] could not place it in their decay schemes. The present coincidence measurement confirm the existence of this level at 1510.28 keV. This level depopulatesthe 1410.15 keV transition and 1180.88 keV to the 100.1 and 329.43 keV levels, respectively. The spin of the 1510.25 level was confirmed from the α_k values of the 1410.15 keV (Table 6.4). The spin and parity were also confirmed from logft values (Table 6.5). The IBM prediction of this level is in good agreement with the experimental values (Table 6.6).

6.3.1.11 The 1553.24 keV (4⁻) level

This level belongs to the $k^\pi = 4^-$ band and is assigned 4^- as suggested by previous works[167,186,187]. Coincidence measurements also established this level which is depopulated by the 1453.22, 1224.00, 264.03, 222.08, 179.27,110.15 and 65.78 keV transitions to the $2^+, 4^+, 2^-, 3^+, 3^-, 4^+$ and 4^-. The spin of the

1553.24 keV level was confirmed from the α_k values (Table 6.4). The spin and parity were also confirmed from logft values (Table 6.5).

6.3.1.12 The 1624.07 keV (5$^+$) level

The new level at 1624.07 keV is suggested by the transition at 1294.57 and 136.65 keV: the former is in weak coincidence with the 100.10 and 229.33 keV gates, so it can go to the   established level at 329.43 keV. The 136.65 keV transition is seen in strong coincidence with the 1289.15 keV gated spectrum. The logft values of 9.30 is consistent with a spin and parity of 5$^+$ for this level and is considered as a member of γ-band. This assignment is supported by Jeltema et al[188], Galan et al[189] and Harmatz et al[190] from ^{182}Re decay.

6.3.1.13 The 1656.64 keV (5$^-$) level

The new level at 1656.64 keV is suggested by the observation of a new transitions at 146.72 and 169.34 keV which depopulated this level to the 1510.28 and 1487.41 keV levels, respectively. The spin 5$^-$ is reported previously[189−190] from the ^{182}Re decay. The 146.72 keV transition is seen in coincidence with the 100.10 and 229.33 keV gated spectrum. The 169.34 keV transition is seen in coincidence with the 100.10, 229.33, 1001.69, 1121.33 and 1289.15 keV spectra. The logft value of 8.78 is consistent with a spin and parity of 5$^-$.

6.4 Nuclear Model Calculations

6.4.1 Collective Model

The ^{182}W nucleus is considered as a deformed nucleus. Nuclei possessing a nonspherical shape show a rotational spectra[27]. In axially symmetric deformation nuclei, the calculation based on rotational theory will be applied to it. The two parameters A and B from Eq. (2.2.2.6) were determined by fitting the experimental energy values of the first two excited states of the bands. Table (6.6) shows together the energies found experimentally and also the theoretical calculation. Fig. (6.9) shows the experimental and theoretical (rotational) energy levels as determined in this study. The value of the parameters A and B for rotational bands are given in Fig. (6.9).

The ratio $E(4^+)/E(2^+)$ of the ground band is 3.29, while the ratio $E(6^+)/E(4^+)$ is 6.81. These two ratios are in agreement with the theoretical predictions of the symmetric rotor[27,162]. The general feature of the calculations of the rotational spectra is the good agreement between theory and experimental which indicates that ^{182}W is true deformed nucleus with axial symmetry.

6.4.2 The Interacting Boson Model

The IBM approach has proved useful for describing the collective behavior of medium and heavy nuclei in terms of proton and neutrons pairs[9,168,176,177]. The number of bosons for the ^{182}W nucleus is 13 and the ratio $E(4^+)/E(2^+)$ is 3.29. The ^{182}W nucleus is considered to be deformed and lie on the SU(3) limit of
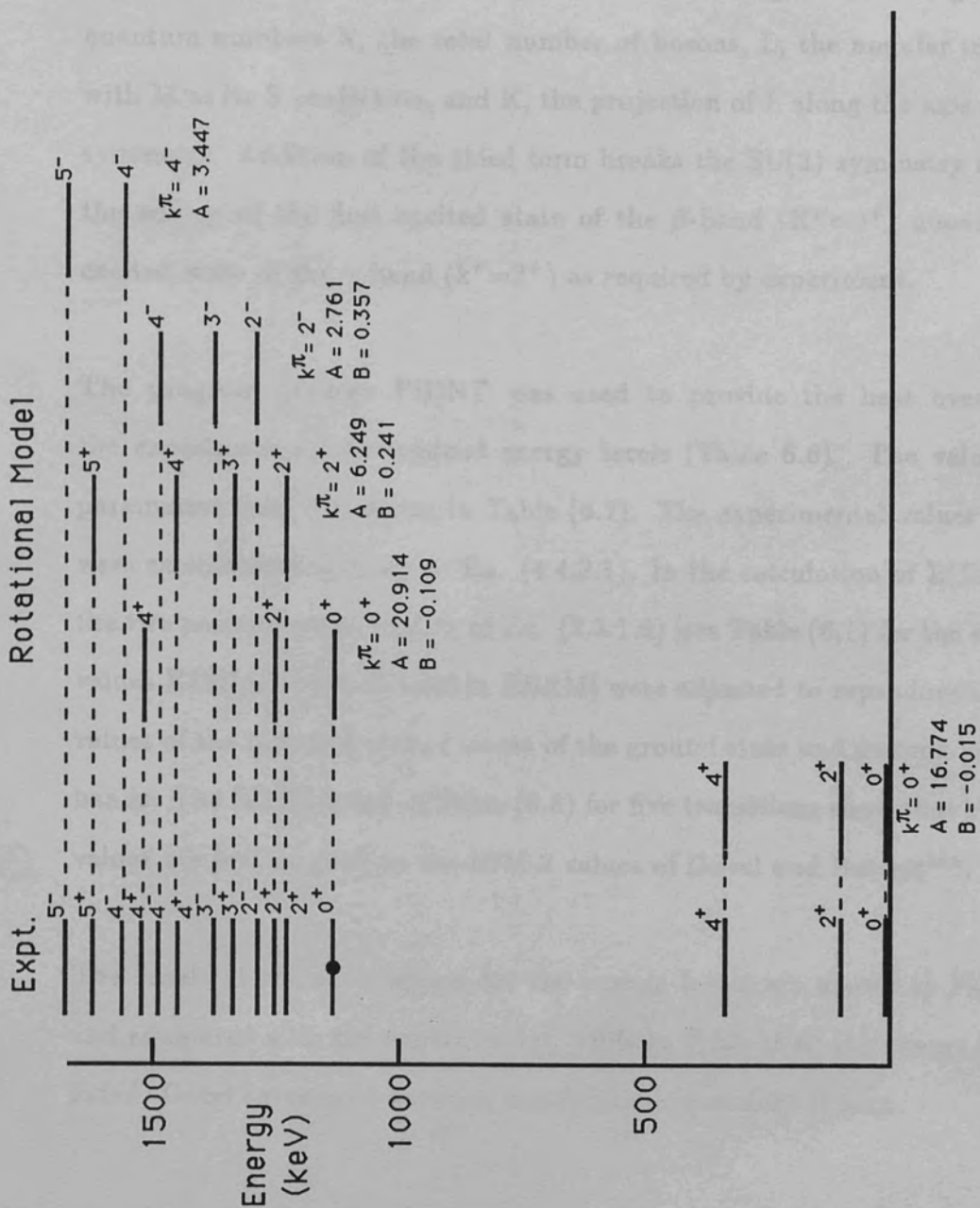
231

Fig (6.9) Low-lying rotational k^{π} bands in ^{182}W compared with experiment. The adopted level is marked with dot in the middle.

the IBM[7]. The Hamiltonian required is

$$H = \frac{1}{2}\text{ELL}(\mathbf{L}.\mathbf{L}) + \frac{1}{4}\text{QQ}(\mathbf{Q}.\mathbf{Q}) + \text{PAIR}(\mathbf{P}.\mathbf{P}) \qquad (6.5.2.1)$$

where the parameters ELL, QQ and PAIR characterise the magnitude of the angular momentum, the quadrupole-quadrupole and pairing interactions. The first two terms give the exact SU(3) limit in which eigenstates are given by the quantum numbers N, the total number of bosons, L, the angular momentum with M as its Z projection, and K, the projection of L along the axis of nuclear symmetry. Addition of the third term breaks the SU(3) symmetry and raises the energy of the first excited state of the β-band ($K^\pi = 0^+$) above the first excited state of the γ-band ($k^\pi = 2^+$) as required by experiment.

The program package PHINT was used to provide the best overall fit to the experimentally determined energy levels (Table 6.6). The values of the parameters used are shown in Table (6.7). The experimental values of B(E2) were calculated according to Eq. (4.4.2.1). In the calculation of B(E2) values, the two parameters α_2 and β_2 of Eq. (2.3.1.6) [see Table (6.7) for the equivalent values E2SD and E2DD used in FBEM] were adjusted to reproduce the B(E2) values of the first and second states of the ground state and gamma-vibrational bands. The B(E2) listed in Table (6.8) for five transitions show that the IBM-1 values are just as good as the IBM-2 values of Duval and Barrett[168].

The result of the calculations for the energy levels are shown in Fig. (6.10) and compared with the experimental, while in Table (6.6) the energy levels are listed. Good agreement between theory and experiment is seen.

Table (6.7)

Values of the parameters corresponding to the Variable Names in Programs PHINT and FBEM (N=13).

PAIR (MeV)	ELL (MeV)	QQ (MeV)	E2SD (eb)	E2DD (eb)
0.0016	0.2222	-0.2999	0.0471	-0.6711

Fig (6.10) Experiment levels in ^{182}W compared with the results of the IBM calculations. The parameters used are the first three of the table (6.7). The adopted level is marked with dot in the middle.

Table (6.8)

Experimental reduced transition probability B(E2) for ^{182}W transitions compared with the nuclear models theory.

Energy (keV)	$J_i \to J_f$	B(E2) Value						
		Experiment*	IBM-1	Duval et al[168]	Hess et al[201]	Kumar et al[200]	Hubert et al[202]	Gunye et al[203]
100.10	$2_1^+ \to 0_1^+$	0.82	0.82	0.84	0.77	0.80	0.84	0.66
1221.43	$2_2^+ \to 0_1^+$	0.057	0.057	0.022	–	–	–	–
1257.43	$2_3^+ \to 0_1^+$	0.015	0.009	0.006	–	–	–	–
1221.33	$2_2^+ \to 2_1^+$	0.086	0.091	0.056	–	–	–	–
229.33	$4_1^+ \to 2_1^+$	1.15	1.15	1.19	–	–	1.20	–

* Lifetime is taken from Firestone[170].

6.4.3 Discussion of Individual Bands

6.4.3.1 The ground state band

This band consists of the levels 100.10 (2^+) and 329.43 (4^+) keV in the ^{182}W nucleus, and is also observed in the ^{182}Re (64 h) decay. The values of the rotational theory is in full agreement with the experiment, while the IBM predicts 333.7 keV for the 4^+. The prediction of the VMI[159] provides the best agreement with the experimental (Table 6.6), but these calculations are given only for the ground state band.

The B.Rs of the 100.10 and 329.43 keV levels are 0.06% and 0.09% depending on the decay-feeding balance of the gamma-rays. These values are supported by Firestone[170], and are in agreement with the assigned spins and parities as predicted from logft values. The experimental B(E2) values and the quadrupole moment (Q) for the transitions depopulating these levels are shown in Table (6.8) together with different theoretical models. The best agreement between theory and experiment is achieved when IBM calculations are used.

6.4.3.2 The γ-band ($k^\pi=2^+$)

The $2^+, 3^+, 4^+$ and 5^+ levels of this band are observed at 1221.34, 1331.37, 1442.88 and 1624.07 keV, respectively. This study suggests that the last level is new. The K quantum number is assigned in view of the comparison between the experimental and the theoretical branching ratios $B(\sigma L)/B'(\sigma L)$, which are shown in Table (6.9). The rotational theory calculation for the energy spectrum is in full agreement with the experimental values. The IBM calculations are also in good agreement with experimental values (Table 6.6). The spins and parities

of the first three levels were assigned in view of the α_k values (Table 6.4) and from the logft values (Table 6.5).

6.4.3.3 The β-band ($k^\pi=0^+$)

This band consists of the two levels at 1257.46 (2^+) and 1510.28 (4^+) keV. The 1135.81 keV is the band-head of the β-band observed by Sapyta et al[167], Galan et al[191] and Gravrilyuk et al[192]. The present IBM calculations predicted this band-head at 1160 keV which is higher than the experimental value, while the 2^+ and 4^+ are in very good agreement with the experimental values. The rotational theory calculations show a full agreement with the experimental values (Table 6.6).

The K quantum number for this band is assigned also in view of the comparison between the experimental and theoretical B(E2) ratios as given in Table (6.9). The spins and parities of these levels were confirmed from logft values (Table 6.5) and from α_k values (Table 6.4).

Sapyta et al[167] assigned the values ($2^+,3^+,4^+$) for the spin of the 1510.28 keV level, while Rikovska et al[175] could not observe this level in their decay scheme. The above theoretical calculation for the energies of this band support the assignment of 4^+ for this level.

6.4.3.4 The negative parity state ($k^\pi=2^-$)

The $2^-,3^-$ and 4^- levels of this octupole rotational band[185] observed in this study and have energies of 1289.17, 1373.85 and 1487.41 respectively. The

Table (6.9)

Relative experimental B(E2) branching ratios for transitions from positive parity states in ^{182}W compared with theory.

Transition (keV)	Energy level (keV)	$\dfrac{J_i^\pi \to J(K)_f^\pi}{J_i^\pi \to J(K)_f^\pi}$	Present Experiment	B(E2) Values for different K_i			Deduced K_i
				K_i	Sapyta et al[167]	Davidson et al[204]	
$\dfrac{1221.43}{1121.33}$	1221.34	$\dfrac{22^+ \to 00^+}{22^+ \to 20^+}$	0.510 (003)	2	0.70	0.52	2
$\dfrac{891.73}{1121.33}$	—	$\dfrac{22^+ \to 40^+}{22^+ \to 20^+}$	0.0050 (0003)	—	0.05	0.09	2
$\dfrac{1001.67}{1131.03}$	1331.37	$\dfrac{32^+ \to 40^+}{32^+ \to 22^+}$	0.500 (005)	2	0.40	0.80	2
$\dfrac{1342.73}{1113.50}$	1442.88	$\dfrac{42^+ \to 20^+}{42^+ \to 40^+}$	0.22 (02)	2	0.34	0.16	2
$\dfrac{1157.53}{1257.43}$	1257.46	$\dfrac{20^+ \to 20^+}{20^+ \to 00^+}$	0.94 (07)	0	1.43	1.41	0
$\dfrac{927.90}{1257.43}$	—	$\dfrac{20^+ \to 40^+}{20^+ \to 00^+}$	1.86 (03)	0	2.57	2.58	0
$\dfrac{1157.53}{927.90}$	—	$\dfrac{20^+ \to 20^+}{20^+ \to 40^+}$	0.51 (04)	0	0.56	0.55	0

calculations of Soloviev et al[193] and Pyatov et al[194] show that small admixture of other two-quasiparticle states also show the transition probability for the 1289.15 keV, M2 transition proceeding from this level. This is supported by the present α_k (Table 6.4). The logft values calculation assigned the 1289.17 keV as 2^- state and classified as allowed/forbidden transition for β-decay to occur. The rotational theory calculations agree with the experimental values (Table 6.6). It was mentioned before (6.4.1.5) that the transition 959.69 keV which depopulates the 1289.17 keV level to the 329.43 keV (4^+) level is of a single particle nature. This supports the idea of broken symmetry in this band. The spins and parities of these levels are assigned in view of logft values (Table 6.5) and from α_k values (Table 6.4). The K quantum number for this band is assigned in view of the B(σL) B.R as given in Table (6.10).

6.4.3.5 The negative parity state ($k^\pi=4^-$)

The 1553.24 keV level was assigned as 4^- by Grigorev et al[187] and from (d,d') reaction[186]. The large E3 component of 1453.22 transition is consistent with k=4 assigned for 1553.21 keV level, although the B(E2) ratios shown in Table (6.10) for transitions proceeding from this level do not support this assignment.

Grigorev et al[187] have considered possible admixture in the 1553.24 keV state using the band-mixing parameters given by Mikhailov[195]. Their analysis indicates that admixture of other k-values are large for the levels of the $k^\pi=4^-$ and $k^\pi=2^-$ band. The calculations of Soloviev et al[196] indicate that negative parity states with K>2 are more properly classified as quasiparticle states rather than octupole vibrational states. The spins and parity of the 1553.24 keV level were confirmed from logft values (Table 6.5) and from the α_k (Table 6.4).

Table (6.10)

Relative experimental B(σL) branching ratios for transitions from negative parity states in ^{182}W compared with Bohr and Mottelson model[205].

Transition (keV)	Energy level (keV)	$\dfrac{J_i^\pi \rightarrow J(K)_f^\pi}{J_i^\pi \rightarrow J(K)_f^\pi}$	Present Experiment	B(σL) Values for different K_i					Deduced K_i
				0	1	2	3	4	
$\dfrac{1289.15}{1189.11}$	1289.17	$\dfrac{22^- \rightarrow 00^+}{22^- \rightarrow 20^+}$	0.07 (01)	—	2.80	0.70	—	—	2
$\dfrac{1044.39}{1273.75}$	1373.85	$\dfrac{32^- \rightarrow 40^+}{32^- \rightarrow 20^+}$	0.67 (02)	1.33	0.75	0.75	0.75	—	2
$\dfrac{42.74}{152.42}$	—	$\dfrac{32^- \rightarrow 32^+}{32^- \rightarrow 22^+}$	1.87 (03)	8.75	8.75	1.40	0.35	—	2

6.5 Conclusions

Certain features of the ^{182}W structure are rather well established[167,170,174,175]. The ground state rotational band is populated up to J=10 in the (α,2n) reaction[197], while in the present work it is populated up to J=4. This study proved that 351 keV is a background transition, supported by Huibin et al[179]. It was not seen in the coincidence spectra and therefore the level 680 (6$^+$) keV could not be placed in the ^{182}Ta decay. This is also supported by Rikovska et al[175], Firestone[170] and Huibin et al[179]. The B(E2) values for deexcitation of the 100.10 and 329.43 keV states are listed in Table (6.8). The 1221.34, 1331.37 and 1442.88 keV states have been classified as belonging to the k$^\pi$=2$^+$ band built on the 1221.34 keV state which was observed for the first time in coulomb excitation studies[198] and explained as asymmetric rotor states[49]. These three states have been treated as γ-rotational states in agreement with the present assignment (Tables 6.4, 6.5).

The excitation of the 1257.46 keV level by inelastic deuteron scattering[186] favours k=0 β-vibrational assignment for this level. This is in agreement with the present choice of large E2 for the 1157.53 keV transition (Table 6.4), since collective vibrational levels deexcite through enhanced E2 transitions. The 1135.81 keV (0$^+$) state reported by Firestone[170], has been predicted by present IBM calculations as an (0$^+$) state and considered as a band-head for the β-band. However, Rikovska et al[175] did not place a 1510.28 keV level in their decay scheme. The present coincidence measurements show that the 1410.15 and 1180.88 keV transitions are in coincidence with 100.10 and 229.33 keV transition, respectively, establishing the 1510.28 keV level. This has been supported by previous works[167,170,174].

The 1289.17, 1373.85, and 1487.41 keV states are from a $k^{\pi}=2^{-}$ rotational band built on the 1289.17 keV state, which according to Gallager and Soloviev[199] can be characterized as a proton two-quasiparticle state. Also the mixing ratios of the 84.64 and 113.75 keV transitions, (Table 6.4), which connect states of the $k^{\pi}=2^{-}$ rotational band, are identical, a result which is expected for rotational band. The 84.64 and 113.75 keV transitions have multipolarity M1, while the 179.27 keV transition from the 4^{-} to 2^{-} band ($\Delta k=2$) is E2/M1. These mixing ratios are thus in qualitative agreement with the k assignments of the negative-parity levels. These assignments are in agreement with present calculation for the spin and parity for these states (Table 6.5). The 1553.24 keV state is characterized as a neutron two-quasiparticle state[199] with $k^{\pi}=4^{-}$. The large E3 component of the 1453.22 keV transition is consistent with a k=4 assignment for the 1553.24 keV level. This is supported from logft value for the spin and parity, and by Sapyta[167].

The new level at 1624.07 keV is assigned to be 5^{+} from its logft value. The IBM calculations predicted this level as member of a γ-vibrational band. This assignment is in agreement with Firestone[170] and Bohr et al[4].

The new level at 1656.64 keV is assigned to be (5^{-}) from logft value (Table 6.5). The assignment of this level is in agreement with other studies[188-190].

Nuclei which lie in the mass range 155<A<185 are considered as strongly deformed and therefore possess rotational spectra. The ^{182}W lies within this range, hence it should show rotational characteristics. The rotational theory was applied to ^{182}W and the results are given in Table (6.6). The SU(3) rotational limit of the IBM was applied with the addition of a very small amount of the pairing (P.P) interaction This allowed the energy of the first excited state of

the β-band ($k^{\pi}=0^+$) to be raised above the first excited state of the γ-band ($k^{\pi}=2^+$), and to get the best fit to the experimental values. Table (6.6) shows the experimental values for the energy levels, compared with the predictions of five different theoretical nuclear models. The calculation of the Pairing Plus Quadrupole Moment (PPQM)[200], Variable Moment of Inertia (VMI)[159], and the General Collective Model (GCM)[201] provide varying degrees of agreement with experiment for the low spin states. However, the IBM calculations gives the best agreement overall.

The agreement between both the rotational theory and the SU(3) limit of the IBM calculations with the experimental values of the energy levels supports the assumption that ^{182}W is a deformed nucleus and is very much like an axially symmetric rotor[162], as is suggested by the energy ratios $E(4^+)/E(2^+)=3.29$ of the ground band states and the $B(E2, 2_\gamma \rightarrow 0_g^+)/B(E2, 2_\gamma \rightarrow 2_g^+)=0.26$. The assumption that the transition between β and γ bands and the ground state band is absolutely forbidden as stated in the SU(3) limit was investigated and experimentally supported.

CHAPTER VII
SUMMARY

In the present work, comprehensive studies of the γ-radiations from the two radioactive isotopes ^{152}Eu and ^{182}Ta were undertaken. The work has succeeded in resolving many of the discrepancies raised by previous workers regarding the transitions and level schemes. In addition, the use of Ge(Li) detectors in singles measurements and in γ-γ coincidence mode allowed a larger number of transitions and levels than before to be included in the decay scheme. The use of an intrinsic Ge detector has given a good check for low energy transitions.

The additional levels and transitions led to the construction of new decay schemes of ^{152}Gd, ^{152}Sm and ^{182}W. The properties of these isotopes which have been explained in the context of the IBM, enabled new aspects of the collective nuclear dynamics to be revealed. Other models were applied as a matter of comparison and were found not to give such a good overall agreement with experiment.

7.1 The ^{152}Gd nucleus

The levels of the ^{152}Gd nucleus are populated by β^- decay of ^{152}Eu. The results of singles measurements were able to confirm the previously reported transitions, and also to suggest eight new transition which were placed in the decay scheme. The decay scheme of ^{152}Gd, established from energy sum relations and γ-γ coincidence measurements employing four gates, includes three new levels at 1312.41, 1485.67 and 1698.34 keV.

245

The new levels at 1485.67 and 1698.34 were assigned spin and parity values of 0^+ and 2^+, to form a third β-band. The new level at 1312.41 keV was assigned to be (1^-), and together with the level 1123.19 keV (3^-) forms an octupole band[118,120,121].

The placement of the 674.66 keV transition between levels 1605.58 keV (2^+) and 930.58 keV (2^+) in ^{152}Gd is confirmed, while the transition 1643.60 keV, which was detected by Sharma et al[105] who could not place it in the decay scheme, has also been observed in the singles only and is considered as due to summing effects.

The spin of the level at 1550.37 keV was confirmed as 4^+, while that of level at 1605.58 keV was confirmed to be 2^+. A new value of 4^+ was confirmed to the level at 1692.48 keV. These levels were assigned by the IBM calculations and logft values.

Ismail et al[111] has proposed a new level at 1381 keV (4^+), which depopulates by the 258 keV transition. This could not be supported experimentally nor predicted by the IBM calculation. It is therefore believed that the 258 keV is a transition background from ^{214}Pb in the reactor.

Conversion electron coefficients have been measured by combining present γ-ray intensities with the conversion electron intensities reported from conversion electron experiments, thereby allowing the multipolarities of transitions contributing to the conversion electron process be deduced. This is achieved by comparing the experimental conversion coefficients with the theoretical values predicted for different multipole orders. Branching ratios of β^- decay, and therefore logft values, have been determined from the intensity balance

between transitions feeding and depopulating a level; using the logft values and multipolarities obtained the spin/parity assignment of seventeen excited states of ^{152}Gd were determined consistent with β decay and γ-emission selection rules.

In the IBM space, the subgroup decomposition of this space has three subgroub, SU(5), SU(3) and O(6). The first two correspond to the familiar vibrational and rotational limits, while the O(6) limit corresponds to the γ-unstable picture. One of the most powerful and appealing aspects of the IBM is the treatment of the transitional regions between these extreme limiting coupling schemes. The information offered by structure properties of the ^{152}Gd nucleus has allowed a valuable test of the applicability of the IBM in such transitional region. The test has been carried out using the computer program PHINT which calculates the energy levels. Also, the electromagnetic transition rates are calculated using the program FBEM.

Earlier work on the ^{152}Gd nucleus indicated that it could be purely vibrational and initial attempt to fit the energy levels (and transition probabilities), incorporating the new transitions and levels was accordingly made using the SU(5) limit of the IBM. The result indicated that the energy levels were not well reproduce and agreement with transition probabilities was poor: a new β-band found experimentally could not be predicted. On the other hand, applying the transitional SU(5) $\rightarrow$ SU(3) IBM gave excellent agreement for both the energies and B(E2) values (Eq. 2.3.3.a.1) and Tables [(4.6),(4.11)]. The parameters used in the IBM calculations are listed in Table (4.10). No improvement was found by using the full Hamiltonian. It may be concluded that the nuclear shape is more that of an oblate ellipsoid, than that of a prolate ellipsoi d.

7.2 The ^{152}Sm Nucleus

Singles measurements of the ^{152}Eu decay reveal the existence of five new γ-ray transitions. The result of γ-γ coincidence measurements and energy sum relations enabled twenty excited states to established. Two levels at 1436.65 and 1681.56 keV are new suggestions. The (2^+) assignment to the new level at 1436.65 keV is supported by the present IBM calculation which predicts it as band-head for the second γ-band in ^{152}Sm (Table 5.5). The new level at 1681.56 keV is suggested according to singles and coincidence data (Table 5.1, 5.2). The spin and parity are assigned to this level in view of logft values, and this is in agreement with the prediction of Konijn et al[71] for this level from $(\alpha,2n)$ reaction.

The 1315.32 keV transition, previously reported by Sharma et al[105] and Baker et al[104] but unplaced in their decay scheme, could be placed between 1681.56 keV level and the level 366.46 keV. The 964.10 keV transition is considered to be a doublet by Baglin[113] and Warburton et al[123] which is confirmed in this work.

^{152}Sm considered as a deformed nucleus would be expected to show rotational spectra. The energy level ratios for the ground state band supported a mainly rotational character, but could allow some vibrational degrees of freedom since experimentally $E(4_1^+)/E(2_1^+)=3.02$ and $E(6_1^+)/E(2_1^+)=5.79$ compared to the pure rotational values of 3.33 and 7.0 respectively. Many models, including the (VMI)[159], (PPQM)[150,200],(BET)[152,160] and (RVM)[161], have been used to calculate both the band energy and the B(E2) ratios for ^{152}Sm with varying degree of success; indications being found that there is a coupling between the

248

rotational and the intrinsic motions of the nucleus, suggesting a transitional nature for ^{152}Sm.

In the case of ^{152}Sm it was verified that the previous use of the SU(5) → SU(3) transitional IBM was in quite good agreement with the experimental results. Nonetheless this could not predict a second β-band in which was placed a 2^+ level at 1293 keV, and whose 0^+ band-head at 1082 keV was one of three 0^+ states found by Passaija et al[141]. When the complete Hamiltonian was used these three 0^+ states could be obtained, and also a fourth 0^+ states at 1485 keV was predicted which could be the band-head of a third β-band in which the 2^+ level at 1768.98 keV could be placed. Also, it was found that much better agreement was obtained overall, Tables (5.5.5.13), when the complete Hamiltonian was used for the IBM calculations, The present results of the IBM calculations are listed in Table (5.5) and shown in Fig. (5.10). The values obtained for the parameters, Table (5.10),reveal that the nucleus can be regarded as deformed showing SU(5) → SU(3), properties coupled to some O(6) characteristics.

7.3 The ^{182}W Nucleus

The level scheme of ^{182}W was established from singles and γ-γ coincidence measurements with Ge(Li) detector following the β^- decay of ^{182}Ta. A pure Ge detector was also used to confirm the intensities of low energy γ-rays and as a further check on background energies. The singles measurements reveal the existence of forty two γ-rays; of these five are new. It has thus been possible to establish the new levels at 1624.07 and 1656.64 keV in the levels scheme of ^{182}W. The new level at 1624.07 keV is assigned to be 5^+ from its

logft value. The IBM calculations predicted this level as member of a γ-band. This assignment is in agreement with Firestone[170] and Bohr et al[4]. The new level at 1656.64 keV is assigned to be 5^- from logft value Table (5.5). The assignment of this level is in agreement with other studies[188-190]. The 681 keV level was depopulated by a transition at 351 keV which Huibin et al[179] regarded as background. This is supported by this work and it could not be seen in the coincidence spectra, therefore the level 681 (6^+) could not be placed in the ^{182}Ta decay. The spin/parity of 1510.28 keV level was uncertain. The present IBM calculation also predicts an 0^+ state at 1135 keV, which was reported by Firestone[170], and it is, considered to be the band-head of the β-band in which the IBM also gives a 4^+ assignment for the 1510.28 keV level. The γ-γ coincidence measurements also suggest the 1410.15 and 1180.88 keV transitions which decay from the very mentioned level are in coincidence with spectra gated by 100.10 and 229.33 keV γ-rays at logft of 9.85. This supports a 4^+ assignment for 1510.3 keV level.

According to the energy ratio $E(4_1^+)/E(2_1^+)=3.29$, the ^{182}W nucleus could be classified as deformed, and can be treated as a symmetric rotor as in Bohr et al[209], or as an example of a nucleus on the SU(3) limit of the IBM. The placement of new level is supported by the new IBM calculation which shows that the SU(3) Hamiltonian gives a good description of the ^{182}W nucleus. With the addition of a small pairing interaction a valuable improvement to the agreement with the experiment is obtained as shown in Table (6.6) and Fig. (6.10). The Hamiltonian used is in Eq. (6.5.2.1). The addition of third term breaks the SU(3) symmetry and raises the energy of the first excited state of the β-band $(k^\pi=0^+)$ above the first excited state of the γ-band $(k^\pi=2^+)$ as required by the experiment. The program PHINT was used to provide the best overall fit to the experimentally determined energy levels Table (6.6) and Fig.

(6.10). The B(E2) values were obtained from the program FBEM are listed in Table (6.8); the parameters obtained are given in Table (6.7).

REFERENCES

(1) Rainwater, J.: Phys. Rev. **79**, 432 (1950).

(2) Bohr, A.: Nat. Fys. Medd. Dan. Vid. Selsk. **26**, No.14 (1952).

(3) Bohr, A. and Mottelson, B.R.: Nat. Fys. Medd. Dan. Vid. Selsk. **27**, No.16 (1953).

(4) Bohr, A. and Mottelson, B.R.: Nuclear Structure, Vol. II (Benjamin W.A, Reading (1975).

(5) Brink, D.M., Toledo Piza A.F.R and Kerman A.K.: Phys. Lett **19**, 413 (1965); Gneuss, G. and Greiner, W.: Nucl. Phys. **A171**, 449 (1971).

(6) Kishimoto, T. and Tamura, T.: Nucl. Phys. **A192**, 246 (1972); A270, 317 (1976).

(7) Janssen, D., Jolos, R.V. and Donan, F.: Nucl. Phys. **A224**, 93 (1974).

(8) Arima, A., and Iachello, F.: Ann. Phys. (N.Y) **99**, 253 (1976).

(9) Arima, A., and Iachello, F.: Ann. Phys. (N.Y) **111**, 201 (1978).

(10) Arima, A., Iachello, F.: Ann. Phys. (N.Y.) **123**, 468 (1979).

(11) Scholten, O., Iachello, F., and Arima, A.: Ann. Phys. (N.Y.) **115**, 325 (1978).

(12) Iachello, F.: Interacting Bosons in Nuclear Physics, (Plenum Press New York, 1979).

(13) Otsuka, T., Arima, A., Iachello, F. and Talmi, I.: Phys. Lett **B76**, 139 (1978).

(14) Otauka, T., Arima, A. and Iachello, F.: Nucl. Phys. **A309**, 1 (1978).

(15) Talmi, T.: in "Proc. Int. Conference Of Dynamical Properties of Heavy-Ion Reaction" S. Afr, J. Phys. **1** (1978) 183; in "Frontier Research in Nuclear Physics". Edit by Feng D.H., et.al. (Plnum Press, New York, 1981) and Ref. 8, P.79.

(16) Ginocchio J.N and Kirson M.: Phys. Rev. Lett. **44**, 1744 (1980); Nucl. Phys. **A350**, 31 (1980).

(17) Dieperink, A.E.L, Sholten, O. and Iachello, F.: Phys. Rev. Lett **44**, 1747 (1980).

(18) Dieperink, A.E.L and Sholten, O.: Nucl. Phys. **A346**, 125 (1980).

(19) Van Roosmalen, D.S and Dieperink, A.E.L.: KVI-283, preprint (1980).

(20) Bateman, H., Proceeding Cambridge Philosophical Society.: **15**, 423 (1910).

(21) Wilson, B.J.: The Radiochemical Manual, Second Edition, (1966).

(22) Moszkowski, S.A.: Phys. Rev. **82**, 35 (1951).

(23) Verral, R.I, Hardy, J.C. and Bell, R.E., Nucl. Instrum. Methods **42**, 258 (1966) and references therein.

(24) Raman, S., and Gove, N.B.: Phys. Rev. **C7**, 1995 (1973).

(25) Arya, A.: Fundamentals of Nuclear Physics, Allyn and Bacon, INC., (1966) P.260.

(26) Blatt, J.M. and Weisskopf, V.F.: Theoretical Nuclear Physics, (1952), (John Willey & Son, New York).

(27) Alder, K., Bohr, A., Huus, T., Mottelson, B.R., and Winther, A.: Rev. Mod. Phys. **28**, 433 (1956).

(28) Löbner, K.E.G.: The Electromagnetic Interaction in Nuclear Spectroscopy, North-Holland Pub. Co. (1975).

(29) Hahn, O. and Meitner, L.: Z. Physik **29**, 161 (1924).

(30) Church, E.L. and Weneser, J.: Ann. Rev. Nucl. Sc. **10**, 193 (1960).

(31) Rose, M.E.: Goetzel, G.H., Spinrod, B.I, Hater, J and Strong, P. Phys. Rev. **83**, 79 (1951).

(32) Rose, M.E.: <u>Alpha, Beta and Gamma-ray Spectroscopy</u> Edited by Seigbahn K., (north-Holland).

(33) Rösel, F., Fries, H.M., Alder, K., and Pauli, H.C.: Atomic Data and Nuclear Data Tables **21**, 325, 268, 258 (1978).

(34) Bohr, A., and Mottelson, B.R.: <u>Nuclear Structure</u> Vol. I. (W.A. Benjamin, inc. Amsterdam, 1969).

(35) Mayer, M.G.: Phys. Rev. **74**, 235 (1948).

(36) Elasser, W.M.: J. Phys. et radium **4**, 549 (1933).

(37) Mayer, M.G.: Phys. Rev. **75**, 1969 (1949).

(38) Haxel, O., Jensen, J.H.D., and Suess, H.E.: Phys. Rev. **75**, 1766 (1949).

(39) Feehberg, E., Hammack, K.C.: Phys. Rev. **75**, 1877 (1949).

(40) Nathan, O., and Nilson, S. G.: <u>Alpha, Beta and Gamma-ray spectroscopy</u>, Edited by Siegbahn, K. (North-Holland publishing Co., Amsterdam, 1965) Chap. II.

(41) Gallagher, C. J. in <u>Selected Topic in Nuclear Spectroscopy,</u> Verhaar B. J. (ed.), p.133, North-holland publishing Co., Amsterdam (1964).

(42) Hecht, K.T.: <u>Selected Topic in Nuclear Spectroscopy</u>, op cit., p.51.

(43) Preston, M. A.: <u>Physics of the Nucleus</u>, Addison-Wesley publishing Co., Massachusetts (1962).

(44) Sheline, R.K.: Rev. Mod. Phys. **32**, 1 (1966).

(45) Bayman, B.F., and Alexander Lande.: Nucl. Phys. **77**, 1 (1966).

(46) Wilets, L., and Jean, M.: Phys. Rev. **102**, 788 (1956).

(47) Pauli, E.P.: <u>Nuclear and Particle Physics</u>, North-Holland publishing. ,Co., p.299 (1969).

(48) Alaga, G., Alder, K., Bohr, A., and Mottelson, B.R.: Mat. Fys. Medd. Dan. Vid. Selsk. **29** No.9 (1955).

(49) Davydov, A.S., and Fillippov, G.F., Nucl. Phys. **8**, 237 (1958); and refrences therein.

(50) Davydov, A.S., and Rostovsky, V.S.: Nucl. Phys. **12**, 58 (1959).

(51) Davydov, A.S., and Chaban, A.A.: Nucl. Phys. **20**, 499 (1960).

(52) Davydov, A.S., Rostovsky, V.S., and Chaban, A.A.: Nucl. Phys. **27**, 134 (1961).

(53) Nilsson, S.G.: Mat. Fys. Modd. Dan. vid. Selsk. **29**, NO. 16 (1955).

(54) Leander, G.: Nucl. Phys. **A273**, 286 (1976).

(55) Meyer-ter-vehn, J.: Nucl. Phys. **A249**, 141 (1975).

(56) Iachello, F., and Arima, A.: Phys. Lett. **53B**, 309 (1974).

(57) Arima, A., and Iachello, F.: Phys. Rev. Lett. **35**, 1069 (1975).

(58) Arima, A., and Iachello, F.: Phys. Rev. Lett. **40**, 385 (1978).

(59) Arima, A., and Iachello, F.: Ann. Rev. Nucl. Part. Sci., **31**, 75 (1981).

(60) Iachello, F.: Nukleonika **22**, 107 (1977).

(61) Iachello, F.: in <u>Proc. Int. Summer School on Nuclear Structure</u>, Dronten, The Netherlands, Plenum Press, (1981).

(62) Scholten, O.: Computer Code PHINT, K.V.I., GroningenHolland.

(63) Elliott, J.P.: Proc. Roy. Soc., **A245**, 128 (1958).

(64) Bjornholm, S., Boehm, F., Knutsen, A.B., and Nielsen, O.B.: Nucl. Phys. **42**, 469 (1963).

(65) Lipas, P.O.: <u>Progress in Particle and Nuclear Physics,</u> Vol.9, Collective Bands in Nuclei, Ed. Wilkinson, D., (Pergamon, Oxford) P. 511 (1983).

(66) Lipas, P.O., Kumpulainen, J., Hammaren, E., Honkaranta, T., Finger, M., Kracikova, T.I., Prochazka, I., and Ferencci, J.: Phys. Scr. **27**, 8 (1983).

(67) Cizewski, J.A., Casten, R.F., Smith.G.J., Stelts, M.L., Kane, W.R., Borner, H.G., and Davidson W.F.: Phys. Rev. Lett. **40**, 167 (1978); Cizewski, J.A., Casten, R.F., Smith.G.J., Macphail, M.R., Stelts, M.L., Kane, W.R., Borner, H.G., and Davidson W.F.: Nucl. Phys. **A323**, 349 (1979).

(68) Hatch, R.L., and Levit, S.: Phys. Rev. **C25**, 614 (1982).

(69) Casten, R.F., and Von Brentans, P.: Phys. Lett. **152B** 22 (1985).

(70) Sakai, M., and Rester, A.C.: Atomic Data and Nuclear Data Table **20**, 441 (1977).

(71) Konijn, J., Berhout, J.B.R., Hesselink, W.H.A., Van Tuijven, J.J., Van Nes, P., Verheul, H.: Nucl. Phys. **A373**, 397 (1982).

(72) Casten, R.F., Warner, D.D.: Rev. Mod. Phys. **60**, 389 (1988).

(73) Iachello, F., and Arima, A.: <u>The Interacting Boson Model</u>, Cambrigde University Press., Cambrigde (1987)

(74) Cizewiski, R.F.: Thesis, (1978).

(75) Debertin, K. and Schotzig, U.: Nucl. Instrum. Methods **140**, 337 (1977).

(76) Debertin, K. and Schotzig, U.: Nucl. Instrum. Methods **158** 471 (1979).

(77) Routti, J. and Prussin, S.: Nucl. Instrum. Methods **72** 125 (1969).

(78) The T.R.C. Set Radiochemical Centre, Amersham, Buckinghamshire, U.K.

(79) Knoll, G.F.: <u>Radiation Detection and Measurement</u> (J. Wiley and Sons, New York, 1979).

(80) Gallager, W.J., and Cipolla, S.J.: Nucl. Instrum. Methods **122**, 405 (1974).

(81) Goulging, F.S.: <u>Semiconductor Detectors for Nuclear Spectroscopy</u> UCRL-16231 (1965).

(82) Freck, D.V., and Wakefield, J.: Nature **193**, 309 (1962).

(83) <u>A Handbook of radioactivity Measurements Procedures</u>, NCRP Report No. 58, Second Edition. Februray (1985).

(84) Ewan, G.T. and Tavendale, A.J.: Can. J. Phys. **42**, 2286 (1964).

(85) An 34 Experiments in Nuclear Science, second edition, published by Ortec, (1976).

(86) Fairstein, E.: Conference on Semiconductor Nuclear Particle Detectors and Circuits, Gatlinburg, Tennessee (1967).

(87) Harris Jr, R.J., and Shuler, W.B.: Nucl. Inst. Methds., **51**, 341 (1967).

(88) Radiation Spectroscopy and Analysis Instruments for Research and Industry Catalogue 1004, 1976.

(89) Barton, R.D., and King, M.E.: Nucl. Instrum. Methods **100**, 165 (1972).

(90) Johansson, B.: Nucl. Instrum. Methods **1**, 274 (1957).

(91) Meilling, W., and Stroy, F.: <u>Nonosecand Pulse Technique</u> (Gorden and Dreach N.Y. 1968).

(92) Gedrke, D.A., and McDonald, W.J.: Nucl. Instrum. Methods **55**, 337 (1967); **56**, 148 (1967); **58**, 253 (1968).

(93) Bengtson, B., and Moszynski, .: Nucl. Instrum. Methods **81**, 109 (1970); **85** 133 (1970).

(94) Wapstra, A.H.: <u>Alpha, Beta and Gamma-ray spectroscopy</u>, ed. Siegbahn, K., (North Holand, Amsterdam, 1965) P.539.

(95) Gibson, W.M., Millerand, G.L., and Denovan, P.F., <u>Alpha, Beta and Gamma-ray Spectroscopy</u>, ed. Siegbahn, K., (North Holland, Amsterdam, 1965).

(96) Casten, R.F.: Phys. ReV. Lett. **54**, 1991 (1985).

(97) Barratte, J., Barratte, M., Boutard, A., Lamoureux, G., Monaro, S., Markiza, S.: Can. J. Phys. **49** 2462 (1971).

(98) Riedinger, L.L., Johnson, R., Hamilton, J.H.: Phys. ReV.**C2**, 2358 (1970).

(99) Toth, K.S., Faler, K.T., Rasmussan, J.O.: Phys. ReV. **115**, 158 (1959).

(100) Gromov, K., Kuzentsov, V.V., Kuznetsova, M.Y., Finger, N., Urbanec, J., Nilsen, O.B., Wilsky, K., Skilbreid, O. and Jorgensen, M.: Nucl. Phys. **A99**, 585 (1967).

(101) Gono, Y.: Proceedings of the international symposium on nuclear structure contributions, Dubna 1968 (International Atomic Energy Agency, Vienna, Austria, 1969).

(102) Zolnowski, D.R., Hughes, M.B., Hunt, J., and Sugihara, T.T., Phys. Rev. **C3**, 2556 (1980).

(103) Bloch, R., Elbeck, B., and Tjøm, P.O.: Nucl. Phys. **A91**, 576 (1967).

(104) Baker, K., Hamilton, J.H., and Ramayya, A.V.: Z.Physik **256**, 387 (1972).

(105) Sharma, A.K., K umar, R., Verma, H.R., Terhan, P.N.: J. Phys. Soc. Jap. **48**, 1407 (1980).

(106) Yoshizawa, Y., Iwata, Y., Inuma, Y.: Nucl. Instrum. Methods **174**, 133 (1980).

(107) Debertin, K.: Nucl. Instrum. Methods **158**, 479 (1979).

(108) Meyer, R.: Lawrence Livermore Laboratory M-100 (1978).

(109) Gehrke, R.J., and Helmer, R.G.: Nucl. Instrum. Methods **147**, 405 (1977).

(110) Debertin, K., Shotzig, U., Weiss, H.M.: PTB-Mitteilungen **85**, 187 (1977).

(111) Ismail, H.A., Hanafi, H., Morsy, M., Nada, A., and Abu-Laila, H.: Acta. Phys. Acad., Sci. Hung. **50**, 391 (1981).

(112) Iwata, Y., Yasuhara, M., Meada, K., and Yoshizawa, Y.: Nucl. Instrum. Methods Phys. Res., **219**, 123 (1984).

(113) Baglin, C.M.: Nucl. Data Sheets **30**, 1 (1980).

(114) Malmsten, G., Nilsson, O., and Anderson, I.: Arkiv Fysik **33**, 361 (1966).

(115) Dzhelepov, B.S., Zhukovskii, N.N, and Maloyan, A.G.: Yad. FiZ., **1**, 941 (1965) (Transl. Sov. J. Nucl. Phys. **1**, 671 (1965).

(116) Varnell, L., Bowman, J.D., and Trischuk, J.: Nucl. Phys. **A127**, 270 (1969).

(117) Gono, Y.: J. Phys. Soc. Jap. **29**, 543 (1970).

(118) Zolnowski, D.R., Funk, E.G., and Mihelich, J.W.: Nucl. Phys. **A177**, 513 (1971).

(119) Barrette, J., Barrette, M., Bountard, A., Lamoureusx, G., and Moharo, S.: Can. J. Phys., **48**, 2011 (1970).

(120) Markund, I., Nathan, O., and Nielsen, O.B.: Nucl. Phys. **15**, 199 (1960).

(121) Zolnowiski, D.R., Kihmoto, T., Gono, Y., Sugihara, T.T.: Phys. Lett., **55B**, 453 (1975).

(122) Schick, W.C., and Grodzins, L.: Nucl. Phys. **62**, 254 (1965).

(123) Warburton, E.K., Alburger, D.E.: Nucl. Instrum. Methods **A253**, 38 (1986).

(124) Grabowski, Z.: Arkiv Fysik **20**, 177 (1961).

(125) Bisgoard, K.M., Nielson, K.B., and Sodemann, J.: Phys. Lett., **7**, 57 (1963).

(126) Larsen, J.S., Skilbreid, O., and Visiten, L.: Nucl. Phys. **100**, 248 (1967).

(127) Schneider, W.: Nucl. Phys., **21**, 55 (1960).

(128) Sheline, R.K.: Rev. Mod. Phys. **32**, 1 (1960).

(129) Sakai, M.: Nucl. Phys. **A104**, 301 (1967).

(130) Meyer, R.A.: Phys. Rev., **170**, 4 (1968).

(131) Andesson, G.I, and Ewan, G.T.: Nucl. Phys. **A123**, 609 (1969).

(132) Soloviev, V.V., Vogel, P., and Komeichuk, A.A.: Sov. Phys. Doki. **9**, 45, (1964).

(133) Gupta, J.B.: Phys. ReV. **C28**, 1829 (1983).

(134) Venkova, Ts., Andrejtscheff, W.: Atomic Data and Nucl. Data Tables **26**, 94 (1981).

(135) Casten, R.F., Warner, D.D., Brenner, D.S., Gill, R.L.: Phys. Rev. Lett. **16**, 1433 (1981).

(136) Kalfas, C.A., Hamilton, W.D., and Fox, R.A.: Nucl. Phys. **A196**, 615 (1972).

(137) Schneider, U., and Hauser, U.: Z. Phys. **A273**, 239 (1975).

(138) Johnson, N.R.: Bull. Am. Phys. Soc., **16**, 130 (1971).

(139) Schick, W.C.: Bull. Am. Phys. Soc. **15**, 75 (1970).

(140) Hinds, S., Bierregaard, J.H., Hansen, O., and Nathan, O.: Phys. Lett. **14**, 48 (1965).

(141) Passoja, A., Kantele, J., Luontama, M., Julin, R., Hammaren, E., Lipas, P.O., and Toivoen, P.: J. Phys. **G12**, 1047 (1986).

(142) Canstanos, O., Frank, A., and Fedreman, P.: Phys. Lett., **88B**, 203 (1979).

(143) Lederer, N., and Shirley, V.: Table of Isotopes, 7th ed. (J. Wiley and Sons, New York, 1978).

(144) Friedlander, G., Kennedy, J., and Miller, J.: <u>Nucler and Radioactivity</u> (J. Wiley and Sons, inc., New York, 1964).

(145) Seaman, G.G., Greenberg, J.S., Bromley, D.A., and McGowan, F.K.: Phys. Rev. **149**, 925 (1966).

(146) Fraser, I.A., Greenberg, J.S., Sie, S.H., Stockstad, R.G., Burginyon, G.A.: Phys. ReV. Lett. **23**, 1047 (1969).

(147) Sayer, R.O., Stelson, P.H., McGowan, F.K., Milner, W.T., and Robinson, R.L.: Phys. ReV. **1**, 1525 (1970).

(148) Lonsjo, O., and Hagemann, G.B., Nucl. Phys. **88**, 624 (1966).

(149) Veje, E., Elbek, B., Herskind, B., and Olesen, M.C.: Nucl. Phys. **A109**, 489 (1968).

(150) Kumar, K., Nucl. Phys. **A213**, 189 (1974).

(151) Riedinger, L.L., Johnson,N.R., Hamilton, J.H.: Phys. ReV.**179**, 1214 (1969).

(152) Tamura, T, Weeks, K., and Kishimoto, T.: Phys. Rev. **C20**, 307 (1979).

(153) Reidinger, L.L., and Johnson, N.: Phys. Rev. Lett. **19**, 1243 (1967).

(154) Mclatchie, W., Kitching, J.E., and Darcey, W.: Phys. Lett. **30B**, 529 (1969).

(155) Yamamoto, H., Kawade, K., Ikeda, Y., and Katoh, T.: J. Phys. Soc. Jap. **43**, 8 (1977).

(156) De-shalit, A., and Feshbach, H.: Theoretical Nuclear Physics Vol. 1, Nuclear Structure (J. Wiley and Sons, Inc., New York 1974).

(157) Schonen, J., and Lipas, P.O.: Nucl. Phys. **A442**, 189 (1985).

(158) VanIsacker,P., Private Communication (1988).

(159) Mariscott, and M.A., Buck, B.: Phys. Rev. **178**, 1864 (1969).

(160) Tamura, T., and Kishimoto, T., Nucl. Phys. **A270**, 317 (1976).

(161) Bhradwaj, S.K., Gupta, K.K., Gupta, J.B., and Gupta, D.K.: Phys. Rev. **C27**, 872 (1983).

(162) Alaga, G., Alder, K., Bohr, A., and Mottelson, B.R., Mat. Fys. Medd. Dan. Vid. Selsk. **29** No.9 (1955).

(163) Lipas, P.O.: Nucl. Phys. **39**, 468 (1962).

(164) Mikhailove, V.M.: Bull. Acad. Sci., USSR Phys. Ser. **30**, 1392 (1966).

(165) Griporiev, E.P., and Avotina, M.P.: Nucl. Phys. **19**, 248 (1960).

(166) Murray, J.J., Boehm, F., Marmier, P., and Dumond, J.W.M.: Phys. rev. **97**, 1007 (1955).

(167) Sapyta, J.J., Funk, E.G., and Mihelich, J.W.: Nucl. Phys. **A139**, 161 (1969).

(168) Duval, D.P., and Barrett, B.R.: Phys. Rev. **C23**, 492 (1981).

(169) Schmorak, M.R.:Nucl. Data. Sheets, **14**, 599 (1975).

(170) Firestone, R.B.: Nucl. Data. Sheets, **54**, 307 (1988).

(171) Helmer, R.G.: Nucl. Phys. **A272** 269 (1976).

(172) Roney, W.M., and Sale, W.A.: Nucl. Instrum. Methods **171**, 389 (1980).

(173) Schötzig, U., Deberton, K., and Walz, K.F.: Nucl. Instrum. Methods **169**, 43 (1980).

(174) Jin, J., Takada, J., Iwata, Y., and Yoshizawa, Y.: Nucl. Instrum. Methods **212**, 259 (1983).

(175) Rikovska, J., and Novakova, D.: Z. Phys. **A311**, 185 (1983).

(176) Casten, R.F., and Cizewski, J.A.: Nucl. Phys. **347**, 173 (1980).

(177) Frank, A., and Federman, P.: Phys. Lett. **88B**, 203 (1979).

(178) Stewart, N.M., and Shaban., A.M.: Z. Phys. **A296**, 165 (1980).

(179) Huibin, S., Fangji, W., and Yunzov, L.: Herrogate Conferance P.367, 1986.

(180) Bashandy, E., El-sarrah, A.H., and El-naser.: Nucl. Phys. **52**, 61 (1964).

(181) Gove, N.B., and Martin, M.J.: Nucl. Data Table **10**, No. 3 (1971).

262

(182) Nilsson, ö., Höberg, S., Karlsson, S.G., and El-sayed, G.M.: Nucl. Phys. **A100**, 351 (1967).

(183) Venkova, T., Andrejtscheff, W.: Atomic Data and Nuclear Data Tables **26**, No. 2 (1981).

(184) Neergard, K., and Vogel, P.: Nucl. Phys. **A145**, 33 (1970).

(185) Herzog, P., Canty, M.J., and Killing, K.D.: Nucl. Phys. **A187**, 49 (1972).

(186) Günther, C., Kleinheinz, P., Casten, R.F., and Elbek, B.: Nucl. Phys. **A172**, 273 (1971).

(187) Griugorev, E.P., Zolotavin, A.V., Sergeev, B.O., and Bekrenev, V.S.: Sov. J. Nucl. Phys. **4**, 5 (1967).

(188) Jeltema, B.D., Bernthal, F.M., Khoo, T.L., and Dors, C.L.: Nucl. Phys. **A280**, 21 (1977).

(189) Galan, P., and Veji, M.: Czech. J. Phys. **22b**, 18 (1972).

(190) Harmatz, B., and Handley, T.H.: Nucl. Phys. **A121**, 481 (1968).

(191) Galan, P., Galanova, T., Malek, Z., Voinova, N., Preibisz, Z., and Stryczniewicz, K.: Nucl. Phys.: **A136**, 673 (1969).

(192) Gavrilyuk, V.I., Kupryashkin, V.T., Latyshev, G.D., Lyutyi, I.N., Makovetskii, Y.V., and Feoktistov, A.I.: Bull. Acad. Sci. USSR, Phys. Ser. **35**, 2027 (1972).

(193) Soloviev, V.G.: At. Energy ReV. **3**, 2117 (1965).

(194) Pytaov, N.I.: Acta Phys. Polon. **25**, 21 (1964).

(195) Mikhailov, V.M.: Bull. Acad. Sci. USSR Phys. Ser. **28**, 225 (1964).

(196) Soloviev, V.G., Fogel, P., and Korneichuk, A.A.: Bull. Acad. Sci. USSR Phys. Ser. **28**, 1495 (1964).

(197) Lark, N.L., and Morinaga H: Nucl. Phys. **63**, 466 (1965).

(198) Johnson, N.R., Reidinger, L.L., and Hamilton, J.H.: Proc. Int. Conf. on Nuclear Structure, Ed. Sanada, J. (Tokyo, September 1967).

(199) Gallager, C.J., and Soloviev, V.G.: Mat. Fys. Medd. Dan. Vid. Selsk. **2**, 2 (1962).

(200) Kumar, K., and Baranger, M.: Nucl. Phys. **A122**, 273 (1968).

(201) Hess, P.O., Marnhn, J., and Greiner, W.: Nucl. Phys. **G7**, 737 (1981).

(202) Hubert, Ph., and Johnson, N.R.: Nucl. Phys. **A321**, 213 (1979).

(203) Gunye, M.R., Kumar, A.: Phys. Rev. **C22**, 869 (1980).

(204) Davidson, J.P., Davidson, M.G.: Phys. Rev. **B138**, 316 (1965).

(205) Bohr, A., Mottelson, B.R.: **14**, 225 (1953).

ACKNOWLEDGEMENTS